

California AHMCT Research Center
University of California at Davis
California Department of Transportation

DEVELOPMENT OF A TELESCOPIC MANIPULATOR ARM FOR HIGHWAY MAINTENANCE

Todd Lawrence Baker

AHMCT Research Report
UCD-ARR-98-02-03-01

Interim
~~Final~~ Report of Contract
IA65X875 T.O. 95-12

March 2, 1998

* This work was supported by the California Department of Transportation (Caltrans)
Advanced Highway Maintenance and Construction Technology Center at UC, Davis

Development of a Telescopic Manipulator Arm for Highway Maintenance

BY

TODD LAWRENCE BAKER

B.S. (University of California, Davis) 1996

THESIS

Submitted in partial satisfaction of the requirements for the degree of

MASTER OF SCIENCE

in

Engineering

in the

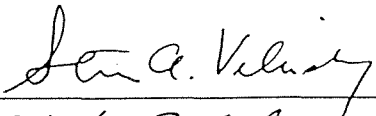
OFFICE OF GRADUATE STUDIES

of the

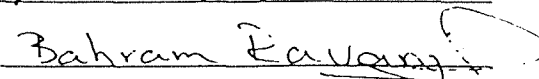
UNIVERSITY OF CALIFORNIA

DAVIS

Approved:







Committee in Charge

1998

ABSTRACT

Annually, governments spend millions of taxpayers' dollars maintaining a highway infrastructure that is continually growing as we near the 21st century. In order to maintain this vast infrastructure, highway workers put their lives on the line each day, subjecting themselves to the ever-present threat of inattentive drivers. The Advanced Highway Maintenance and Technology (AHMCT) Center, of the University of California, Davis, has developed numerous machines aimed at increasing the productivity, quality and safety of highway maintenance operations.

This thesis presents the design and development of a Telescopic Manipulator Arm that comprises part of the Operator Controlled Crack Sealing Machine (OCCSM). This machine is designed to provide a cost-effective means of improving the safety, productivity, and quality of transverse crack sealing operations through the use of a long-reach R- θ Telescopic Manipulator arm that is capable of encompassing a 3.6m square workspace. In addition, the manipulator is designed to attain maximum rapid travel speeds to 0.91 m/s. Crucial to the development of this machine is the invention of a novel Prismatic Ball Screw Actuator which provides accurate high speed telescopic extension throughout the workspace.

This thesis details the design of the R- θ Telescopic Manipulator from concept formulation through detailed prototype design, testing and conclusions and proceeds with recommendations aimed at directing future development.

TABLE OF CONTENTS

ABSTRACT	ii
TABLE OF CONTENTS	iii
LIST OF FIGURES	vii
LIST OF TABLES	ix
CHAPTER 1: INTRODUCTION	
1.1 Current Crack Sealing Methods	2
1.1.1 Crack Identification	3
1.1.2 Crack Preparation	3
1.1.3 Crack Sealing	3
1.2 The Automated Crack Sealing Machine (ACSM)	4
1.2.1 ACSM Drawbacks.....	5
1.3 The OCCSM Prototype	6
1.4 Problem Description and Objective	8
CHAPTER 2: MACHINE CONCEPT SELECTION	
2.1 Project Specifications	10
2.1.1 Crack Definition	10
2.1.2 Workspace Definition	11
2.1.3 Sealing Specifications	12
2.1.3.1 Manipulator Speed	13
2.1.3.2 Manipulator Loading.....	13
2.1.3.3 Positioning Accuracy	13
2.1.3.4 Control Specifications	13
2.1.4 Environmental Conditions.....	13
2.1.5 Life Expectancy.....	14
2.1.6 Vehicular Requirements	14
2.1.7 Safety Requirements.....	14
2.2 Conceptual Design	15
2.2.1 Preliminary Concepts	16
2.2.1.1 X-Y Table.....	16
2.2.1.2 Horizontal and Vertical Articulating Robots.....	17
2.2.1.3 Wheeled Carts	18
2.2.1.4 Telescopic R- θ Arm	19
2.2.2 Trade-Off Analysis.....	20
2.3 Summary	21
CHAPTER 3: TELESCOPIC R- θ ARM CONCEPTUAL DESIGN	
3.1 Telescopic Arm Structural Concept	23
3.1.1 Telescopic Arm Structural Specifications	24
3.1.2 Telescopic Arm Structural Design Concepts	24
3.1.2.1 Custom Aluminum Extrusions	24
3.1.2.2 Steel Rectangular Extrusions	24
3.1.2.3 Thin Wall Steel Composite	25
3.1.2.4 Fiber Composites.....	26

3.1.3	Trade-Off Analysis.....	26
3.1.4	Summary	26
3.2	Telescopic Actuation Concept Selection.....	28
3.2.1	Telescopic Actuation Specifications	28
3.2.2	Preliminary Concepts	29
3.2.2.1	Cable-Pulley Configurations	29
3.2.2.2	Parallel Screw Configurations.....	30
3.2.2.3	Telescopic Hydraulic Cylinders	31
3.2.2.4	Telescopic Screw Actuator.....	31
3.2.3	Trade-Off Analysis.....	35
3.3	Rotational Actuation	37
3.3.1	Rotational Specifications.....	37
3.3.2	Preliminary Concepts	37
3.3.2.1	Planetary Gearbox	37
3.3.2.2	Chain / Gear Drive	38
3.3.2.3	Hydraulic Cylinder	38
3.3.2.4	Harmonic Drive	39
3.3.3	Trade-Off Analysis.....	40
3.3.4	Summary	41
3.4	Vehicle Integration and Stowage System.....	43
3.4.1	Specifications	43
3.4.2	Preliminary Concepts	44
3.4.2.1	Compound Slides	44
3.4.2.2	Support Plate / Roller	44
3.4.2.3	Curved Rail	45
3.4.3	Trade-Off Analysis.....	46
3.4.4	Summary	46
3.5	Summary	46

CHAPTER 4: OCCSM DETAILED DESIGN

4.1	Telescopic Arm Structural Design	49
4.1.1	Specifications	50
4.1.2	Telescopic Sections	50
4.1.2.1	Base Cross Section	50
4.1.2.2	Intermediate Cross Section.....	53
4.1.2.3	Fly Cross Section	55
4.1.3	Vertical Support Systems	55
4.1.3.1	Primary Loading Rollers	56
4.1.3.1.1	Intermediate and Fly Sections	56
4.1.3.2	Secondary Loading Rollers	59
4.1.4	Horizontal Support Systems.....	59
4.1.5	Summary	60
4.2	Telescopic Actuator System.....	61
4.2.1	Specifications	61
4.2.2	Telescopic Ball Screw Actuator Design.....	62
4.2.2.1	Ball Screw Selection	62

4.2.2.2	Ball Screw Gun-Drilling	63
4.2.2.3	Drive Tube Design	63
4.2.2.4	Actuator Supports.....	64
4.2.2.5	Actuator / Section Integration	65
4.2.3	Concentric Output Planetary Gearbox Design	67
4.2.3.1	Kinematic Constraints	67
4.2.3.2	Detailed Design	69
4.2.3.2.1	Bevel Gear Selection	70
4.2.3.2.2	Planetary Gear Selection	70
4.2.3.2.3	Input Shaft	70
4.2.3.2.4	Outer Output Shaft	71
4.2.3.2.5	Inner Output Shaft	71
4.2.3.2.6	Bearing Selections	71
4.2.3.2.7	Gearbox Housing Design	72
4.2.3.2.8	Lubrication	73
4.2.3.3	Summary	73
4.3	Rotational Actuation	74
4.3.1	Specifications	75
4.3.2	Harmonic Drive Selection	75
4.3.2.1	Torque Requirements	76
4.3.2.2	Speed Requirements	77
4.3.2.3	Accuracy Requirements	77
4.3.3	Servo Motor.....	77
4.3.3.1	Torque Requirements	78
4.3.3.2	Speed Requirements	78
4.3.3.3	Accuracy Requirements	78
4.3.4	Summary	79
4.4	Vehicle Integration and Stowage System Design	79
4.4.1	Specifications	79
4.4.2	Base-End Pivot Plate.....	80
4.4.3	Curved Rail Support System	80
4.4.4	Stowage System	81
4.4.5	Summary	83
4.5	Summary	84

CHAPTER 5: OCCSM EXPERIMENTAL VERIFICATION

5.1	Telescopic Arm Structure.....	85
5.1.1	Qualitative Analysis	85
5.1.1.1	Arm Sections	85
5.1.1.2	Joint Connections	86
5.1.1.3	Qualitative Conclusions	86
5.1.2	Quantitative Analysis	87
5.1.2.1	Vertical Stiffness	87
5.1.2.2	Quantitative Conclusions	87
5.2	Telescopic Ball Screw Actuator.....	92
5.2.1	Qualitative Analysis	92

5.2.1.1 Qualitative Observations	92
5.2.1.2 Qualitative Conclustions	92
5.2.2 Quantitative Analysis	93
5.2.2.1 Positioning Accuracy	93
5.2.2.2 Actuator System Backlash.....	93
5.2.2.3 Quantitative Conclusions	94
5.3 Concentric Output Planetary Gearbox	96
5.3.1 Qualitative Analysis	96
5.3.1.1 Pre-Operation	96
5.3.1.2 Bevel Gear Noise.....	96
5.3.1.3 Qualitative Conclusions	96
5.3.2 Quantitative Analysis	97
5.3.2.1 Gearbox Backlash.....	97
5.3.2.2 Quantitative Conclusions	97
5.4 Vehicle Integration and Stowage System.....	97
5.4.1 Qualitative Analysis	97
5.4.1.1 Curved Rail Support	98
5.4.1.2 Stowage System	98
5.4.1.3 Rotational Pivot Plate.....	98
5.4.1.4 Qualitative Conclusions	98
5.4.2 Quantitative Analysis	99
5.4.2.1 Stowage Time.....	99
5.4.2.2 Quantitative Conclusions	99
5.5 Summary	99

CHAPTER 6: CONCLUSIONS AND RECOMMENDATIONS

6.1 Conclusions and Recommendations.....	100
6.1.1 Project Goals	100
6.1.2 Telescopic Sections Design / Performance	100
6.1.3 Actuator Systems Design / Performance.....	101
6.1.4 Vehicle Integration Design / Performance	102
6.1.5 Further Testing	102

REFERENCES	104
------------------	-----

APPENDIX A: CALCULATIONS

APPENDIX B: DETAILED DRAWINGS

LIST OF FIGURES

Figure 1.1	ACSM Longitudinal and Transverse Sealing Mechanisms	5
Figure 1.2	3-D Rendition of OCCSM Prototype Sealing a Transverse Crack	7
Figure 2.1	3-D Rendition of X-Y Table Concept.....	16
Figure 2.2	Adept 550 Horizontal and CRS Robotics A255 Vertical Articulating Robots	17
Figure 2.3	The AHMCT TMR Wheeled Mobile Robot.....	18
Figure 2.4	Commercially Available Telescopic Boom Lift	19
Figure 3.1	Thin-Wall Steel Composite Section.....	25
Figure 3.2	Cable-Pulley Actuation Method.....	29
Figure 3.3	Parallel Screw Configuration	30
Figure 3.4	Telescopic Hydraulic Cylinder	31
Figure 3.5	“Floating” Telescopic Screw Actuator	32
Figure 3.6	Bevel Gear Reduction	38
Figure 3.7	Hydraulic Cylinder Rotational Actuator	39
Figure 3.8	Cup-Type Harmonic Drive	39
Figure 3.9	Harmonic Drive Operation Sketch.....	40
Figure 3.10	Curved Rail Support / Storage System	45
Figure 4.1	OCCSM Prototype Telescopic Manipulator	49
Figure 4.2	Deflection Analysis Program.....	52
Figure 4.3	Base Cross Section.....	53
Figure 4.4	Intermediate and Fly Beam’s Cross Sections	54
Figure 4.5	Intermediate Section Outer Support System.....	57
Figure 4.6	Intermediate Section Rear Support System	57
Figure 4.7	Fly Section Outer Support System.....	58
Figure 4.8	Fly Section Rear Support System	59
Figure 4.9	Split Tube for Driving the Intermediate Ball Screw	63
Figure 4.10	Rear Intermediate Section Fixed Support (left) and Intermediate Ball Screw Rolling Support (right)	65
Figure 4.11a	Detailed View of Actuator Gearbox Connection.....	66
Figure 4.11b	Detailed View of Intermediate Ball Screw Joint	66
Figure 4.11c	Detailed View of Fly Ball Screw Connector.....	66
Figure 4.11d	Detailed View of Fly End Support	66
Figure 4.12	Apex40 Servo Motor and Concentric Dual Output Planetary Gearbox Assembly	67
Figure 4.13	Concentric Output Planetary Gearbox	68
Figure 4.14	Telescopic Gearbox After Five Hours of Operation.....	74
Figure 4.15	Rotational Actuator System	75
Figure 4.16	End Support System - Curved Rail	81
Figure 4.17	Roller Truck Directing Loading into Curved Plate.....	83
Figure 4.18	OCCSM Stowage System	84
Figure 5.1	Force vs. Deflection Plot for $r=4.57m$	89
Figure 5.2	Plot Depicting Nonlinear Stiffness of Arm.....	90
Figure 5.3	Plot of Force vs. Deflection Data for Various Beam Extensions	91

Figure 5.4 End Support Deflection Measurement During Vertical End Deflection Test	92
Figure 5.5 CET Measuring Apparatus for Validation of Positioning Accuracy	94
Figure 5.6 Plots of Measured Error vs. Extended Length(Top) and Retracted (Bottom) Beam Length	95
Figure 6.1 Improved Telescopic Beam Cross Section	101

LIST OF TABLES

Table 2.1	Machine Concept Trade-Off Analysis.....	22
Table 3.1	Telescopic Section Trade-Off Analysis.....	27
Table 3.2	Telescopic Actuation Trade-Off Analysis.....	36
Table 3.3	Rotational Actuation Trade-Off Analysis.....	42
Table 3.4	End Support / Stowage System Trade-Off Analysis	48
Table 5.1	Force vs. Deflection Data for $r=4.57$ m.....	88

CHAPTER 1: INTRODUCTION

Each year, local and federal government agencies spend millions of taxpayers' dollars maintaining our nation's immense highway infrastructure. The California state Department of Transportation (Caltrans) spends upwards of a \$100 million dollars annually preserving over 46,000 miles of California's highways against the ever-increasing threat of a soaring population (Velinsky, 1993). From 1983 to 1990, the U.S. Department of Transportation reported that the miles of vehicle travel had increased 41% (1990), a rate that is only expected to increase as we near the 21st century. The Advanced Highway Maintenance and Construction Technology (AHMCT) Center, of the University of California, Davis, has recognized this problem and has been redefining the future of highway maintenance with the aim of improving the productivity, quality and safety of highway maintenance procedures.

One specific highway maintenance task that is receiving major attention at the AHMCT Center is crack sealing. Cracks often form as a result of cyclic loading, faulty material compositions, subgrade failures, and environmental conditions including temperature and moisture fluctuations. After a crack is formed, harsh environments and heavy traffic perpetuate the crack axially along the road surface and downward toward the sublayer of the road. If left untreated, moisture will flow into the sublayer and further accelerate the degradation of the roadway. Therefore, crack sealing is crucial in preventing the high cost of complete rehabilitation of a crack-damaged highway. However, crack sealing does have its own cost, most of which is related to labor costs.

Crack sealing is a tedious task requiring Caltrans to spend about \$10 million dollars annually. Of this budget, 66% is used to maintain a crew of eight individuals which can typically seal from one to two lane-miles per day (Velinsky, 1993). This lack of productivity leads to extended lane closures, causing traffic congestion and increased exposure of highway workers to a very harsh environment. Since crack sealing can only be performed when the roadway is dry, sealing is often limited, regionally, to the late spring through summer months when the temperatures can soar to above 43°C (110° F) on the road surface. In addition, the workers are often forced to work only feet away from traffic flowing at speeds up to 100 kph (62 mph), subjecting their safety to an increasing number of inattentive drivers.

To alleviate these problems, the AHMCT Center has developed a number of machines aimed at automating the crack sealing procedures to increase productivity, quality and safety. The latest of these machines is the Operator Controlled Crack Sealing Machine (OCCSM), a machine that has its origins tied to the first AHMCT crack sealing machine, the Automated Crack Sealing Machine (ACSM), which will be briefly discussed. The interested reader is referred to Velinsky (1993) for more detailed information.

1.1 Current Methods of Crack Sealing

Although crack sealing operations vary greatly by state, crack sealing can be generalized into three operations: crack identification, preparation, and sealing. Crack identification consists of determining whether a crack is suitable for sealing. Crack preparation methods concern cleaning, and preparing the crack to accept the sealant. Finally, sealing concerns methods used in applying the sealant to the road. It should be

noted that the standards presented here are formulated by analyzing the current methods used by Caltrans.

1.1.1 Crack Identification

Crack width, depth, length and occurrence are all factors that determine whether a roadway should be sealed. Caltrans will usually seal cracks that range in width from 6-12 mm (0.23-0.47 in) for transverse cracks and up to 51 mm (2 in) for longitudinal cracks (Velinsky, 1993). Cracks that are larger than these dimensions can be indicative of a roadway that is beyond repair since crack depth usually increases proportionally to crack width. A crack that extends down to the sublayer is most likely to have already allowed erosion. This erosion may cause movement of the sublayer drastically reducing the life of any seal and causing further cracking. A roadway with this state of degradation is likely to be marked for complete renovation.

1.1.2 Crack Preparation

Crack preparation can include any of the following procedures: routing, cleaning, drying, and heating. For transverse cracks, Caltrans will usually clean cracks with compressed air or a stiff brush. Occasionally, some states will rout smaller cracks to increase the penetration of the sealant into the surface and achieve a stronger seal. However, this can be a time consuming process. Drying can be achieved by compressed air, the use of a heat gun or other means. The advantage of a heat gun or other heat source for drying is that it will also heat the interior surfaces of the crack creating improved sealant adhesion.

1.1.3 Crack Sealing

Crack sealing is currently a very low-tech operation in which sealant is applied to the roadway by a simple fill operation. Operators manually move a sealant wand over the crack that they are sealing. Sealant is forced out of the wand by a small amount of pressure exerted by an upstream sealant melter. This system relies on gravity and low sealant viscosity to obtain a solid fill in the crack.

1.2 The Automated Crack Sealing Machine (ACSM)

The ACSM was developed by AHMCT, through the Strategic Highway Research Program's H107A project at the University of California, Davis. The ACSM, Figure 1.1, is a fully automated crack sealing machine outfitted with subsystems for sealing longitudinal and transverse cracks in the roadway. The two subsystems are operated by the same support systems requiring only a single sealant melter and power supply. The machine uses separate sensing systems to locate the cracks on the roadway. This information is then processed to provide path planning for each subsystem.

A longitudinal apparatus is located on the side of the truck and incorporates a local sensing system, router, vacuum, heat source and a crack sealing head. Each of these subsystems is placed in line, such that a single hydraulic cylinder can accurately follow the crack measured by the local sensing system (Velinsky, 1993).

A side mounted GMF-A510 SCARA manipulator located at the rear of the vehicle seals transverse cracks. Path planning for this manipulator is acquired through a vision sensing system mounted on the front of the vehicle. As the vehicle travels along the roadway, a vision sensing system generates a full image of the roadway from which cracks are identified. This information is then transformed into real world coordinates

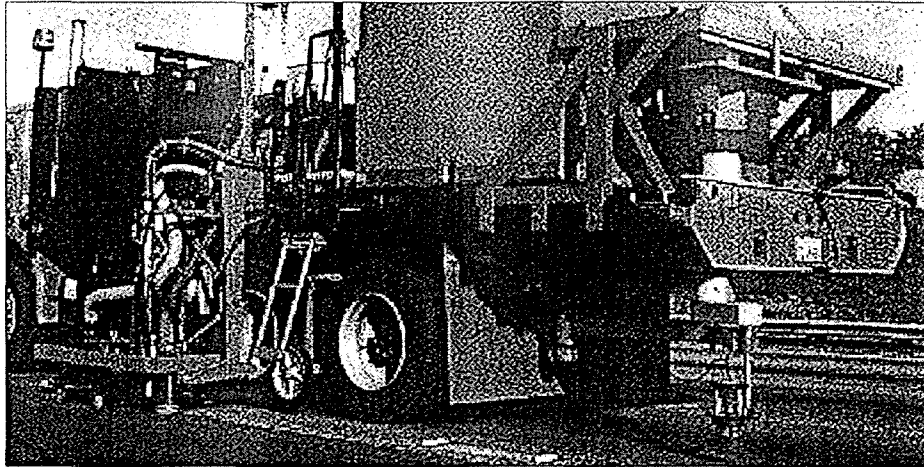


Figure 1.1: ACSM Longitudinal and Transverse Sealing Mechanisms

through a vehicle orientation and control system. Once the path is planned and translated into relative coordinates, the SCARA robot manipulates the sealant head throughout the workspace (Velinsky, 1993).

1.2.1 ACSM Drawbacks

The most prevalent drawback of the ACSM is its complexity and associated high cost of manufacturing and operation. Through a preliminary market report contracted to the Technology Development Center (1993) it was determined that the ACSM was too cost prohibitive to sell as a complete machine. Recommendations by members of focus groups were in favor of the development of advanced crack sealing technology. However, they believed that a machine with less automation would gain wider acceptance at a lower cost. For example, one member from the Nevada State Department of Transportation stated that worker comfort and acceptance was crucial. In addition, many members felt that safety of the crack sealing operation would be greatly increased through this type of automation.

This marketing report and the desire to meet the needs of the users has led to the concept of an Operator Controlled Crack Sealing Machine (OCCSM). Specifically, this

machine targets the sealing of transverse cracks in the roadway with reduced automation and thus reduced machine cost.

1.3 The OCCSM Prototype

The Operator Controlled Crack Sealing Machine (OCCSM) project was undertaken with the goal of producing a machine that would better meet the needs of the end-user. To this extent, the OCCSM uses concepts developed by the ACSM project, but reduces the automation, while maintaining the increased productivity, quality and safety.

The OCCSM prototype is designed to be a general crack sealing machine capable of sealing random transverse and small longitudinal cracks. The prototype uses a telescoping manipulator arm, located under the rear of the vehicle, to manipulate a pressurized sealant head over the roadway. The robotic arm is controlled from the cab of the vehicle by using a virtual interface. A computer shows a real captured image depicting the full workspace on the screen, from which the operator locates any cracks suitable for sealing. Using a digitizing device, such as a mouse or touch screen, the operator follows the crack to be sealed. The computer interprets this motion on the screen, and relays commands to the main control program. The control program then actuates the telescopic arm to mimic the operator's motion.

The telescopic manipulator arm operates as an R- θ manipulator to encompass a 3.6 m (12 ft) square workspace and is arguably the most crucial component of the OCCSM. The manipulator arm is mechanically capable of attaining positioning accuracy within 1.5 mm (1/16 in) throughout the workspace with a maximum end-effector velocity of 0.91 m/s (3 ft/s). Actuation of the manipulator arm is achieved through two subsystems, the rotational actuator and the telescopic actuator. The rotational actuator

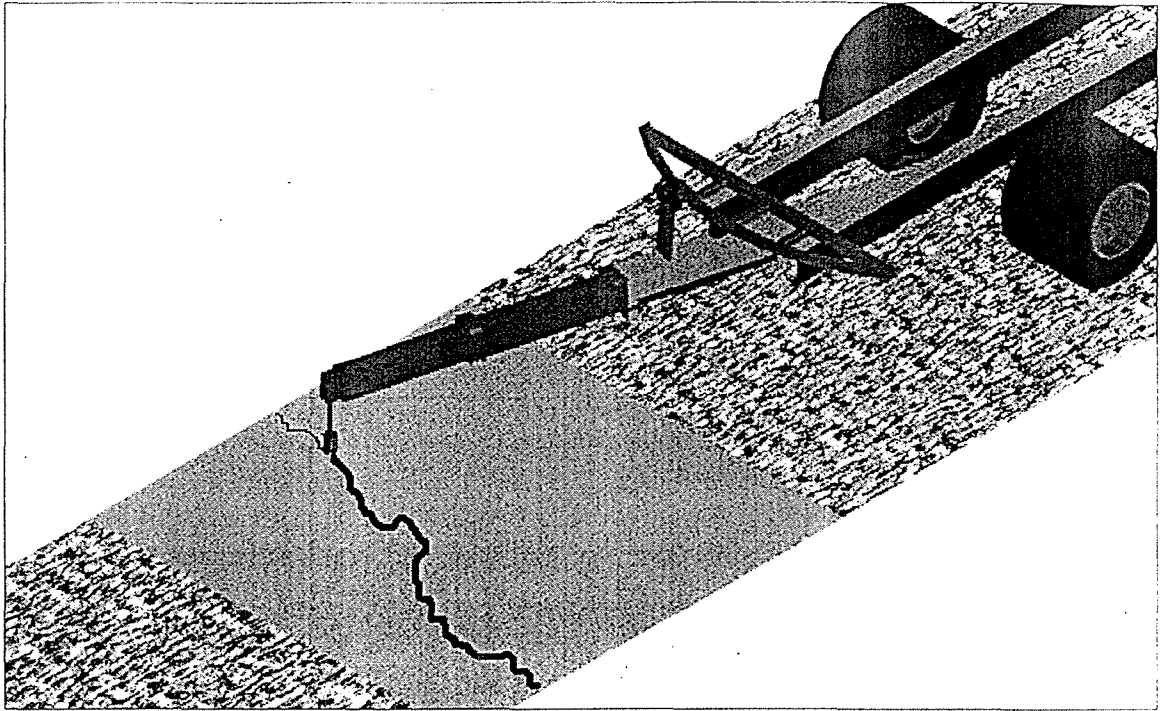


Figure 1.2: 3-D Rendition of OCCSM Prototype Sealing a Transverse Crack

incorporates a servo motor and harmonic drive gear reducer to obtain a peak torque of over 1782 Nm (1320 ft-lb). This torque is capable of accelerating the arm, at maximum extension, to a speed of 0.91 m/s (3ft/sec) in less than 0.5 seconds. The telescopic actuation system uses a novel prismatic ball screw actuator to provide high positioning accuracy and high-speed actuation over the entire workspace. A servo motor and custom planetary gearbox drive the ball screw actuator to attain positioning accuracy within 1.5 mm (1/16 in) with accelerations to 0.91 m/s (3 ft/s) in less than 0.5 seconds.

Structurally, the OCCSM telescopic manipulator arm is comprised of three prismatic sections that collapse to a length of 2.67 m (105 in) and extend to a total length of 6.7 m (264 in). The three prismatic sections are sized such that the base arm is the heaviest and largest, while the fly arm is the smallest and lightest. In addition, each section is optimized to have a high stiffness to weight ratio. This is accomplished by using custom-made thin wall sections made from mild steel. These thin wall sections

also allow for the passage of the sealant hose as well as the telescopic actuation system within the telescopic arm.

The integrated manipulator arm is then mounted onto the vehicle by using a rotating joint at the end of the base section. The rotational actuator is connected at this point to provide torque actuation of the arm. At the other end of the base section, a rotating support system further supports the arm and provides a mechanism to lift the arm into a storage position.

1.4 Problem Description and Objective

In an effort to increase the safety and productivity of highway maintenance tasks, the AHMCT research center is developing means to automate many labor-intensive tasks such as crack sealing. The ACSM was developed with the aim of fully automating the crack sealing procedures. This machine became a groundbreaking step in proving the feasibility of and need for such machines. However, in spite of the success of this first project, a marketing analysis report had shown that the machine was too costly to be pursued. This has led to the development of the OCCSM prototype. The OCCSM reduces the automation associated with the crack identification process by allowing the operator to identify and command which cracks should be sealed. This allows the OCCSM to be a more cost-effective solution while maintaining the improved productivity, quality and safety of crack sealing maintenance.

This thesis will present the complete mechanical design of the OCCSM robotic manipulator arm from concept formation to a first generation prototype. The project specifications and machine concept selection are discussed in Chapter 2, from which Chapter 3 proceeds with the discussion of the detailed conceptual design of the machine

components. A detailed design of these components is presented in Chapter 4 with validation, through testing and qualitative analyses, following in Chapter 5. This thesis concludes with a discussion of conclusions and recommendations, aimed at directing the future OCCSM development, in Chapter 6.

CHAPTER 2: MACHINE CONCEPT SELECTION

The machine concept selection for the OCCSM was the most important phase in the design process. In this phase, goals and limitations regarding the machine's performance were chosen carefully in order to obtain a cost-effective and productive crack sealing machine. The first step was to determine the project specifications, such as workspace size, target crack size, life expectancy, vehicle requirements, crack sealing speeds, etc. These specifications were then used as guidelines to form and evaluate design concepts through brainstorming sessions and a trade-off analysis, respectively. Throughout this trade-off analysis, concepts were pitted against one another to ensure that the final machine concept selection would most closely fit the project specifications. This chapter presents the OCCSM concept selection process and concludes with a detailed explanation of the OCCSM machine concept.

2.1 Project Specifications

Project specifications for the OCCSM were developed by considering factors from crack sealing procedures, control specifications and common sense. The specifications were then studied and weighted according to their importance in the overall design process with the goal of producing a productive and cost-effective machine.

2.1.1 Crack Definition

Crack sealing procedures were used in determining the sizes and configurations of target cracks. Through research into current Caltrans methods, the target crack widths for general crack sealing were determined to be between 6 mm (0.23 in) to 12 mm (0.47 in) for transverse cracks and up to 51 mm (2 in) for longitudinal cracks. However, large

longitudinal cracks presented a problem for current automated crack sealing machines. The problem was that current sealant melters were designed to operate with a manually sealing crew that was not capable of sealing at the high rates of automated sealing machines. Therefore, when an automated machine was used with these large cracks, the melter was not powerful enough to maintain a constant flow of melted sealant. To alleviate this problem, either the OCCSM machine would need to be outfitted with a larger, more expensive sealant melter, or the machine would need to be limited to smaller cracks. Through a careful cost-benefit evaluation, it was determined that the larger melter had extra costs associated with the need for a larger vehicle and higher power consumption, all of which raised the cost-benefit ratio. Therefore, it was determined that a target crack width of 6 mm (0.23 in) to 12 mm (0.47 in) would provide the most cost-effective solution, while maintaining productivity.

2.1.2 Workspace Definition

The OCCSM workspace definition became a critical part of the conceptual design. From an early stage, it was determined that an operator-controlled machine would be very difficult to operate unless the vehicle was stationary. This necessitated a large workspace to minimize lost time required to move the vehicle ahead to the next workspace. To further increase productivity, the OCCSM workspace was required to extend through the entire lane width (3.6 m/12 ft) to eliminate the need for a second pass sealing operation. Through careful analysis it was determined that a workspace 3.6 m (12 ft) wide by 3.6 m (12 ft) long would be necessary for a productive machine.

2.1.3 Sealing Specifications

Sealing specifications were prescribed by previous experience in automated sealing as well as the operations of Caltrans. These specifications included sealing speed, manipulator load requirements, positioning accuracy and control specifications.

2.1.3.1 Manipulator Speed

Speed of the OCCSM manipulator was determined by considering situations that the operator might encounter, such as cracks at opposite ends of the workspace, as well as mechanical limitations. To improve the productivity of the machine, it was determined that the machine should operate at the highest speed possible. However, higher speeds required higher power consumption, and bulkier mechanical designs to accommodate the higher inertial loading. In addition to structural design, there was concern that the higher sealant rates would require larger, more costly sealant melters. Based on careful consideration of the preceding factors, the rapid travel speed for the OCCSM was set to 0.91 m/s (3 ft/s), with an acceleration time of 0.5 seconds, recognizing that the end-effector speed during crack sealing would lie well below this goal.

2.1.3.2 Manipulator Loading

Speed requirements were then used with sealant head data to determine the loading that the OCCSM end-effector would endure. A vertical loading requirement of 445 N (100 lb) was determined from the weight of the sealant head. In addition, the manipulator was required to handle side loading due to inertial effects and friction between the sealant head and the workspace. Specifically, the manipulator was required to handle accelerations of the sealant head to 0.91 m/s (36 in/s) in 0.5 seconds and estimated frictional forces of 89 N (20 lb) at the bottom of the sealant head. As with

sealing speed, the ability to handle these loads varied greatly for each preliminary conceptual design.

2.1.3.3 Positioning Accuracy

Accuracy requirements for the OCCSM were influenced largely by target crack specifications. It was determined that the machine should be capable of placing the end-effector within the dimensions of the smallest target crack, 6 mm (0.23 in). Therefore, the target accuracy for the OCCSM was set to 3 mm (0.12 in), one-half of the smallest target crack width.

2.1.3.4 Control Specifications

Lastly, control specifications for the OCCSM were determined based on the above specifications and others. The goal of the OCCSM was to have simplified control, and as such, it was determined that the mechanical design of the OCCSM should aid in this quest. Specifically, control specifications required the mechanical design to minimize vibrations, provide maximum accuracy and minimize the complexity of the required control.

2.1.4 Environmental Conditions

Environmental conditions were determined to contribute significantly to the design of the OCCSM due to harsh operating environments. It was determined that road maintenance machinery must be designed to be robust to many environmental factors such as corrosion, caused by salt and moisture exposures. In addition, the design must be able to operate in a wide temperature range depending on geographical area. In California alone, conditions vary drastically from desert conditions in Death Valley to

the frigid Sierra Nevada. Therefore, OCCSM conceptual designs were required to be robust in any of these environmental conditions.

2.1.5 Life Expectancy

The life expectancy of any machine has a direct relation to its operating environment and as such is difficult to ascertain. For this reason, life expectancies for the OCCSM were not quantified, rather each conceptual design was compared against the robustness of current highway maintenance machinery. On a detailed mechanical design basis, component specifications were set such that the fatigue life of all components should exceed two years, operating for six hours per day and 365 days per year.

2.1.6 Vehicular Requirements

Vehicle requirements for the OCCSM project concerned the power, weight, size and specialized needs of each machine concept. Each mechanical concept was analyzed to determine the exact impact on the OCCSM vehicle in terms of vehicle size, cost, and power requirements.

2.1.7 Safety Requirements

Safety was also a major concern in the design of the OCCSM. Although the OCCSM was to be operator controlled, a computer was responsible for the physical actuation of the individual components, possibly leading to unsafe situations during power failures, software problems, etc. Therefore, safety specifications were made requiring that the OCCSM be designed with foresight into all possible scenarios. In addition, the OCCSM was required to be incapable of operating at unsafe speeds, or with unsafe forces. Parallel to the safety of the actuation systems, the structural composition was also required to be safe. Due to uncertainties in material composition, exact

operating environment and other factors, all components that made up the mechanical design of the OCCSM were required to be designed with a factor of safety of at least two. Following these guidelines and developing foresight and consideration into possible unsafe operating scenarios all but guaranteed the development of a safe and productive machine.

2.2 Conceptual Design

The conceptual design phase began with a series of brainstorming sessions in which critical evaluation of the previously discussed project specifications allowed several machine design concepts to be generated. Each concept was then critically examined based on a series of weighted design specifications. The results were then tabulated in trade-off tables, from which the designs could be compared. The results of these comparisons would ideally reveal the best conceptual design.

The development of the OCCSM began with the most general concept selection concerning the type of manipulator that would be used. Through research and brainstorming, several concepts were formulated. These concepts included an X-Y table, horizontal and vertical articulating arms, wheeled carts and an R- θ telescoping arm. Criteria were then developed considering the previous project specifications and other considerations specific to each concept. These criteria were then used in a trade-off analysis, Table 2.1, from which the most optimum design configuration could be selected. Once the optimum machine configuration was selected, subsequent designs concerning actuation and hardware design were each optimized using the same method until the entire OCCSM conceptual development was complete.

2.2.1 Preliminary Concepts

The initial brainstorming and project specifications yielded a number of competing machine concepts including an X-Y table, horizontal and vertical articulating arms, a wheeled cart, and an R- θ telescoping arm.

2.2.1.1 X-Y Table

The X-Y table concept, Figure 2.1, consists of a frame that holds two compound linear slides. In the figure shown, the Y-axis is the main slide upon which X-axis motion is obtained. The actuation requires two actuators operating simultaneously to yield compounded linear motion in any direction. The principle advantage of this design is the simplicity of the mechanical structure requiring a simple frame and commercially available actuators. The principle disadvantage is that the frame must extend beyond the active workspace. In crack sealing this would place the frame into the adjacent lanes requiring multiple lane closures.

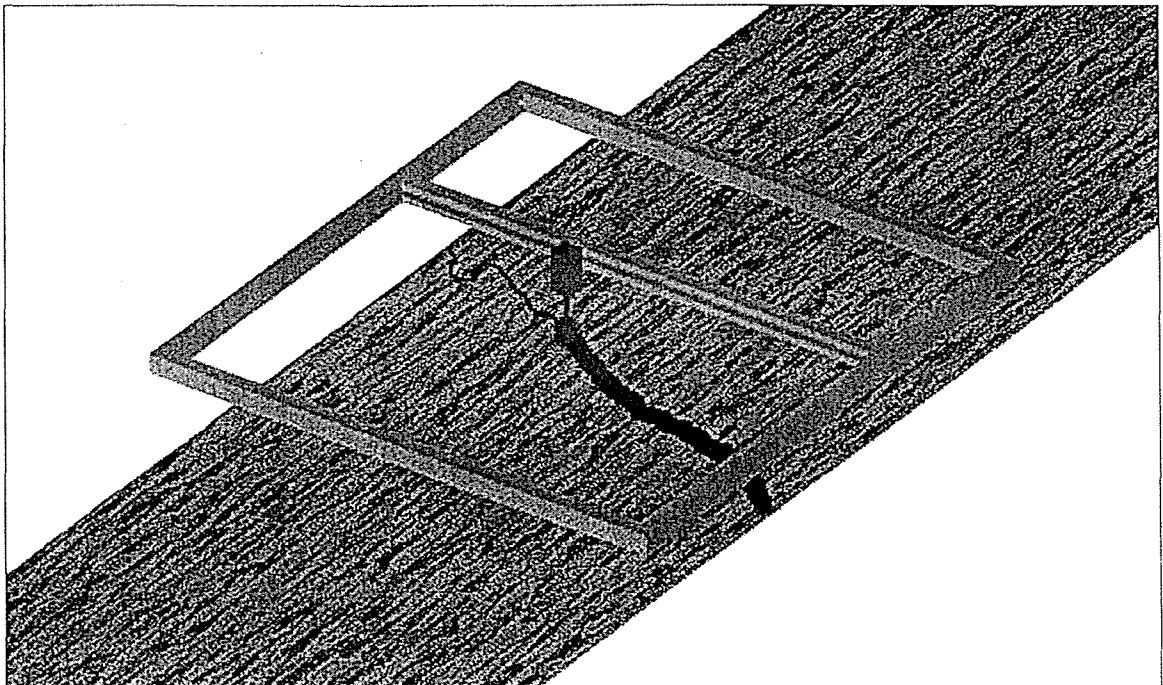


Figure 2.1: 3-D Rendition of X-Y Table Concept

2.2.1.2 Horizontal and Vertical Articulating Manipulators

Horizontal and vertical articulating manipulators are common to many robotic applications and are becoming increasingly available on the commercial market. Figure 2.2 depicts examples of two commercially available articulating robots. Horizontal articulating robots, similar to the GMF-A510 SCARA manipulator used on the ACSM, can require as little as two actuators, depending on the number of linkages, and accurate positioning can be accomplished by solving the linkage kinematics of the articulating system.

Vertical articulating arms operate similarly to horizontal robotic manipulators with the exception that the arms are oriented vertically as in Figure 2.2. This type of robot requires four-axis control and has built in accuracy control by solving the linkage kinematics.

Both of these designs have vast applications in industry, but are rather limited for the current application due to their complexity and limited workspace.

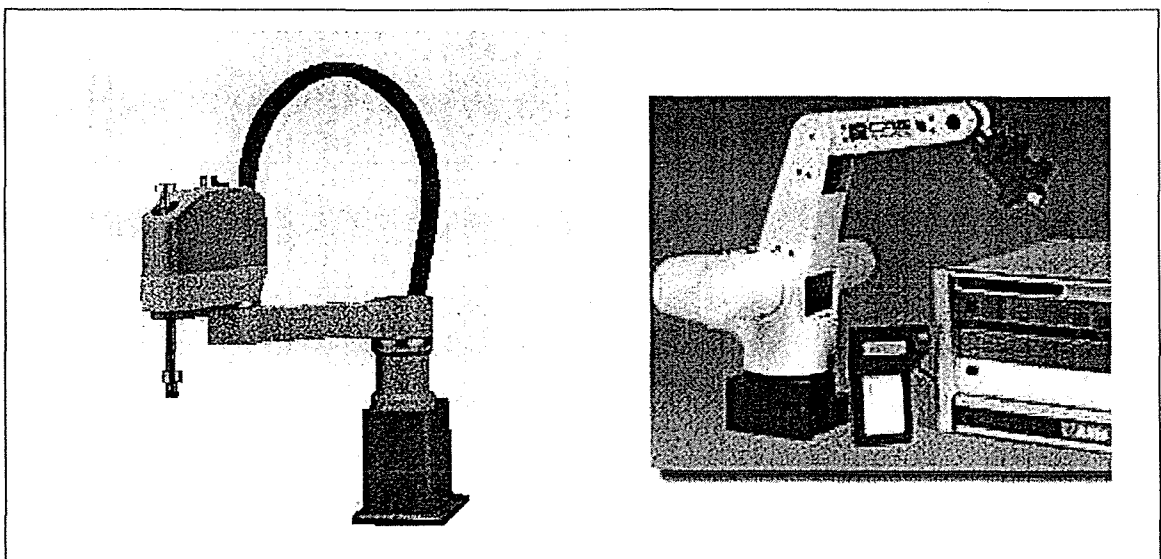


Figure 2.2: Adept 550 Horizontal and CRS Robotics A255 Vertical Articulating Robots

2.2.1.3 Wheeled Cart

Another form of manipulator that has applications in highway maintenance is the wheeled cart. This technology consists of a cart type vehicle that is able to manipulate the sealant head over the workspace and seal the cracks. The advantage of a wheeled cart robot is its ability to handle high tooling loads. For instance, the AHMCT Center has developed a Tethered Mobile Routing Robot (TMRR), Figure 2.3, which is designed to track, rout and seal cracks in the pavement. The cart design is necessary to handle the intense loading required by routing operations. There are two disadvantages of this type of concept. The first is that the wheels are required to track over the workspace including freshly applied sealant. This can limit the amount of cracks that can be sealed in a specific area or necessitate a drying agent to help cure the sealant surface. The second disadvantage is caused by tire slip and requires external measuring devices that relate the cart's position to the vehicle and workspace.

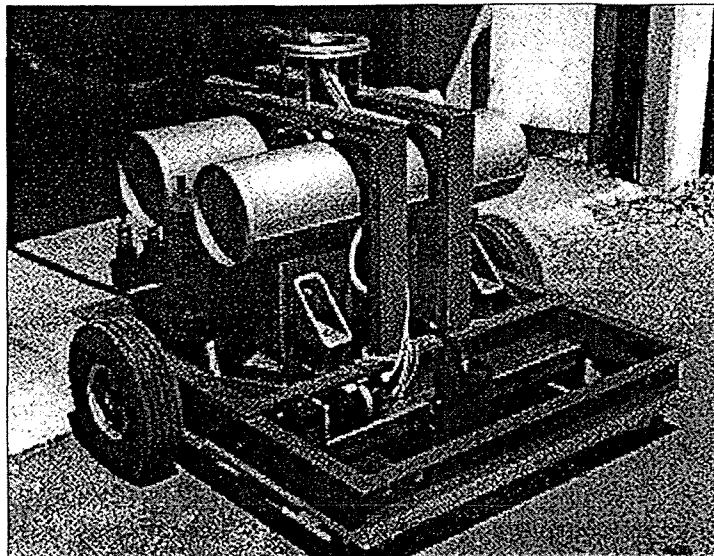


Figure 2.3: The AHMCT TMRR Wheeled Mobile Robot

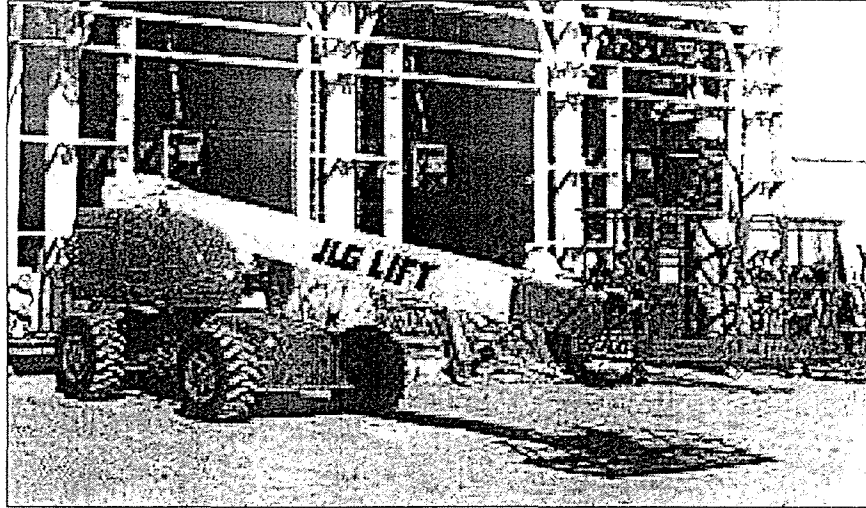


Figure 2.4: Commercially Available Telescopic Boom Lift

2.2.1.4 Telescopic R- θ Arm

The last proposed concept was an R- θ telescopic manipulator arm. This design is commonly referred to as a cylindrical type robot and uses telescopic and rotational motion to manipulate throughout the workspace. This design is similar to common telescopic boom lifts, Figure 2.4, with the imposed limitation of planar motion, parallel to the workspace. The telescopic structure is accomplished through a series of prismatic sections that are rotated from the largest, base section. The sealant head would then attach to the smallest, outermost section and extend downward to seal the workspace. Rotational and telescopic actuators control the arm movement and provide complete end-effector position measurements. The advantages of this design include the simplicity of the two-axis kinematics, compact storage size, and the vast workspace coverage. The main disadvantage is the lack of commercially available components, such as sections, actuators, etc. Although there are numerous material handling machines similar to Figure 2.4, these machines are designed for carrying much larger loads and do not incorporate accurate positioning systems.

2.2.2 Trade-Off Analysis

The next step was to determine the optimum design based on the project specifications as well as the other desired specifications. These specifications were then given weightings from one to ten based on how crucial they were in developing a productive and economical machine. Next, each of the competing conceptual designs was given a rating for each criterion in the trade-off analysis table, Table 2.1. Each rating was then converted into a numerical score from one to five, where one is the worst, five is the best. These numerical ratings were then multiplied by the weight of each criterion to determine each concepts score in that criterion. The subtotals were then summed to find the overall score for each concept. The trade-off analysis yielded two competing designs that were close enough to require extra consideration. These two designs were the X-Y table and the R- θ telescoping manipulator arm.

The X-Y table and the R- θ telescopic manipulator arm differed in only two of the comparative categories, machine boundary dimensions and mechanical complexity. Although, the mechanical complexity of the telescopic arm was high compared to that of the X-Y table, the fact that the X-Y table extended beyond lane width precluded it from being selected. It was perceived that the only solution to this problem would be to have multiple lane closures or to reduce the workspace and have the machine perform multiple passes, all of which would sacrifice the machine's productivity.

2.3 Summary

At this stage in the design process, project specifications had been developed based on the goal of producing a cost-effective and productive crack sealing machine. These specifications were then used in brainstorming sessions to develop preliminary

machine concepts. To quantify the value of each of the preliminary concepts, a trade-off analysis table was formed which numerically rated how well each concept met the specifications. As a result, the R- θ telescopic manipulator arm concept was chosen as the most ideal concept for a productive and cost-effective machine. The next step in the design process was to determine the conceptual design of the subsystems that would form the R- θ telescopic manipulator arm.

	Weighting (1-10)	X-Y Table			Vertical Articulating Arm			Horizontal Articulating Arm			Wheeled Cart			Telescopic R-Theta Arm		
		Rating	Score	Total	Rating	Score	Total	Rating	Score	Total	Rating	Score	Total	Rating	Score	Total
Controllability																
# of Actuators required(min)	5	2	5	25	2 to 3	4	20	3	1	5	2	5	25	2	5	25
kinematic complexity	7	low	5	35	high	1	7	high	1	7	high	1	7	low	5	35
Accuracy																
External measurement req'd.	7	no	5	35	no	5	35	no	5	35	yes	1	7	no	5	35
Workspace																
12'x14' attainable workspace	10	yes	5	50	yes	5	50	yes	5	50	yes	5	50	yes	5	50
Machine Boundary Dimensions																
Vertical height	4	low	5	20	high	1	4	low	5	20	low	5	20	low	5	20
Within lane width	10	no	1	10	yes	5	50	no	1	10	no	1	10	yes	5	50
Sealing																
Able to transverse over sealant	10	yes	5	50	yes	5	50	yes	5	50	no	1	10	yes	5	50
Machine Setup																
Truck stabilization required?	8	no	5	40	yes	1	8	no	5	40	no	5	40	no	5	40
Move ahead time	8	low	5	40	med	3	24	low	5	40	high	1	8	low	5	40
Cost																
commercially available	4	no	1	4	no	1	4	no	1	4	no	1	4	no	1	4
control complexity	8	low	5	40	high	1	8	high	1	8	med	3	24	low	5	40
mechanical complexity	8	low	5	40	high	1	8	high	1	8	med	3	24	high	1	8
Score				389			268			277			229			397

Table 2.1: Machine Concept Trade-Off Analysis

CHAPTER 3: TELESCOPIC R- θ ARM CONCEPTUAL DESIGN

The design process to this point had included the conceptual design of and optimum machine configuration using a telescopic R- θ manipulator. The next step in the design process was to determine the configurations of each of the subsystems.

Specifically, the OCCSM telescopic arm was broken down into three basic subsystems: telescopic arm structural design, telescopic and rotational actuation, and vehicle integration and stowage. Within each of these subsystems, concepts were formulated and evaluated through the use of trade-off tables to determine their ability to meet the machine specifications.

3.1 Telescopic Arm Structural Concept

The conceptual design selection for the R- θ telescopic arm included section geometry, joint connections and material considerations. Research into techniques used in telescopic crane booms and material handlers was performed to gain insight into the current state of the art. This research yielded valuable information regarding commercially available beam sections and joint connections. However, it was easy to recognize that these designs were developed according to a different set of standards based on high lifting capacities. To the contrary, the OCCSM machine would require minimal tooling loads and high positioning accuracy common to robotic machines, thus eliminating the usefulness of commercially available techniques. To accommodate this, several concepts were developed ranging from custom aluminum extrusions to thin wall steel composite beam sections. These designs were then evaluated against a set of specifications in a trade-off analysis to determine the optimum structural design concept.

3.1.1 Telescopic Arm Structural Specifications

Several factors were considered in determining the optimal structural design of the telescopic arm. These factors included design considerations such as stiffness to weight ratios, overall weight, size and strength. In addition, factors concerning cost, robustness, versatility and simplicity were considered. Specifications were developed through consideration of the performance requirements set forth in the project specifications as well as consideration into the preceding factors. This analysis yielded several major design criteria that were then used to evaluate each of the competing conceptual designs.

3.1.2 Telescopic Arm Structural Design Concepts

3.1.2.1 Custom Aluminum Extrusions

Aluminum alloys are widely used in robotic applications due to their high strength to weight ratios and manufacturing versatility. However, the usefulness of these aluminum alloys for the OCCSM project was limited due to the lack of commercially available sections. The principle drawback is the high cost of large, custom, closed form extrusions which become cost-prohibitive in prototype design. Alternative methods using aluminum alloys have been considered for future prototypes. These methods include a particular design that combines two half-extrusions by adhesive or fasteners to form a custom closed section. This has a lower initial cost due to the open extrusions and offers the benefit of geometric versatility.

3.1.2.2 Steel Rectangular Extrusions

Steel rectangular extrusions were investigated because of their low cost and commercial availability. In addition, steel extrusions offer increased robustness and

stiffness over aluminum alloys. The principle disadvantages of these extrusions include the lack of close fit sizes and thin wall sections. These disadvantages cause the arm sections to be larger than required, adding excessive weight to the machine which causes increases in the total beam deflection, rotational inertia, and machine power.

3.1.2.3 Thin Wall Steel Composite

Thin wall steel composite sections were developed to address the drawbacks of the previous steel rectangular sections. From research into the steel rectangular sections, it was found that the excessive wall thickness was the principle cause of all of the major drawbacks. To remedy this, it was proposed to design a steel section out of a formed light gauge material. The idea was to form a dimensionally large section to gain high stiffness, but with thin walls to maintain low weight. The proposed design would need to maintain a thicker bottom surface to which all of the high contact loading from the section joints could be directed. Figure 3.1 shows the geometric shape of the conceptual section. While increasing the stiffness to weight ratio, the formed section also offered the advantage of low cost. Associated drawbacks of the section included questionable

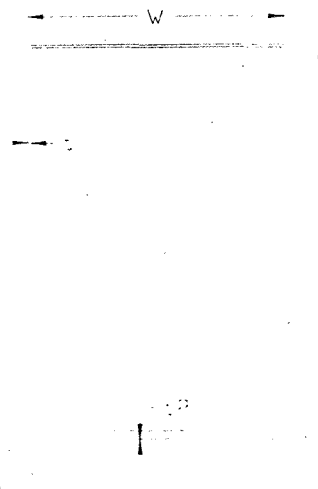


Figure 3.1: Thin wall Steel Composite Section

robustness, low dimensional accuracy, and the possibility of localized buckling in the thin sidewalls. However, these drawbacks would prove to be manageable when dealing with a prototype machine.

3.1.2.4 Fiber Composites

Fiber composites were also considered for the OCCSM telescopic arm. These composites offered many advantages including the highest stiffness to weight ratios, low section weight and manufacturing versatility. However, fiber composites have similar drawbacks to aluminum alloys in that they are very costly and hard to procure. These drawbacks precluded the use of fiber composites in the OCCSM prototype design, where rapid prototyping is crucial.

3.1.3 Trade-Off Analysis

To help quantify the selection of the best telescopic section design, a trade-off table, Table 3.1, was formed. Each of the competing conceptual designs was rated against a set of weighted specifications. Each concept's individual score for each criterion was then summed to form a total "value" of the design. The criteria used were simplicity, manufacturing versatility, stiffness to weight ratio, robustness, size, overall weight, commercial availability and cost.

3.1.4 Summary

The results of the trade-off analysis clearly showed that the thin wall steel composite section was the most appropriate design for the proof-of-concept machine. Although the mechanical complexity is higher for these sections due to the limitation on the geometric shapes, the low cost, high stiffness to weight ratio, and high commercial availability outweigh this disadvantage.

	Weighting (1-10)	Aluminum Alloy Extrusions			Steel Rectangular Tubing			Thin-Wall Steel Composite			Fiber Composite		
		Rating	Score	Total	Rating	Score	Total	Rating	Score	Total	Rating	Score	Total
Simplicity	7	high	5	35	med	3	21	med-high	4	28	high	5	35
Manufacturing Versatility	6	high	5	30	low	1	6	med-high	4	24	high	5	30
Stiffness/Weight Ratio	10	low-med	2	20	med	3	30	high	5	50	high	5	50
Robustness	5	low	1	5	high	5	25	med	3	15	low-med	2	10
Size	4	high	1	4	low-med	4	16	low	5	20	low	5	20
Overall Weight	10	low	5	50	high	1	10	low	5	50	low	5	50
Commercial Availability	9	low	1	9	high	5	45	med-high	4	36	low	1	9
Cost	10	high	1	10	low	5	50	low	5	50	low	1	10
Score				163			203			273			214

Table 3.1: Telescopic Section Trade-Off Analysis

3.2 Telescopic Actuation Concept Selection

Determining the actuation system for the telescopic sections began with brainstorming and research into current methods used in telescoping boom cranes, material handlers, and personnel lifts. Through this research, several actuation concepts were formulated including cable-pulley configurations, parallel screw configurations, and telescoping hydraulic cylinders. However, each of these methods of actuation had associated drawbacks that encouraged development of a novel telescopic ball screw design. All of these designs were then compared against the desired project specifications in a trade-off analysis table to determine the most appropriate design.

3.2.1 Telescopic Actuation Specifications

Project specifications were examined and refined to develop a series of telescopic actuation specifications (see Table 3.2). The specifications were then used in a trade-off analysis table to evaluate the conceptual designs. The most crucial specifications concerned concept accuracy, velocity constraints, and space requirements. Specifically, each design was required to have positioning accuracy within 3 mm (0.125 in), taking system backlash into consideration. In addition, each actuator had to provide for constant velocity actuation of the sealant head throughout the workspace, and be capable of attaining the target speed of 0.91 m/s (36 in/s). Finally, space requirements were imposed to ensure that sealing hoses and control lines for the sealant head could be routed within the telescopic sections. Other less crucial constraints concerned efficiency, robustness, weight, mechanical complexity, cost, and control complexity.

3.2.2 Preliminary Concepts

3.2.2.1 Cable-Pulley Configurations

Cable-pulley configurations provide for a simple cost-effective means of actuating nested telescopic sections. The simplest design is shown for a single telescopic section in Figure 3.2. One end of a continuous drive cable is connected to the inner end of the section to be actuated. The cable is then routed outward along the inside of the outer section around a pulley located at the outer end of the outer section. The cable is then routed along the outside of the outer section and wrapped around a cable drum several times. Next, the cable is routed around a pulley and into the base end of the outer section. Finally, the cable is connected to the base end of the inner section. A motor initiates extension and retraction by rotating the cable drum clockwise and counterclockwise, respectively. Additional telescopic sections can be actuated using the single cable drum and a more complex cable routing.

The principle advantages of this design are its simplicity, lightweight construction and corresponding low cost. The principle disadvantage is low accuracy associated with cable compliance and winding on the drum.

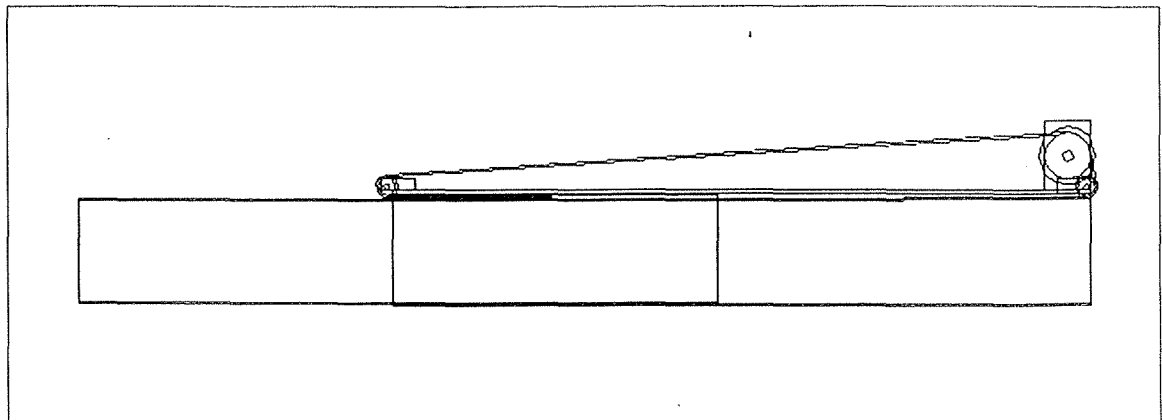


Figure 3.2: Cable-Pulley Actuation Method

3.2.2.2 Parallel Screw Configurations

Parallel screw configurations are another common method used in telescopic applications. Figure 3.3 is a patent sketch of a parallel configuration. This design incorporates a series of ball/lead screws aligned parallel within the telescopic sections. The screws are connected such that rotation of the first screw causes rotation of the remaining screws at the same rate. To actuate the sections, each screw's nut is connected to the corresponding section, i.e. the first screw's nut to the first telescopic section. In addition the subsequent screws are connected to the previous sections such that they extend along with the sections. For example, in Figure 3.3, the first screw is rotated causing the second screw to rotate simultaneously. The first screw's nut is attached to the first telescopic section causing it to extend. The second screw is also attached to this section causing it to extend simultaneously. The second telescopic section is then extended by the second screw's nut, fixed to the second section.

This design offers advantages over cable-pulley methods in increased accuracy and robustness. However, this design includes disadvantages in large space requirements and high system backlash.

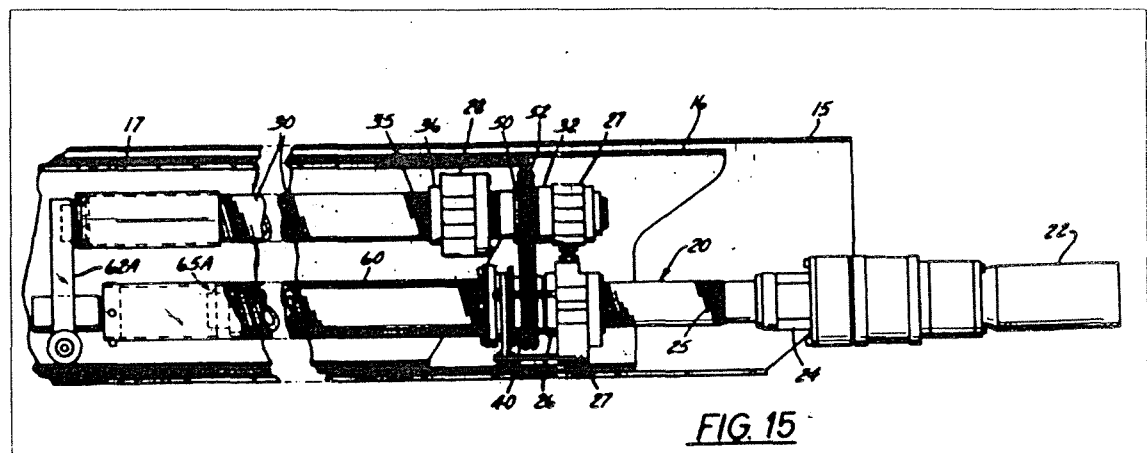


Figure 3.3: Parallel Screw Configuration (U.S. Patent: 4337868)

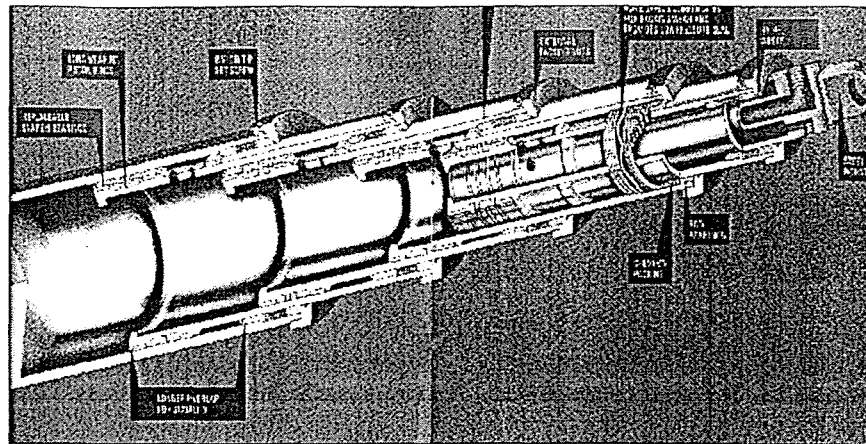


Figure 3.4: Telescopic Hydraulic Cylinder

3.2.2.3 Telescopic Hydraulic Cylinders

Telescopic hydraulic cylinders, as shown in Figure 3.4, are another method commonly used in telescopic crane booms, and other industrial applications. Telescopic cylinders are composed of a series of prismatic hollow tubes concluding with a smallest solid rod. As fluid enters the cylinder, the solid rod is pushed outward, subsequently pulling the nested hollow tubes along with it.

Advantages of this design include commercial availability, robustness and simplicity of design. However, there are associated disadvantages of telescopic hydraulic cylinders. The first is the lack of constant velocity motion due to volumetric changes within the cylinder through extension and retraction. In addition, in order to obtain accurate positioning from the cylinder, an external measurement device and complex hydraulic control would be required.

3.2.2.4 Telescopic Screw Actuator

To alleviate many of the above problems, a novel design was invented in which a series of screws could be nested together in a prismatic manner. The idea incorporates the accurate positioning of a parallel screw mechanism with reduced backlash and the space saving features associated with telescopic hydraulic cylinders. The original

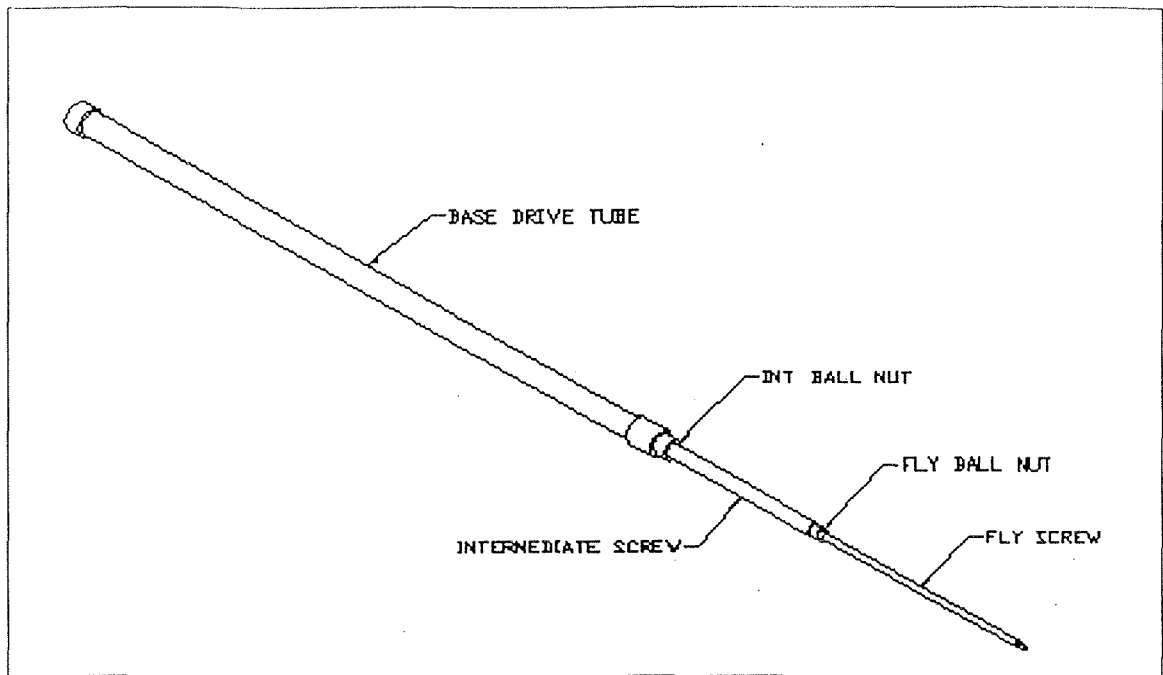


Figure 3.5: "Floating" Telescopic Screw Actuator

conceptual design included the use of a series of nested prismatic ball screws, each of the same lead, interconnected such that rotation of the largest screw's nut would cause constant velocity translation of the smallest screw which is fixed from rotating. This is best described for a simple actuator, Figure 3.5, consisting of two ball screws. A base tube is connected to a drive motor at its base end and to the nut of the largest screw at its outer end. The largest screw is then threaded within its nut such that it resides within the base drive tube. The smaller screw's nut is then attached to the outer end of the intermediate screw and a hole is drilled throughout this screw to allow for the smaller screw to pass within. Next, the smaller screw is threaded into its nut such that its base-end resides within the larger screw. Finally, the outer end of the smallest screw is attached to the item to be actuated, thus restricting its rotation. If each of these screws are of the same lead, simply turning the base drive tube will cause three possible

scenarios, all of which will result in the same constant velocity translation of the smallest screw.

The first scenario is that rotation of the base drive tube, and thus the larger nut, causes pure translation of the larger screw. Therefore, the smaller screw's nut will not rotate causing the larger screw and the smaller screw to translate as a rigid body. The actuator will continue to extend until the larger screw approaches its end-of-travel, at which point an energy absorbing stop will cause the larger screw to rotate and cease to translate. The rotation of the larger screw will then cause the smaller screw to translate with respect to the larger screw until the desired position is reached.

The next possible scenario is that the larger screw rotates with the base drive tube until the smaller screw reaches its end-of-travel. At this point, an energy absorbing stop on the smaller screw will stop the larger screw from rotating, causing it to translate until the desired position is reached.

The final scenario is a combination of the two absolute velocity scenarios. The larger screw rotates at a slower rate than the base drive tube such that it translates and rotates. Therefore, each screw will translate with respect to its nut until the desired position is reached.

Determination of which scenario will prevail will depend on several factors including friction, accelerations, and telescopic position. However, due to the fact that both of the screws are of the same lead, the actuation will always result in a translation proportional to the input drive tube angular velocity and the lead of the screws. This method was referred to as the floating prismatic actuator, due to the fact that the larger screw's position is uncertain.

The advantages of this design include its simplistic, robust design that allows for accurate positioning with low backlash over an extended reach. In addition, the design offers the same space saving advantages associated with telescopic hydraulic cylinders.

There are a few disadvantages associated with the “floating” nature of the larger screw. The first is that high-speed travel is limited due to the fact that the screws are often extended to their end-of-travel limits. At these locations, a tremendous amount of energy is required in accelerating and decelerating the larger screw. This energy must be absorbed in the stops at each screw’s end-of-travel, leaving the possibility that the screw’s may jam and become locked. The second disadvantage is that the rotational inertia of the arm varies greatly with the location of the larger screw. Since this location is uncertain, there was concern as to whether control of the arm’s rotational motion would be jeopardized.

Therefore, the telescopic actuator concept was revised to include a means of “controlling” the larger screw. By placing a slotted tube inside the base drive tube, the larger screw could be rotated through a key connecting it to the slotted tube. The slotted tube could then be rotated at a prescribed rate slower than the base drive tube. The larger screw would then be forced to translate and rotate at prescribed rates proportional to the angular velocities of the base drive tube and the inner slotted tube. This allowed the actuator to be reconfigured such that each of the screws would translate with respect to their nuts at the same rate, thus eliminating the possibility of screw overrun and jamming, within the normal operating range of the actuator. The disadvantages of this design were the increased weight, complexity and the need for a gearbox to prescribe rotation of the inner and outer drive tubes at different rates.

3.2.3 Trade-Off Analysis

Through a complete trade-off analysis, Table 3.2, the conceptual designs were evaluated based on the previous weighted specifications in order to determine the most ideal design. The results of the trade-off analysis concluded that the “controlled” telescopic ball screw actuator was the most ideal with the “floating” design as the second most ideal design. It was determined that the “controlled” actuator design had benefits that outweighed its increased complexity and cost. These benefits included its improved controllability and protection against screw jamming due to overrun at high speeds.

	Weighting (1-10)	Cable Extension			Hydraulic Cylinder			Parallel Screw Configuration			"Floating" Telescopic Screw			"Controlled" Telescopic Screw		
		Rating	Score	Total	Rating	Score	Total	Rating	Score	Total	Rating	Score	Total	Rating	Score	Total
Efficiency	6	high	5	30	med	3	18	low-med	2	12	high	5	30	high	5	30
Accuracy	10	low-med	2	20	low	1	10	med	3	30	high	5	50	high	5	50
Backlash	10	med-high	2	20	high	1	10	med-high	2	20	low	5	50	low	5	50
Constant Velocity	10	yes	5	50	no	1	10	yes	5	50	yes	5	50	yes	5	50
Robustness	7	low-med	2	14	med-high	4	28	med-high	4	28	low-med	2	14	high	5	35
Max. Speed Attainable	10	yes	5	50	yes	5	50	yes	5	50	maybe	3	30	yes	5	50
Weight	7	low	5	35	high	1	7	med	3	21	med	3	21	med-high	2	14
Mechanical Complexity	7	high	1	7	low	5	35	med	3	21	low-med	4	28	med-high	2	14
Cost	6	low	5	30	med-high	2	12	low-med	4	24	med	3	18	high	1	6
Control Complexity	8	low	5	40	high	1	8	low	5	40	med-high	2	16	low	5	40
Space Requirements	9	high	1	9	high	1	9	med-high	2	18	low-med	4	36	low-med	4	36
Commercial Availability	6	yes	5	30	yes	5	30	no	1	6	no	1	6	no	1	6
Ease of Integration into arm	6	low	1	6	high	5	30	med	3	18	high	5	30	high	5	30
Score				341			257			338			379			411

Table 3.2: Telescopic Actuation Trade-Off Analysis

3.3 Rotational Actuation Concept Selection

Concept selection of a rotational actuation method proceeded similarly by first prescribing critical specifications. These specifications were then used as guidelines in brainstorming sessions and research to develop a number of conceptual designs. These conceptual designs were then evaluated through a trade-off analysis to determine the best conceptual design.

3.3.1 Rotational Specifications

Specifications for the rotational actuation system were developed by considering the project specifications set forth in the project conceptual design. Specifically, the rotational actuation system was to be capable of handling the maximum torque requirements, attaining the maximum speed, and maintaining the required accuracy. On a more general basis, the design should be compact, lightweight, robust, and commercially available.

3.3.2 Preliminary Concepts

3.3.2.1 Planetary Gearbox

The concept of using a planetary gearbox was formulated with consideration into the large gear reductions that are typical of planetary systems with low space requirements. In addition, planetary systems can offer high efficiency and low backlash. The planetary gearbox concept would include a set of right angle bevel gears in order to allow for the motor to be directed along the longitudinal axis of the arm. This advantage would allow significant vertical space savings. The main disadvantage of this design is the lack of commercial availability due to the stringent torque requirements arising from OCCSM performance specifications and the extreme rotational inertia of the telescopic

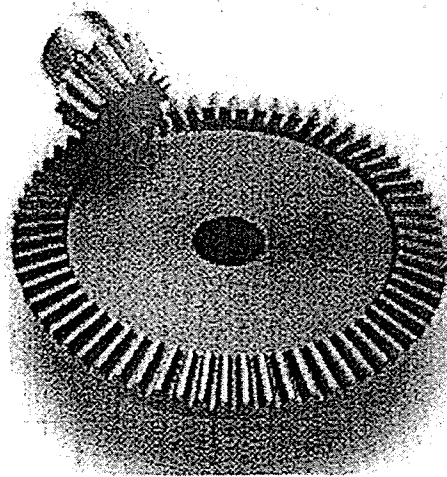


Figure 3.6: Bevel Gear Reduction

arm. This lack of commercial availability is an especially large factor in planetary systems resulting in a cost-prohibitive design.

3.3.2.2 Chain/Gear Drive

Chain and gear drives are common forms of actuation in many commercially available telescopic crane booms due to their simplistic design. Figure 3.6 shows an example of a bevel gear type drive in which the reduction ratio is about 5:1. The principle advantage of this type of design is its low mechanical complexity and associated low cost. The principle disadvantage is the large space requirements needed to achieve reduction ratios on the order of 60:1.

3.3.1.3 Hydraulic Cylinder

Hydraulic cylinders are often used in industrial machines to cause rotations. This is accomplished by placing a cylinder in a leverage position as depicted in Figure 3.7. There are a number of advantages of this design including low mechanical complexity, commercial availability and associated low cost. However, hydraulic cylinders are often difficult to use in robotics applications due to the need for external measurement devices.

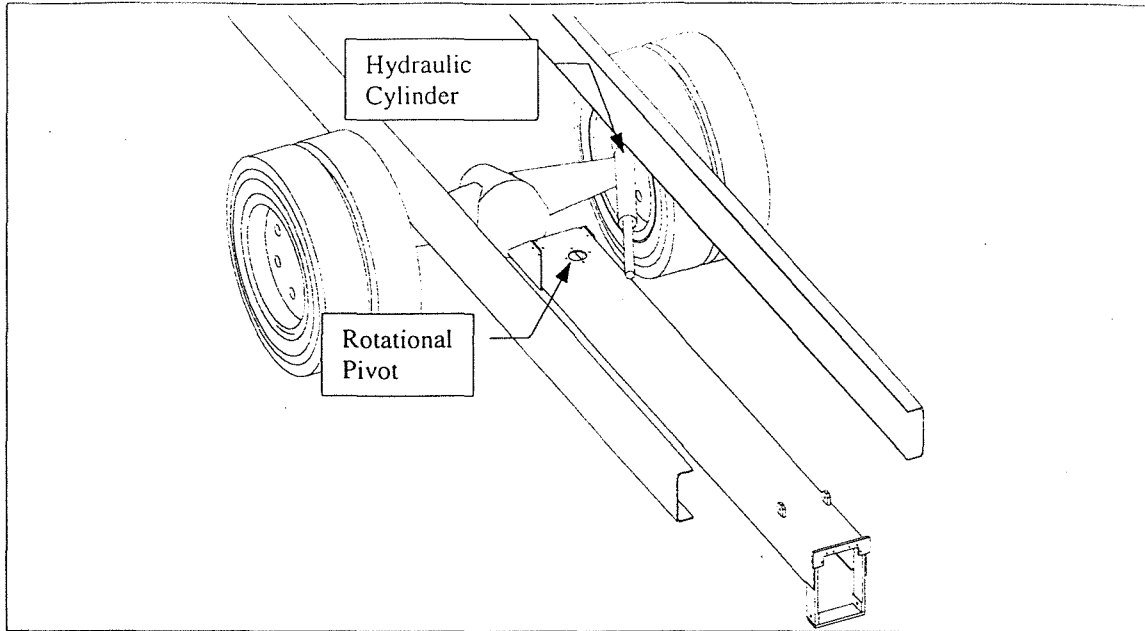


Figure 3.7: Hydraulic Cylinder Rotational Actuator

In addition, this type of design would require non-linear flow control to obtain constant velocity rotation of the arm.

3.3.1.4 Harmonic Drive

Harmonic drives are specialized gear reduction devices that are becoming more prevalent in robotic applications due to high reduction ratios, compact space

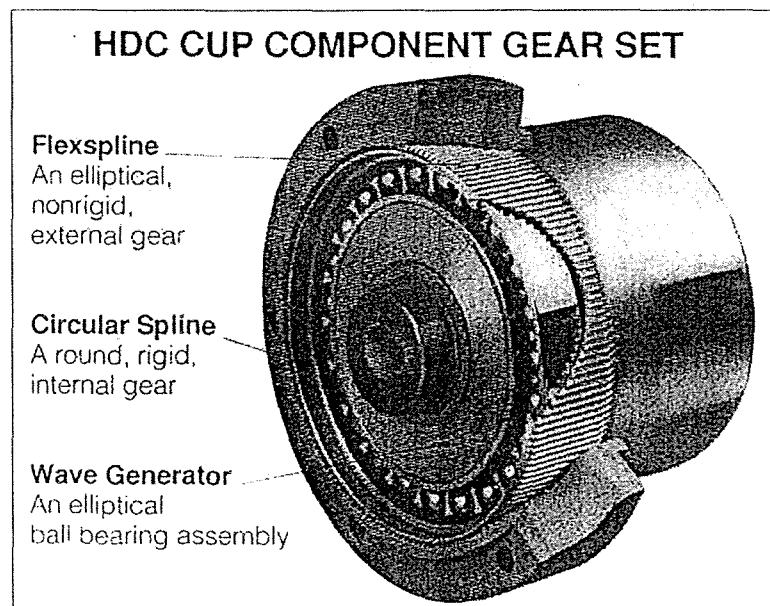


Figure 3.8: Cup-Type Harmonic Drive

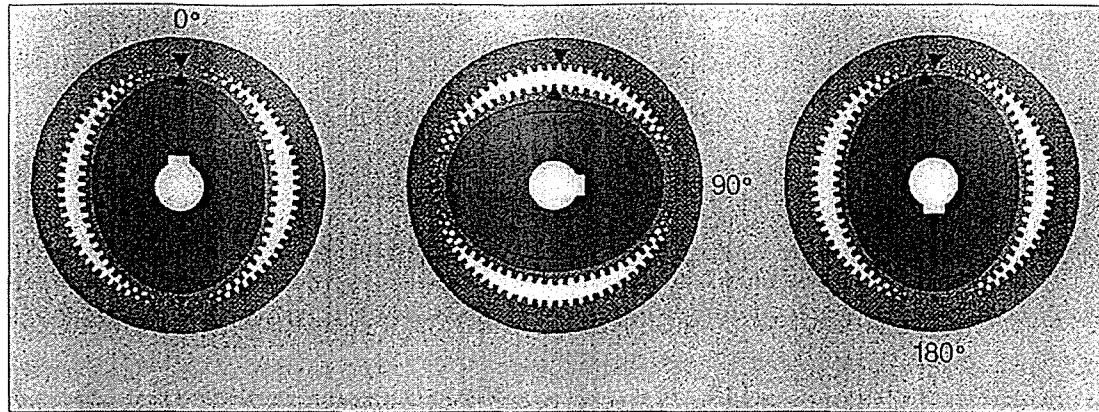


Figure 3.9: Harmonic Drive Operation Sketch

requirements, and high torque capacities. Figure 3.8 is a detailed view of a cup type harmonic drive. The central component to the operation of a harmonic drive is an elliptical bearing known as a wave generator. The wave generator is fitted within a flexible external gear, called a flexspline. The deformed flexspline is then fitted into a rigid internal gear such that contact is only made along the major axis of the ellipse. The gear reduction is accomplished by the fact that the flexible spline contains two less teeth than the rigid internal ring gear with which it is engaged. Therefore, for each revolution of the wave generator, the flexspline will rotate slightly in the reverse direction at a ratio equal to one-half the number of teeth on the flexspline. Figure 3.9 is a sketch depicting the reduction accomplished through one-half rotation of the wave generator.

3.3.3 Trade-Off Analysis

A complete trade-off analysis, Table 3.3, was performed in order to determine which of the above concepts would best satisfy the rotational specifications. Each of the conceptual designs was evaluated based on efficiency, accuracy, backlash, robustness weight, and a variety of other factors. The totals for each concept were summed with the totals along the bottom of the table. The highest total would reveal the best conceptual design.

3.3.4 Summary

Results of the trade-off analysis showed that the harmonic drive concept best fit the OCCSM requirements. The determining factors were the high torque capacities, low space requirements, low cost due to commercial availability, and excellent positioning accuracy. The next competing design was the chain/gear drive due to its simplicity and low weight. The major downfall of this design was its large planar space requirements.

	Weighting (1-10)	Planetary Gearbox			Chain/Gear Drive			Hydraulic Cylinder			Harmonic Drive		
		Rating	Score	Total	Rating	Score	Total	Rating	Score	Total	Rating	Score	Total
Efficiency	6	med	3	18	med/high	4	24	med	3	18	med/high	4	24
Accuracy	10	high	5	50	med/high	4	40	low	1	10	high	5	50
Backlash	10	low,med	4	40	high	1	10	high	1	10	low	5	50
Constant Velocity	10	yes	1	10	yes	5	50	no	1	10	yes	5	50
Robustness	7	med/high	4	28	med	3	21	high	5	35	low/med	2	14
Max. Speed Attainable	10	yes	5	50	yes	5	50	yes	5	50	yes	5	50
Weight	3	med/high	4	12	low	1	3	med	3	9	low/med	2	6
Mechanical Complexity	7	high	1	7	low	5	35	low	5	35	med/high	2	14
Cost	7	high	1	7	low	5	35	low	5	35	med	3	21
Control Complexity	8	low	5	40	low	5	40	med/high	2	16	low	5	40
Space Requirements	5	med	3	15	med/high	2	10	med	3	15	low	5	25
Commercial Availability	8	no	1	8	yes	5	40	yes	5	40	yes	5	40
Score				285			358			283			384

Table 3.3: Rotational Actuation Trade-Off Analysis

3.4 Vehicle Integration and Stowage System

The conceptual design for the vehicle integration and stowage system addressed details of how the telescopic arm would be mounted onto a vehicle. This mounting would include the main pivot for the arm, an end support capable of tracking the radius generated by the end of the base section, as well as a means of stowing the arm away from the ground to aid in clearance. Specifications were developed concerning each of these subsystems, from which conceptual designs were formulated and evaluated. Using trade-off analyses, the conceptual designs were evaluated and the best concept was chosen for each subsystem.

3.4.1 Specifications

Based on the retracted length of the OCCSM telescopic arm, it was determined that the arm should mount to the rear underside of the vehicle, directly behind the wheels. When fully retracted for stowage, the arm should reside within the boundaries of the vehicle to provide for maximum protection against incidental damage. To accomplish this, it was suggested that the arm pivot up away from the road into a storage position. This would then allow sufficient ground clearance at the end of the vehicle. In addition to the stowage of the arm, the vehicle mount must also provide for an end support for the telescopic arm at all positions in the workspace. This would require a moving support that could track the radius generated by the end of the base section while providing a rigid, frictionless support. The final part of the vehicle integration system was the main pivot mount that allows the arm to rotate in the horizontal plane and the vertical plane for stowage.

3.4.2 Preliminary Concepts

3.4.2.1 Compound Slides

A simple, commercially available design was formulated which would use compounded linear slides for the end support. This idea uses multiple slides, one mounted lengthwise along the arm and a longer slide mounted transversely across the back of the vehicle. The slides are joined together such that they support the weight of the arm and provide for x-y tracking of the end radius. The advantages of this design include commercial availability, simplistic design and relatively low weight. The principle disadvantage of this design is that it does not allow for easy lifting of the arm into a retracted position. To stow the arm using this design would require a separate system that could lift the entire slide assembly, or a system that detached the two slides to lift the arm. Another disadvantages include low robustness associated with commercially available slides.

3.4.2.2 Support Plate/Roller

Another idea that was proposed was the use of a flat plate upon which a roller, fixed on the arm, could track a radius. The plate could be located below the arm, thus allowing for stowage by simply lifting the plate upward toward the truck. Advantages of this design include high robustness, low cost and weight. Disadvantages relate to the stowage system that would require an entire separate system to lift the support plate. In addition, this support further reduces the amount of ground clearance.

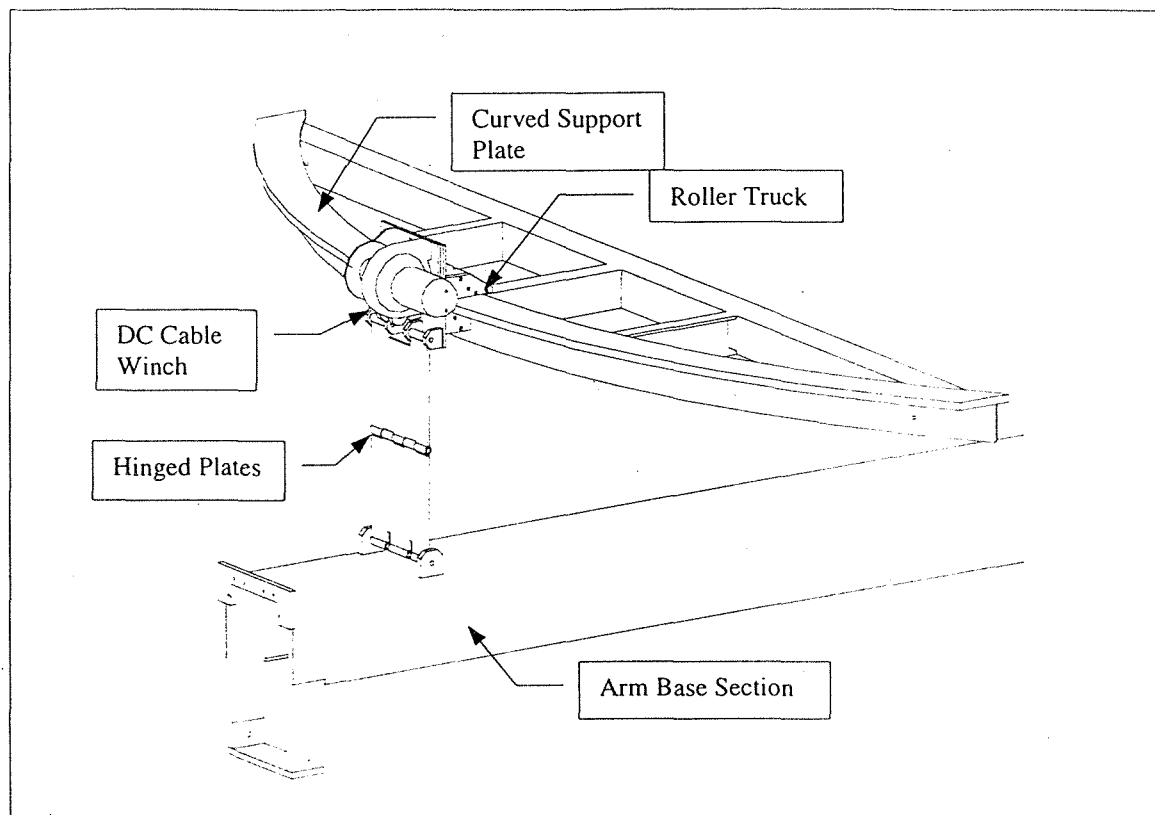


Figure 3.10: Curved Rail Support / Stowage System

3.4.2.3 Curved Rail

The last proposed idea was to use a curved rail, Figure 3.12, located on the back end of the truck. The rail would have a roller truck that would run back and forth on the rail. The roller truck would be outfitted with a set of hinged plates to connect to the arm. The system would also include a cable winch, attached to the roller truck, which would raise the arm into its stowage position. When fully dropped into its operational position, the hinged plates would extend straight and support the full load of the arm. The advantages of this design include high robustness, low cost, integrated stowage system, and no reduction in ground clearance. The disadvantages of this design are lack of commercial availability and higher mechanical complexity.

3.4.3 Trade-Off Analysis

To help evaluate the competing designs, a trade-off analysis, Table 3.4, was performed. In this analysis, the competing designs were evaluated and given numerical scores based on how well they would meet the specific design criteria. The highest scoring design was selected as the best fit based on the design criteria and weighting.

3.4.4 Summary

The trade-off analysis showed that the curved rail design best fit the specifications and weighting for the OCCSM end support and stowage system. The main benefit of this system was the integrated, compact stowage system that provided a rigid support in the full down position. In addition, this system offered the highest ground clearance in the stowed position and the least reduction in ground clearance while in the lowered position.

The design of the rotational mount for the OCCSM telescopic arm was conceptualized to be a plate that would run between the frame rails of the vehicle. The plate would contain a hole in the center to allow for the passage of the rotational actuator system and contain a set of pivots at the interface to the frame rails to allow for stowage rotation.

3.5 Summary

This chapter has presented the conceptual design of each of the subsystems that combine to form the OCCSM telescopic manipulator. These subsystems included the telescopic arm structural design, telescopic and rotational actuation systems, and the vehicle integration and stowage system. Conceptual designs for each of these subsystems were formulated to adhere to the machine specifications through the use of trade-off

analyses. These trade-off analyses helped quantify the conceptual designs to ensure the best machine design.

The next stage in the design process was to expand the conceptual designs into a fully detailed state. This will require quantifying the machine specifications on an engineering basis and localizing these constraints to each subsystem's conceptual design.

	Weighting (1-10)	Compound Slides			Support Plate/Roller			Curved Rail		
		Rating	Score	Total	Rating	Score	Total	Rating	Score	Total
Radius Tracking	10	yes	5	50	yes	5	50	yes	5	50
Commercial Availability	4	high	5	20	med	3	12	low/med	2	8
Weight	5	low/med	2	10	low	1	5	low/med	2	10
Robustness	10	low	1	10	high	5	50	high	3	30
Stowage Complexity	8	med/high	2	16	med/high	2	16	low	5	40
Maximumize Ground Clearance	8	high	5	40	low	1	8	high	5	40
Space Requirements	3	med	3	9	low/med	4	12	med	3	9
Cost	8	med	3	24	low	5	40	med	3	24
Score				179			193			211

Table 3.4- End Support / Stowage System Trade-Off Analysis

CHAPTER 4: DETAILED DESIGN

The conceptual design of the OCCSM R- θ Telescopic Manipulator had been completed with formulated designs for the three main subsystems: rotational and telescopic actuation, telescopic arm structure, and vehicle integration and stowage. The next step was to elaborate these concepts and formulate a working detailed design that would meet all of the project specifications. This chapter presents this detailed prototype design in a natural progression from the conceptual design phase to form the first prototype Telescopic R- θ Manipulator, Figure 4.1.

4.1 Telescopic Arm Structural Design

The conceptual design for the telescopic arm structure was used to gain insight into the material and geometry configurations that would best meet the machine specifications. It was determined that fiber-reinforced composites would yield the

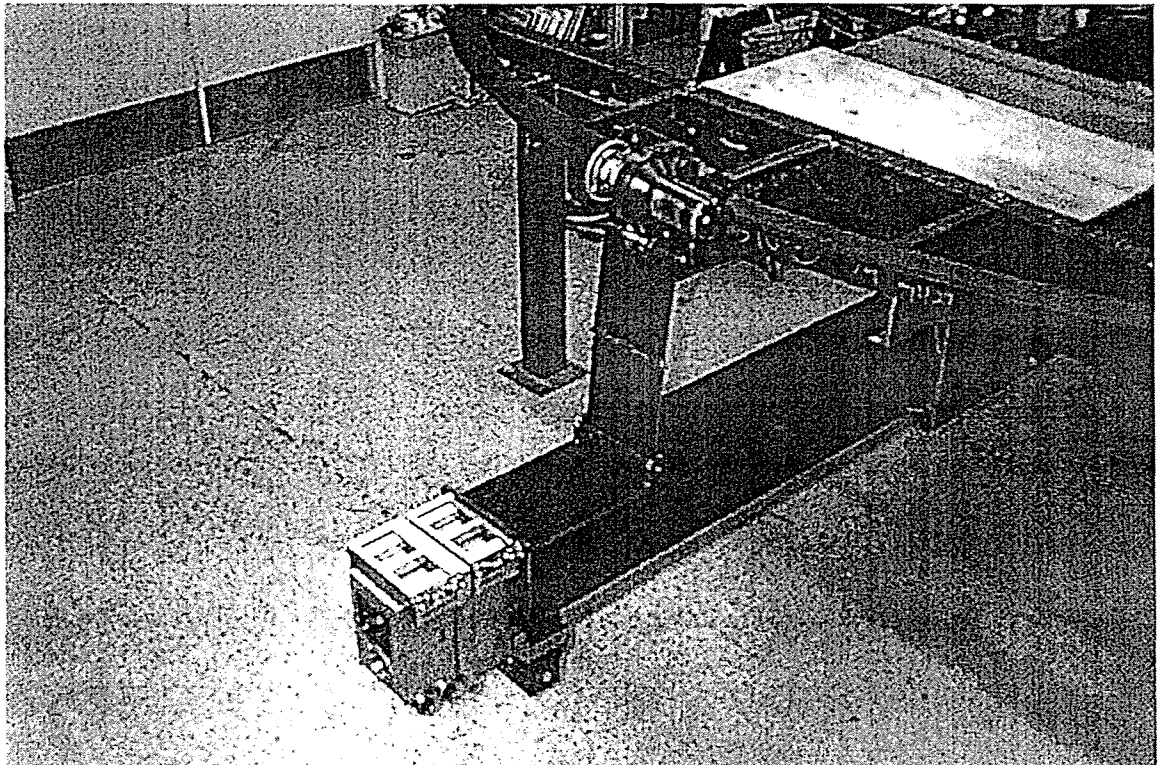


Figure 4.1 OCCSM Prototype Telescopic Manipulator

highest performance, but were ruled out in this prototype design phase due to availability, cost and the need for rapid prototyping. The next best design was to use custom formed sections with properties optimized to yield the largest stiffness to weight ratio possible, and thus the smallest weight. The material and dimensions of these custom sections were selected from a detailed analysis of the beam deflection. Through this analysis, the section dimensions were optimized to yield the highest stiffness to weight ratio possible while maintaining robustness considerations. Detailed calculations for the telescopic arm structural design can be found in Appendix A, pages A-1 through A-18.

4.1.1 Specifications

Specifications for the OCCSM telescopic arm were generated from machine and project specifications and used to determine the optimum configurations of the telescopic sections. Detailed specifications imposed constraints on the stiffness and strength of the sections such that the arm would support a 445 N (100 lb) vertical end load with less than 12.7 mm (0.50 in) deflection at maximum extension. The end loading constraint was derived from a conservative estimate of the sealant applicator weight. The deflection constraint was set in order to ensure proper actuator operation as well as ensuring high beam stiffness. Side loading was estimated to be minimal and included 89 N (20 lb) due to the frictional force of the sealant applicator and inertial loading resulting from rotational accelerations. Additional constraints on the design included robustness, controllability, and stiff joint connections between the mating sections.

4.1.2 Telescopic Sections

The design of the telescopic sections began with an examination of the detailed specifications. Through a detailed analysis of the stress and deflection of the telescopic

arm, it was determined that the critical design specification was the arm vertical deflection constraint. To optimize the design of the arm sections, a program was created in which the cross sectional and material properties could be varied. This program, Figure 4.2, used the deflection formulae, along with section properties to evaluate the end deflection of the arm. The sections' material and geometry were then iterated to determine the optimum design configuration.

After numerous iterations, the deflection behavior was generalized and several conclusions were formed. First, while limiting the material selection to aluminum, steel and titanium, it became apparent that steel would provide the highest stiffness to weight ratio, and thus produce the lightest section. This is easily seen from a comparison of the ratio of the modulus of elasticity to the density for each material. In addition, since the loading is significantly higher in the vertical plane, the sections' vertical dimensions should be larger in this direction, thus eliminating circular and square cross sections. Finally, since the beams are telescopic in nature, high wall thickness reduces the boundary dimensions of the succeeding sections and thus increases the overall deflection and weight of the arm. Therefore, it was concluded that the sections should be made of thin wall steel with vertical plane dimensions exceeding horizontal plane dimensions. In addition, examination of the section properties suggested that the heavier wall thickness at the top and bottom of the sections would further optimize the stiffness to weight ratio of the sections.

4.1.2.1 Base Cross Section

The design of the Base section was significantly different than that of the Intermediate and Fly sections. Low weight and high stiffness were not as crucial as the

Deflection Analysis For Beam with Varying Cross-Section									
Material: Section 1 Section 2 Section 3									
Steel Steel Steel									
Given			Reactions				Cross Sections		
End Load	P=	100	Due to P				Base(in)	Height(in)	
Dist. to Support	L0=	87	R1=	100 Lbf			Section 1:	9.375	7
Dist. to 1st Sect.	L1=	101	M=	-26900 Lbf/in			Section 2:	6	10
Dist. to 2nd Sect.	L2=	185	Due to w				Section 3:	5.8	8.8
Dist. to 3rd. Sect.	L3=	269	R1=	458.0941 Lbf			Ib=	41.47594 in^4	
Mod. of Elasticity	Eb=	3.00E+07	M=	-45917.8 Lbf/in			Ii=	37.825 in^4	
	Ei=	3.00E+07	Support				Ii=	24.05475 in^4	
Sections	Ef=	3.00E+07	R1=	-1005.18 Lbf			X-Area1=	6.21875 in^2	
Dist. Weight	w1=	2.643688	R2=	1005.182 Lbf			X-Area2=	2.963552 in^2	
Dist. Weight	w2=	1.550722	M=	87450.84 Lbf/in			X-Area3=	2.124328 in^2	
Dist. Weight	w3=	0.72406	Nat Reactions				Specific Section 1:	0.282	
Ball Screws	Seal./Actuator		R1=	-447.088 Lbf			Weight Section 2:	0.282	
Base Dist. Weight	w1=	0.89	R2=	1005.182 Lbf			(Lbf/in^3) Section 3:	0.282	
Int. Dist. Weight	w2=	0.715	M=	14633.05 Lbf/in			Weight of Beam (Lbf)	314.8615	
Fly Dist. Weight	w3=	0.125					Hanging Weight(lbf)	120.5217	
Slopes and Displacements									
Base-1 x=		87	Base-2 x=		120	Int. x=	216	Fly x=	312
Slope		Disp.	Slope		Disp.	Slope	Disp.	Slope	Disp.
Due to P		-0.00158 -0.073	-0.00202 -0.13251		-0.00289	-0.37599 -0.00307		-0.67924	
Due to w(W/O SPRT)		-0.00205 -0.10433	-0.00239 -0.17803		-0.00278	-0.43267 -0.00284		-0.70429	
Support Deflect.		0.003057 0.177322	0.003057 0.278213		0.003057	0.571712 0.003057		0.865211	
Total Deflection(in.)		-0.00057 0	-0.00135 -0.03233		-0.00261	-0.23695 -0.00285		-0.51832	
Material Data									
Mat'l	Aluminum	Steel	Titanium						
E:(psi)	1.00E+07	3.00E+07	1.65E+07						
Spec. Wt.(lbf/in^3)	0.098	0.282	0.17						

Figure 4.2: Deflection Analysis Program

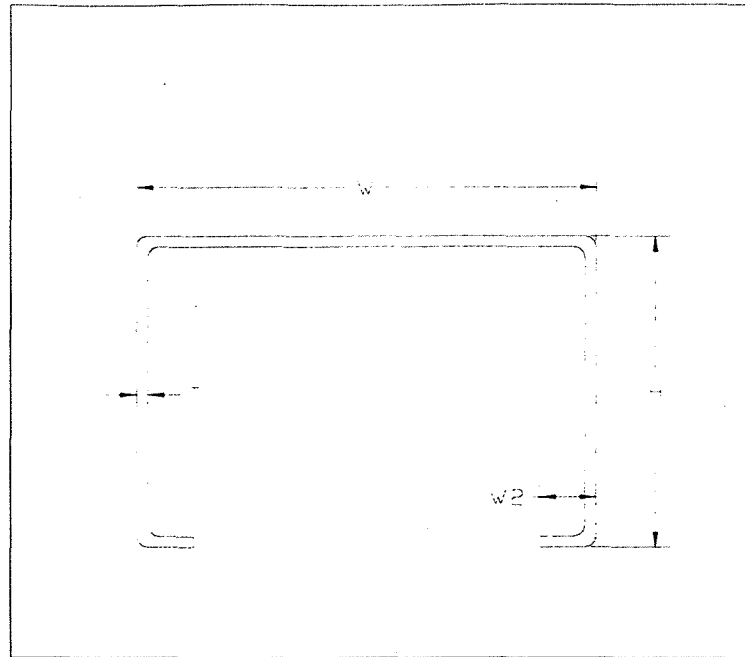


Figure 4.3: Base Cross Section

Intermediate and Fly sections due to the fact that the Base section would remain close to the pivot and be rigidly supported by the frame of the vehicle at each end. Therefore, the design of the base section was directed around the design of the Intermediate and Fly sections as well as the vehicle integration requirements.

The prototype Base section design is shown in Figure 4.3. The section was made from 6.35 mm (0.25 in) thick hot roll steel plate that was formed into a C-shape, slightly closed in on the bottom surface to provide greater side wall strength as well a ledge for the rear vertical support system of the Intermediate section. The dimensions for this section were determined by iteration through the beam deflection program, as well as consideration of support constraints imposed by the Intermediate section.

4.1.2.2 Intermediate Cross Section

Design of the Intermediate cross section began through iteration of the developed deflection program while maintaining project specifications concerning size, robustness, and concentrated loading. Through extensive analysis and brainstorming, the

Intermediate section was designed as shown in Figure 4.4. The design calls for a large thin wall U-shaped section around the top of the section which mates to a heavy short C-shaped section along the bottom. The edges of the heavy bottom structure were designed to handle the contact stresses from support rollers and provide a means of supporting the section against side loading. In addition, this overlap would allow for proper joining of the sections through a continuous resistance seam weld. In essence, the section was designed to have a large bending inertia, be lightweight, and direct all of the loading down to the thicker section base.

Specific dimensions for this section were determined through the beam deflection program such that the arm would meet the loading and end-deflection constraints. To meet these requirements, the minimum arm dimensions were as follows:

$H=254 \text{ mm (10.0 in)}$

$H_2=25.4 \text{ mm (1.0 in)}$

$W=152.4 \text{ mm (6.0 in)}$

$t_2=4.77 \text{ mm (0.188 in)}$

$t=0.762 \text{ mm (0.030 in)}$

where the variables were defined as in Figure 4.4.

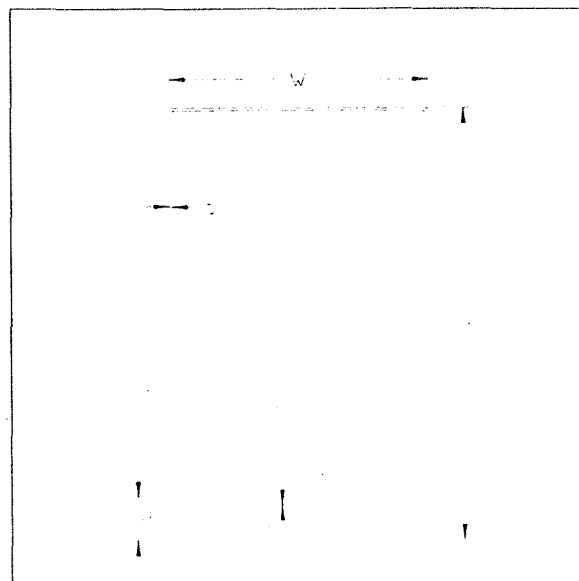


Figure 4.4: Intermediate and Fly Beam's Cross Sections

4.1.2.3 Fly Cross Section

Design of the Fly section proceeded exactly as that of the Intermediate section with the exception of reduced loading. To accommodate for this reduced loading the section's bottom channel thickness and height were reduced in addition to the reduction in the overall height to fit into the Intermediate section. The wall thickness of the main beam section was kept constant with that of the Intermediate due to robustness constraints and concerns of localized sidewall buckling. The resulting dimensions for the Fly section were as follows:

H=226.10 mm (8.9 in) H2=14.99 mm (0.59 in)

W=147.32 mm (5.8 in) t2=3.17 mm (0.125 in)

t=0.762 mm (0.030 in)

where the variables were again defined as in Figure 4.4. These dimensions would produce a clearance between the Intermediate and Fly section sidewalls of 1.78 mm (0.070 in) and 0.89 mm (0.035 in) for the top and bottom edges. This clearance was kept small in order to maximize the stiffness to weight ratio of the arm.

The preceding analysis and design of the telescopic sections had been accomplished using ideal deflection calculations based on engineering assumptions that could be questioned for a telescopic beam unless the joints could be designed with adequate stiffness. Therefore, an extensive amount of work was necessary to ensure that the telescopic arm would emulate the deflection analysis.

4.1.3 Vertical Support Systems

The joint connections were divided into two main support systems, the vertical support systems and the horizontal support systems. The vertical support systems were

the most crucial in aligning the sections and ensuring that the arm would meet the deflection specifications. The first step in designing the vertical supports for the telescopic sections was to determine the loading at each of these joints. A complete analysis of this loading was performed at maximum extension of the arm to yield the largest joint loading. This loading was then used to design the primary support roller systems to handle loading at the end of the arm in the vertical down direction, and secondary support roller systems to handle loading in the vertical up direction. Due to the high loading, wear and necessary reliability of the vertical support systems, rollers were deemed necessary to ensure proper arm operation.

4.1.3.1 Primary Loading Rollers

The primary loading rollers are depicted in Figures 4.5-4.8 for both the Intermediate and Fly sections. These primary rollers were designed to handle the primary loading caused by the weight of the arm and the end load. High loading for these support rollers was distributed along the section using a series of rollers in an effort to reduce the localized contact stresses on the section. To ensure full contact between the rollers and sections, roller trucks were used wherever possible.

4.1.3.1.1 Intermediate and Fly Sections

The primary vertical support system for the Intermediate section was designed to use two pair of roller trucks, one located on the outer end of the base section, Figure 4.5, and the other pair located at the top back of the Intermediate section, Figure 4.6. The Fly section was designed to use a similar roller truck on the back of the section, Figure 4.8,

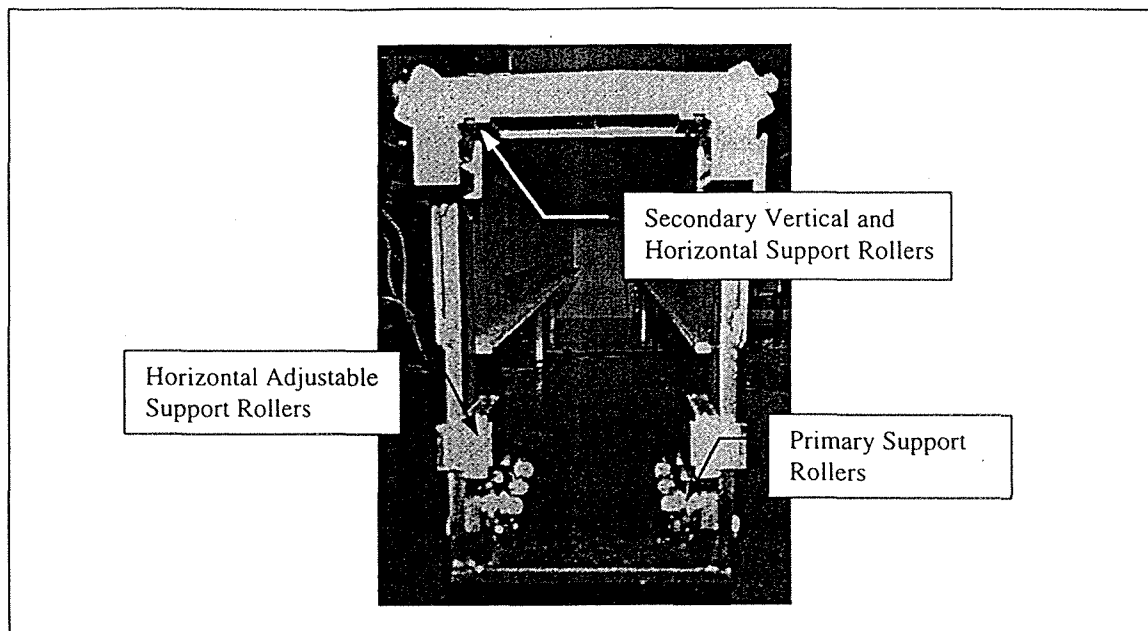


Figure 4.5: Intermediate Section Outer Support System

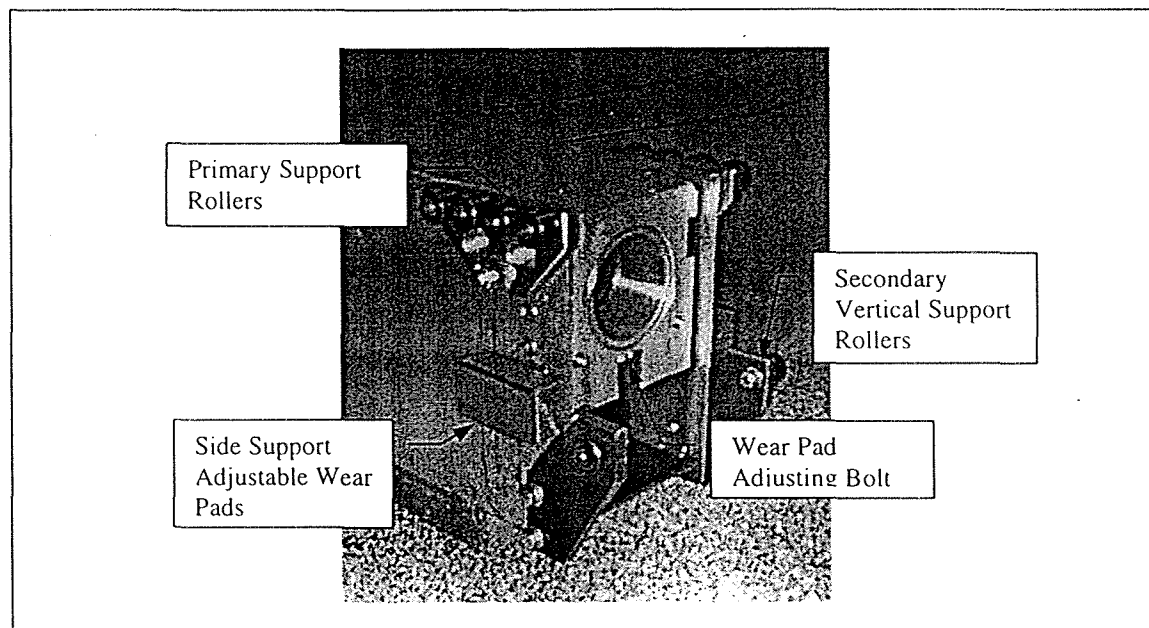


Figure 4.6: Intermediate Section Rear Support System

with a set of fixed rollers for the outer support, see Figure 4.7. This was possible due to the reduced loading on the Fly section rollers. The roller trucks were designed to handle the specified arm loading with a factor of safety of about four based on the Maximum Shear Stress Theory. On the other hand, the rollers on the trucks were designed to carry up to five times the designed loading to allow for concentrated loading on a single roller due to misalignments.

A crucial part of the Fly section rear primary support was to design the roller truck such that the loading could be directed into the sidewall of the Intermediate section. This required that the roller truck be placed as close to the upper corner of the section as possible. To accomplish this, the side of the Fly section was notched out and the side support was integrated onto the roller truck, see Figure 4.8

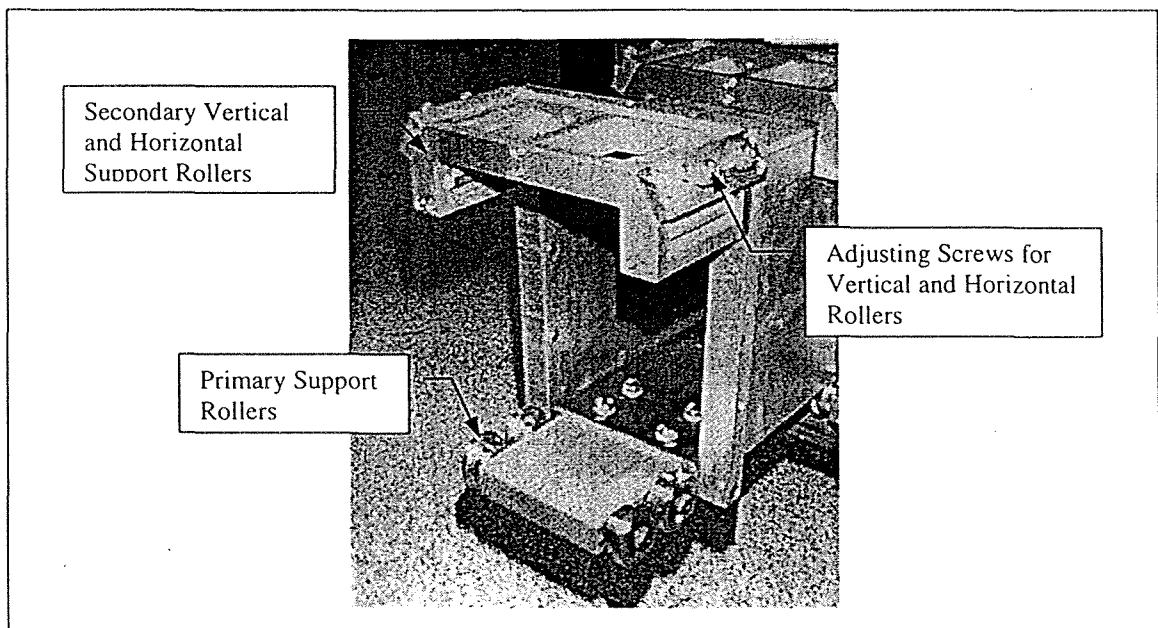


Figure 4.7: Fly Section Outer Support System

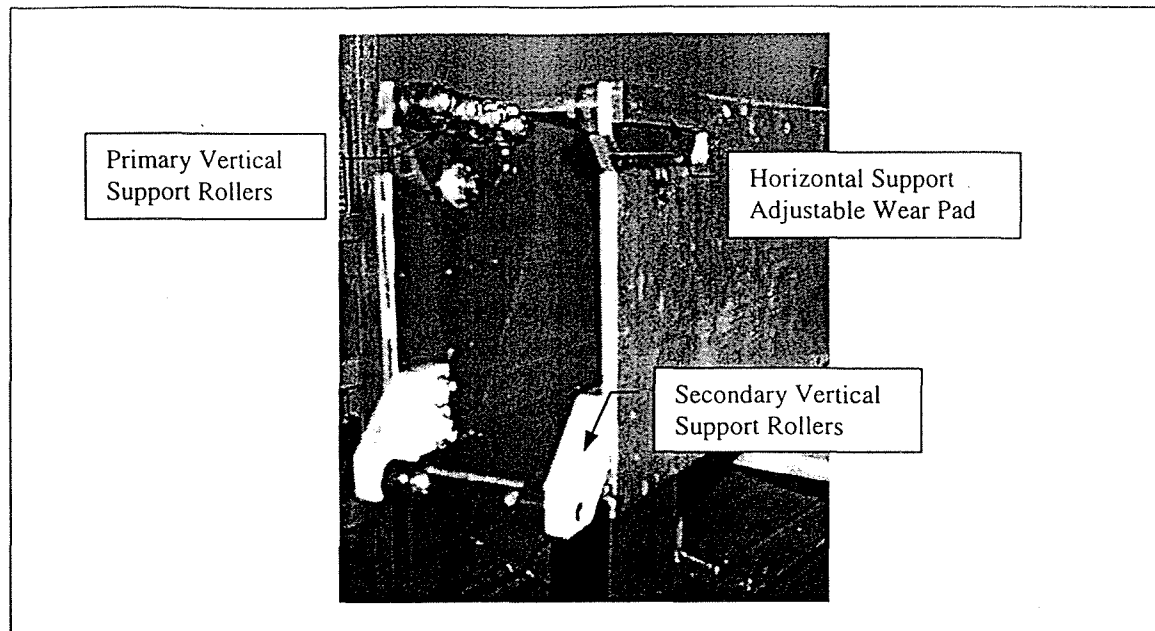


Figure 4.8: Fly Section Rear Support System

4.1.3.2 Secondary Loading Rollers

The secondary loading rollers were far less crucial than the primary support rollers. Loading on these rollers would come from incidental upward loading on the end of the arm and from the weight of the arm sections upon retraction. The secondary support systems for each section are shown in Figures 4.5-4.8.

Lower loading requirements enabled each of these supports to be adjustable such that the arm sections could be preloaded to account for any misalignment. In addition, the outer supports for each section were designed to use the same adjustable part, with the Fly section support adjusted smaller.

4.1.4 Horizontal Support Systems

Horizontal supports for the telescopic arm are shown in Figures 4.5-4.8. These supports were designed by first analyzing the loading caused by friction between the sealant head and the road as well as acceleration loading caused during peak

accelerations to the maximum velocity. As a worst case, the analysis was performed at maximum extension. These calculations yielded horizontal loading for the Intermediate section on the order of 4.45 KN (1000 lb), and on the order of 1.3 KN (300 lb) for the Fly section side supports. The designs for each section joint were then customized around the available clearances and loading to ensure a factor of safety of at least two. In addition, adjustable designs were used wherever possible.

4.1.5 Summary

The detailed design of the OCCSM telescopic arm structure began with a detailed deflection and loading analysis to ensure that the prototype arm would meet the project specifications. Through a detailed analysis of the arm cross sections and materials, it was determined that steel thin wall composite sections would be the most ideal design for the cantilevered sections. The base section included more flexibility since it remained under the vehicle where it could be rigidly supported. The resulting design of the Base section was designed around the Intermediate section constraints as well as arm deflection constraints. A program that enabled quick calculation of the end deflection for various cross sections and materials was developed and proved invaluable.

Once the sections were optimized, design began on the joint connections to ensure that the anticipated arm deflection and operation would evolve. Within this design, detailed analysis of the section loading under maximum operating parameters was performed. This analysis enabled the support systems to be designed safely and economically with factors of safety exceeding two in all components.

4.2 Telescopic Actuator System

The invention of the telescopic ball screw actuator offered large improvements over conventional linear actuation methods. As mentioned in the conceptual design phase, Chapter 3, the “controlled” ball screw actuator consisted of a series of two nested ball screws, each of different, prescribed leads, connected together with the small ball screw inside the larger ball screw. To prescribe rotation on the larger ball screw, a “split tube” was used which contained a slot down one side equal in length to the large ball screw stroke. The tube was sized to allow clearance for the large ball screw to pass within and a key was used to lock the rotation of the large screw to the split tube. The nut of the large ball screw was then connected to another shaft that enclosed the aforementioned split tube and large ball screw. To drive the two concentric shafts at different rates, a custom dual output planetary gearbox was designed. The gearbox used a single input shaft, a ninety-degree bevel reduction, and a conventional 3:1 planetary set to prescribe rotation of the actuator shafts to obtain constant velocity extension for each screw with respect to their ball nuts. The principle advantage of this design was the elimination of jamming and overrun during normal operation.

With the concept in hand, the next step was to determine the exact specifications of each of the components in order to achieve the desired actuator performance. Detailed calculations concerning the design of the Telescopic Actuation System may be found in Appendix A, pages A-25 through A-40.

4.2.1 Specifications

Numerous specifications were developed to guide the design of the telescopic actuator system. General stroke specifications required the actuator to have a stroke

equal to 4.03 m (159.0 in) in order to reach the outer corner of a 3.6 m (12 ft) square workspace. On a performance level, the actuator was required to operate at a maximum speed of 0.91 m/s (36 in/s) with acceleration time of 0.5 seconds. In addition, the actuator was required to perform with sufficient accuracy to position the sealant head throughout the workspace within 3.1 mm (0.125 in) with minimal backlash. Once the design was started, more specific specifications were developed to ensure smooth motion of the arm. A major concern for the actuator of this long length was rotational vibrations associated with support misalignments. Adjustable supports were required to address these misalignment concerns.

4.2.2 Telescopic Ball Screw Actuator Design

4.2.2.1 Ball Screw Selection

The selection of the appropriate ball screws for this design began with analysis into the required performance specifications. The high velocity requirements and support misalignments necessitated ball screws of very high lead in order to avoid whip of the Intermediate screw. Additional geometry constraints imposed by the telescopic nature of the screws were used to size the diameters of the screws. To meet these specifications, the Intermediate ball screw was selected with a diameter of 50.8 mm (2.0 in) and a lead of 50.8 mm/rev (2.0 in/rev). The Fly ball screw was then selected with a diameter of 25.4 mm (1.0 in) and a lead of 25.4 mm/rev (1.0 in/rev). The ratio of the leads was arbitrary and was selected as a ratio of the Intermediate/Fly equal to two based on commercial availability.

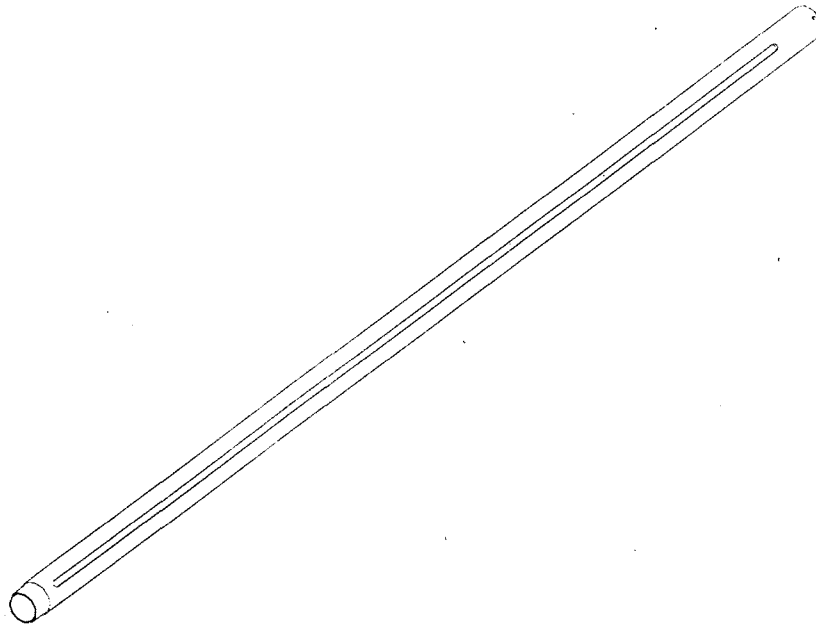


Figure 4.9: Split Tube for Driving the Intermediate Ball Screw

4.2.2.2 Ball Screw Gun-Drilling

The telescopic nature of the actuator required a hole through the Intermediate ball screw to allow for the passage of the Fly ball screw. Concentricity of this hole was crucial to avoid lowering the critical speed of the Intermediate ball screw. In order to fabricate the high lead ball screw with a 26.9 mm (1.062 in) hole, 2.4 m (96 in) long, through the entire screw, the screw was sent to a precision gun-drilling company. The hole was drilled to a maximum runout in concentricity of 0.381 mm (0.015 in) at the middle of the screw. In addition, the hole was drilled through the entire 2.4 m (96 in) length from one end in order to eliminate any ridges on the interior hole surface.

4.2.2.3 Drive Tube Design

With the ball screws specified, the focus shifted to the design of the two drive tubes that would cause rotation of the Intermediate ball screw and its nut. The crucial

component in this design was the inner drive tube, split tube, shown in Figure 4.9, with a key slot down the length of one side to cause rotation of the Intermediate ball screw. The principle concern in this design was the torsional stress and deflection in the tube as the Intermediate screw would extend outward. A complete analysis was performed to determine the stress and deflection at the maximum driving torque. From this analysis, it was determined that deflection was more of a concern than wall thickness. However, this deflection would not result in a steady state error, rather it would result in torsional windup with a spring rate related to the stiffness of the tube. An acceptable torsional deflection of 0.0266 rad was achieved with a wall thickness of 6.35 mm (0.25 in). This torsional deflection would result in a linear windup of about 0.32 mm (0.012 in) at maximum acceleration.

The outer drive tube, see Figures 4.11a and 4.11b, was designed around the constraints of the split tube and the Intermediate ball nut. The size constraints necessitated by the split tube eliminated stress and deflection as a concern in the drive tube. This allowed the implementation of a thin wall tube with the wall thickness limited only by dimensional stability.

4.2.2.4 Actuator Supports

The actuator supports were designed to include four total supports, three of which were fully adjustable. The supports included the dual concentric output gearbox, a fixed bronze bearing in the rear of the Intermediate section, a rolling support attached to the end of the Intermediate ball screw, and a support at the end of the Fly section which restrained the Fly ball screw from rotating. Figures 4.10 shows the fixed support in the Intermediate section and the fully adjustable Intermediate ball screw rolling support.

4.2.2.5 Actuator / Section Integration

The integration design of the actuator and sections concerned the actuation of each of the telescopic sections. The Fly screw end support was attached to the end of the Fly section to cause extension. However, a method of driving the Intermediate section still needed to be devised. It was determined that to ensure good controllability and performance, the sections should extend in a similar manner as the actuator such that each section would reach the end of its travel at the same time. This required the use of a connection plate between the end of the Intermediate ball screw and the rear of the Intermediate section. The plate was required to connect to the rear of the Intermediate due to the telescopic nature of the arm. In addition to good performance and controllability, this design optimized the strength of the arm throughout the workspace.

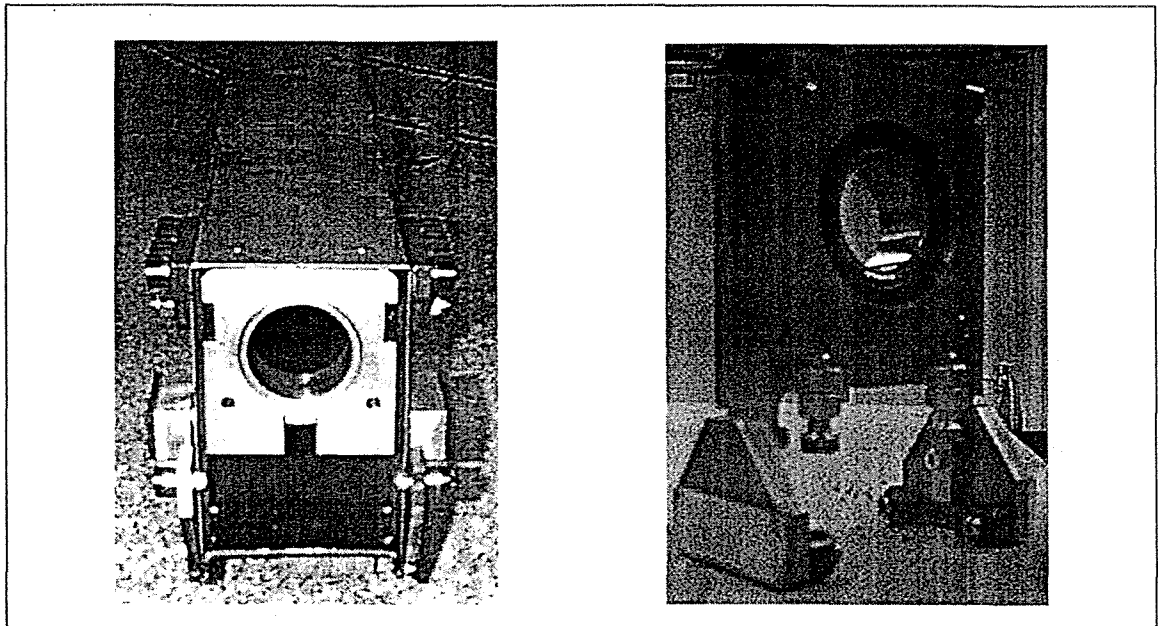
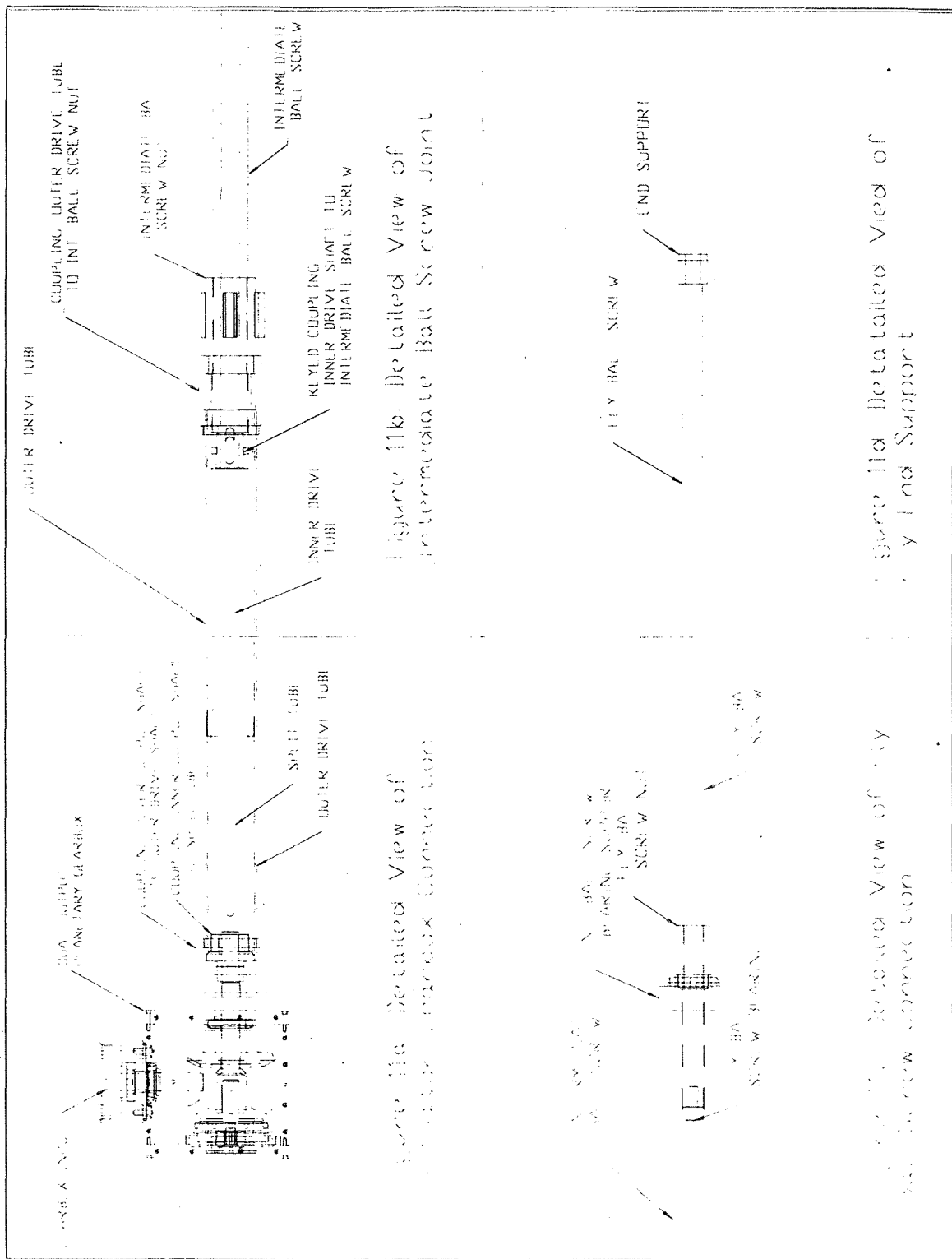


Figure 4.10: Rear Intermediate Section Fixed Support (left) and Intermediate Ball Screw Rolling Support (right)



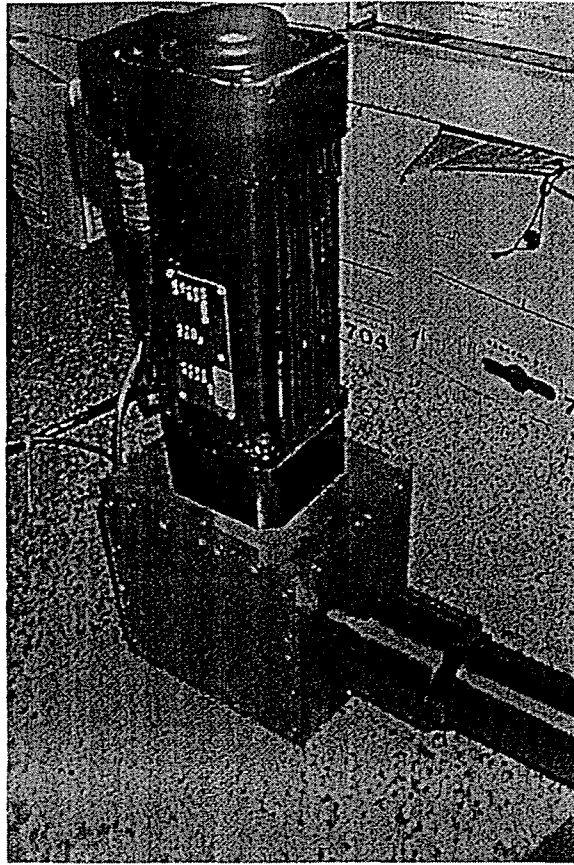


Figure 4.12: Apex 40 Servo Motor and Concentric Dual Output Planetary Gearbox Assembly

4.2.3 Concentric Output Planetary Gearbox Design

4.2.3.1 Kinematic Constraints

The detailed design of the gearbox began with specifications describing the required kinematic relationships between the input and output shafts as well as the means of achieving these relationships. From the detailed design of the telescopic actuator, it was decided to design the actuator with the smaller screw having a lead equal to one-half the lead of the larger screw. Through a simple calculation, it was shown that in order for each screw to travel out of its respective nut at the same rate, the gearbox outer output shaft should rotate at a rate of 3/2 that of the inner gearbox shaft or:

$$\frac{\omega_{outer}}{\omega_{inner}} = 1.5$$

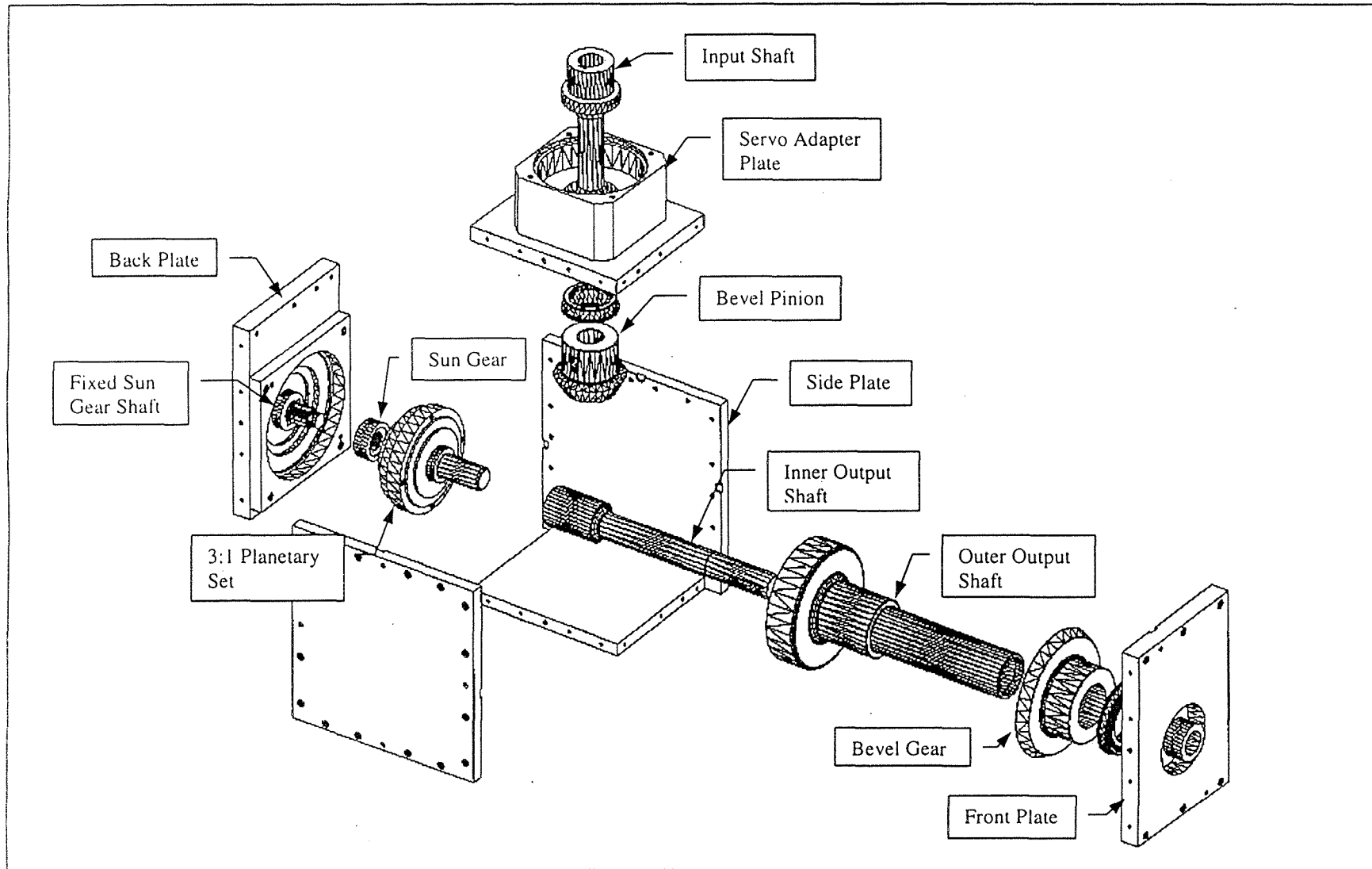


Figure 4.13: Concentric Output Planetary Gearbox

With this constraint as a design specification, a method was to be developed to generate this relationship through concentric output shafts, with minimal backlash, and a single input.

The design selected, see Figures 4.12 and 4.13, included the use of a 3:1 (conventionally driven) planetary set, and a set of 2:1 reduction bevel gears. The input shaft entered in through the top of the gearbox and drove the pinion of the 2:1 bevel gear set. The gear of this bevel gear set was mounted directly onto the outer output shaft such that the outer output shaft is constrained by the relation $\omega_{out} = \frac{1}{2}\omega_{motor}$. The other end of this output shaft was then connected to the ring gear of the conventional 3:1 planetary set. The sun gear of this set was then fixed providing the inner output shaft to be driven by the planet carrier. Therefore, the inner output shaft was constrained according to the kinematic relation, $\omega_{inner} = \frac{1}{3}\omega_{motor}$. Therefore, the required kinematic constraints for the output shafts were satisfied.

4.2.3.2 Detailed Design

The kinematic analysis had yielded a general description of the gearbox components. However, the sizing of these components had yet to be determined. The first step was to calculate the required gearbox input torque and speed based on machine specifications and the previously developed gearbox kinematics. Through this analysis, it was determined that the required motor torque was 4.95 N-m (44 in-lb). The required input speed was then calculated to be 339 rad/sec (3240 rpm). These values were then

used to select appropriate gear sets for the bevel gear reduction as well as the planetary set.

4.2.3.2.1 Bevel Gear Selection

The bevel gear set was chosen through use of manufacture's ratings as well as a detailed failure analysis based on tooth bending stresses and contact stresses. It was determined that a hardened 2:1 bevel gear set with a 127 mm (5.00 in) bevel gear would provide a factor of safety of about 2 for each of the two critical failure modes. For the tooth bending stress, the peak torque and speed were used to determine the factor of safety, while for the contact stresses (wear), the continuous duty torque and speed were used.

4.2.3.2.2 Planetary Gear Selection

Due to the limitation on fabrication of custom planetary gear sets, the gearbox was designed to use a 3:1 planetary set out of a commercially available Bayside® RA-115 gearhead. Strength and wear considerations were then derived from the manufacturer's specifications by examining the rated input torque and speeds.

4.2.3.2.3 Input Shaft

With the gear sets determined, the next step was to size the shafts that would connect them. The sizing of the input shaft was determined by the bore of the bevel pinion, torque and deflection considerations. Through a detailed calculation, it was determined that the critical design specification was not torque or deflection related. The only critical design factor was geometry. Therefore, the input shaft was sized to meet requirements of other connecting parts, such as the bevel pinion, the motor output shaft, input bearings, and the motor adapter plate.

4.2.3.2.4 Outer Output Shaft

The outer output shaft sizing proceeded in a similar manner as the input shaft with similar results. The fact that the outer output shaft had to contain the inner input shaft within, caused the dimensions to be large enough such that the stress and strain of the shaft became insignificant under the required gearbox loading. Therefore, the outer output shaft was optimized to allow for easy mating to the planetary ring gear, the bevel gear, bearings, as well as the actuator base tube. The ring gear was connected to the outer output shaft through a set of four 4.77 mm (0.188 in) diameter steel dowel pins. The bevel gear was then connected to the middle of the output shaft through a standard keyway and set screw configuration. Finally, the connection to the base tube of the actuator was attained through the application of a self-centering, tapered, locking bushing.

4.2.3.2.5 Inner Output Shaft

The final shaft within the gearbox was the inner output shaft. This shaft was simply an extender shaft for the original output shaft of the 3:1 Bayside® planetary set. The sizing of this shaft was based on a peak torque of 14.9 N-m (132 in-lb) and minimal angular deflections. Connections to the shaft included a keyed connection to the planetary set with a setscrew and a taper pin connection to the actuator split tube. Both of these connections were designed to hold at maximum operating torque with a factor of safety of two.

4.2.3.2.6 Bearing Selections

The bearing selection became rather limited with the addition of a bevel gear reduction into the system. This created the need for axial as well as radial support in the

shaft connections. To handle this combined loading, the gearbox was outfitted with a series of tapered roller bearings. The fact that the shafts were quite large eliminated the possibility of overloading the bearings and introduced a more crucial problem, underloading the bearings. If the bearings were to be loaded under the critical minimal loading, the rollers would begin to slide instead of rolling along the races. This would cause premature failure of the bearings due to wear. Therefore, the critical design specification for the bearings was to keep the loading above the minimal required loading through preloading and proper sizing. Through a detailed analysis, it was shown that the bearings would have a low enough load for virtually infinite life and were loaded enough to maintain rolling contact between the rollers and races.

4.2.3.2.7 Gearbox Housing Design

The design of the gearbox housing was centered around the two gear set arrangement and their corresponding supports. Due to the large size of the gearbox, it was decided to fabricate the box out of assembled aluminum plates. This would keep the cost and weight low. However, additional problems would need to be addressed to maintain proper gear alignment. To help ensure this proper alignment, the gearbox plates were machined from cast aluminum tool plate that is known for its great dimensional stability and flatness. On the other hand, this tool plate had disadvantages associated with weak threads on tapped holes, the inability to be anodized, and high malleability.

In addition to selecting a stable material to machine the plates, additional steps were taken in the design to ensure proper gear alignments. Dimensions for the prototype plates were all specified from a common edge as to eliminate the possibility of tolerance

accumulation. Finally, alignment pins were provided to allow for proper reassembly to the original state.

Stresses in the gearbox housing exist only from the axial loading produced by the bevel gear set as well as the tapered roller bearings. These loads were calculated and were eliminated as a critical design factor in the gearbox housing. Therefore, the gearbox housing wall thickness was determined by the bearing widths, seals, and other constraints associated with the internal gearbox components.

4.2.3.2.8 Lubrication

Lubrication specifications were derived by examining the operating speeds of the gearbox as well as maintenance considerations. Through this analysis, it was determined that the gearbox components would operate at a low enough speed as to allow for conventional grease. Grease was preferable to minimize leakage along the plate seams as well as ease the process of disassembly of the gearbox. The only question was whether the grease would work as well as oil in lubricating all of the components. There was concern that the grease would flow to the bottom of the gearbox away from the bevel gear areas. This would cause a shortage of grease for the bevel pinion.

Figure 4.14 shows an inside view of the gearbox after approximately 5 hours of use. From this picture, it was determined that the grease was remaining around the gears and that proper lubrication was achieved.

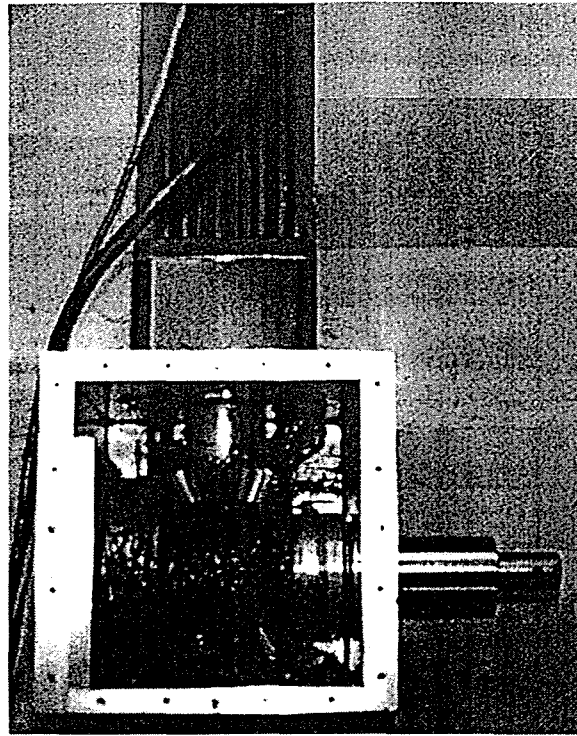


Figure 4.14: Telescopic Gearbox after Five Hours of Operation

4.2.4 Summary

The design of the novel dual concentric output gearbox began from a specification of the required output kinematics and proceeded through detailed analysis and thought to form a complete working prototype. The key to the gearbox was the application of a conventional 3:1 planetary gearbox that was taken from a production gearhead. This gear set was driven through the ring gear, with the sun gear fixed to prescribe motion to the inner output shaft. On a detailed basis all gears, shafts and bearings were sized accordingly to ensure long life and high robustness.

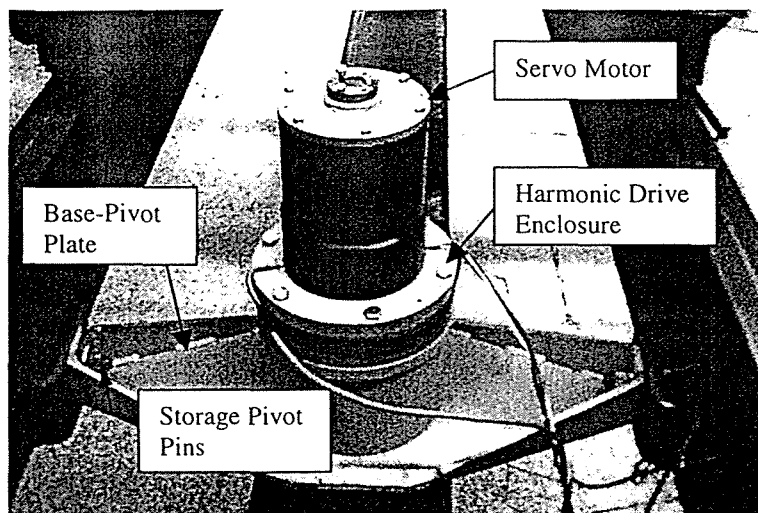


Figure 4.15: Rotational Actuator System

4.3 Rotational Actuator System

Detailed calculations for the Rotational Actuation System can be found in Appendix A, pages A-19 through A-25.

4.3.1 Specifications

Design of the rotational actuation system, Figure 4.15, began with calculations of the necessary torque requirements to meet the machine specifications. Within these calculations, two critical operating scenarios were considered. The first scenario is at maximum extension where the rotational inertia of the arm is the largest but the angular acceleration is the lowest. The second scenario occurs at the minimum extension where the rotational inertia is lowest and the angular acceleration is highest. Through a detailed analysis, the first scenario at maximum extension was proved to require the highest torque. The maximum required torque to actuate the arm to 0.91 m/s (3 ft/s) in 0.5 seconds was calculated to be 895 N-m (7951 in-lb).

In addition to handling the torque requirements of the arm, the rotational actuator must be capable of maintaining the required accuracy. To maintain this accuracy, two factors were considered, backlash and encoder resolution. Both of these factors affect the accuracy of the arm at maximum extension. Therefore, a large gear reduction should be used to increase the accuracy.

The final specifications used to design the rotational actuation system concerned robustness, size, weight, cost and commercial availability. Through the extensive trade-off analysis, it was shown that the harmonic drive gear reducer would best satisfy these specifications and be capable of attaining the required torque and accuracy.

4.3.2 Harmonic Drive Selection

The harmonic drive, Figure 3.8, was chosen because of its high gear reduction capabilities, compact space requirements and low backlash. This section presents the selection of the appropriate model for this application. The details of operation will not be discussed further here, the reader is referred to Chapter 3 for a detailed explanation.

4.3.2.1 Torque Requirements

The selection of the appropriate harmonic drive was performed concurrently with the selection of the motor. The torque calculations yielded a maximum required torque of 895 N-m (7951 in-lb). The harmonic drive was then selected such that the rated output torque would not exceed this value. The gear ratio of the harmonic drive was dependent on the torque requirements as well as the maximum output speed of the motor. It was desired to obtain the largest gear ratio possible while still maintaining the necessary speed in order to increase the stiffness of the arm and provide better workspace accuracy.

Through a careful consideration of the motor and performance specifications, a gear ratio of 60:1 was selected.

4.3.2.2 Speed Requirements

The speed requirements for the rotational joint were defined from the project specifications and the rotational velocity at minimum extension. Through a simple calculation, the maximum rotational speed of the arm was calculated to be 0.348 rad/sec (3.3 rpm), which was then translated to an input speed of 21 rad/sec (199 rpm). From a comparison against the manufacturers acceptable speeds, it was determined that this design was well within the design limits of the harmonic drive which is rated at speeds up to 3000 rpm.

4.3.2.3 Accuracy Requirements

To determine the effect of the harmonic drive backlash on the workspace, the input backlash was transferred through the harmonic drive gear reduction and translated into a x-deviation along the road surface at maximum extension. In order to meet the project specifications, the x-deviation must be within 3 mm (0.125 in). For the Harmonic Drive - model 65, the input backlash was given as 13 arc-min. The calculation was performed to yield a maximum x-deviation of 0.43 mm (0.017 in). Therefore, the harmonic drive backlash would satisfy the project specifications.

4.3.3 Servo Motor

Selection of the proper servomotor was constrained by two factors that separated this design from conventional servo motor applications. These factors included very low speed requirements and high torque requirements. To fit this application, a Dynaserv®

DR-5030B Direct Drive Brushless motor was selected. The motor specifications include a rated speed of 240 rpm and a peak output torque of 30 N-m (22 ft-lb).

4.3.3.1 Torque Requirements

The torque requirements for the servomotor were defined as before by the performance specifications as well as the gear reduction ratio. Although the selections of the motor and gear reduction unit were performed in parallel, the details are given here with the assumption of a pre-selected gear ratio. With the gear reduction specified as 60:1, a quick calculation was performed to yield the required motor torque as 15 N-m (11 ft-lb). The motor specifications rate the peak torque output at 30 N-m (22 ft-lb) with the continuous torque ratings at two-thirds of the peak value, or 20 N-m (14.7 ft-lb).

Therefore, the motor will have ample torque to meet the machine performance requirements.

4.3.3.2 Speed Requirements

To determine the maximum required speed of the motor, the arm maximum speed at minimum extension was converted through the pre-selected 60:1 ratio to attain a value of 20.9 rad/sec (3.32 rev/sec). This value was then compared to the rated speed of the motor, 25 rad/sec, to ensure that the motor would be adequate.

4.3.3.3 Accuracy Requirements

The final consideration in the selection of a motor was encoder resolution. As mentioned earlier, backlash and encoder resolution were the two factors that would combine to give position error at the end-effector. The motor's encoder resolution, 278,528 steps/rev, was translated through the gear reduction ratio and the maximum extension of the arm to determine the positioning capabilities of the motor. Assuming

zero backlash, the calculation yielded a positioning resolution on the workspace of 389 steps/mm (10132 steps/in), or 0.0025 mm (9.9E-5 in).

4.3.4 Summary

The design of the rotational actuator system was directed through definition of the project specifications and rotational specifications. The servomotor and Harmonic Drive selections were performed in parallel in order to obtain the most ideal configuration. With the selection of a 60:1 gear reduction and a specialized servomotor, all of the required specifications were met and exceeded. The finished system specifications include a peak torque of 1800 N-m (1320 ft-lb), maximum arm angular velocity of 25 rad/sec, with mechanical workspace accuracy of ± 0.22 mm (0.009 in).

4.4 Vehicle Integration and Stowage System Design

Conceptual design of the vehicle integration and stowage system had led to the development of an idea to use a curved rail upon which a roller truck would run to track the radius formed by the end of the base section. The arm was then connected to the roller truck through a hinged linkage. The other component of the vehicle integration included the design of the rotational pivot mount. A key part of this mount was a compound joint that would allow the arm to rotate in the horizontal plane, as well as rotate in the vertical plane for stowage between the frame-rails. The task at hand was to transfer these qualitative ideas into a detailed working design capable of meeting all specifications. Calculations for the Vehicle Integration and Stowage System can be found in Appendix A, pages A-42 through A-43.

4.4.1 Specifications

The specifications for the vehicle integration and stowage system were separated into two categories describing the end support and the rotational pivot discretely. The end support specifications required the support to hold the arm through the entire workspace. To accomplish this, the end support was required to track the radius formed by the end of the arm. In addition, the end support must allow for a simple stowage design that is highly reliable when in the unstowed position. In other words, the end support should not require active means to maintain the vertical position of the arm.

The pivot support specifications assured that the pivot was strong enough to handle the loading of the arm at all workspace locations, provided for easy mounting of the rotational actuator, and pivoted such that both horizontal and vertical motion of the arm is allowed.

4.4.2 Base-end Pivot Plate

The pivot plate, Figure 4.15, was designed according to calculations yielding the maximum reaction force at the pivot. This force varied for different extensions with the arm creating a maximum upward force of 2.1 KN (477 lb), from Figure 4.2, to a downward force of about 0.9 KN (200 lb) at full retraction, to support the weight of the arm. Horizontal motion was achieved by direct mounting of the rotational actuator system through a hole in the plate. Vertical motion of the arm was allowed through the two pivot bolts that connect the plate to the frame-rails.

4.4.3 Curved Rail Support System

The design of the curved rail, Figure 4.16, was derived through consideration of the project specifications and manufacturing considerations. From an early stage, it was



Figure 4.16: End Support System-Curved Rail

realized that the end support would be highly critical in maintaining the height of the manipulator arm with respect to the workspace. The idea to use a curved rail would require that the radius of the rail exactly match the radius tracked by the arm or the result would be up and down motion in the arm. To solve this problem, the roller truck was designed to support the arm through a moment applied onto a curved support plate, see Figure 4.17. This design used a double row of rollers inside the roller truck to support the moment imposed by the plates extending to support the arm. Axial support for the roller truck required only a single roller that tracked the edge of the support plate. This edge was known to capable of being accurately manufactured to the proper radius either by flame cutting or machining.

4.4.4 Stowage System

The key component to the stowage system, Figure 4.18, was the hinged plates which allowed the arm to be raised and eliminated the need for active support when in normal crack sealing operation. To raise the arm, a cable winch was provided onto the

back of the roller truck. The cable from this winch extended down behind the plates to the bottom of the lower hinge plate. As the cable was raised, the hinged plates were forced to buckle out toward the end of the arm by the shortening of the cable. The arm was then allowed to rise until the top of the base section contacted the bottom of the winch mount. A rigid connection was then made between the arm and the truck frame through a simple pin connection to ensure safe transport.

Strength considerations were addressed through a detailed analysis of the end support loading. The critical components in the design were the hinged plates and the roller truck. The hinged plates were designed to force the connecting pins into direct shear through close alignment of the interconnecting joints. Through a quick calculation of the maximum shearing stress, it was determined that 9.5 mm (0.375 in) diameter rods would be sufficient to support the maximum loading. A factor of safety of four was calculated based on material yield strength of 372 Mpa (54 ksi) and the Maximum Shear Stress Theory.

The roller truck was analyzed in a similar manner by transferring the moment of the plate loading force into radial loading on the bearings. This allowed the bearings, shafts and plate walls to be sized accordingly. Another critical section that was addressed was that of the backbone of the roller truck. The C-shape of the roller truck under moment loading will try to open up, thus bending the backbone of the roller truck. To prevent this, the backbone was designed with a factor of safety of 2.5 based on maximum loading.

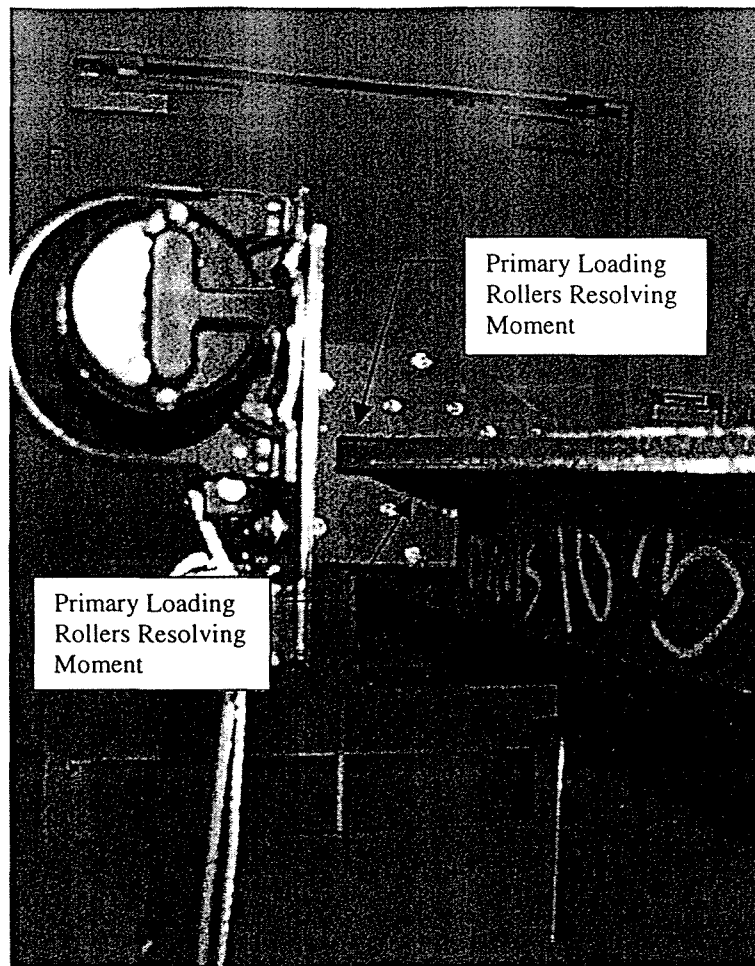


Figure 4.17: Roller Truck Directing Loading into Curved Plate

4.4.5 Summary

The vehicle integration and stowage design had resulted in a clean and robust solution for supporting and stowing the OCCSM Telescopic R- θ Manipulator. Detailed design was initiated through a complete loading analysis to determine the maximum support loading. This loading was then used along with the system specifications to ensure a safe design that would meet all specifications.

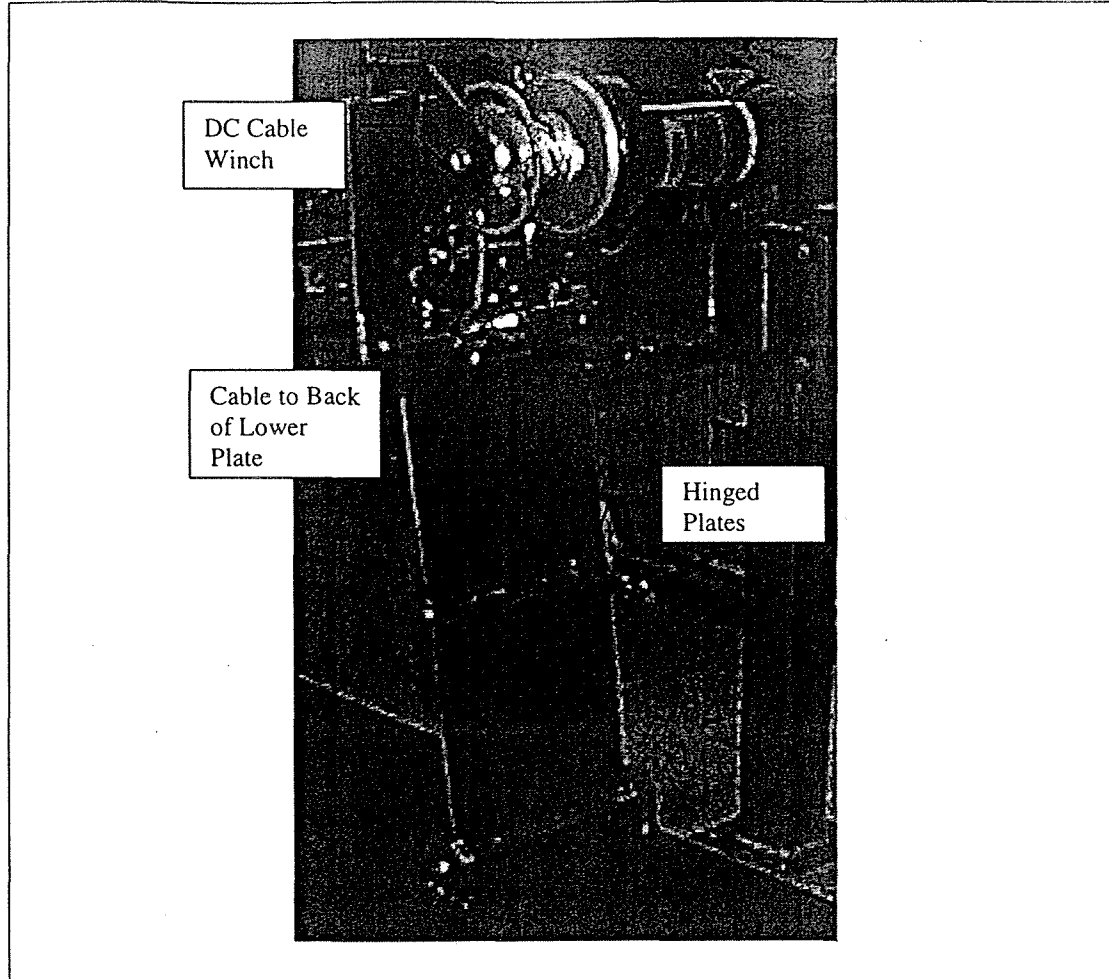


Figure 4.18: OCCSM Stowage System

4.5 Summary

The detailed design of the OCCSM Telescopic R- θ Manipulator had been completed and the working prototype was ready for testing. The machine was designed through detailed analyses and brainstorming all in order to try to develop a machine that could perform up to specifications. From this point, Chapter 5 will be used to discuss the testing that was performed to evaluate the successfulness of the first prototype Telescopic R- θ Manipulator. Furthermore, conclusions from these tests will be discussed on a subsystem specific level with a broader based project conclusions and recommendations presented in Chapter 6.

CHAPTER 5: EXPERIMENTAL VERIFICATION

5.1 Telescopic Arm Structure

The telescopic arm structure was evaluated through both qualitative and quantitative measurements. Qualitative measurements included observations based on dynamic actuation of the arm and static robustness considerations. On the other hand, quantitative testing was performed statically to determine the stiffness of the structure and the overall deflections under loading. Data from this quantitative analysis was then recorded and plotted to yield insight into the non-linear stiffness of the beam as a function of radial extension.

5.1.1 Qualitative Analysis

Qualitative analysis of the arm began at the beginning of fabrication and continued through the prototype assembly and operation. This analysis included testing of the robustness, quality, and performance of the various parts that comprised the telescopic arm including arm sections and joint connections.

5.1.1.1 Arm Sections

A major concern to be tested in the qualitative analysis was that of localized buckling in the sidewalls of the Intermediate and Fly sections. To address this concern, each of the sections was loaded in a test setup with up to three times the designed loading.

In addition to the concern of sidewall buckling, all sections were inspected to determine dimensional accuracy and integrity. Each section dimension was allowed 0.76 mm (0.030 in) deviance from nominal for the entire length. This strict tolerance was

necessary to ensure that the section joints would remain in contact through the entire stroke of the arm and that the beam sections would extend out straight.

5.1.1.2 Joint Connections

The joint connections were another critical component of the telescopic arm. Qualitative analysis included inspection of the various support systems along the entire stroke of the telescopic arm. For this inspection, the aim was to ensure that the supports were contacting the sections for the entire length such that the sections had no “play” or movement in the joints.

5.1.1.3 Qualitative Conclusions

The qualitative analysis from an early stage in the project led to a major design change in the formation of the Intermediate and Fly steel composite sections. Through the localized buckling test, it was found that the 0.76 mm (0.030 in) wall thickness was too thin to support the concentrated loading at the primary support rollers. The result was localized buckling in the sidewalls directly above the center of the roller truck. This led to a revised design in which the wall thickness was increased to 1.52 mm (0.060 in). The test was successfully repeated with the improved sections with up to three times the design loading.

The other main concern was that of the welds which connected the bottom channel to the thin wall U-section for the composite beams. The original design called for a resistance seam weld along the bottom of each composite section. However, due to availability, this continuous seam weld was replaced by an array of spot welds spaced about 25 mm (1.0 in) apart. To test these welds, the sections were loaded with up to three times the designed loading. The only problems that occurred were in locations where

there was poor penetration of the welds. As a result, these welds were reinforced and the testing was successfully repeated.

Finally, each section was inspected to determine dimensional accuracy. From this inspection, it was determined that the great care must be taken in the manufacturing to ensure proper sizing. Each section was continuously remade until the desired tolerances were achieved.

5.1.2 Quantitative Analysis

5.1.2.1 Vertical Stiffness

The vertical stiffness at various extensions was measured by applying known loads to the end of the arm and measuring the corresponding deflection. The loading was applied through a pneumatic air cylinder for which the pressure could be varied to achieve precise force variations. To measure the corresponding deflection, a travel dial indicator was used. The results of these experiments were then recorded, see Table 5.1, for various extensions of the arm. This data was then plotted in force vs. deflection plots, see Figure 5.1, from which a linear line was fit to the data to yield the stiffness of the arm at each location. Figure 5.2 shows a plot of the arm stiffness vs. radial extension from which it is easy to depict the nonlinearity. Finally, in Figure 5.3, all force-deflection data was plotted on the same scale from which it becomes clear of the increasing stiffness as radial extension decreases due to the arm's telescopic construction.

5.1.2.2 Quantitative Conclusions

The results of the data clearly showed a nonlinear deflection characteristic for the telescopic arm. This nonlinearity is mainly attributed to the nested telescopic sections which become increasingly stiff as the arm is retracted. The data showed a slightly larger

Radial Extension(m)	Pressure (kPa)	Force (N)	Deflection (mm)
4.57	0.00	0.00	0.000
4.57	13.78	36.70	0.406
4.57	27.56	73.40	0.787
4.57	41.34	110.09	1.219
4.57	55.12	146.79	1.575
4.57	68.90	183.49	1.981
4.57	82.68	220.19	2.362
4.57	103.35	275.23	2.972
4.57	137.80	366.98	3.810
4.57	172.25	458.72	4.826
4.57	206.70	550.47	5.766
4.57	241.15	642.21	6.629
4.57	275.60	733.95	7.518
4.57	310.05	825.70	8.407
4.57	344.50	917.44	9.144
4.57	378.95	1009.19	9.982
4.57	413.40	1100.93	10.541

Table 5.1: Force vs. Deflection Data for $r=4.57m$

deflection at maximum extension than what was anticipated, about 135% of the predicted deflection. Possible sources of this discrepancy lie in the assumptions made for the calculations. The calculations assume infinitely stiff joints and zero support deflection, neither of which is true in the prototype arm. It was suspected that the majority of the error was occurring in deflection of the end support due to deflection of the mock-up truck frame. To quantify this, a dial indicator was placed under the end support, see Figure 5.4, and the arm was loaded at both the maximum and design loading cases at maximum extension (6.35 m (250 in)). The end support deflection for these two cases was found to be 3.2 mm (0.125 in) and 1.27 mm (.050 in), respectively. These values were then translated into vertical deflection at the end of the arm by assuming rotation about the rotational pivot point. The contribution of these deflections at the end of the arm were then calculated to be 9.7 mm (0.383 in) at maximum loading and 3.9 mm (0.150 in) for design loading. The data at this loading and extension was then corrected

for the rotation and the measured deflection was found to only be 7% higher than calculated values.

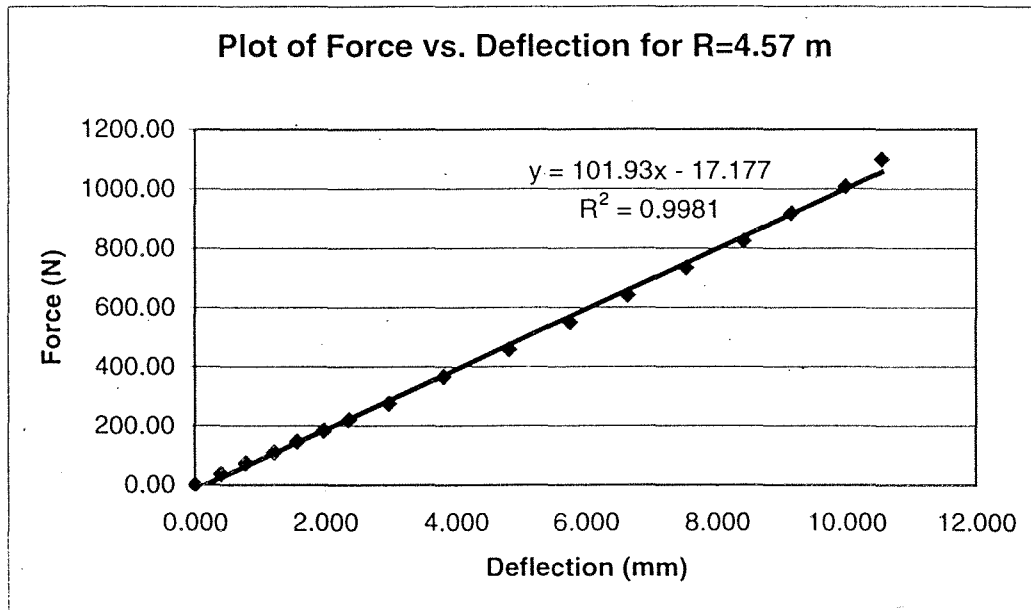


Figure 5.1: Force vs. Deflection Plot for r=4.57m

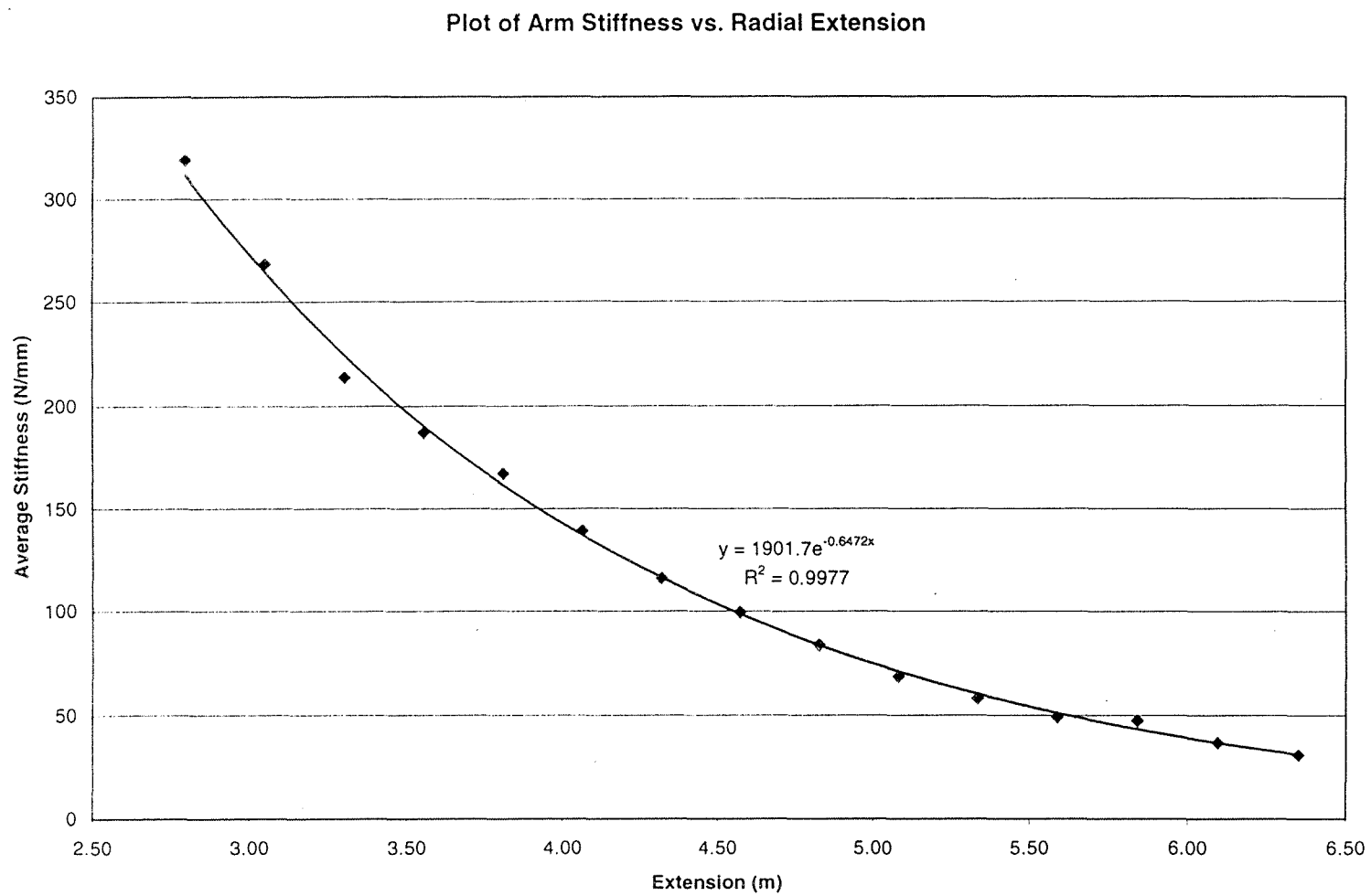


Figure 5.2: Plot Depicting Nonlinear Stiffness of Arm

Plot of Force vs. Vertical Deflection for Various Beam Extensions

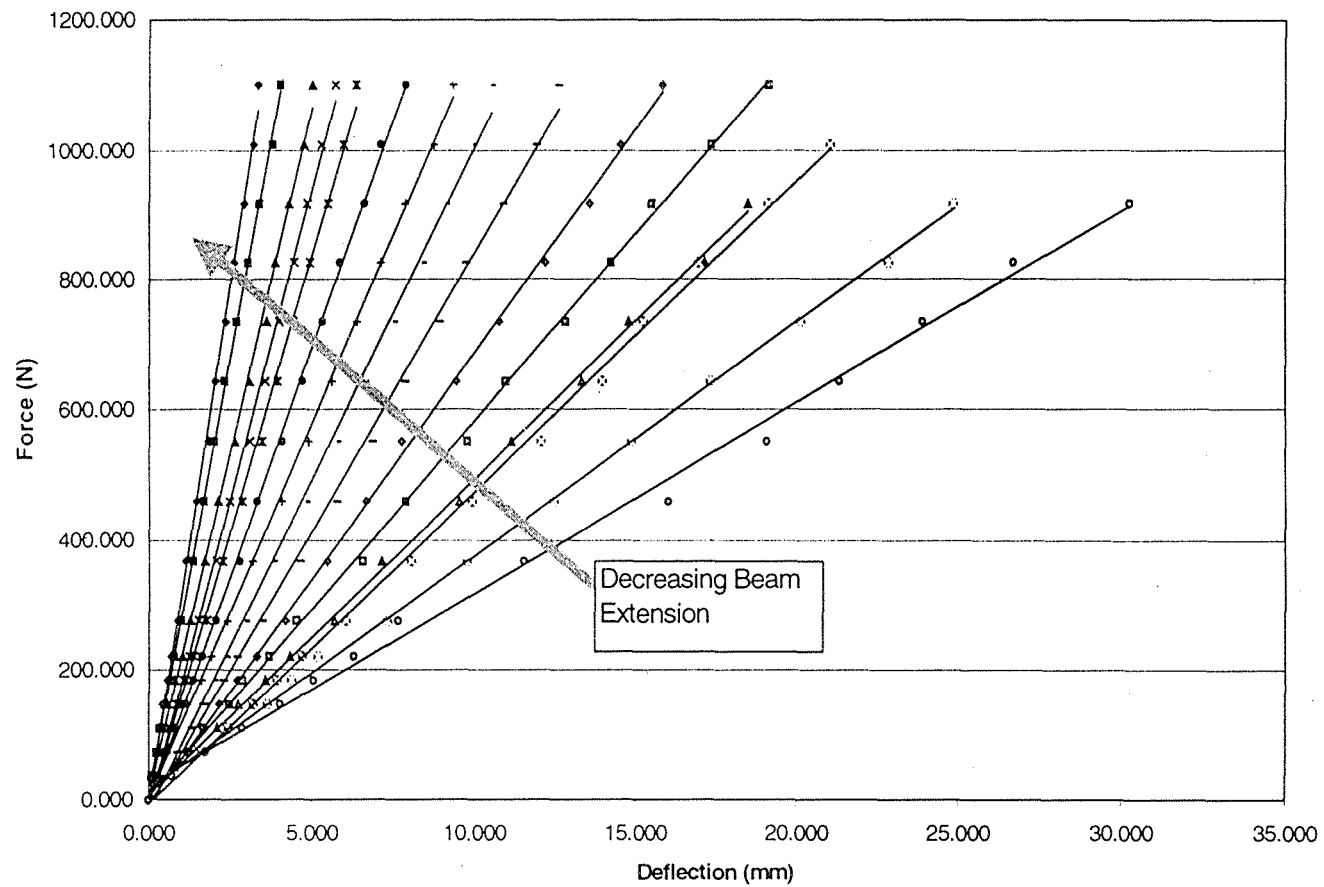


Figure 5.3: Plot of Force vs. Deflection Data for Various Beam Extensions

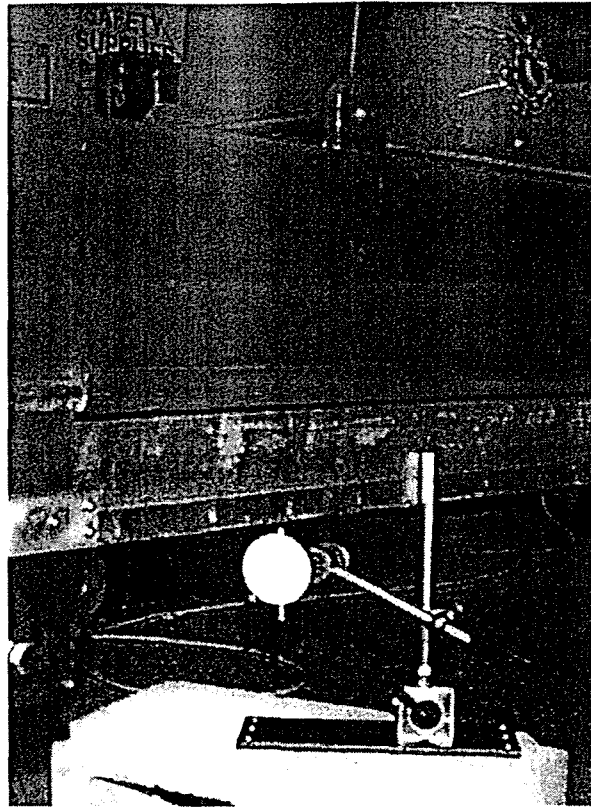


Figure 5.4: End Support Deflection Measurement during Vertical End Deflection Test

5.2 Telescopic Ball Screw Actuator

5.2.1 Qualitative Analysis

5.2.1.1 Qualitative Observations

The telescopic actuator was evaluated qualitatively from the start of the assembly phase through its operation inside the telescopic arm. Qualitative observations such as noise, vibrations and misalignments were recorded.

5.2.1.2 Qualitative Conclusions

The telescopic ball screw actuator operated very well from a qualitative analysis. All of the components assembled with ease and fit well into the arm. The only major problem was due to misalignment of the actuator supports caused by poor assembly of the telescopic arm sections. This misalignment caused the actuator to bend at large

extensions where the stiffness was reduced. To correct the problem, the sections will need to be readjusted to extend straight.

Another problem that was encountered due to misalignment and poor shaft concentricity was low amplitude vibrations in the arm. The vibration was of a higher frequency at smaller extensions and reduced as the arm was extended. This is consistent with the reduced stiffness in the actuator joints as it is extended. The problem was narrowed down to the curvature in the outer drive tube and support misalignment. Both of which are easily remedied.

5.2.2 Quantitative Analysis

5.2.2.1 Positioning Accuracy

The positioning accuracy for the telescopic actuator was evaluated through the use of a Cable Extension Transducer (CET) fixed at the base section as shown in Figure 5.5. The CET cable was then attached to the end of the arm to measure the extension concurrently with the drive motor's encoder. The arm was then commanded through the entire workspace to generate two sets of positioning data, one set for extension and another for retraction. The results are shown in Figure 5.6.

5.2.2.2 Actuator System Backlash

The data used above in the accuracy verification experiment was then used to determine the average actuator system backlash. Since the data was collected for both extension and retraction, the difference in the CET readings for each commanded position would represent the system backlash. The system backlash was evaluated from these seventy data points and averaged to yield an average linear system backlash of 0.381 mm (0.015 in).

5.2.2.3 Quantitative Conclusions

The data recorded for the accuracy validation of the telescopic actuator showed an increasing error as the arm was extended. The accuracy of these CET measurements is given by the manufacturer as 0.003% of the maximum extension capabilities of the CET. This calculates to an accuracy of ± 0.254 mm (0.010 in) for the CET used. This accuracy error was not enough to account for the over 2 mm (0.078 in) error measured by the CET.

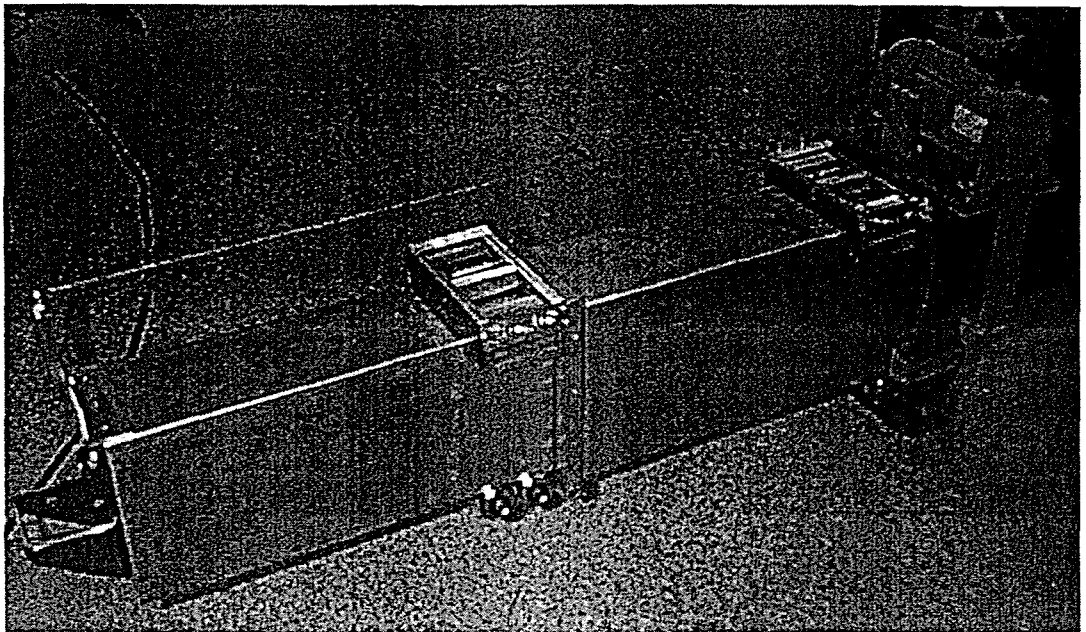


Figure 5.5: CET Measuring Apparatus for Validation of Positioning Accuracy

One possible source of this error relates back to the misalignment in the ball screw actuator. If the ball screw was not traveling in a straight line, the measurement by the CET would be greater than the actual translate distance. This would account for some of the error present and is very plausible considering the misalignment in the telescopic sections.

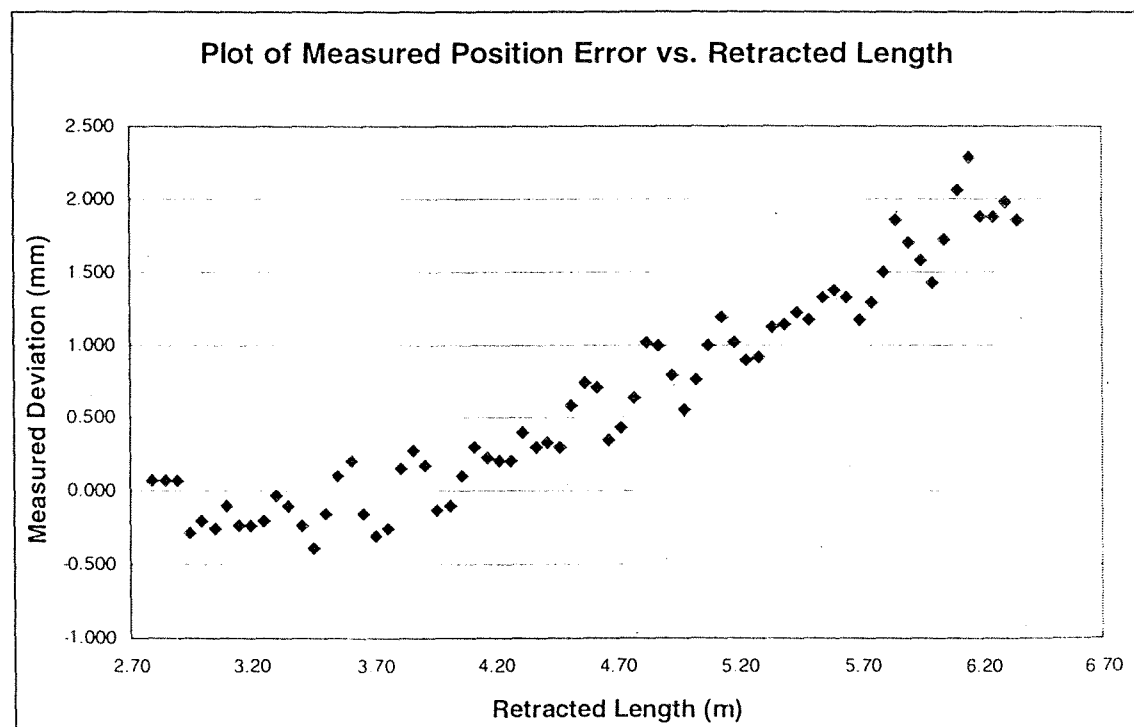
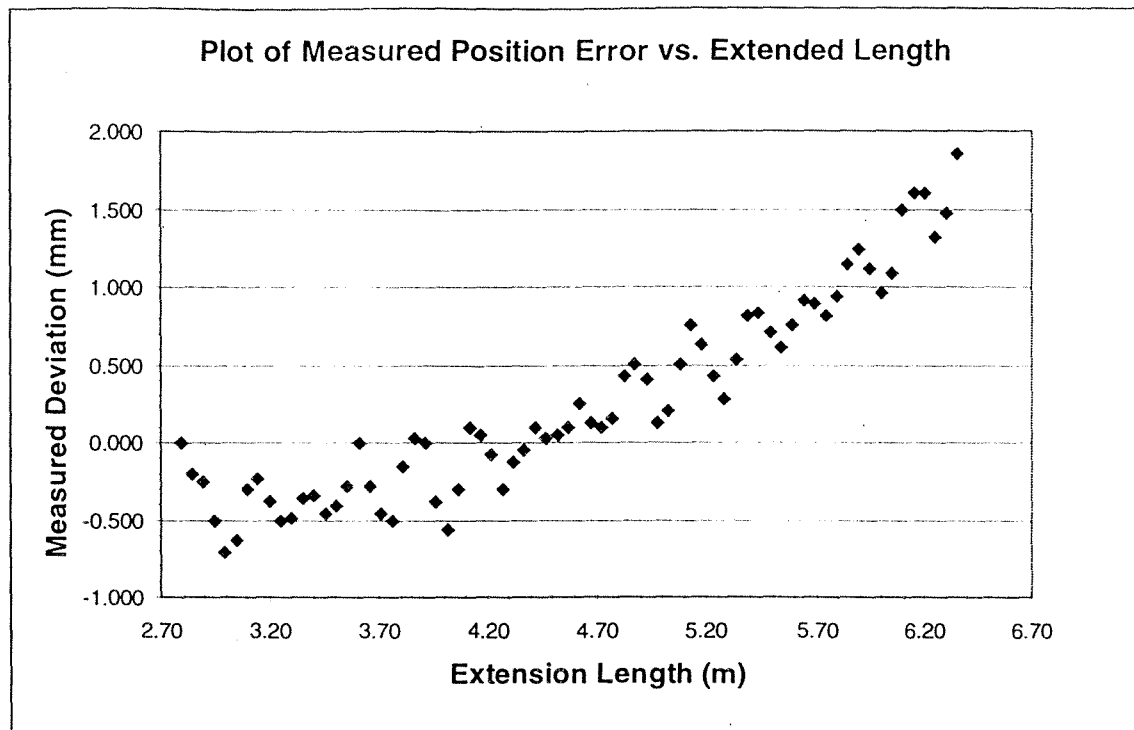


Figure 5.6: Plots of Measured Error vs. Extended (Top) and Retracted (Bottom) Beam Length

5.3 Concentric Output Planetary Gearbox

5.3.1 Qualitative Analysis

Evaluation of the planetary gearbox began in the assembly phase and continued through operation. The evaluation concerned alignments, ease of assembly and fits in the assembly phase and included factors such as vibrations and noise in the operation phase.

5.3.1.1 Pre-Operation

Qualitatively, the assembly of the gearbox was very smooth. The setting of the center distances for the bevel gear reduction was an iterative and tedious process that was highly reliant on the machining tolerances of the gearbox plates. In addition, the support for the ring gear and outer output shaft had to be replaced with a tapered roller bearing that could support an axial load. With the radial bearing, as the front gearbox plate was tightened, the outer output shaft was forced towards the back of the gearbox, thus, locking the radial bearing (see Figure 4.13 for clarification).

5.3.1.2 Bevel Gear Noise

The dynamic testing of the gearbox was very successful except for the noise resulting from the bevel gear reduction. Due to the fact that the noise was louder in one direction than the other, it was assumed that there was some slight misalignment in the shafts. To remedy this, the gearbox was disassembled and readjusted until the noise was at an acceptable level.

5.3.1.3 Qualitative Conclusions

The qualitative analysis through the assembly and operation phases resulted in a number of modifications to the gearbox in both design and adjustments. Misalignment in the gearbox shafts was blamed for the high noise emission from the gearbox. However,

this noise was reduced to an acceptable level by more closely setting the correct center distance of the bevel gears.

5.3.2 Quantitative Analysis

5.3.2.1 Gearbox Backlash

The gearbox backlash was measured directly off of the gearbox shafts using a dial indicator. In this method, the gearbox input shaft was fixed, while the two output shafts were allowed to rotate. A thin plate was attached to each output shaft, from which horizontal deflection was measured. The measurement was repeated five times for each shaft and recorded. This data was then averaged and converted through trigonometry to find the output shafts' backlash. The measured outer output shaft had an average backlash of about 8 arc-min and the inner output shaft had an average backlash of about 11 arc-min. These values are in line with expectations assuming that the bevel gears are assembled correctly with 0.127 mm (0.005 in) backlash in the teeth. Translating this value to the outer output shaft yields a backlash of 6.8 arc-min.

5.3.2.2 Quantitative Conclusions

This measured backlash correlates well with the manufacturers prescribed backlash for the planetary set as well as the bevel gear set. It is slightly higher than these specifications, but well within acceptable limits.

5.4 Vehicle Integration and Stowage System

5.4.1 Qualitative Analysis

5.4.1.1 Curved Rail Support

Qualitative testing of the curved rail included visual inspections from a static loading as well as from dynamic operation of the arm. Statically, the rail support seemed

to provide a reliable support for the end of the arm with no visible deflections at maximum loading. On other hand, dynamic testing resulted in a stick-slip motion of the roller truck on the curved plate. This stick slip motion of the roller truck was then propagated into the arm to yield a jerking motion at the tip of the arm.

5.4.1.2 Stowage System

The stowage system was tested by raising and lowering the arm through the use of the DC winch system. The hinged plates folded as expected resulting in smooth lifting and lowering of the arm.

5.4.1.3 Rotational Pivot Plate

The rotational pivot plate was inspected by operating the arm throughout the workspace and into the storage position. The joint provided a rigid support throughout the workspace with minor deflections detected around the pivot hole during the vertical deflection analysis. The only problem with this pivot plate was the lack of reinforcing of the frame rail around the connection points. However, this frame was merely a mock-up of the real truck that is expected to have reinforced frame rails.

5.4.1.4 Qualitative Conclusions

There was only one main problem that surfaced through the evaluation of the curved rail support. Stick-slip motion of the roller truck caused horizontal vibration at the tip of the arm. The rail and roller truck were inspected and the problem was determined to be the curved plates rough surface. The plate is made from hot rolled steel and as such has scale that is causing the roller truck to stick as the scale loosens on the plate. To solve this problem, it has been proposed to machine the curved plate on the top and bottom surface.

5.4.2 Quantitative Analysis

5.4.2.1 Stowage Time

The stowage time was measured using a hand crank through the winch as well as through DC power. The hand crank required minimal force through a significant number of rotations and took about 3 minutes to fully store the arm. Using the DC Winch, the arm was stowed in less than 1 minute with virtually no effort.

5.4.2.2 Quantitative Conclusions

The stowage system operated well through stowage system testing. It remains to be determined if the winch is required or if a simple hand crank should be used. The advantages of the winch in less effort, faster stowage and possible automatic control are virtually cancelled out by the wiring requirements necessary to power the winch.

5.5 Summary

Testing of the first prototype arm was based on qualitative evaluations as well as quantitative experiments. Each of the three main systems that comprise the arm was tested and in each case, either design changes or suggestions for changes were made. The major quantitative testing was limited to a vertical stiffness calculation for the arm and telescopic actuator accuracy verification due to time constraints. Future testing to include structural vibration analyses and dynamic end-effector accelerations through operation would be of great value to future development of the OCCSM.

CHAPTER 6: CONCLUSIONS AND RECOMMENDATIONS

This thesis has presented the development of the first prototype R- θ telescopic manipulator arm from concept phase through detailed design, testing and test conclusions. This Chapter presents project-wide conclusions of the total R- θ telescopic manipulator concept and proceeds with recommendations for future research into second-generation prototypes as well as enhanced testing of the current prototype.

6.1 Conclusions and Recommendations

6.1.1 Project Goals

The goal of this project was to produce an operator controlled crack sealing machine with the aim of increasing the productivity, quality, and safety of current crack sealing operations while maintaining affordability. The most important phase in this quest was the design and fabrication of the R- θ Telescopic Manipulator. Through extensive research, conceptual design, detailed design, and testing, the first-generation full-scale R- θ telescopic manipulator arm has been successfully lab tested and proven to meet or exceed all critical project specifications.

6.1.2 Telescopic Sections Design / Performance

Preliminary crack following has shown excellent arm response and tracking. The main drawback of this prototype is the lack of manufacturing precision in the telescopic sections and the complexity of the joint supports. The sections were conceptualized around the need for rapid prototyping to prove the concept. The next step in this progression is to reevaluate the conceptual design selection. It is recommended that

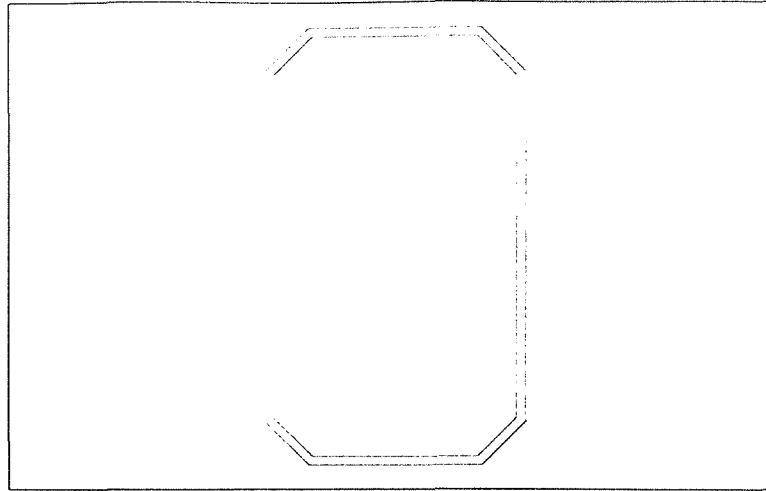


Figure 6.1: Improved Telescopic Beam Cross Section

aluminum open-form extrusions be considered. Although these sections will not offer the high stiffness to weight ratio of steel, they can be held to far higher dimensional tolerances. In addition, these sections will allow the complexity of the joint connections to be reduced by breaking the corners of the section as shown in Figure 6.1. This would combine the horizontal and vertical support systems together to further reduce the weight and simplify the design.

6.1.3 Actuation Systems / Performance

The actuator systems work very well in the prototype R- θ Telescopic Arm. The rotational actuation system exceeds all performance specifications and proves to be a clean and efficient design. The telescopic ball screw actuator has a few minor tuning problems that are related to the telescopic beam sections. Since the beam sections provide the support for the actuator components, it is very critical that they be aligned straight and true. The result of this misalignment is a whip type oscillation at larger extensions, corresponding to less joint stiffness in the sections as well as the actuator.

With this exception, the actuator operates very well, meeting all performance specifications.

The only recommendation concerns the fabrication of the telescopic ball screw actuator. It is recommended that research be directed into reducing the cost of fabricating the hollow ball screw, possibly through grinding the threads onto a center-less ground tube. This would drastically reduce the cost of the actuator. In addition, V-thread screws can be substituted for the ball screws to reduce the cost. However, these screws will sacrifice positioning accuracy and efficiency. In addition, at the time of this research, V-thread screws were not available in leads up to 51 mm/rev. This will require higher rotational velocities and thus more precise alignment of the supports.

6.1.4 Vehicle Integration / Performance

The vehicle integration system was found to be a very robust, economical and clean solution to supporting and stowing the telescopic arm. Preliminary operation has shown problems associated with the raw finish on the roller plate. The current roller plate, made from hot roll steel, has problems associated with pitting and a general bad surface finish that causes the roller truck to move in a stick-slip fashion at slow speeds. This induces a vibration in the arm and affects end-effector movement.

To alleviate this problem it is recommended that the surfaces of the support plate be machined. In addition, research should be directed into increasing the side stiffness of the hinged plates in an effort to provide more smooth motion. However, it is anticipated that the former suggestion will alleviate the problem.

6.1.5 Further Testing

Testing of the current R- θ telescopic manipulator presented in this thesis was limited. It is recommended that further testing be performed to quantify the static and dynamic behavior of the arm under varying conditions. It is recommended that the horizontal stiffness, vibrational responses / natural frequency, true actuator positioning accuracy, as well as frame deflection under loading all be researched to yield further insight into possible design improvements for the second generation R- θ Telescopic Manipulator.

REFERENCES

- Kane, Thomas R. and David A. Levinson. Dynamics: Theory and Applications. McGraw-Hill, Inc., 1985.
- Roarke, Raymond J. Formulas for Stress and Strain. McGraw-Hill, Inc., 1938.
- Shigley, Joseph and Charles Mischke. Mechanical Engineering Design. New York, McGraw-Hill, Inc., 1989.
- Technology Development Center. Preliminary Market Report: Commercialization of Road Maintenance Technology-Crack/Joint Sealing Devices. Technology Development Center, 1993.
- Timoshenko, Stephen. Theory of elasticity. New York, McGraw-Hill, Inc., 1934.
- Velinsky, S. A. Fabrication and Testing of Maintenance Equipment Used for Pavement Surface Repairs. *Final Report of SHRP H-107A*, National Research Council Strategic Highway Research Program, Washington D.C.

APPENDIX A CALCULATIONS

TABLE OF CONTENTS

Telescopic Arm Structure Calculations

Beam Cross-Sectional Properties	A-1
Deflection Analysis-End Load	A-4
Deflection Analysis-Distributed Load.....	A-6
Deflection Analysis-Reaction Force	A-8
Telescopic Arm Stress Analysis.....	A-11
Joint Connections Loading Analysis.....	A-14
Torsional Analysis of Telescopic Arm.....	A-18

Rotational and Telescopic Actuation Calculations

Rotational Motor / Gearbox Specifications.....	A-19
Calculation for Rotational Inertia as a Function of Radial Extension.....	A-21
Rotational Axis Torque Requirements	A-24
Telescopic Actuator System.....	A-25
Ball Screw Actuator: Kinematic Analysis.....	A-27
Gearbox Calculations	A-30
Gearbox Bevel Gear Analysis	A-32
Shaft Reactions (FBD)	A-35
Shaft Strengths	A-37
Planetary Analysis.....	A-39
Split Tube Analysis	A-40

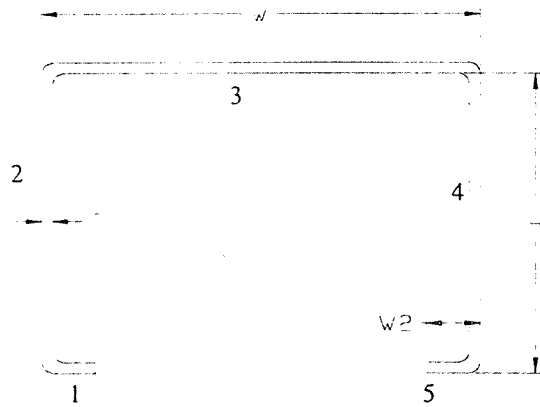
Vehicle Integration and Stowage Calculations

Hinged Support Plates	A-42
Roller Truck Stress Analysis.....	A-43

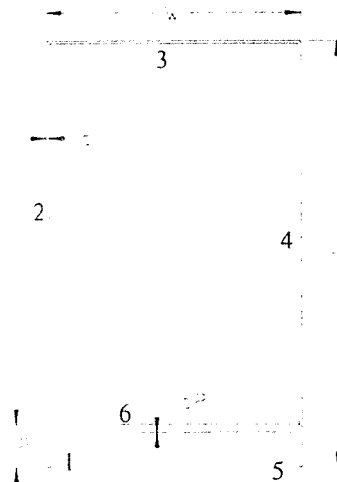
Beam Cross Sectional Properties

Formed Section Geometry

Base Section



Fly/Intermediate Sections



In order to calculate the beam section properties, each section was separated into i rectangular sections (1,2,3...). These i -sections were then used to determine the bending moments of inertia, centroid and other properties as shown in the following tables.

Base Section(w=9.375,t=.25,h=7,w2=1.25)

i	bi(in)	hi(in)	Ai(in ²)	Si(in)	Ai*Si(in ³)	di(from si*)	I0(in ⁴)	Ai*di ² (in ⁴)
1.000	1.250	0.250	0.313	0.125	0.039	-4.177	0.002	5.453
2.000	0.250	6.500	1.625	3.250	5.281	-1.052	5.721	1.799
3.000	9.375	0.250	2.344	6.875	16.113	2.573	0.012	15.515
4.000	0.250	6.500	1.625	3.250	5.281	-1.052	5.721	1.799
5.000	1.250	0.250	0.313	0.125	0.039	-4.177	0.002	5.453
Sum			6.219		26.754		11.458	30.018

Base Section Properties

si* (height to c.g.) 4.302 in
 Material Density 0.283 lb/in³
 Section Length 96.000 in
 Section Volume 597.000 in³
 Section Weight 168.951 lb
 I section=I0+Ai*di²= 41.476 in⁴

Intermediate Section(w=6,t=.06,h=10,t2=.188,h2=1)

i	bi(in)	hi(in)	Ai(in ²)	Si(in)	Ai*Si(in ³)	di(from si*)	I0(in ⁴)	Ai*di ² (in ⁴)
1.000	0.188	0.812	0.153	0.406	0.062	-3.185	0.008	1.549
2.000	0.060	10.000	0.600	5.000	3.000	1.409	5.000	1.191
3.000	5.880	0.060	0.353	9.970	3.517	6.379	0.000	14.355
4.000	0.060	10.000	0.600	5.000	3.000	1.409	5.000	1.191
5.000	0.188	0.812	0.153	0.406	0.062	-3.185	0.008	1.549
6.000	5.880	0.188	1.105	0.906	1.002	-2.685	0.003	7.971
Sum			2.964		10.643		10.020	27.805

Intermediate Section Properties

si* (height to c.g.) 3.591 in
 Material Density 0.283 lb/in³
 Section Length 96.000 in
 Section Volume 284.501 in³
 Section Weight 80.514 lb
 I section=I0+Ai*di²= 37.825 in⁴

Fly Section(w=5.75,t=.06,h=8.9,t2=.109,h2=.59)

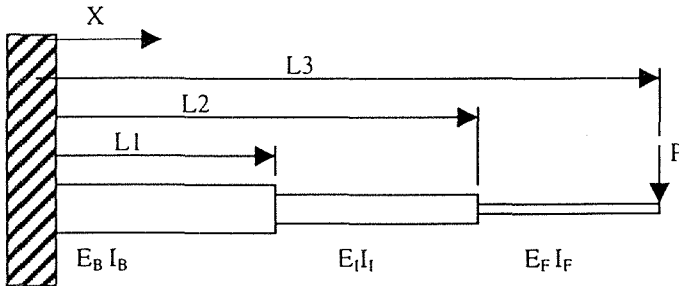
i	bi(in)	hi(in)	Ai(in ²)	Si(in)	Ai*Si(in ³)	di(from si*)	I0(in ⁴)	Ai*di ² (in ⁴)
1.000	0.109	0.481	0.052	0.241	0.013	-3.574	0.001	0.670
2.000	0.060	8.900	0.534	4.450	2.376	0.636	3.525	0.216
3.000	5.630	0.060	0.338	8.870	2.996	5.056	0.000	8.634
4.000	0.060	8.900	0.534	4.450	2.376	0.636	3.525	0.216
5.000	0.109	0.481	0.052	0.241	0.013	-3.574	0.001	0.670
6.000	5.630	0.109	0.614	0.536	0.329	-3.279	0.001	6.597
Sum			2.124		8.103		7.052	17.002

Fly Section Properties

si* (height to c.g.) 3.814 in
 Material Density 0.283 lb/in³
 Section Length 96.000 in
 Section Volume 203.935 in³
 Section Weight 57.714 lb
 I section=I0+Ai*di²= 24.055 in⁴

Deflection Analysis – End Load

Deflection due to end load for varying cross sections and materials.



Engineering Assumptions

- Infinitely stiff joints between cross sections.
- Linear elastic deflections.
- Sections remain plane, no localized buckling in side-walls.

Statics

$$\sum F_y = 0 \Rightarrow R_1 = P$$

$$\sum M = M_1 = -PL_3$$

$$0 < x < L_1$$

$$E_B I_B v_1''(x) = M(x) = -PL_3 + Px$$

$$E_B I_B v_1'(x) = P \frac{x^2}{2} - PL_3 x + C_1$$

$$E_B I_B v_1(x) = P \frac{x^3}{6} - PL_3 \frac{x^2}{2} + C_1 x + C_2$$

B.C.

$$v_1'(0) = 0 \Rightarrow C_1 = 0$$

$$v_1(0) = 0 \Rightarrow C_2 = 0$$

$$L_1 < x < L_2$$

$$E_I I_I v_2''(x) = M(x) = -PL_3 + Px$$

$$E_I I_I v_2'(x) = P \frac{x^2}{2} - PL_3 x + C_{12}$$

$$E_I I_I v_2(x) = P \frac{x^3}{6} - PL_3 \frac{x^2}{2} + C_{12} x + C_{22}$$

B.C.

$$v_2'(L1) = v_1'(L1) \Rightarrow C_{12} = \frac{E_I I_I}{E_B I_B} \left(\frac{PL_1^2}{2} - PL_1 L_3 \right) - \frac{PL_1^2}{2} + PL_1 L_3$$

$$v_2(L1) = v_1(L1) \Rightarrow C_{22} = \frac{E_I I_I}{E_B I_B} \left(\frac{PL_3 L_1^2}{2} - \frac{PL_1^3}{3} \right) - \frac{PL_1^3}{3} + \frac{PL_3 L_1^3}{2}$$

L2 < x < L3

$$E_F I_F v_3''(x) = M(x) = -PL_3 + Px$$

$$E_F I_F v_3'(x) = P \frac{x^2}{2} - PL_3 x + C_{13}$$

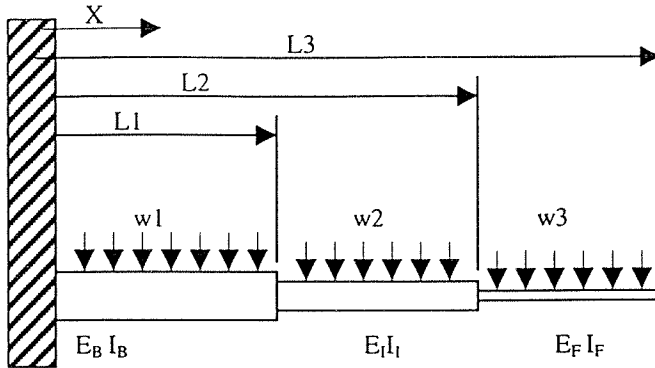
$$E_F I_F v_3(x) = P \frac{x^3}{6} - PL_3 \frac{x^2}{2} + C_{13} x + C_{23}$$

B.C.

$$v_3'(L_2) = v_2'(L_2) \Rightarrow C_{13} = \frac{E_F I_F}{E_I I_I} \left(\frac{PL_2^2}{2} - PL_2 L_3 + C_{12} \right) - \frac{PL_2^2}{2} + PL_2 L_3$$

$$v_2(L_2) = v_1(L_2) \Rightarrow C_{23} = \frac{E_F I_F}{E_I I_I} \left(\frac{PL_2^3}{6} - \frac{PL_3 L_2^2}{2} + C_{12} L_2 + C_{22} \right) - \frac{PL_2^3}{6} + \frac{PL_3 L_2^2}{2} - C_{13} L_2$$

Deflection due to distributed weight for varying cross sections and materials.



Engineering Assumptions

- Infinitely stiff joints between cross sections.
- Linear elastic deflections.
- Sections remain plane, no localized buckling in side-walls.
- Distributed loads act as point loads for static analysis.

Statics

$$\sum F_y = 0 \Rightarrow R_1 = w_1 L_1 + w_2 (L_2 - L_1) + w_3 (L_3 - L_2)$$

$$\sum M = M_1 = -\frac{w_1 L_1^2}{2} - w_2 (L_2 - L_1) \left(\frac{L_1 + L_2}{2} \right) - w_3 (L_3 - L_2) \left(\frac{L_3 + L_2}{2} \right)$$

Deflection

$$0 < x < L_1$$

$$E_B I_B v^{IV} = -w_1$$

$$E_B I_B v''' = -w_1 x + C_1$$

$$E_B I_B v'' = -w_1 \frac{x^2}{2} + C_1 x + C_2$$

$$E_B I_B v' = -w_1 \frac{x^3}{6} + C_1 \frac{x^2}{2} + C_2 x + C_3$$

$$E_B I_B v = -w_1 \frac{x^4}{24} + C_1 \frac{x^3}{6} + C_2 \frac{x^2}{2} + C_3 x + C_4$$

Boundary Conditions

$$E_B I_B v'''(0) = R_1 \Rightarrow C_1 = R_1$$

$$E_B I_B v''(0) = M_1 \Rightarrow C_2 = M_1$$

$$v'(0) = 0 \Rightarrow C_3 = 0$$

$$v(0) = 0 \Rightarrow C_4 = 0$$

Similarly for $L_1 < x < L_2$

$$E_I I_I v = -w_2 \frac{x^4}{24} + C_{12} \frac{x^3}{6} + C_{22} \frac{x^2}{2} + C_{32} x + C_{42}$$

Boundary Conditions

Applying continuity to all of the differential equations at the position $x=L_1$ will yield...

$$C_{12} = \frac{E_I I_I}{E_B I_B} (-w_1 L_1 + R_1) + w_2 L_1$$

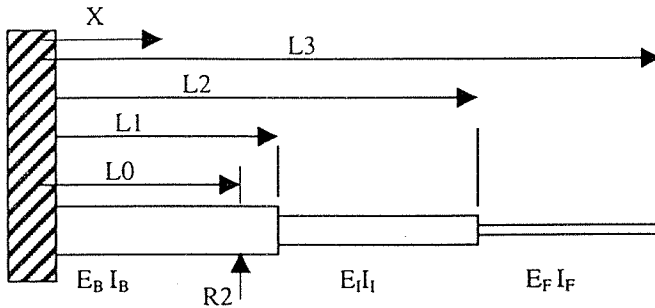
$$C_{22} = \frac{E_I I_I}{E_B I_B} \left(-w_1 \frac{L_1^2}{2} + R_1 L_1 + M_1 \right) + w_2 \frac{L_1^2}{2} - C_{12} L_1$$

$$C_{32} = \frac{E_I I_I}{E_B I_B} \left(-w_1 \frac{L_1^3}{6} + R_1 \frac{L_1^2}{2} + M_1 L_1 \right) + w_2 \frac{L_1^3}{6} - C_{12} \frac{L_1^2}{2} - C_{12} L_1$$

$$C_{42} = \frac{E_I I_I}{E_B I_B} \left(-w_1 \frac{L_1^4}{24} + R_1 \frac{L_1^3}{6} + M_1 \frac{L_1^2}{2} \right) + w_2 \frac{L_1^4}{24} - C_{12} \frac{L_1^3}{6} - C_{12} \frac{L_1^2}{2} - C_{32} L_1$$

Similar Equations will result for $L_2 < x < L_3$ and can be found by replacing all L_1 by L_2 and the beam subscripts for the intermediate (I) and the fly sections (F).

Determination of Reaction Force at Base End / Deflection due to R2



Note: The reaction force R2 is determined by adding the deflections of the applied loads, P and the distributed weight, at the location L0 and then applying the constraint that the deflection at L0 must be zero.

Engineering Assumptions

- Infinitely stiff joints between cross sections.
- Linear elastic deflections.
- Sections remain plane, no localized buckling in side-walls.

Statics

$$\sum F_y = 0 \Rightarrow R_1 = -R_2$$

$$\sum M_1 = R_2 L_0$$

Deflections

$$0 < x < L_0$$

$$M = R_2 L_0 - R_2 x = E_B I_B v''$$

$$E_B I_B v' = R_2 L_0 x - \frac{R_2 x^2}{2} + C_1$$

$$E_B I_B v = \frac{R_2 L_0 x^2}{2} - \frac{R_2 x^3}{6} + C_1 x + C_2$$

Boundary Conditions

$$E_B I_B v'(0) = C_1 = 0 \Rightarrow C_1 = 0$$

$$E_B I_B v(0) = C_2 = 0 \Rightarrow C_2 = 0$$

L0< x < L1

$$M = R_2 L_0 - R_2 x + R_2 (x - L_0) = E_B I_B v'' = 0$$

$$E_B I_B v_2' = C_1$$

$$E_B I_B v_2 = C_1 x + C_2$$

Boundary Conditions

$$v_2'(L_0) = v_1'(L_0) \Rightarrow C_1 = \frac{R_2 L_0^2}{2}$$

$$v_2(L_0) = v_1(L_0) \Rightarrow C_2 = -\frac{R_2 L_0^3}{6}$$

L1< x < L2

$$E_I I_I v_3'' = 0$$

$$E_I I_I v_3' = C_1$$

$$E_I I_I v_3 = C_1 x + C_2$$

Boundary Conditions

$$v_3'(L_0) = v_2'(L_0) \Rightarrow C_1 = \frac{E_I I_I R_2 L_0^2}{2 E_B I_B}$$

$$v_3(L_0) = v_2(L_0) \Rightarrow C_2 = \frac{E_I I_I R_2 L_0^3}{6 E_B I_B}$$

L2< x < L3

$$E_I I_I v_4'' = 0$$

$$E_I I_I v_4' = C_1$$

$$E_I I_I v_4 = C_1 x + C_2$$

Boundary Conditions

$$v_3'(L_0) = v_2'(L_0) \Rightarrow C_1 = \frac{E_I I_I R_2 L_0^2}{2 E_B I_B}$$

$$v_3(L_0) = v_2(L_0) \Rightarrow C_2 = \frac{E_I I_I R_2 L_0^3}{6 E_B I_B}$$

Solving for the reaction force R_2 as a function of the distributed load and the applied end load P .

From R_2 :

$$E_B I_B v = \frac{R_2 L_0 x^2}{2} - \frac{R_2 x^3}{6} \Rightarrow v(L_0) = \frac{R_2 L_0^3}{3 E_B I_B}$$

From the distributed loading:

$$E_B I_B v = -w_1 \frac{x^4}{24} + R_1 \frac{x^3}{6} + M_1 \frac{x^2}{2} \Rightarrow v(L_0) = \frac{-w_1 \frac{L_0^4}{24} + R_1 \frac{L_0^3}{6} + M_1 \frac{L_0^2}{2}}{E_B I_B}$$

where

$$R_1 = w_1 L_1 + w_2 (L_2 - L_1) + w_3 (L_3 - L_2)$$

$$M_1 = \frac{-w_1 L_1^2}{2} - w_2 (L_2 - L_1) \left(\frac{L_1 + L_2}{2} \right) - w_3 (L_3 - L_2) \left(\frac{L_3 + L_2}{2} \right)$$

Again, point loads were assumed for the distributed loading in determining the statics.

For the applied end load P :

$$E_B I_B v_1(x) = P \frac{x^3}{6} - PL_3 \frac{x^2}{2} \Rightarrow v_1(L_0) = \frac{P \frac{L_0^3}{6} - PL_3 \frac{L_0^2}{2}}{E_B I_B}$$

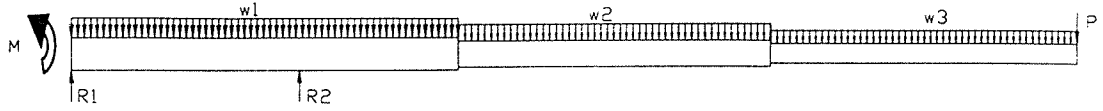
Finally, by applying the constraint that the deflection at L_0 be zero, we have

$$\frac{P \frac{L_0^3}{6} - PL_3 \frac{L_0^2}{2}}{E_B I_B} + \frac{-w_1 \frac{L_0^4}{24} + R_1 \frac{L_0^3}{6} + M_1 \frac{L_0^2}{2}}{E_B I_B} + \frac{R_2 L_0^3}{3 E_B I_B} = 0$$

where R_1 and M_1 are defined as in the distributed loading case. Therefore R_2 can be solved as:

$$R_2 = 3 \left(\frac{w_1 L_0}{24} - \frac{R_{1-DL}}{6} - \frac{M_{1-DL}}{2 L_0} - \frac{P}{6} + \frac{PL_3}{2 L_0} \right)$$

Telescopic Arm Stress Analysis



The critical stress location in the telescopic beams occurs at R2 and is found from the moment at R2:

$$\sum M_{R2} = M_1 - R_1 L_0 + w_1 L_1 \left(L_0 - \frac{L_1}{2} \right) - w_2 (L_2 - L_1) \left(\frac{L_2 + L_1}{2} - L_0 \right) - w_3 (L_3 - L_2) \cdot \dots$$

$$\dots \cdot \left(\frac{L_3 + L_2}{2} - L_0 \right)$$

where L_i are defined as in the deflection diagrams and M_1 , R_1 are found by superposition of the following equations for each loading condition.

End Load

$$\sum F_y = 0 \Rightarrow R_{1-EL} = P$$

$$\sum M = M_{1-EL} = -PL_3$$

Distributed Load

$$\sum F_y = 0 \Rightarrow R_{1-DL} = w_1 L_1 + w_2 (L_2 - L_1) + w_3 (L_3 - L_2)$$

$$\sum M = M_{1-DL} = \frac{-w_1 L_1^2}{2} - w_2 (L_2 - L_1) \left(\frac{L_1 + L_2}{2} \right) - w_3 (L_3 - L_2) \left(\frac{L_3 + L_2}{2} \right)$$

Reaction Force

$$\sum F_y = 0 \Rightarrow R_{1-R2} = -R_2$$

$$\sum M_{1-R2} = R_2 L_0$$

where from before:

$$R_2 = 3 \left(\frac{w_1 L_0}{24} - \frac{R_{1-DL}}{6} - \frac{M_{1-DL}}{2L_0} - \frac{P}{6} + \frac{PL_3}{2L_0} \right)$$

and R_1 and M_1 are from the distributed loading as:

$$R_{1-DL} = w_1 L_1 + w_2 (L_2 - L_1) + w_3 (L_3 - L_2)$$

$$M_{1-DL} = \frac{-w_1 L_1^2}{2} - w_2 (L_2 - L_1) \left(\frac{L_1 + L_2}{2} \right) - w_3 (L_3 - L_2) \left(\frac{L_3 + L_2}{2} \right)$$

Therefore, using some careful bookkeeping the moment at R2 can be evaluated and used to evaluate the maximum bending stress in the beam through the following equation:

$$\sigma_{xx} = \frac{Mc}{I_{xx}}$$

where M is the bending moment, c is the distance from the neutral axis to the outermost edge, and I is the bending inertia of the beam at this location.

The average shear stress in the section can be found by:

$$\tau_{xy} = \frac{V}{A}$$

Where V is the shear force in the section at R2, and A is the cross sectional area of the section at R2. *Note:* This shear stress vanishes at the edges of the section where the bending stress is maximum.

Using the maximum shear stress theory, the maximum shear stress in the section is found from:

$$\tau_{MAX} = \sqrt{\left(\frac{\sigma_{xx}^2}{2} + \tau_{xy}^2\right)} \text{ where } \tau_{xy} \text{ and } \sigma_{xx} \text{ are at the outer edge of the section } \therefore \tau_{xy} = 0.$$

And according to the theory, the maximum shear stress must be such that:

$$\tau_{MAX} \leq \frac{S_{yt}}{2n}$$

where S_{yt} is the tensile yield strength of the material and n is the factor of safety.

Numerical Evaluation

$$L_o = 81 \text{ in}$$

$$L_1 = 103.5 \text{ in}$$

$$L_2 = 183 \text{ in}$$

$$L_3 = 262.5 \text{ in}$$

$$P = 100 \text{ lb/in}$$

$$w1 = 2.54 \text{ lb/in}$$

$$w2 = 1.45 \text{ lb/in}$$

$$w3 = .80 \text{ lb/in}$$

using these values we find...

$$R_{1-EL} = -100\text{lb}$$

$$M_{1-EL} = -26250\text{lb}\cdot\text{in}$$

$$R_{1-DL} = 442\text{lb}$$

$$M_{1-DL} = -44284.60\text{lb}\cdot\text{in}$$

$$R_2 = 784\text{lb}$$

$$R_{1-R2} = -784\text{lb}$$

$$M_{1-R2} = 63512\text{lb}\cdot\text{in}$$

Therefore, we can find M1 and R1 as

$$M_1 = -7023\text{lb}\cdot\text{in}$$

$$R_1 = -242\text{lb}$$

Finally, substitution of these values into the equation for the Moment at R2 yields...

$$\sum M_{R2} = M_1 - R_1 L_0 + w_1 L_1 \left(L_0 - \frac{L_1}{2} \right) - w_2 (L_2 - L_1) \left(\frac{L_2 + L_1}{2} - L_0 \right) - w_3 (L_3 - L_2) \left(\frac{L_3 + L_2}{2} - L_0 \right)$$

$$M_{R2} = -7023 + 19602 + 7689 - 17723 - 14834.7 = -12289.7\text{lb}\cdot\text{in}$$

The corresponding bending stress is found using as:

$$\sigma_{xx} = \frac{Mc}{I_{xx}} = \frac{(-12289.7\text{lb}\cdot\text{in})(4.3\text{in})}{41.476\text{in}^4} = -1.274\text{ksi}$$

where c is the distance from the neutral axis to the bottom of the base section.

The corresponding average shear stress is found as:

$$\tau_{xy} = \frac{V}{A} = \frac{784\text{lb}}{6.22\text{in}^2} = 0.126\text{ksi} \text{ which is significantly lower than the bending stress.}$$

And the maximum shear stress is then found as:

$$\tau_{MAX} = \sqrt{\left(\frac{\sigma_{xx}}{2} \right)^2} = 0.637\text{ksi}$$

Using a yield strength for mild steel of 43ksi, the section has a calculated factor of safety of about 33.

Conclusion

This analysis has proven that the beam section stresses are very low and thus the beams should not fail under normal operation conditions. This analysis has also proven why the deflection was the major design consideration for the telescopic arm.

Joint Connections Loading Analysis

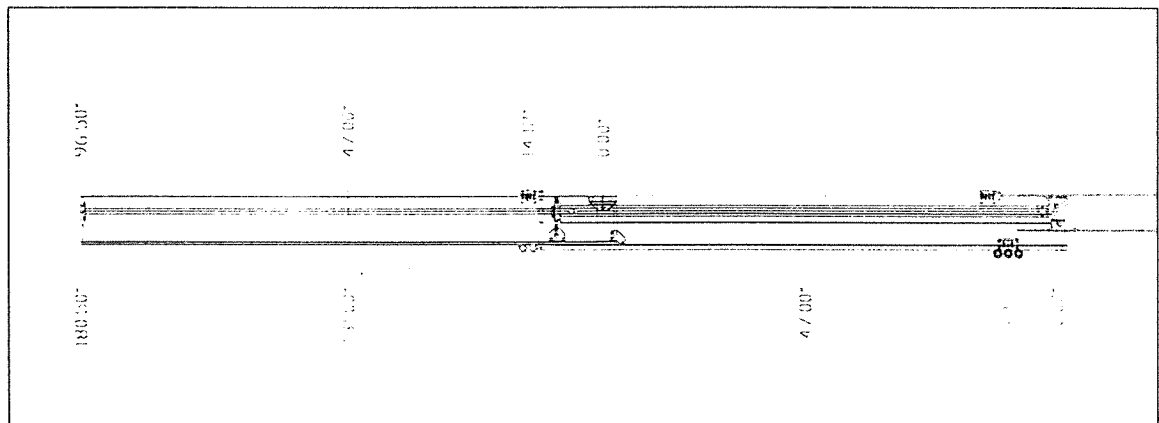
Assumptions:

- Arm components act as point masses.
- Infinitely stiff joint connections.
- Beam deflection is small.

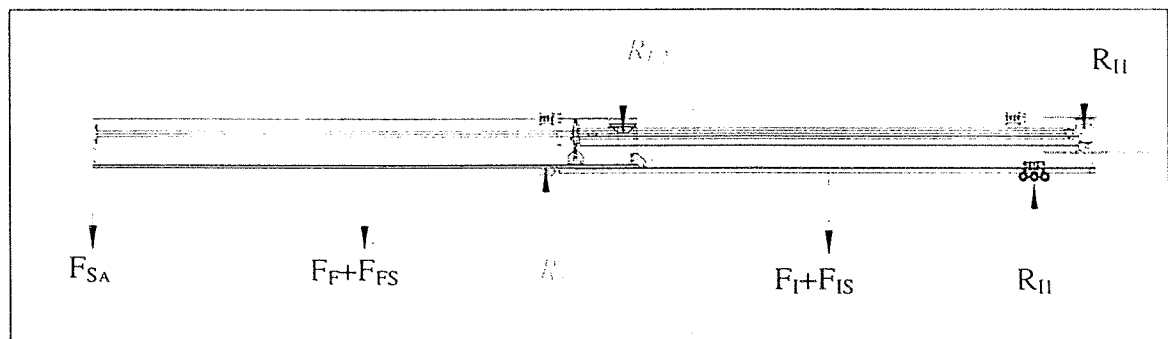
Procedure:

To determine the loading on the section joints, the arm parts were broken down into point masses that act over a distance to form a moment about the joint connection. This moment must be resolved through the two sets of primary support rollers.

Given:



OCCSM Telescopic Arm c.g. / Support Dimensions



OCCSM Telescopic Arm FBD-Joint Analysis

Note: $R_{FI,2}$ do not represent external loads, rather act only on the fly section alone. They are provided here for the Fly joint analysis only.

$$m_B = 169lb$$

$$m_{BS} = 88lb$$

$$m_I = 80.5lb$$

$$m_{IS} = 62lb$$

$$m_F = 57.7lb$$

$$m_{FS} = 21lb$$

$$m_{SA} = 75lb$$

Where the subscripts are defined as follows:

B = base beam

I = intermediate beam

F = fly beam

BS = base screw

IS = intermediate screw

FS = fly screw

SA = sealant applicator

Statics: Intermediate Primary Loading Rollers

$$\sum M_{R12} = -R_{I1}(9.75) + (F_I + F_{IS})(47) + (F_F + F_{FS})(131) + F_{SA}(180.5)$$

$$\therefore R_{I1} = \frac{((F_I + F_{IS})(47) + (F_F + F_{FS})(131) + F_{SA}(180.5))}{9.75} = 3302 \text{ LB} = 14.69 \text{ KN}$$

$$\sum F_Y = 0 \Rightarrow R_{I2} = R_{I1} - F_I - F_{IS} - F_F - F_{FS} - F_{SA} = 3006 \text{ LB} = 13.35 \text{ KN}$$

Statics: Fly Primary Loading Rollers

$$\sum M_{RF2} = -R_{F1}(14.12) + (F_F + F_{FS})(47) + F_{SA}(96.5)$$

$$\therefore R_{F1} = \frac{(F_F + F_{FS})(47) + F_{SA}(96.5)}{14.12} = 774 \text{ LB} = 3.44 \text{ KN}$$

$$\sum F_Y = 0 \Rightarrow R_{F2} = R_{F1} - F_F - F_{FS} - F_{SA} = 620 \text{ LB} = 2.76 \text{ KN}$$

Statics: Horizontal Supports

Assume:

- Sections can be modeled as point masses.
- Inertia Forces will exist due to rotational acceleration, at max. extension ($\alpha=0.274$ rad/sec from previous calculation).
- Same dimensions apply as in the vertical loading analysis.
- FBD from before applies with forces and reactions substituted for the horizontal loading case.

Inertial Forces Sample Calculation

$$IF_{SA} = m_{SA}(\alpha r^2) = (100\text{lbm})(0.274\text{rad/sec})(269\text{in}) \cdot \frac{\text{lbf sec}^2}{386.4\text{lbm in}} = 19.1\text{lbf} = 84.9\text{ N}$$

Therefore, the succeeding inertia forces can be calculated in a similar manner and statics can be performed to yield...

$$IF_{SA} = 19.1\text{lbf}$$

$$IF_I = 7.73\text{lbf}$$

$$IF_{IS} = 5.95\text{lbf}$$

$$IF_F = 8.98\text{lbf}$$

$$IF_{FS} = 3.26\text{lbf}$$

$$F_{FRIC} = 20\text{lbf}$$

Intermediate Horizontal Support Reactions

$$\sum M_{SI2} = -R_{SI1}(9.75) + (IF_I + IF_{IS})(47) + (IF_F + IF_{FS})(131) + (IF_{SA} + F_{FRIC})(180.5)$$

$$\therefore R_{SI1} = \frac{((IF_I + IF_{IS})(47) + (IF_F + IF_{FS})(131) + (IF_{SA} + F_{FRIC})(180.5))}{9.75} = 954\text{ lbf} = 4.2\text{ KN}$$

$$\sum F_Y = 0 \Rightarrow R_{I2} = R_{I1} - F_I - F_{IS} - F_F - F_{FS} - F_{SA} - F_{FRIC} = 889\text{ lbf} = 3.9\text{ KN}$$

Fly Horizontal Support Reactions

$$\sum M_{SI2} = -R_{SI1}(14) + (IF_F + IF_{FS})(47) + (IF_{SA} + F_{FRIC})(96.5)$$

$$\therefore R_{SI1} = \frac{((IF_F + IF_{FS})(47) + (IF_{SA} + F_{FRIC})(96.5))}{14} = 311\text{ lbf} = 1.39\text{ KN}$$

$$\sum F_Y = 0 \Rightarrow R_{I2} = R_{I1} - F_F - F_{FS} - F_{SA} - F_{FRIC} = 259.7\text{ lbf} = 1.15\text{ KN}$$

Sample Roller Truck Bolt Analysis

Intermediate Front Roller Truck

The pin has two failure possibilities, through bending stress or shear stress.

Bending Stress: (From Shigley)

$$F_{\max} = 3302/2 = 1651\text{ lbf}$$

$$M_{\max} = 1651(0.25\text{in}) = 413\text{ lbf-in}$$

$$D = 0.50\text{ in}$$

$$C = 0.25\text{ in}$$

$$I = \frac{\pi D^4}{64} = 3.07e^{-3} \text{ in}^4$$

$$\sigma = \frac{Mc}{I} = \frac{(413)(0.25)}{3.07e^{-3}} = 33 \text{ ksi}$$

Using the Maximum Shear Stress Theory Yields...

$$\tau_{\text{MAX}} = \sqrt{\left(\frac{\sigma_{xx}}{2}\right)^2 + (\tau_{xy})^2} = \frac{\sigma_{xx}}{2} = 16.5 \text{ ksi}$$

$$S_y = 130 \text{ ksi (Grade 8 Bolt)}$$

$$\therefore n = \frac{S_y}{2\tau_{\text{MAX}}} = 3.9$$

Shear Stress: (From Shigley)

$$\tau_{\text{MAX}} = \frac{4V}{3A} = \frac{16(1651)}{3(\pi(0.5)^2)} = 11.2 \text{ ksi}$$

Using the Maximum Shear Stress Theory Yields...

$$\tau_{\text{MAX}} = \sqrt{\left(\frac{\sigma_{xx}}{2}\right)^2 + (\tau_{xy})^2} = \tau_{\text{MAX}}$$

$$S_y = 130 \text{ ksi (Grade 8 Bolt)}$$

$$\therefore n = \frac{S_y}{2\tau_{\text{MAX}}} = 5.8$$

Torsional Analysis of Telescopic Arm

<i>Torsion of OCCSM Telescopic Arm (Roarke p156)</i>				
Theta=T*L/(K*G)	0.000498	rad	0.0031	deg
T=F*H	480	lbf*in		
F=	20	lbf		
H=	24	in		
L=	159	in		
G=	1.15E+07	psi		
t sides=	0.03	in		
Average t-top/btm	0.03	in		
Section Height=	10	in		
Section Width=	6	in		
K=	13.33527	in ⁴		
Sealant Head Error	0.011944	in		

<i>Torsion of OCCSM Telescopic Arm (Timoshenko)</i>				
Theta=T*L/(4*A²*G*t)	1.56E-05	rad	1E-04	deg
T=F*H	480	lbf*in		
F=	20	lbf		
H=	24	in		
L=	159	in		
G=	1.15E+07	psi		
t =	0.03	in		
Section Height=	10	in		
Section Width=	6	in		
A=	59.5218	in		
Sealant Head Error	0.000375	in		

Note: This formula assumes equal wall thicknesses

Note2: A= The mean of the areas enclosed by the inner and outer boundaries of the cross section of the tube.

Rotational Motor / Gearbox Specifications

Motor: *Dynaserv® DR5030B Brushless Servo Motor*

Peak Torque: 22 ftlb.
 Rated Speed: 4 rev/sec
 Resolution: 278528 steps/rev
 Weight: 28.9 lb
 Motor Inertia: 1420 oz-in²
 Max. Power Consumption: 3.6 KVA

Gearbox: *Harmonic Drive® - HDC65*

Gear Ratio: 60:1
 Rated Output Torque: 7880 lbin @ 1750rpm
 Maximum Output Torque: 10200 lbin
 Static Torque Limit: 27750 lbin
 Ratchet Torque Limit: 24000 lbin
 Maximum Input Speed: 3500 rpm
 Inertia: 15.54 lbm-in²
 Input Backlash 13 arc-min

Drive System Requirements:

- Handle maximum torque requirements.
- Capable of attaining maximum speed.
- Capable of attaining required accuracy.

Calculations

Beam Inertia: $J_b = 11.2E6 \text{ lbm-in}^2$
 Gearbox Inertia: $J_g = 15.54 \text{ lbm-in}^2$
 Motor Inertia: $J_m = 1420 \text{ oz-in}^2$
 Vmax: $V = 3 \text{ ft/sec}$
 Time to Accelerate: $t = .5 \text{ sec}$
 Radial Extension: $r = 262.5 \text{ in}$
 Rated Motor Speed: $n = 4 \text{ rev/sec}$
 Gearbox Ratio: $N = 60$
 Motor Resolution: $R = 278528 \text{ steps/rev}$

$$\text{Required Motor Torque} = \tau_R = \frac{1}{386.4} \left(\frac{J_b}{N^2} + \frac{J_m}{16} + J_g \right) \cdot \frac{VN}{rt} = 11.46 \text{ lbft}$$

Inertia Ratio(J_{load}/J_m):

$$\frac{J_{load}}{J_m} = \frac{\frac{J_b}{N^2} + J_g}{\frac{J_m}{16}} = 35.23$$

Required Motor Speed(at minimum extension)

$$n_r = N\dot{\theta} = (60)(0.3478\text{rad/sec}) = 20.868\text{rad/sec} = 3.32\text{rev/sec}$$

Arm Resolution(Steps/in(translation)) at max extension

$$R^* = \frac{NR}{2\pi r_{\max}} = \frac{(60)(278528\text{steps/rev})}{(2\pi\text{rad/rev})(262.5\text{in})} = 10132\text{steps/in}$$

Transferred Backlash (at Maximum extension)



$$\tan \alpha = \frac{x}{r_{\max}} \approx \alpha$$

$$\therefore x = r_{\max} \cdot \alpha$$

where α is in radians.

Current Values

$$r_{\max} = 262.5 \text{ in}$$

$$\alpha = 13 \text{ arc-min/N} = 0.217\text{deg}/60 = 6.33\text{E-}5 \text{ rad}$$

$$\text{Therefore } x = 0.017 \text{ in}$$

Therefore, the calculations show that the specified gearbox and motor will meet and exceed all of the machine performance calculations.

Calculation for Rotational Inertia as a Function of Radial Extension

Variables:

r = radial distance to end of arm.

R_i = Radial distance from pivot to i 'th objects center of mass.

Constants:

I_{0_i} = Inertia of i 'th object about its own center of mass.

M_i = i 'th object mass

Subscripts:

B = base beam

I = intermediate beam

F = fly beam

BS = base screw

IS = intermediate screw

FS = fly screw

SA = sealant applicator

Equations:

For $103.5 < r < 262.5$

$$I(r) = (I_{0_B} + m_B r_B^2) + (I_{0_{BS}} + m_{BS} r_{BS}^2) + (I_{0_I} + m_I r_I^2) + (I_{0_F} + m_F r_F^2) + (I_{0_{IS}} + m_{IS} r_{IS}^2) + \dots$$

$$\dots + (I_{0_{FS}} + m_{FS} r_{FS}^2) + m_{SA} r^2$$

geometric constraints yield

$$r_B = 43.5$$

$$r_{BS} = 45$$

$$r_I = \frac{r - 105}{2} + 50.5$$

$$r_{IS} = \frac{r - 105}{2} + 52.5$$

$$r_F = r - 49.5$$

$$r_{FS} = r - 44.5$$

which yields

$$I(r) = (I_{0_B} + m_B (43.5)^2) + (I_{0_{BS}} + m_{BS} (43.5)^2) + (I_{0_I} + m_I (\frac{r - 105}{2} + 50.5)^2) + (I_{0_F} + m_F (r - 49.5)^2) + \dots$$

$$\dots + (I_{0_{IS}} + m_{IS} (\frac{r - 105}{2} + 52.5)^2) + (I_{0_{FS}} + m_{FS} (r - 44.5)^2) + m_{SA} r^2$$

which expands to

$$\begin{aligned}
 I(r) = & (I_{0_B} + 1892.25m_B) + (I_{0_{BS}} + 2025m_{BS}) + (I_{0_I} + m_I(\frac{r^2}{4} - 29r + 841)) + (I_{0_F} + \dots \\
 & \dots + m_F(r^2 - 99r + 2450.25)) + (I_{0_{IS}} + m_{IS}(\frac{r^2}{4} - 27.25r + 742.56)) + \dots \\
 & \dots + (I_{0_{FS}} + m_{FS}(r^2 - 89r + 1980.25)) + m_{SA}r^2
 \end{aligned}$$

and simplifies to

$$\begin{aligned}
 I(r) = & (\frac{m_I + m_{IS}}{4} + m_F + m_{FS} + m_{SA})r^2 - (29m_I + 99m_F + 27.25m_{IS} + 89m_{FS})r + (I_{0_B} + \dots \\
 & \dots + I_{0_I} + I_{0_F} + I_{0_{BS}} + I_{0_{IS}} + I_{0_{FS}} + 1892.25m_B + 2025m_{BS} + 841m_I + 2450.25m_F + \dots \\
 & \dots + 742.56m_{IS} + 1980.25m_{FS})
 \end{aligned}$$

Current Arm Values:

$$I_{0_B} = 253,429 \text{ lb}_m \text{ in}^2$$

$$I_{0_I} = 66,799 \text{ lb}_m \text{ in}^2$$

$$I_{0_F} = 41,750 \text{ lb}_m \text{ in}^2$$

$$I_{0_{BS}} = 92,602 \text{ lb}_m \text{ in}^2$$

$$I_{0_{IS}} = 48,113 \text{ lb}_m \text{ in}^2$$

$$I_{0_{FS}} = 15,695 \text{ lb}_m \text{ in}^2$$

$$m_B = 169 \text{ lb}_m$$

$$m_{BS} = 88 \text{ lb}_m$$

$$m_I = 80.5 \text{ lb}_m$$

$$m_{IS} = 62 \text{ lb}_m$$

$$m_F = 57.7 \text{ lb}_m$$

$$m_{FS} = 21 \text{ lb}_m$$

$$m_{SA} = 75 \text{ lb}_m$$

Substitution Yields

$$I(r) = 189.3r^2 - 11605r + 1267043 \text{ lb}_m \text{ in}^2$$

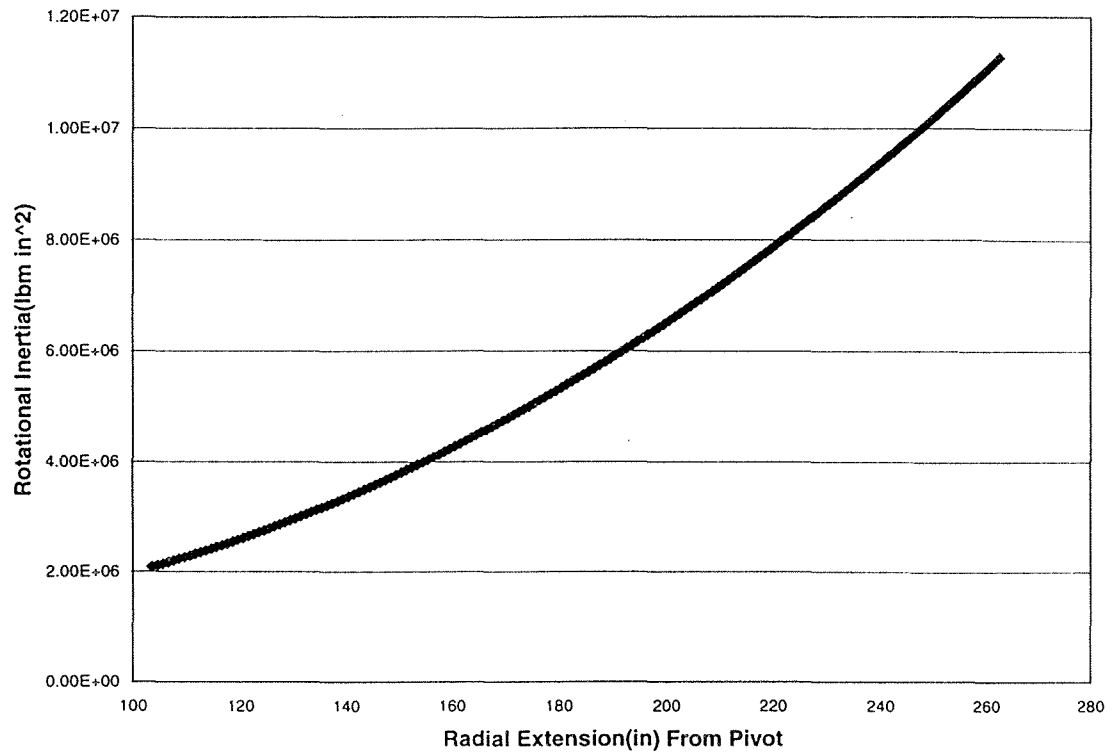
Therefore,

$$I_{\min} = I(103.5) = 2.1\text{E}6 \text{ lb}_m \text{ in}^2$$

$$I_{\max} = I(262.5) = 11.2\text{E}6 \text{ lb}_m \text{ in}^2$$

Graphical Representation

Rotational Inertia Vs. Radial Extension



This plot demonstrates the vast range of the rotational inertia values for the telescopic arm. These large deviations in the characteristics of the arm bring to question the rotational control system performance. The mechanical design of the OCCSM telescopic arm minimizes this deviance by using thin-wall light beam sections in an effort to maintain a stable control system.

Rotational Axis Torque Requirements

There are two possible design scenarios which will result in the maximum torque requirement due to the telescopic nature of the arm. The first is at minimum extension, where the rotational inertia is very low but the angular acceleration must be larger due to the arm's shorter length. The second is at maximum extension where the rotational inertia is very small and the angular acceleration is very low.

Minimum Extension

Radial Extension: $r=103.5$ in
Rotational Inertia: $I=2.1E6$ lbin²
End Effector Velocity: $V=36$ in/s
Time to Max Speed: $t=0.5$ sec

Angular Velocity and Acceleration

$$\dot{\theta} = \frac{v}{r} = \frac{36}{103.5} = 0.3478 \text{ rad/sec}$$

$$\alpha = \frac{\dot{v}}{t} = \frac{0.3478}{.5} = 0.6956 \text{ rad/sec}^2$$

Required Torque(Neglecting Motor Inertia)

$$\tau = J\alpha \Rightarrow (2.1E6)(0.6956) \frac{\text{lb min}^2}{\text{sec}^2} \cdot \frac{\text{lbf}}{32.2 \frac{\text{lbmft}}{\text{sec}^2}} \cdot \frac{1 \text{ ft}}{12 \text{ in}} = 3780 \text{ lbfin}$$

Maximum Extension

Radial Extension: $r=262.5$ in
Rotational Inertia: $I=11.2E6$ lbin²
End Effector Velocity: $V=36$ in/s
Time to Max Speed: $t=0.5$ sec

Angular Velocity and Acceleration

$$\dot{\theta} = \frac{v}{r} = \frac{36}{262.5} = 0.1371 \text{ rad/sec}$$

$$\alpha = \frac{\dot{v}}{t} = \frac{0.1371}{.5} = 0.2743 \text{ rad/sec}^2$$

Required Torque(Neglecting Motor Inertia)

$$\tau = J\alpha \Rightarrow (11.2E6)(0.2743) \frac{\text{lb min}^2}{\text{sec}^2} \cdot \frac{\text{lbf}}{32.2 \frac{\text{lbmft}}{\text{sec}^2}} \cdot \frac{1 \text{ ft}}{12 \text{ in}} = 7951 \text{ lbfin}$$

Therefore, the design case to be used is at maximum extension where the required torque is about 7950 lbfin.

Telescopic Actuator System

Specifications

Motor: Compumotor® Apex 620

Peak Torque:	331 inlb.
Cont. Torque:	116 inlb
Rated Speed:	3700 rev/min
Resolution:	4096 steps/rev
Weight:	29.0 lb
Motor Inertia:	35.87 oz-in ²
Rated Power:	6 hp

Gearbox: Custom Dual Output Planetary System

Weight:	
Lubrication:	Grease
Casing:	Aluminum
Inertia (est.):	40 oz-in ²
Backlash(outer/inner):	8 / 11 arc-min
Input:	
Shaft (Dia.: Mount):	24mm: Keyed
Torque (Cont.):	116 inlb
Torque (Peak):	331 inlb
Speed (Peak):	3600 rev/min

Outer Output:	
Shaft (Dia.: Mount):	25mm: No. 6 Taper Pin
Ratio(I/O):	1/2
Torque (Cont.):	232 inlb
Torque (Peak):	662 inlb
Speed (Peak):	1800 rev/min

Inner Output:	
Shaft (Dia.: Mount):	1.75in: Clamp-on Coupling
Ratio(I/O):	1/3
Torque (Cont.):	348 inlb
Torque (Peak):	993 inlb
Speed (rpm):	1200 rev/min

Prismatic Ball Screw Actuator

Retracted Length:	107 in
Stroke:	159 in
Effective Lead:	0.667 in/motor rev
Peak Translational Speed:	40 in/sec (Motor Limited)

Outer Drive Tube:

Clearance Diameter:	4.0 in
Diameter:	3.0 in
Wall Thickness:	0.125 in
Length:	96 in
Rotational Inertia:	1016 oz in ²
Approx. Weight:	46 lb

Split Tube:

Outer Diameter:	2.563 in
Inside Diameter:	2.060 in
Length:	94.40 in
Slot Length:	88 in
Rotational Inertia:	1047 oz in ²
Approx. Weight:	40 lb

Intermediate Ball Screw

Lead:	2.000 in/rev
Diameter:	2.000 in
# of starts:	2 start
Lead Accuracy:	0.0005 in/ft.
Length:	92 in
Through Hole Diameter:	1.062 in
Rotational Inertia:	603 oz in ²
Approx. Weight:	62 lb

Fly Ball Screw

Lead:	1.000 in/rev
Diameter:	1.000 in
# of Starts:	2 start
Lead Accuracy:	0.0005 in/ft
Length:	96 in
Weight:	21 lb

Ball Screw Actuator: Kinematic Analysis

Notation:

ω_i = Angular Speed of the i^{th} object.

v_i = Translational Speed of the i^{th} object.

L_i = Screw Lead of the i^{th} object. ($L = 1/\text{Pitch}$)

Subscripts:

I = Gearbox input

BT = Base tube

IS = Intermediate screw

FS = Fly screw

Gearbox Equations:

$$\omega_{BT} = \frac{1}{2} \omega_I$$

$$\omega_{IS} = \frac{1}{3} \omega_I$$

Ball Screw Equations:

$$(\omega_{BT} - \omega_{IS})L_{IS} = v_{IS}$$

$$(\omega_{IS} - \omega_{FS})L_{FS} + v_{IS} = v_{FS}$$

$$\omega_{FS} = 0$$

$$\frac{L_{IS}}{L_{FS}} = 2$$

Relation of Motor Input Velocity to End Translation:

$$(\omega_{IS} - \omega_{FS})L_{FS} + v_{IS} = (\omega_{IS})L_{FS} + (\omega_{BT} - \omega_{IS})L_{IS} = v_{FS}$$

$$\left(\frac{\omega_{IS}}{2} + (\omega_{BT} - \omega_{IS}) \right) = v_{FS}$$

Substitute for ω_{BT}, ω_{IS} as functions of ω_I .

$$\left(\frac{1}{2} \omega_I - \frac{1}{6} \omega_I \right) L_{IS} = \frac{1}{3} \omega_I L_{IS} = v_{FS}$$

Note :

All ω_i are in [rev/sec], L_i are in [in/rev] and v_i are in [in/sec].

Current Ball Screw Values:

$$L_{IS} = 2 \text{ in / rev}$$

$$L_{FS} = 1 \text{ in / rev}$$

Therefore, the relational equation is:

$$v_{FS} = \frac{2}{3} \omega_l$$

with $\omega_l(Max) = 61 \text{ rev/sec}$

$$v_{FS}(Max) = \frac{2}{3} \omega_l = 40 \text{ in/sec}$$

Required Gearbox Inner Output Torque Calculation

$$\tau_{Motor} = \frac{1}{386.4} \left(\left(\frac{J_{Load}}{e} + J_{IS} \right) \frac{\omega N}{t} + J_{Motor} + J_{Gearbox} \right) + \frac{T_F}{N}$$

where:

τ_i = Torque[ozin]

J_i = Rotational Inertia[ozin²]

ω = Angular Velocity[rad / s]

t = Time[sec]

e = efficiency[%x100]

Ball Screw Rotational Inertia, J_{IS}

$$J_{IST} = J_{ST} + J_{IS}$$

$$J_i = \frac{1}{2} M_o r_o^2 - \frac{1}{2} M_i r_i^2$$

$$J_i = \frac{1}{2} M_o r_o^2 - \frac{1}{2} M_i r_i^2 = \frac{1}{2} (\rho \pi r_o^2 L) r_o^2 - \frac{1}{2} (\rho \pi r_i^2 L) r_i^2 = \frac{1}{2} \rho \pi L (r_o^4 - r_i^4)$$

For the split tube, $r_o=1.28\text{in}$, $r_i=1.03\text{in}$, $L=94.4\text{in}$:

$$J_{ST} = \frac{1}{2} \rho \pi L (r_o^4 - r_i^4) = \frac{1}{2} \pi (94.4) (1.28^4 - 1.03^4) (0.283) = 65.42 \text{ lb}_m \text{ in}^2$$

For the Intermediate Ball Screw, $r_o=1.0\text{in}$, $r_i=0.53\text{in}$, $L=92\text{in}$:

$$J_{IS} = \frac{1}{2} \rho \pi L (r_o^4 - r_i^4) = \frac{1}{2} \pi (92) (1^4 - 0.53^4) (0.283) = 37.67 \text{ lb}_m \text{ in}^2$$

Therefore...

$$J_{IST} = 65.42 + 37.67 = 102.89 \text{ lb}_m \text{ in}^2$$

Equivalent Load Rotational Inertia

$$J_{Load} = \frac{W}{(2\pi P)^2} = \frac{WL_{IS}^2}{39.47}$$

where W is the weight of all of the moving masses. In this case...

$$W = m_{IS} + m_I + m_F + m_{FS} + m_{SA} = 62 + 81 + 58 + 21 + 75 = 297lb$$

Therefore...

$$J_{Load} = \frac{WL_{IS}^2}{39.47} = \frac{(297)(4)}{39.47} = 30.09lbin$$

Frictional Equivalent Torque:

$$T_F = \frac{F_f L_{IS}}{2\pi e} = \frac{\mu F_n L_{IS}}{2\pi e} = \frac{(0.15)(200)(2)}{2\pi(0.81)} = 11.78lbin$$

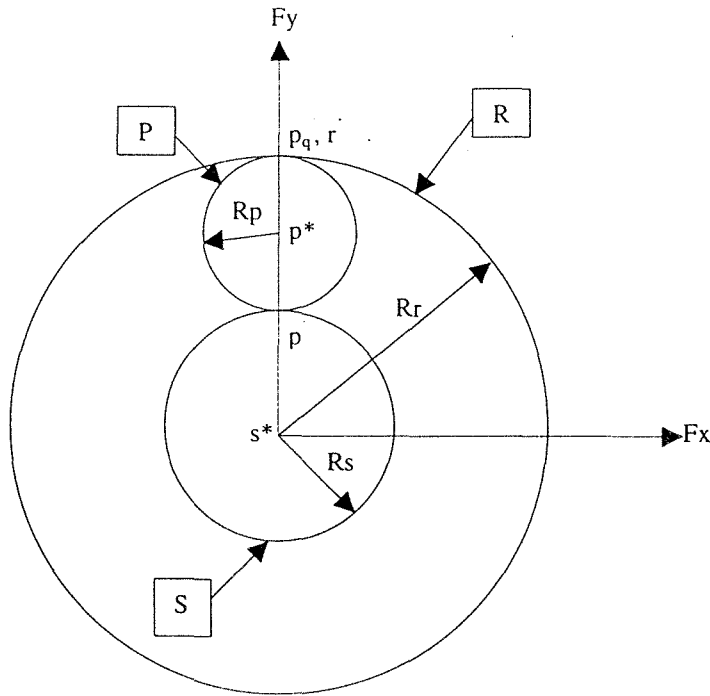
Assuming that the frictional forces in the section arise from the wearpads and that the normal forces on these wear pads total 200lb.

Therefore, the Required Motor Torque is:

$$\tau_{Motor} = \frac{1}{386.4} \left(\frac{\left(\frac{J_{Load}}{e} + J_{IS} \right)}{N^2} + J_{Motor} + J_{Gearbox} \right) \frac{\omega N}{t} + \frac{T_F}{N}$$
$$\tau_{Motor} = \frac{1}{386.4} \left(\frac{\frac{30.09(16)}{0.81} + 102.89(16)}{9} + 35.87 + 40 \right) \frac{127(3)}{0.5} + \frac{(11.78)(16)}{3} = 703ozin$$

Gearbox Calculations

Planetary Kinematic Analysis



Given:

$$** \quad {}^F \tilde{\omega}^R = \Omega \bar{f}_z$$

$$** \quad {}^F \tilde{\omega}^S = 0$$

** Object P rolls on S and R

Desire:

$$N = \frac{\Omega}{\omega_A}$$

Solution:

$${}^F \tilde{v}^{p*} = {}^F \tilde{v}^{p_1} + {}^F \tilde{\omega}^P \times r^{p_1 p*} \quad (1)$$

$${}^F \tilde{v}^{p_1} = {}^F \tilde{v}^{R^*} = {}^F \tilde{v}^{S^*} + {}^F \tilde{\omega}^R \times r^{S^* R^*} = \Omega \bar{f}_z \times r_r \bar{f}_y = -\Omega r_r \bar{f}_x \quad (2)$$

$${}^F \tilde{v}^{p*} = {}^F \tilde{v}^{p_1} + {}^F \tilde{\omega}^P \times r^{p_1 p*}$$

$${}^F \tilde{v}^{p*} = -\Omega r_r \bar{f}_x + \omega_p \bar{f}_z \times -r_p \bar{f}_y = -\Omega r_r \bar{f}_x + \omega_p r_p \bar{f}_x = (-\Omega r_r + \omega_p r_p) \bar{f}_x \quad (3)$$

From 1, 3

$$\omega_p \bar{f}_z \times r_p \bar{f}_y = -\omega_p r_p = -\Omega r_r + \omega_p r_p \Rightarrow \omega_p = \frac{\Omega r_r}{2r_p} \quad (4)$$

Then from 3,4

$${}^F\tilde{v}^{P^*} = \left(-\Omega r_r + \frac{\Omega r_r}{2r_p} r_p \right) \bar{f}_x = \frac{\Omega r_r}{2} \bar{f}_x \quad (5)$$

Then, by connecting an arm from s* to p* we can determine the angular velocity of this arm as...

$${}^F\tilde{v}^{P^*} = {}^F\tilde{v}^{S^*} + {}^F\tilde{\omega}^A \times r^{S^*P^*}$$

$$-\frac{\Omega r_r}{2} \bar{f}_x = \omega_A \bar{f}_z \times (r_p + r_s) \bar{f}_y$$

$$-\frac{\Omega r_r}{2} \bar{f}_x = -\omega_A (r_p + r_s) \bar{f}_x \Rightarrow \omega_A = \frac{\Omega r_r}{2(r_p + r_s)} \quad (6)$$

From geometry, the following equation arises...

$$2r_p + r_s = r_r \Rightarrow r_p + r_s = r_r - r_p \quad (7)$$

Substitution of (7) into (6) yields...

$$\omega_A = \frac{\Omega r_r}{2(r_r - r_p)} \Rightarrow \frac{\omega_A}{\Omega} = \frac{r_r}{2(r_r - r_p)} \quad (8)$$

\therefore given a desired ratio of output ω_A to Input Ω a relationship between r_r and r_p can be found as...

$$r_r = 2 \frac{\omega_A}{\Omega} (r_r - r_p) \Rightarrow r_p = r_r \left(1 - \frac{N}{2} \right) \text{ where } N = \frac{\Omega}{\omega_A} \quad (10)$$

Gearbox Input/Output Kinematics

$$N = \frac{3}{2} \Rightarrow \omega_A = \frac{2\Omega}{3}$$

Ω is the angular velocity of the ring gear which is derived from...

$$\Omega = \frac{\omega_1}{2}, \text{ where } \omega_1 \text{ is the input angular velocity.}$$

Therefore, the outer output shaft is related to the input by a ratio of 1/2 :

$$\Omega = \frac{\omega_1}{2}$$

The inner output shaft is connected to the arm and has the relationship...

$$\omega_A = \frac{2\Omega}{3} = \frac{\omega_1}{3} \text{ (a gear reduction of 1/3.)}$$

Gearbox Bevel Gear Analysis

Peak Input Torque: 350 inlb

Bevel Gear Stress Analysis:

Gear Bending Stresses/Contact Stresses

Assumptions:

- Bending stresses are maximum at peak transmitted torque
- Contact stresses (wear), will occur under continuous transmitted torque
- Centrifugal forces on geartrain are small
- Sun gear stresses are identical to planet stresses

Equations:

From Shigley,

Gear Bending Strength

$$\sigma = \frac{W_t K_a P_s K_s K_m}{K_v F J}$$

where σ =bending stress in gear tooth

W_t =transmitted load

K_a =application factor

P_s =diametral pitch

K_s =size factor

K_m =load distribution factor

K_v =dynamic Factor

F =face width

J =geometry factor

$$\sigma_{all} = \frac{S_t K_L}{K_T K_R}$$

where σ_{all} =maximum allowable stress in gear tooth

S_t = AGMA bending stress

K_L =life factor

K_T =temperature factor

K_R =reliability factor

Gear Contact Stresses

$$\sigma = C_p \left(\frac{W_t C_a C_s C_f C_m}{C_v F d I} \right)^{1/2}$$

where σ =contact stress on gear

C_p =elastic coefficient

W_t =transmitted load

C_a =application factor

C_f =surface factor

C_s =size factor
 C_m =load distribution factor
 C_v =dynamic Factor
 F =face width
 d =pitch diameter
 I =geometry factor

$$\sigma_{all} = \frac{S_c C_L C_H}{C_T C_R}$$

where σ_{all} =maximum allowable contact stress in gear
 S_c = AGMA contact stress
 C_L =life factor
 C_T =temperature factor
 C_R =reliability factor
 C_H =hardness factor

Calculations/Results: See following page

Bevel Gear Analysis

Gearbox Details

Torque Input (in lb)	332	Desired F.S.	2
Continuous Torque(in lb)	166	n-motor(rpm)	3700
Gear Ratio	2	Material Properties	E v
	Pinion Gear	Steel	3.00E+07 0.3
Peak Wt (lb.)	265.6		132.8
Continuous Wt(lb)	132.8		66.4

Stress Analysis:Bevel Gears

	Phi	Diameter	p(teeth/in)	Teeth	E	v	Qv	V(ft/min)	F(in)
Bevel Pinion	20	2.5	8	20	3.00E+07	0.3	9	2421.644	0.83
Bevel Gear	20	5	8	40	3.00E+07	0.3	9	2421.644	0.83

Surface Contact Correction Factors

Cp	2.29E+03
Ca	1.5
Cv(pinion)	0.780845
Cv(gear)	0.780845
A(pinion)	76.87883
B(pinion)	0.520021
A(gear)	76.87883
B(gear)	0.520021

Cs	1
Cm	1.3
Cf	1
I	0.078 0.107131
Mn	1
Mg	2

Sc(pinion)	200000
Sc(gear)	200000
Cl	1
Ch(pinion)	1
Ch(gear)	1.00069
A	0.00069
BHNp	360
BHNg	360

Ct	1
Cr	1

Pinion Contact Stress	103687.8
Allowable Stress	200000
Gear Contact Stress	73318.34
Allowable Stress	200138

Surface Contact Factor of Safety

Gear	2.729713
Pinion	1.928867

Strength Correction Factors

Ka	1.5
Kv(pinion)	0.780845
Kv(gear)	0.780845
Ks	1
Km	1
J(pinion)	0.23
J(gear)	0.21
St(pinion)	60000
St(gear)	60000
Kl	1
Kt	1
Kr	1

Pinion Bending Stress	21381.52
Pinion Allowable Stress	60000
Gear Bending Stress	11708.93
Gear Allowable Stress	60000

Strength Based Factor of Safety

Gear	5.124294
Pinion	2.806161

Shaft Reactions (FBD)

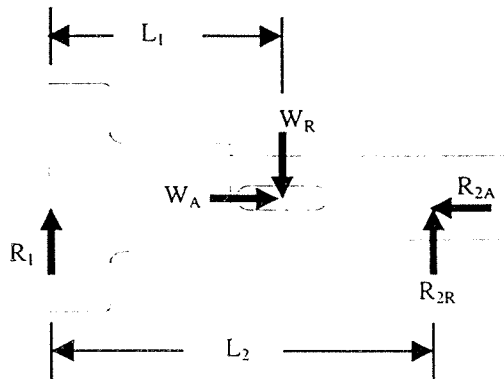
Assumptions:

- All forces are point forces, not distributed
- Reaction load points from tapered roller bearings are at $a=0$
- Bearings cannot support moments

Equations:

$$\begin{aligned} \sum F &= 0 \\ \sum M &= 0 \end{aligned} \quad \text{where } F = \text{applied forces, } M = \text{applied moments}$$

Calculations/Results: (NOTE: The analysis of only the outer output shaft is shown here for simplicity. All other shaft calculations were performed in a similar manner.



Outer Output Shaft: FBD-Vertical Plane

Shaft Loading: 5" Bevel Gear-

$$W_r = W_t \tan \phi \cos \gamma = 140(\tan 20^\circ)(\cos 45^\circ) = 36.0 \text{ lb}$$

$$W_a = W_t \tan \phi \sin \gamma = 140(\tan 20^\circ)(\sin 45^\circ) = 36.0 \text{ lb}$$

$$L_1 = 4.75 \text{ in}$$

$$L_2 = 6.75 \text{ in}$$

Statics (Vertical Plane)

$$\sum F_y = 0 = -W_r + R_{2R} + R_1 : \text{Eq. 1}$$

$$\sum F_x = 0 = W_a - R_{2A} : \text{Eq. 2}$$

$$\sum M_{R1} = 0 = W_r(L_1) - R_{2R}(L_2) : \text{Eq. 3}$$

From Eq. 3:

$$R_{2R} = 25.3 \text{ LB}$$

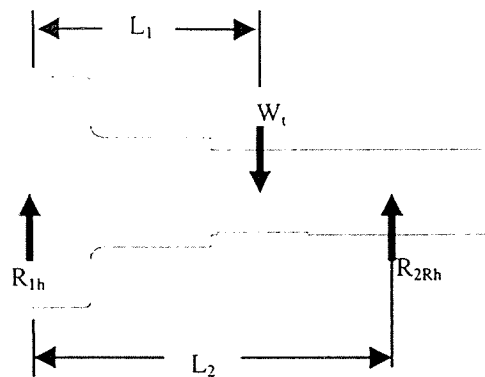
From Eq. 2:

$$R_1 = 10.7 \text{ LB}$$

From Eq. 1:

$$R_{2A} = 36.0 \text{ LB}$$

Outer Output Shaft:FBD-Horizontal Plane



Statics(Horizontal Plane)

$$\sum F_y = 0 = -W_t + R_{2Rh} + R_{1h} : \text{Eq. 1h}$$

$$\sum M_{R1} = 0 = W_t(L_1) - R_{2Rh}(L_2) : \text{Eq. 2h}$$

From eq.3h:

$$R_{2Rh} = 98.5lb$$

From eq. 1h:

$$R_{1h} = 41.5lb$$

Shaft Strengths

Assumptions:

- Maximum shear stress theory is adequate
- Failure will occur under peak torque loading

Equations:

From Shigley

$$\sigma_{xx} = \frac{F}{A} + \frac{Mc}{I} = \frac{4K_{fa}F}{\pi d^2} + \frac{16K_fM}{\pi d^3}$$

$$\tau_{xy} = \frac{Tr}{J} = \frac{32K_{fs}T}{\pi d^3}$$

$$\tau_{max} = \left(\left(\frac{\sigma_{xx}}{2} \right)^2 + (\tau_{xy})^2 \right)^{1/2} = \frac{S_y}{2n}$$

where σ_{xx} =stress due to axial and bending

τ_{xy} = stress due to torsion

F=axial applied load

d=diameter of shaft

c=radius of shaft

I=bending inertia of shaft

T=torque applied to shaft

J=polar moment of inertia

K_{fa} =axial stress concentration factor

K_f =bending stress concentration factor

K_{fs} =torsional stress concentration factor

τ_{max} =maximum shear stress

S_y = material yield stress

n= factor of safety

Calculations/Results:

Outer Output Shaft(see FBD)

Given:

T(peak) input=331in-lb

F=W_a

D_o=1.75in

D_i=1.125in

$$A = \frac{\pi}{4} (D_o^2 - D_i^2) = 2.148 \text{ in}^2$$

$$M_{max} = \frac{(W_R^2 + W_t^2)^{0.5} L_1}{4} = 171.7 \text{ lb-in}$$

$$I = \frac{\pi(D_o^4 - D_i^4)}{64} = 0.707 \text{ in}^4$$

$$J = \frac{\pi(D_o^4 - D_i^4)}{32} = 1.413 \text{ in}^4$$

$$c = \frac{D}{2}$$

$$\therefore \sigma_{xx} = \frac{F}{A} + \frac{Mc}{I} = \frac{36}{2.148} + \frac{171.7(0.875)}{0.707} = 229.26 \text{ psi}$$

$$\tau_{xy} = \frac{Tr}{J} = \frac{(662)(0.875)}{1.413} = 409.9 \text{ psi}$$

$$\tau_{\max} = \left(\left(\frac{\sigma_{xx}}{2} \right)^2 + (\tau_{xy})^2 \right)^{1/2} = 425 \text{ psi} = \frac{S_y}{2n} = \frac{54000 \text{ psi}}{2n}$$

$$n = FS = 63.5$$

Planetary Analysis

Peak inputs to Bayside® RA115 - 3 : 1 planetary system :

$$\text{Torque : } \frac{5.0}{2.5} (T_{input}) = 700 \text{ lbin}$$

$$\text{Speed : } \frac{2.5}{5.0} (\omega_{input}) = 1850 \text{ rev/min}$$

Peak Planetary Outputs :

Torque : 993 inlb

Speed : 1200 rev/min

Bayside® RA115 - 3 : 1 Planetary *Rated Loading* :

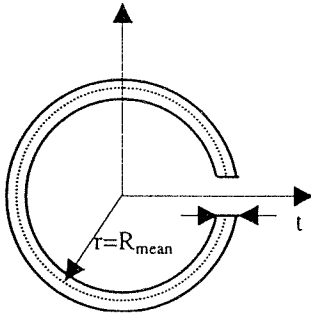
Rated Output Torque : 1600 inlb

Peak Output Torque : 2656 inlb

Input Speed : 5000 rev/min

Therefore, the Bayside® planetary set is operating within the manufacturer's specifications.

Split Tube Analysis



From Roarke, Formulas for Stress & Strain

$$\theta = \frac{TL}{KG} \quad K = \frac{2}{3}\pi r t^3$$

$$\tau_{\max} = \frac{T(6\pi r + 1.8t)}{4\pi^2 r^2 t^2}$$

From the gearbox and motor specifications, the maximum torque applied to the split tube is 132 lbin.

Split Tube Specifications

Outer Diameter:	2.563 in
Inside Diameter:	2.060 in
Length:	94.40 in
Slot Length:	88 in
Rotational Inertia:	1047 oz in ²
Approx. Weight:	40 lb

Applying Roarke's equations yields...

Stress

$$\tau_{\max} = \frac{T(6\pi r + 1.8t)}{4\pi^2 r^2 t^2} = \frac{132 \text{ lbin}(6\pi(1.15 \text{ in}) + 1.8(0.25 \text{ in}))}{4\pi^2 (1.15 \text{ in})^2 (0.25 \text{ in})^2} = 0.878 \text{ ksi}$$

Using the maximum shear stress theory

$$\tau_{\max} \leq \frac{S_y}{2n} = \frac{44}{4} = 11 \text{ ksi}$$

where n is a factor of safety of 2 and S_y is the tensile yield strength of hot roll steel. Therefore, the tube is well below the safe stress limits.

Deflection

$$\theta = \frac{TL}{KG} \quad K = \frac{2}{3}\pi r t^3 = \frac{2}{3}\pi(1.15)(0.25)^3 = 0.03763 \text{in}^4$$

$$\theta = \frac{TL}{KG} = \frac{132 \text{lb in}(88 \text{in})}{(0.03763 \text{in}^4)(11.6 \text{E}6 \text{psi})} = 0.0266 \text{rad}$$

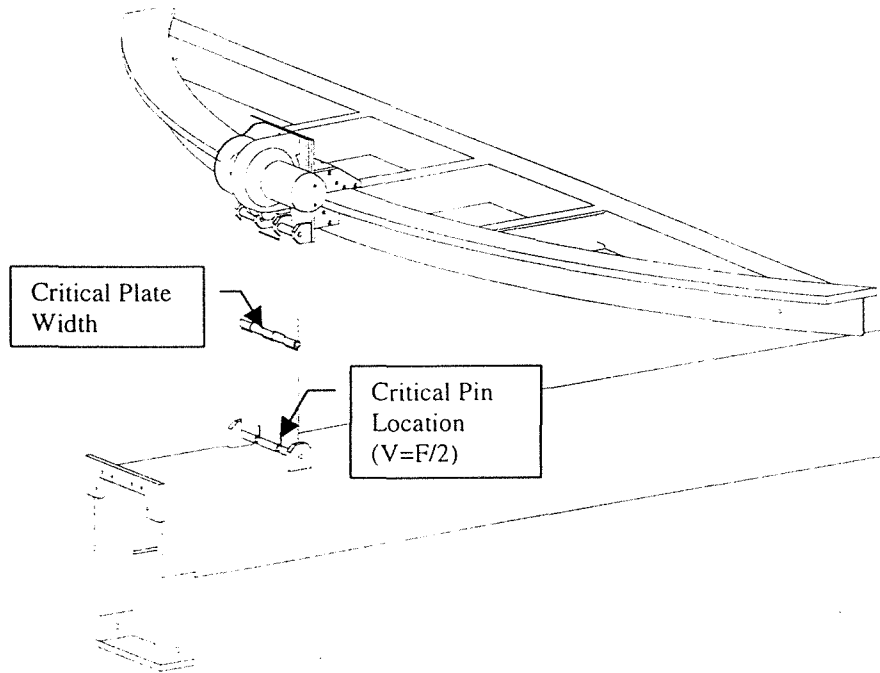
Conclusion

This value is acceptable since it is not a steady state error. Rather it represents torsional windup that will disappear as motion stops. This will represent the lag in the translation of the ball screw under acceleration and deceleration to maximum speeds. During normal operation at slower speeds, this deflection will be negligible.

Hinged Plate Analysis

Assumptions:

- hinge pins are forced into direct shear through close tolerances
- loading in plates in purely axial



Given Dimensions:

Plate width(nominal)-	7.0 in
Plate width at critical section-	4.5in
Plate Thickness-	0.25 in
Pin diameter-	0.375in

Maximum Loading(Axial)- 1100 lb

Calculations:

Plate Stress:

$$\sigma = \frac{F}{A} = \frac{1100}{(4.5)(.25)} = 977 \text{ psi}$$

$$\tau_{\max} = \frac{\sigma}{2} = \frac{S_y}{2n} \Rightarrow n \approx 64 \text{ (based on } S_y = 32\text{ksi)}$$

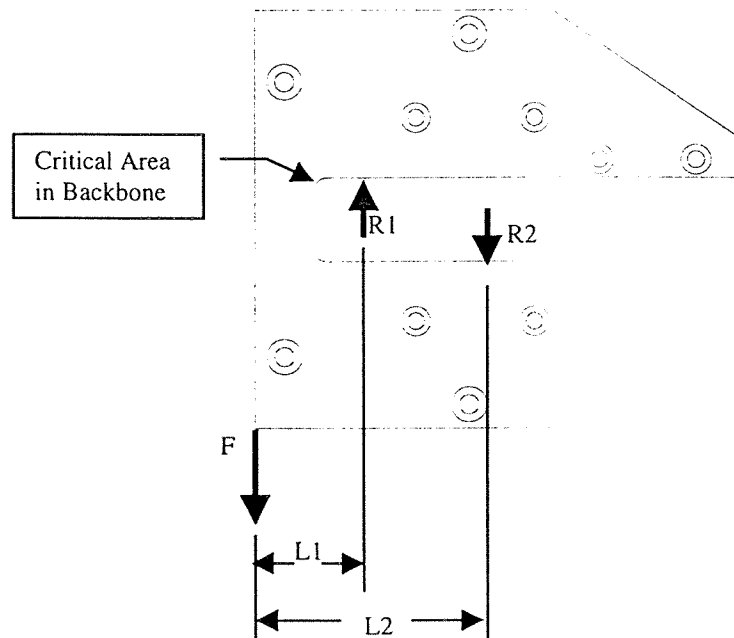
Pin shear:

$$\tau_{\max} = \frac{4V}{3A} = \frac{16(550\text{lb})}{3(\pi(0.375)^2)} = 6.6\text{ksi}$$

$$\tau_{\max} = 6.6\text{ksi} = \frac{S_y}{2n} \Rightarrow n = 4.8 \text{ (based on a } S_y \text{ for steel of } 32\text{ksi)}$$

Support Truck Analysis

Support Truck FBD



Given:

$$F = 1100 \text{ lb}$$

$$L1 = 1.31 \text{ in}$$

$$L2 = 2.56 \text{ in}$$

$$\text{Backbone Thickness} = 0.625 \text{ in}$$

$$\text{Backbone Width} = 6.0 \text{ in}$$

Statics:

$$\sum M_{R2} = R1(L2 - L1) - F(L2) = 0 \Rightarrow R1 = \frac{F(L2)}{L2 - L1} = 2253 \text{ lb}$$

$$\sum Fy = R1 - R2 - F = 0 \Rightarrow R2 = R1 - F = 1153 \text{ lb}$$

Stress Analysis:

$$\sigma = \frac{Mc}{I} = \frac{12(R1(L1 - .625))}{(6)(.625)^3} = 12.7 \text{ ksi}$$

$$\tau_{\max} = \frac{\sigma}{2} = \frac{S_v}{2n} \Rightarrow n = 2.5$$

APPENDIX B

DETAILED DRAWINGS

Table of Contents

Ball Screw Actuator Prints

ACT-001	Base Tube	B-1
ACT-002	Outer Drive Coupling	B-1
ACT-003	Intermediate Nut Coupling	B-2
ACT-004	3-18 Jam Nut	B-2
ACT-005	Base Tube Assembly	B-3
ACT-006A-D	Split Tube	B-3
ACT-007	Split Band	B-5
ACT-008	Split Tube Drive Coupling	B-6
ACT-009	Split Tube Assembly	B-6
ACT-010	Intermediate Ball Screw	B-7
ACT-011	Int. Screw Keyway Drive Coupling	B-7
ACT-012	Int. Ball Screw Assembly	B-8
ACT-013	Fly Ball Screw	B-8

Telescopic Gearbox Prints

G-001	Front Plate	B-9
G-002	Rear Plate	B-9
G-002MOD	Rear Plate Modification	B-10
G-003	Top Plate	B-10
G-004	Side Plates	B-11
G-005	Bottom Plate	B-11
G-006	Outer Output Shaft	B-12
G-007	Input Shaft	B-12
G-008	Inner Output Shaft	B-13
G-009	5" P.D. Bevel Gear	B-13
G-010	Sun Gear Shaft	B-14
G-011	2.5" Bevel Pinion	B-14
G-012	Input Shaft Assembly	B-15
G-013	Ring Gear Modification	B-15
G-014	Bearing Plate	B-16
G-015	Rear Plate Assembly	B-16

Telescopic Arm Prints

Base Section

B-001	Base C-Channel	B-17
B-002	Base Side Strap Assembly	B-17
B-002-1	Base Side Bar	B-18

B-002-2.....	Base Spacer Plate	B-18
B-003	Base Bottom Strap.....	B-19
IBR-001	Intermediate Back Roller Plate.....	B-19
B-010	End Support Pivot Plate	B-20
SR-001.....	Intermediate Support Roller	B-20
NRC-002	New Intermediate Roller Casing	B-21
BSR-001	Base Side Support: Slide Block.....	B-21
BSR-002	Base Side Support: Roller Housing.....	B-22
BSR-003	Base Side Support: Thread Block	B-22
BSR-004	Base Side Support: Top/Bottom Plate.....	B-23
BSR-005	Base Side Support: Side Plate	B-23
BSR-006	Base Side Support: Mounting Plate.....	B-24
BSR-007	Base Side Support: Roller Shaft.....	B-24
SR-0.....	Side Roller Housing	B-25
SR-1.....	Side Support Roller	B-25
SR-2.....	Side Support Roller Shaft.....	B-26
SR-4.....	Side Roller Adjustment Block.....	B-26
SR-5.....	Side Support Front Frame	B-27
SR-5A.....	Side Support Rear Frame	B-27
SR-6.....	Side Support: Side Spacer Bar	B-28
SR-7.....	Side Support: Top Spacer Block	B-28
SR-9.....	Int. Side Support Yoke	B-29

Intermediate Section

OCCSM-002.....	Intermediate Base Cross Section.....	B-30
OCCSM-001.....	Intermediate Cross Section.....	B-30
OCCSM-003	Int. Section Assembly	B-31
OCCSM-004.....	Int. Reinforcing Plate.....	B-31
OCCSM-005.....	Int. Section Machining	B-32
IRT-001	Int. Roller Truck	B-32
B-007	Base Section Wear Block.....	B-33
B-006	Base Tube Bearing Support.....	B-33
B-008	Base Wear Pad Adjusting Screw.....	B-34
SR-8.....	Fly Side Support Yoke	B-34
FSR-1	Fly Support Roller Block.....	B-35
NRC-001	New Fly Roller Casing	B-35

Fly Section

CS-001-b.....	Fly Base Cross Section.....	B-36
CS-001.....	Fly Cross Section.....	B-36
CS-002.....	Fly Cross Section Assembly.....	B-37
RP-2.....	Fly Reinforcing plate	B-37
CS-002M	Fly Cross Section Machining	B-38

RT-1	Fly Upper Roller Truck	B-38
FBR-1;FBR-2	Fly Back Rollers	B-39

Truck Mount

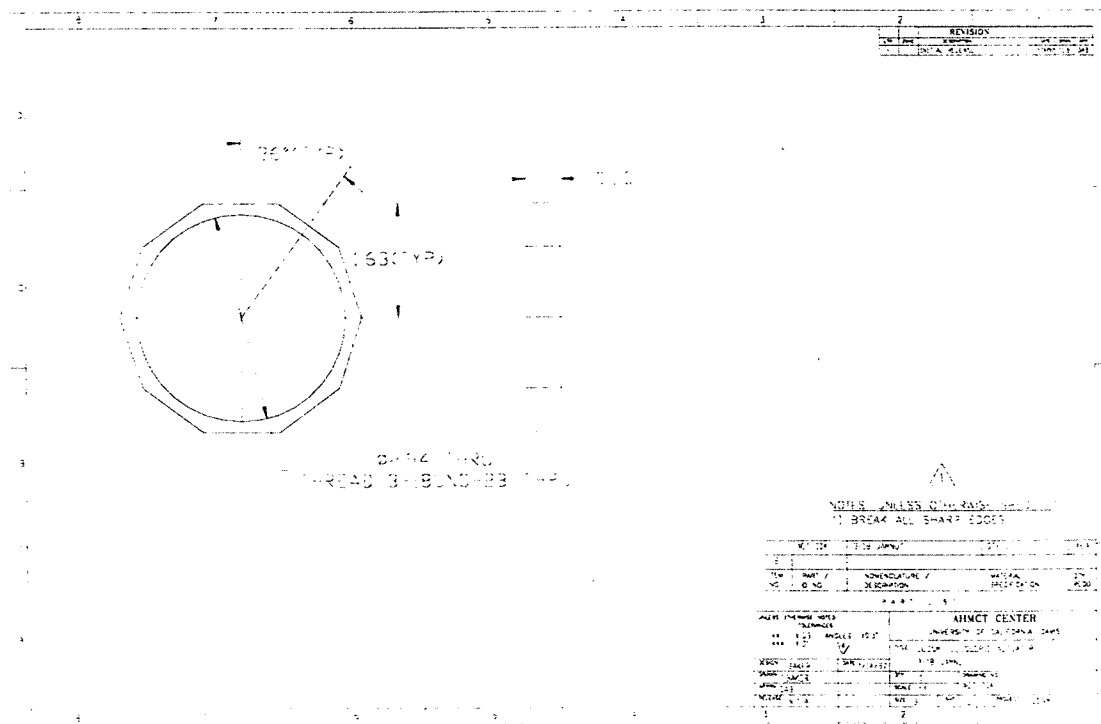
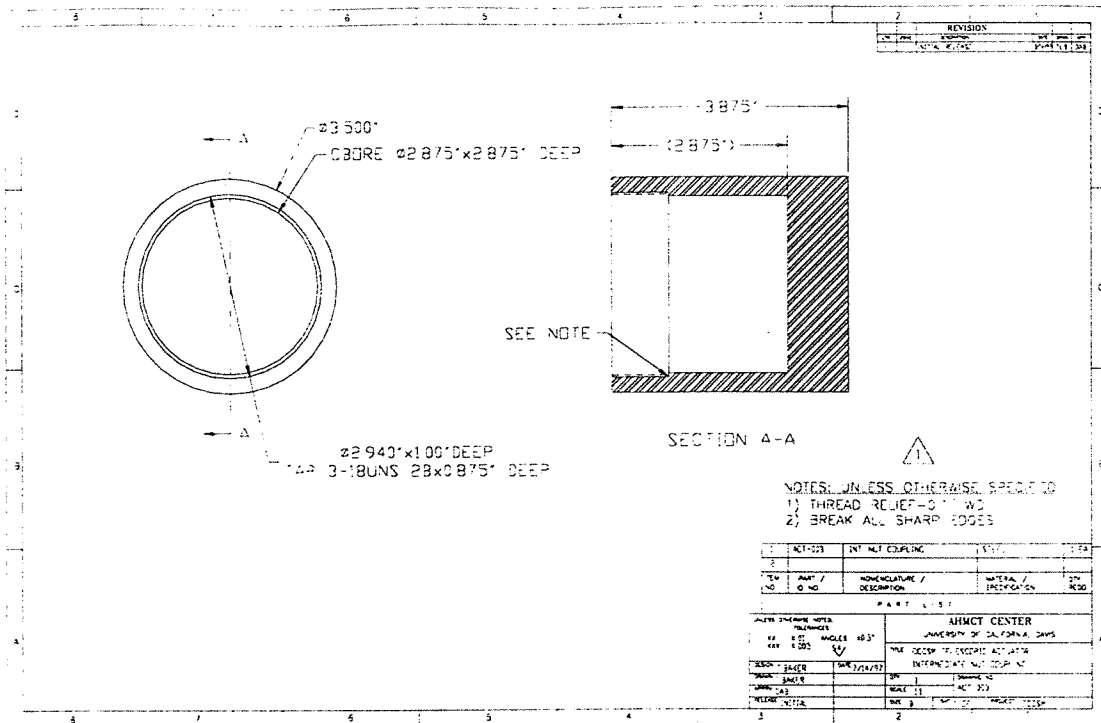
SPRT-001	Strut Rail	B-40
SPRT-002	Roller Plate	B-40
SPRT-003	Main Rail	B-41
SPRT-004	Middle Support Bar	B-41
SPRT-005	Side Support Bar	B-42
STRK-001LH/RH	Support Truck: Side Plates	B-42
STRK-002	Support Truck: Top/Bottom Plates	B-43
STRK-003	Support Truck: Roller Plates	B-43
STRK-004	Support Truck: Front Plate	B-44
STRK-005	Support Truck: Weld Assy	B-44
STRK-006	Support Truck: Horizontal Mount	B-45
WM-ASSY	Winch Mount Assy	B-45
UHNG-ASSY	Upper Hinge Plate	B-46
LHNG-ASSY	Lower Hinge Plate	B-46
B-011	Hinge Pins	B-47
WM-001	Winch Mod: Roller Plate	B-47
WM-002	Winch Mod: Winch Roller	B-48
WM-003	Winch Mod: Cable Roller	B-48

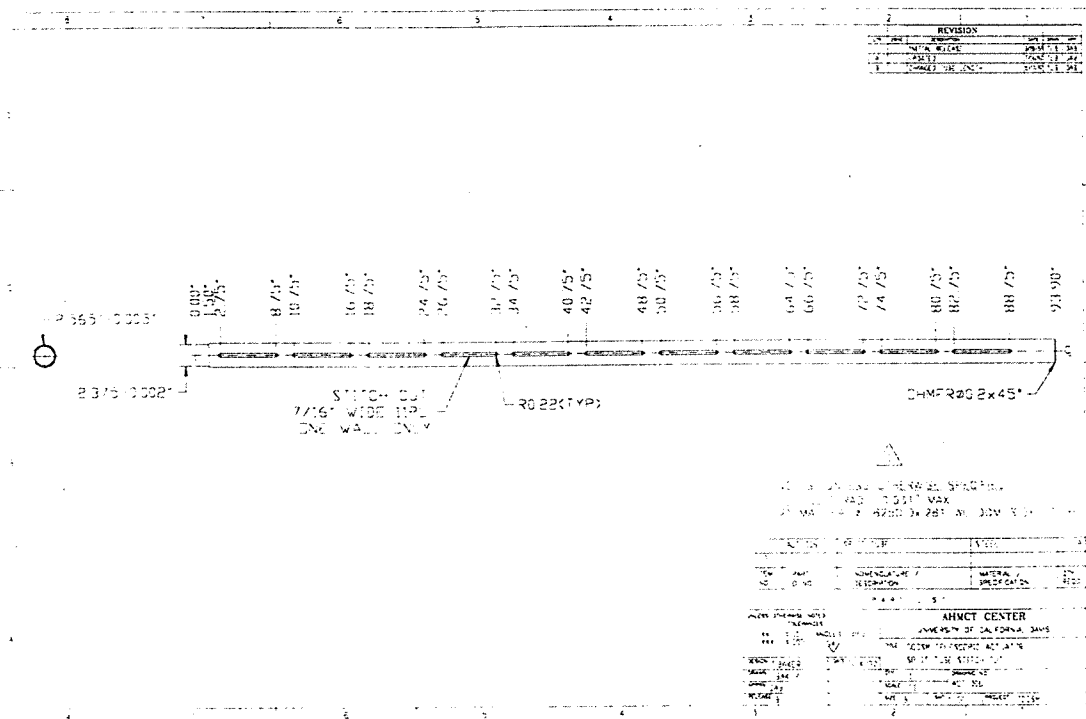
Actuator Supports

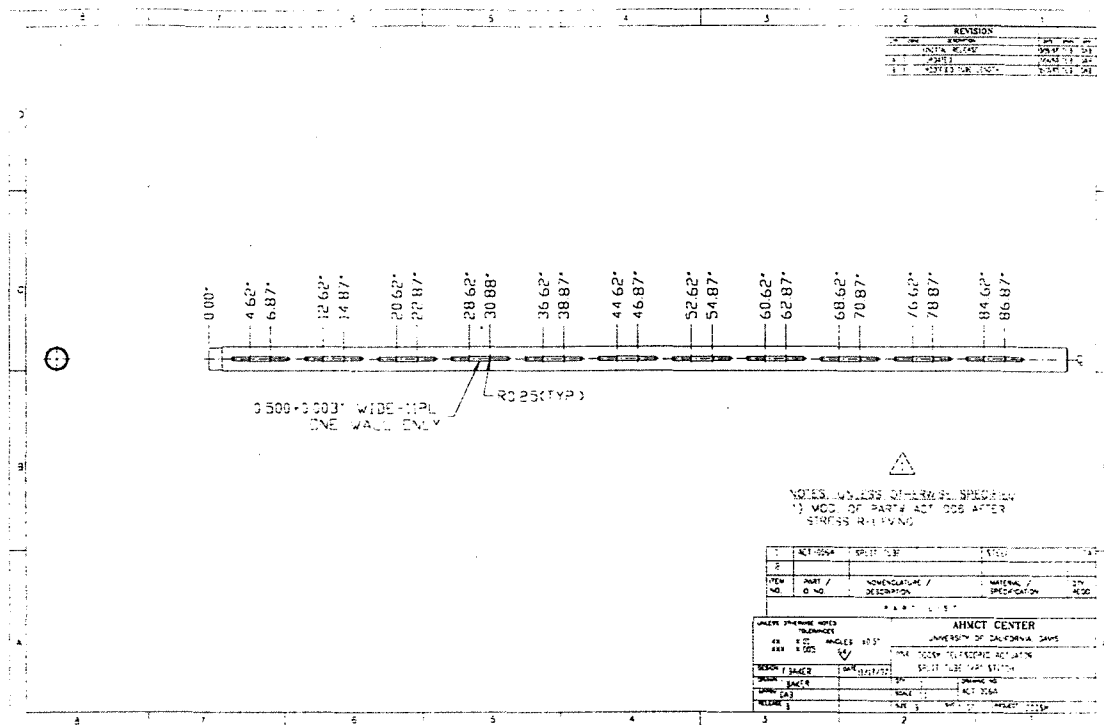
ACTSPRT-001	Fly Support Plate	B-49
ACTSPRT-002	Alignment Plate	B-49
ACTSPRT-003	Coupler Plate	B-50
ACTSPRT-004	Int. Support Base Plate	B-50
ACTSPRT-005	Int. Support Flange Plate	B-51
ACTSPRT-006	Int. Support Bearing Flange	B-51
ACTSPRT-007	Int. Support Roller Truck	B-52
ACTSPRT-008	Int. Section Drive Rail	B-52
ACTSPRT-009	Drive Rail Flange Plate	B-53

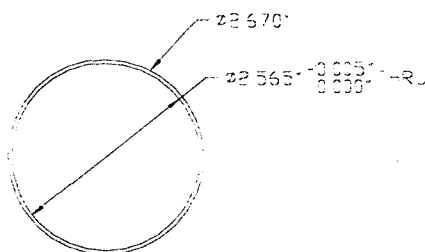
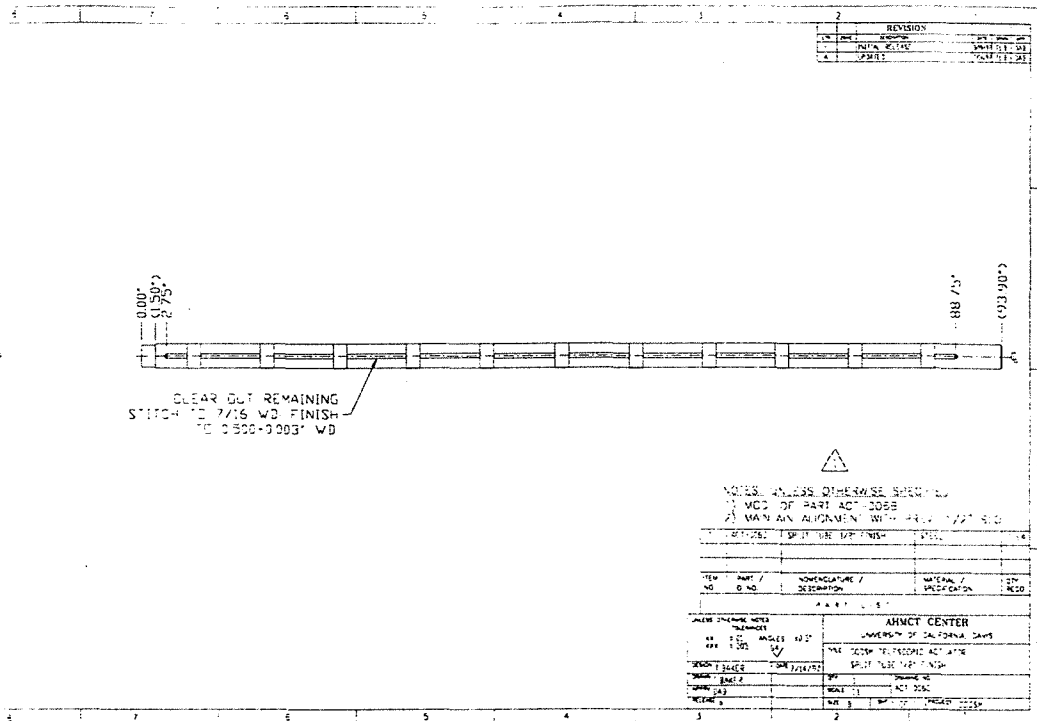
Gearbox Mount

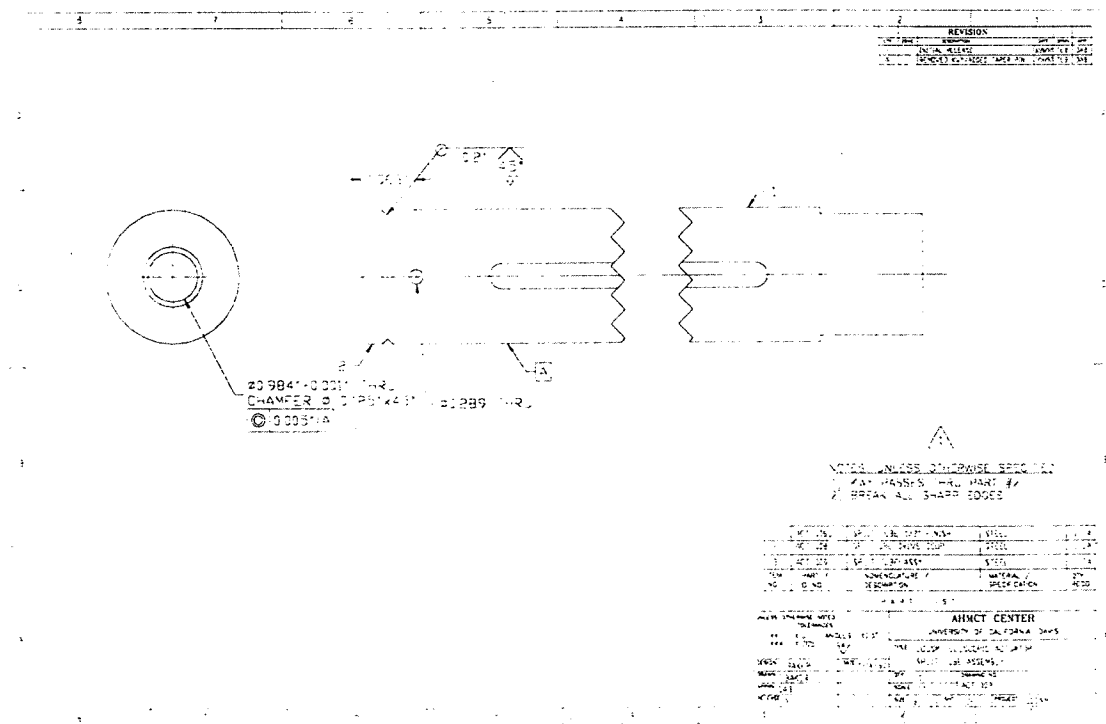
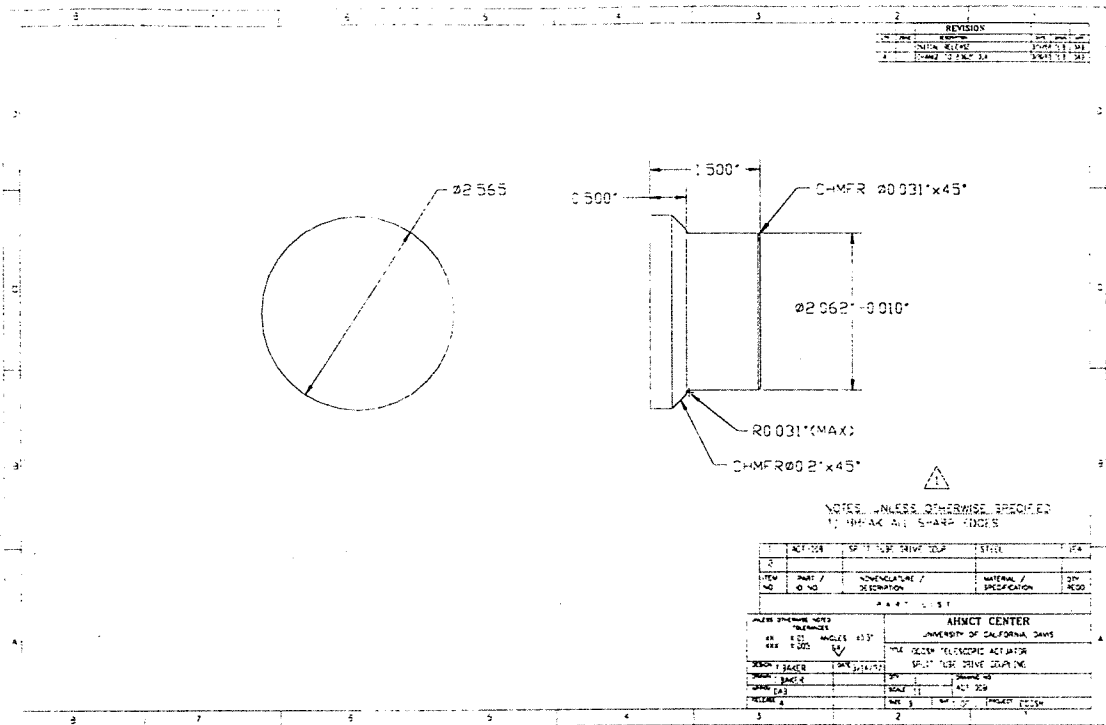
G-001	Gearbox Mount Base Plate	B-54
G-002	Gearbox Mount Side Plate	B-54
G-003	Gearbox Protecting Plate	B-55
G-ASSY	Gearbox Mount Assembly	B-55

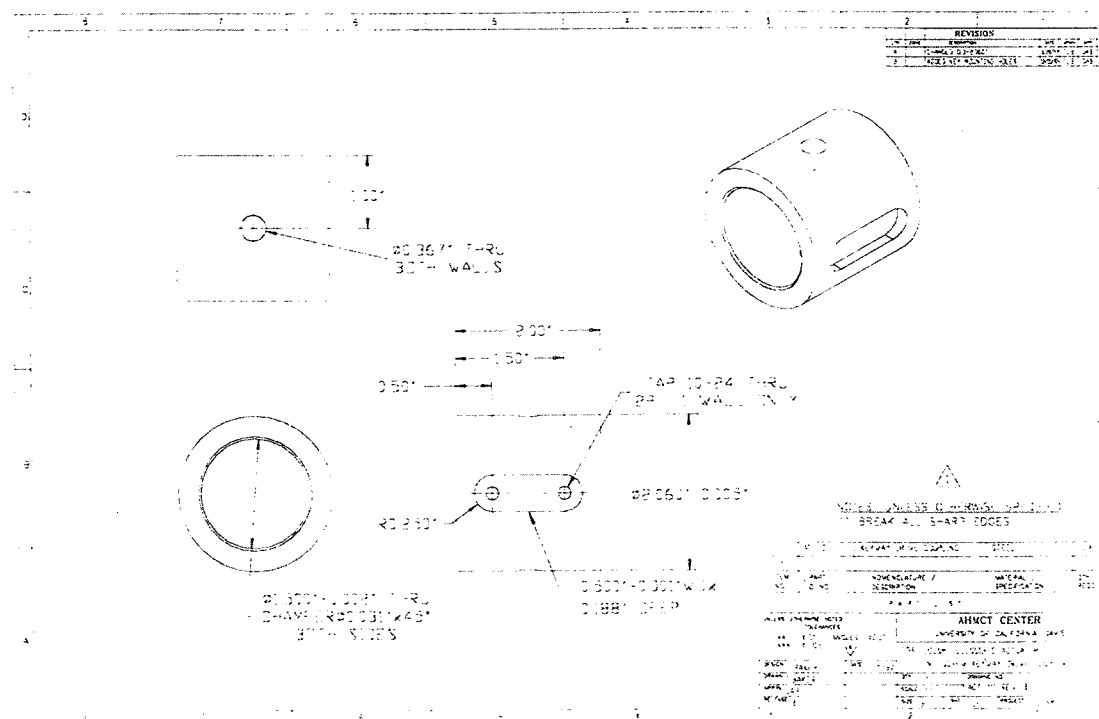




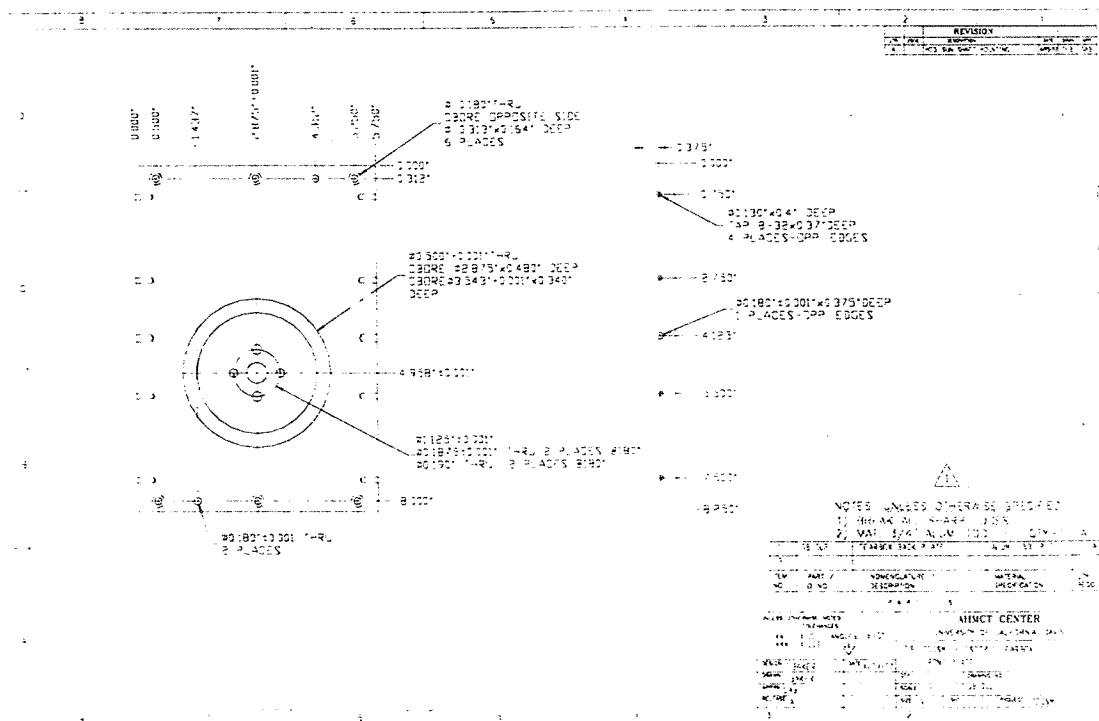
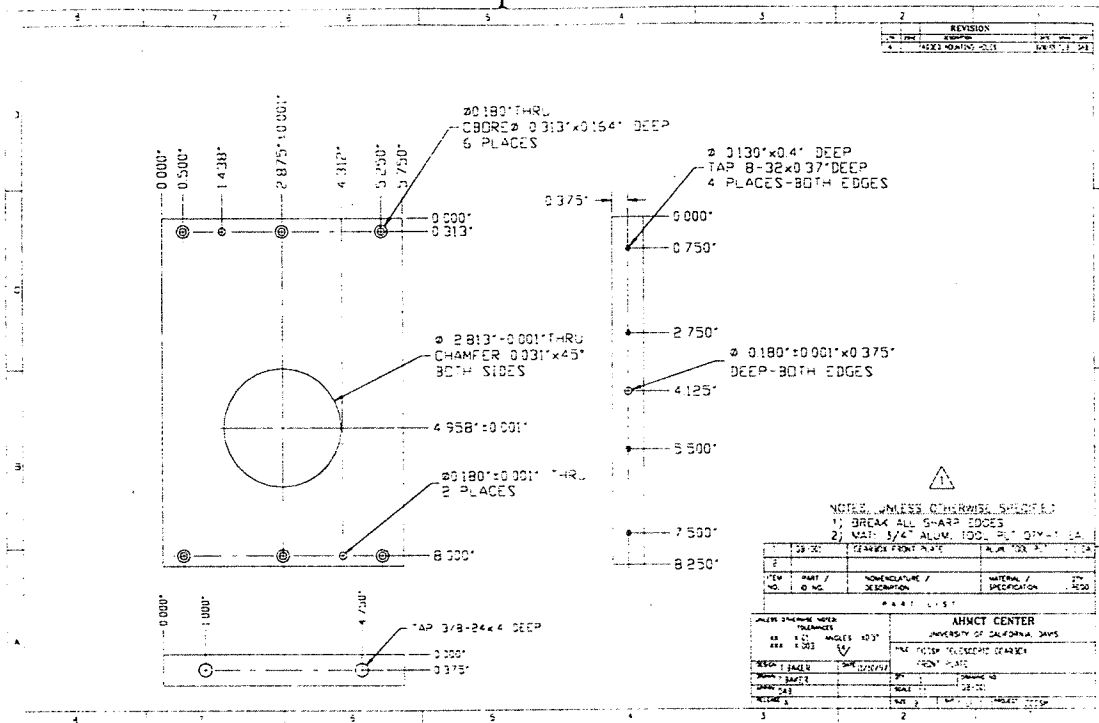


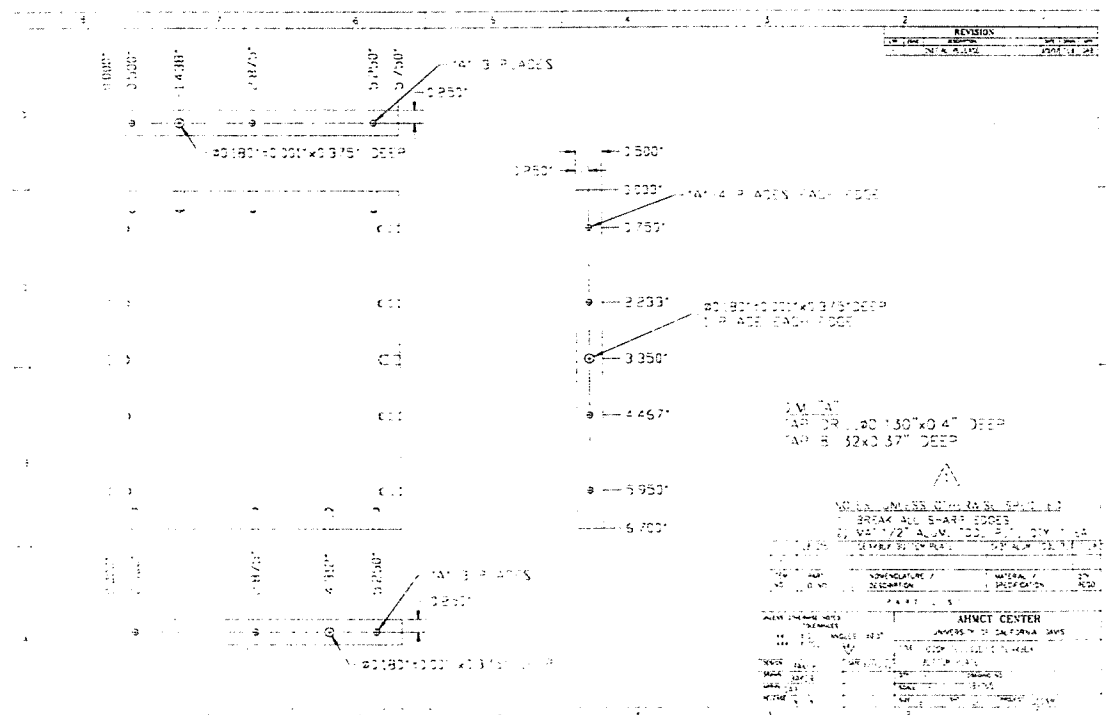
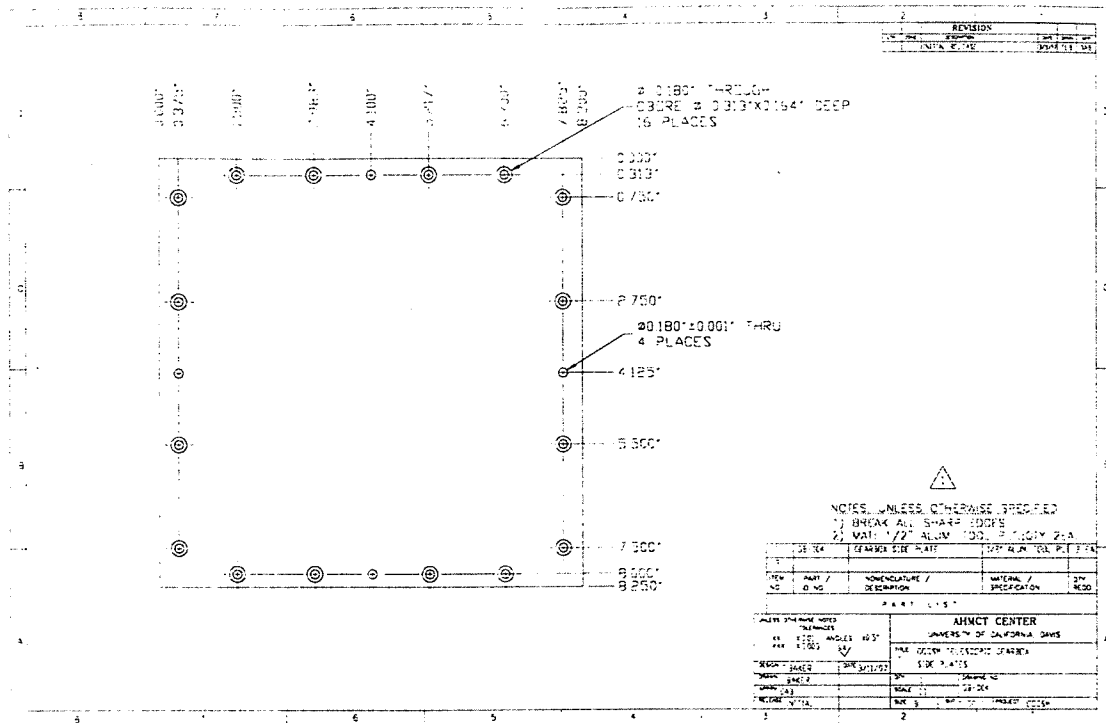


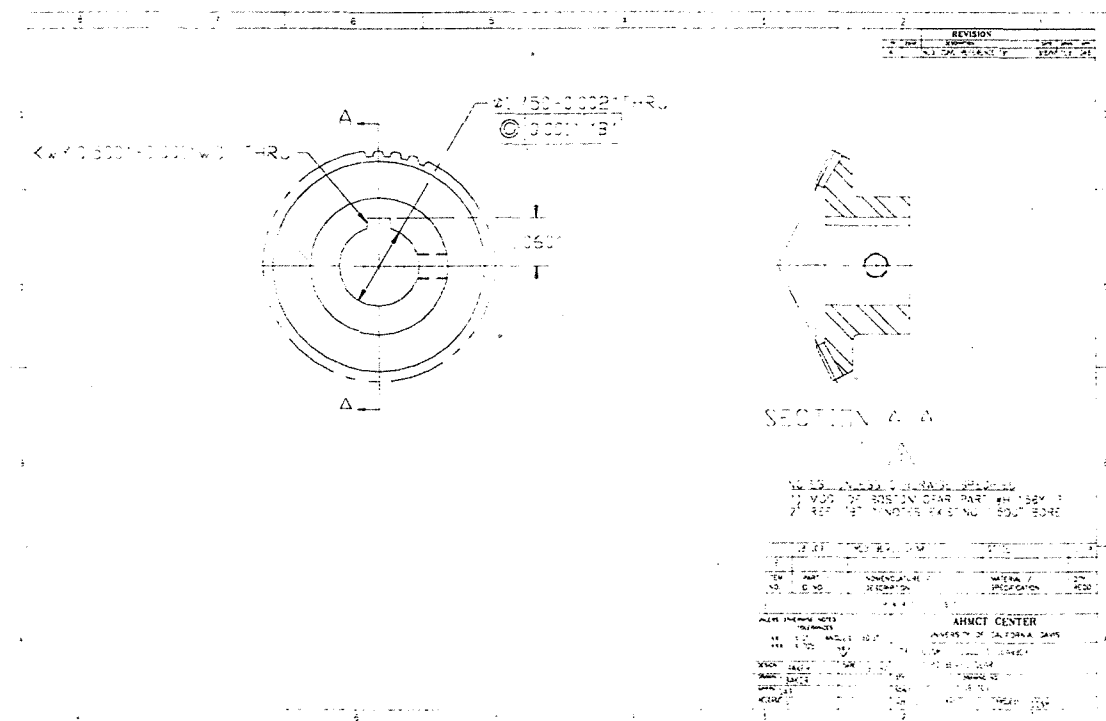
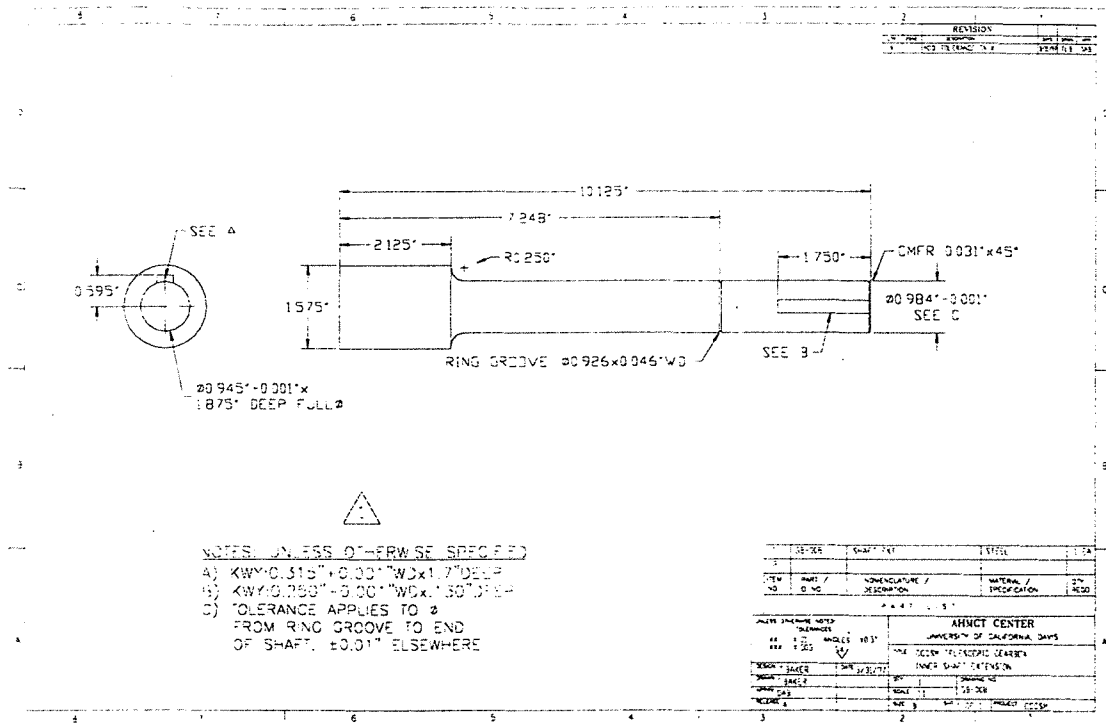


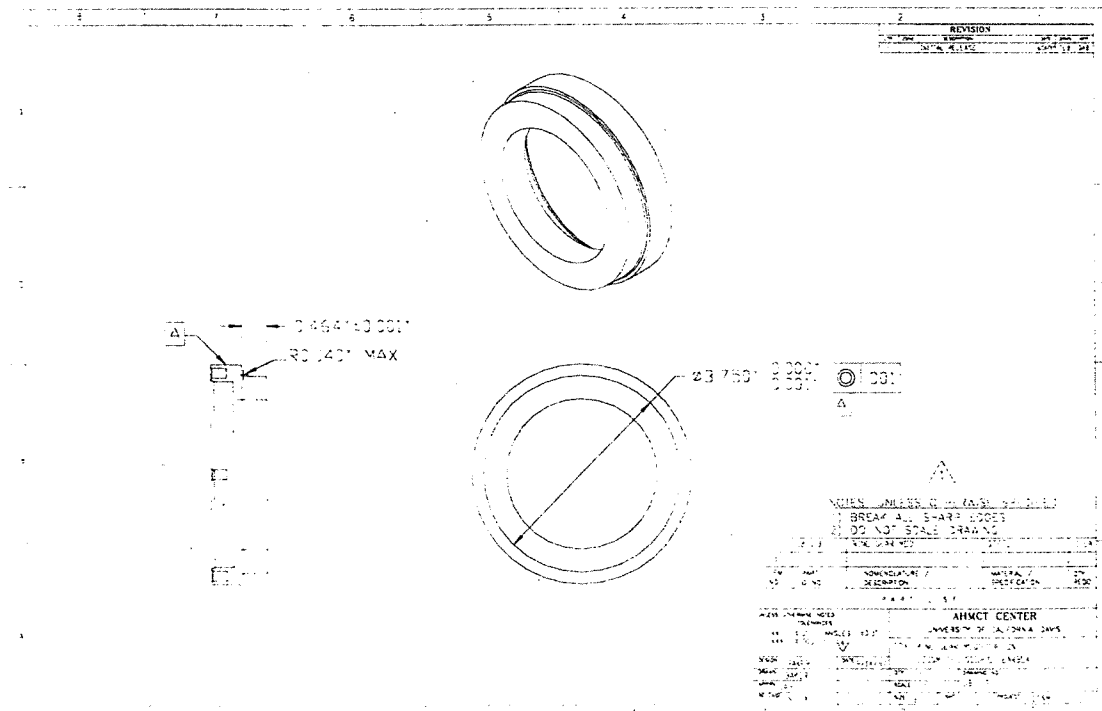
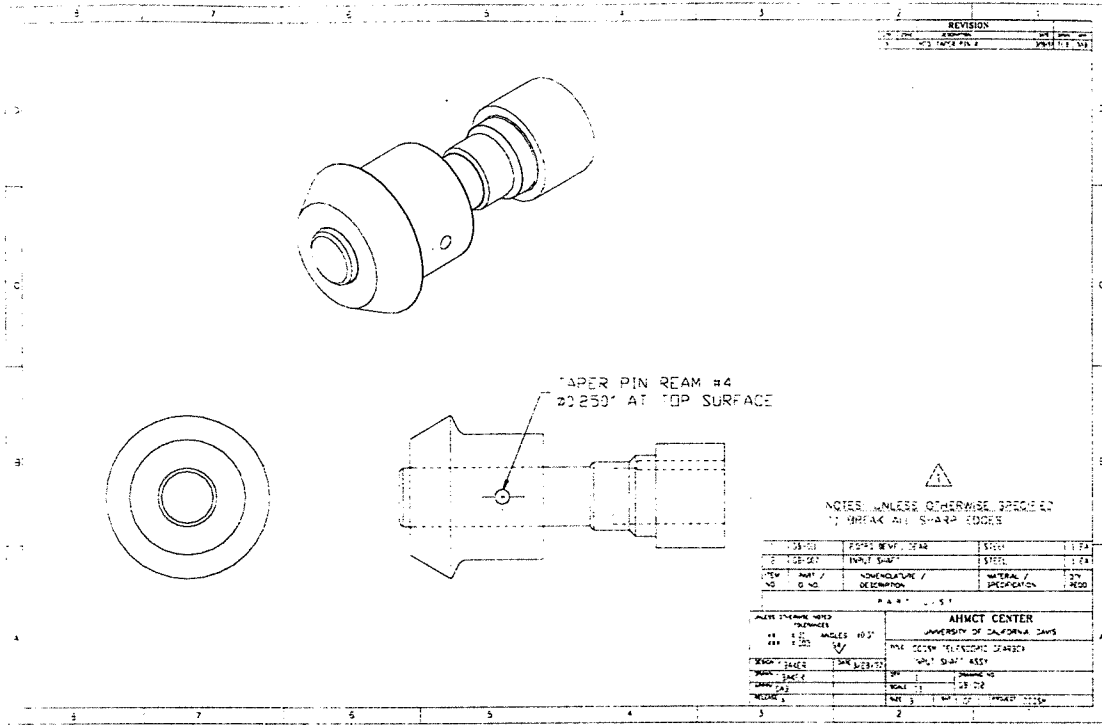


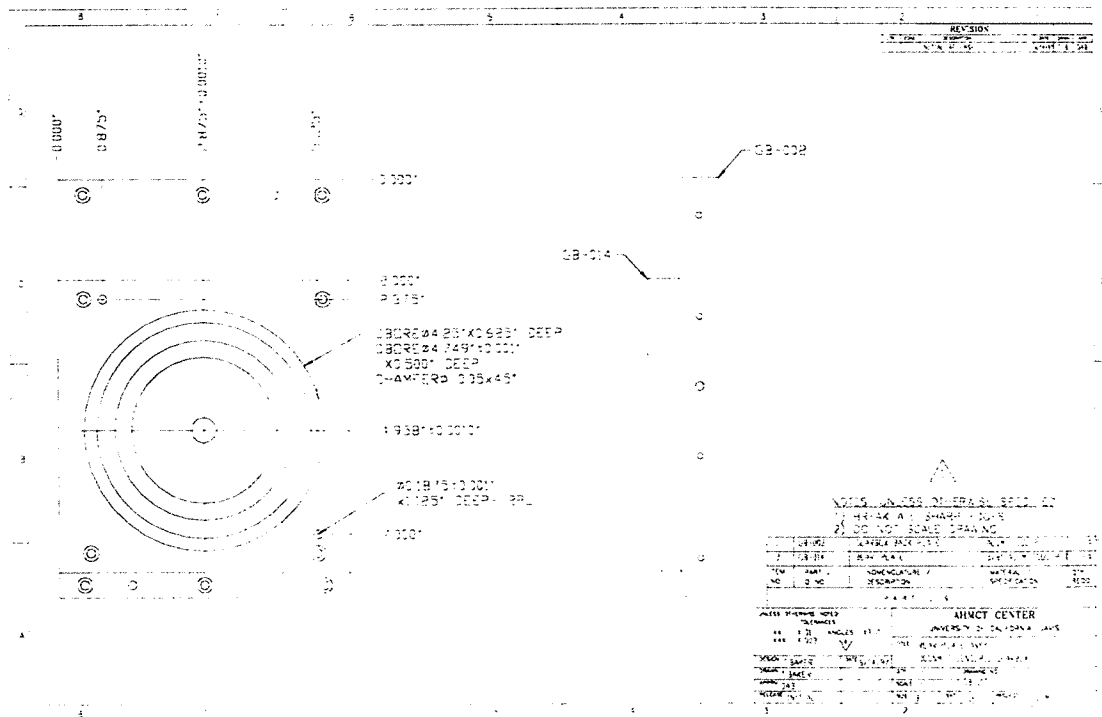
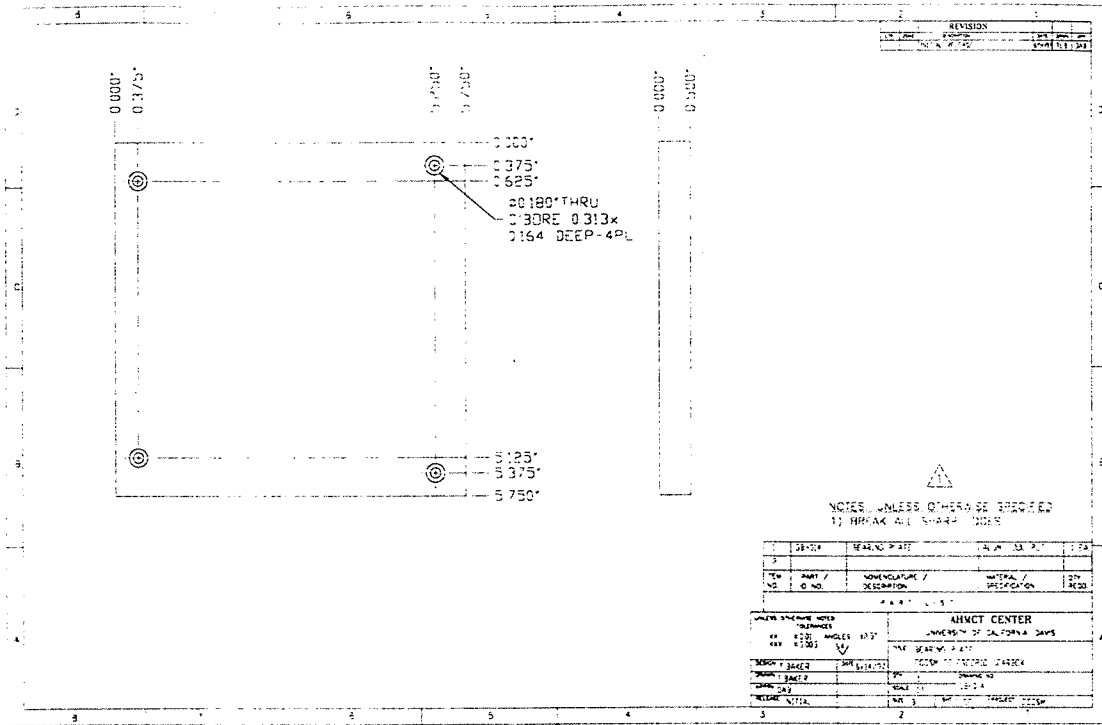
Telescopic Gearbox Prints



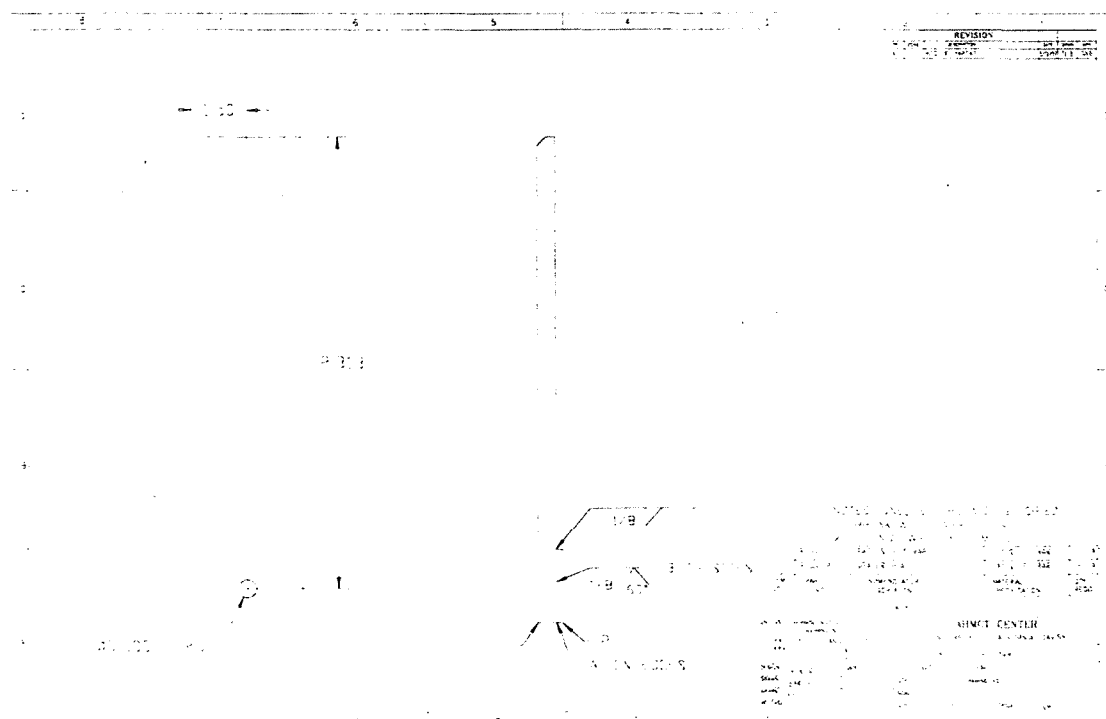
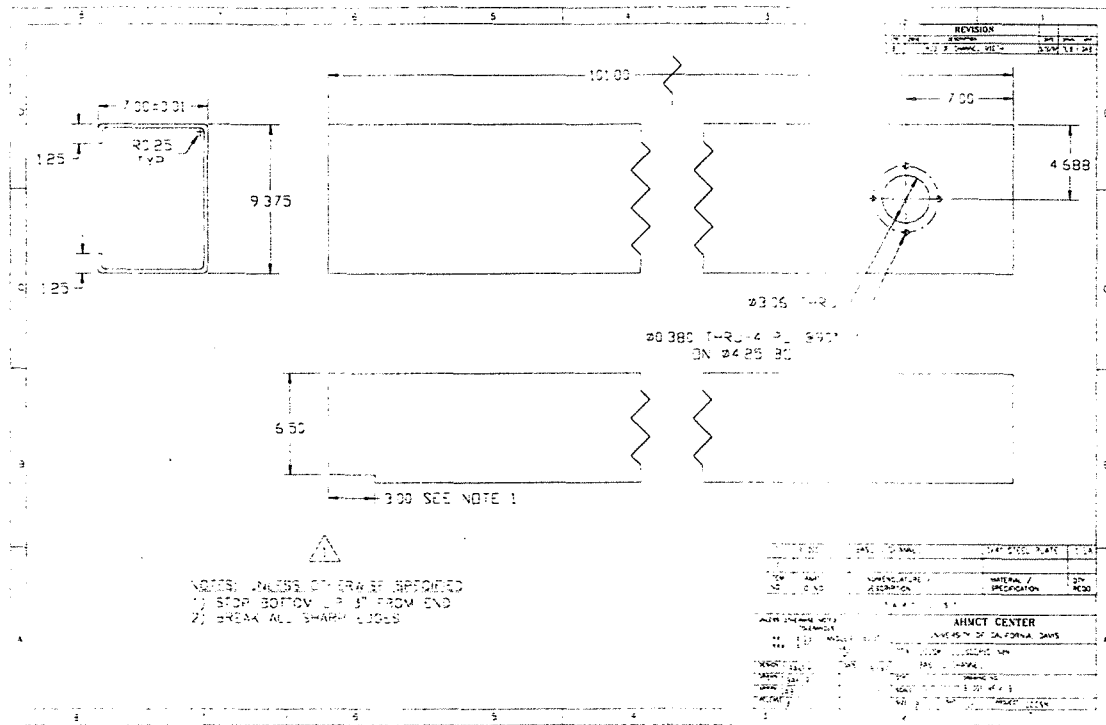


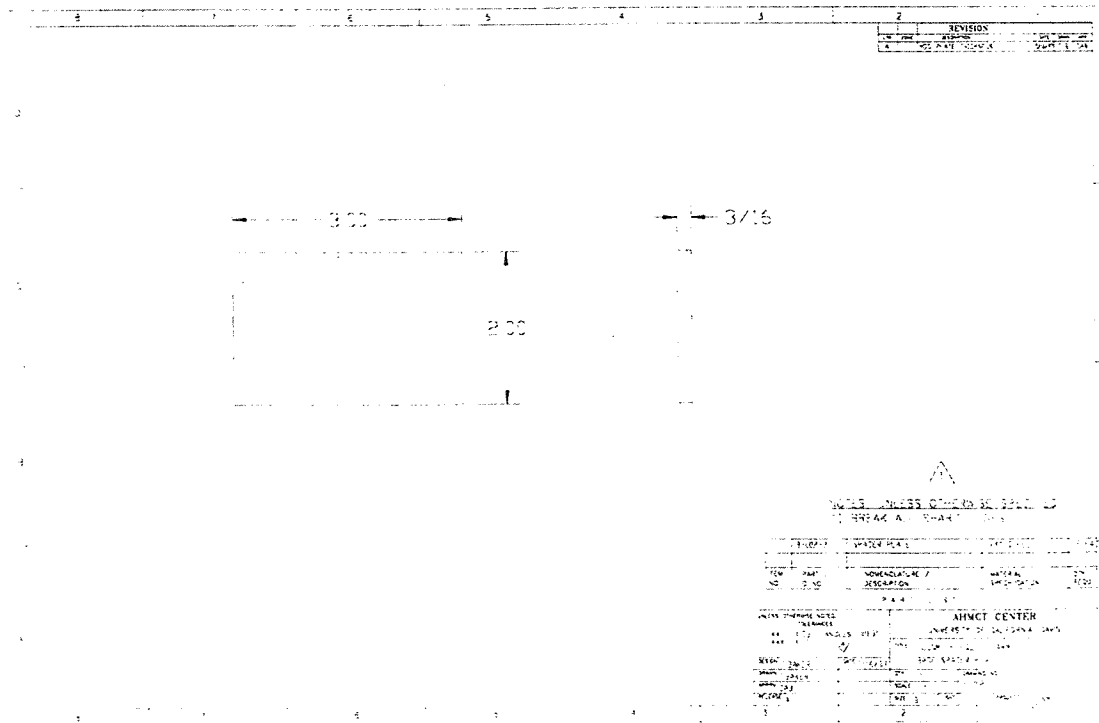
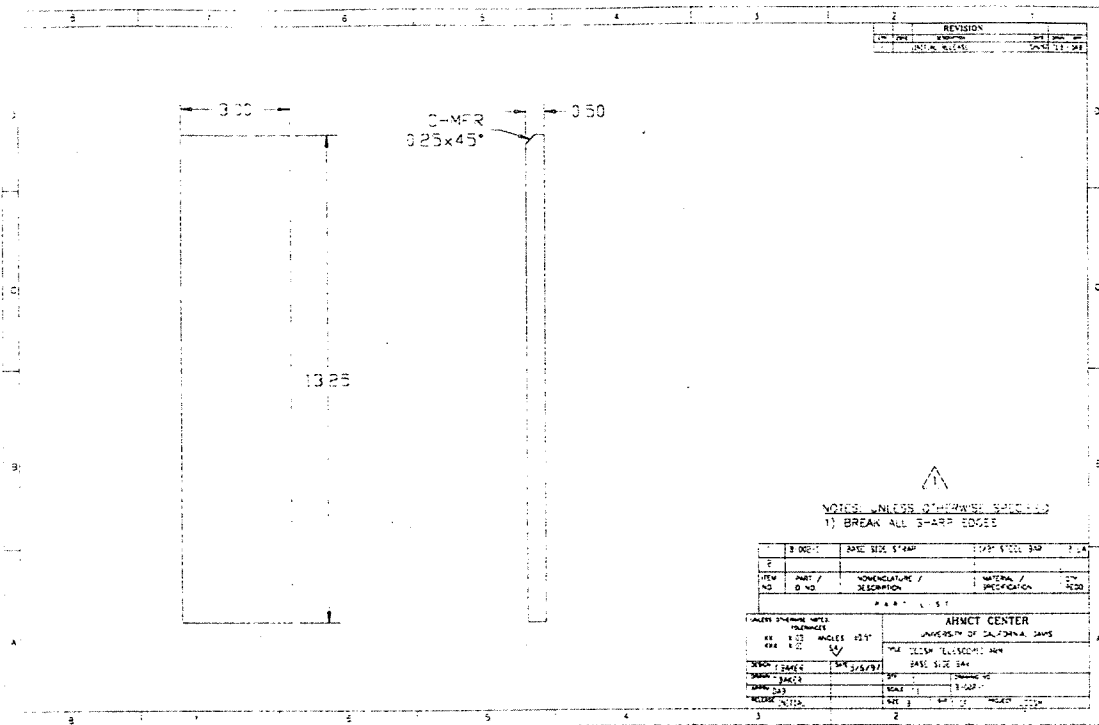


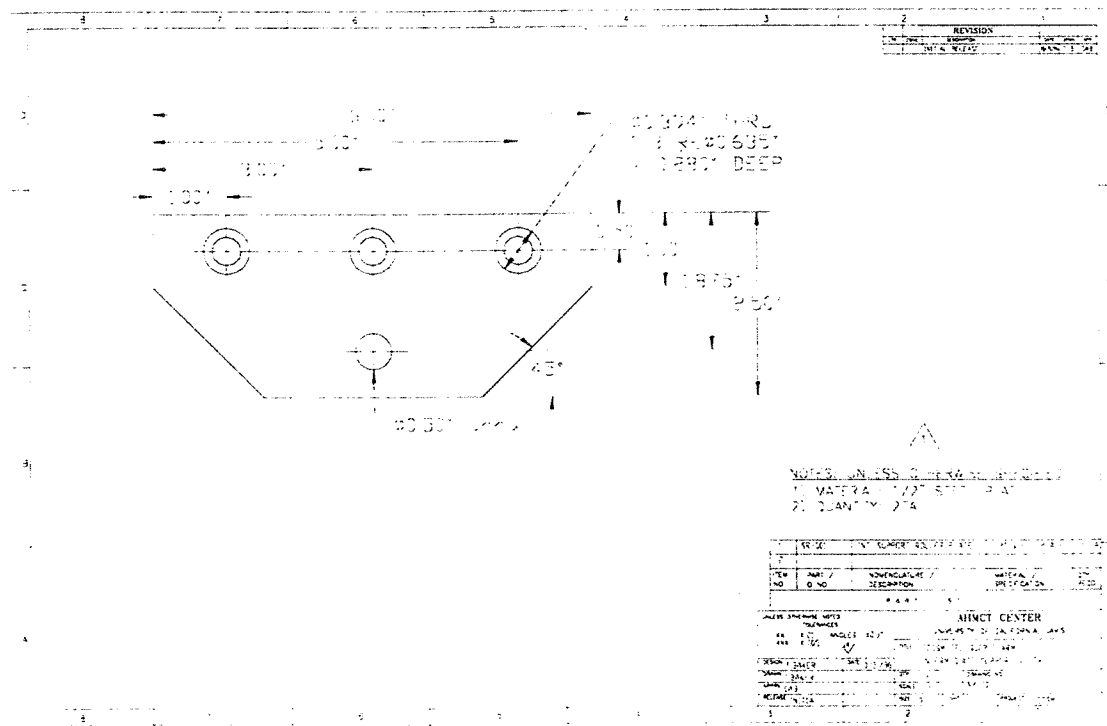
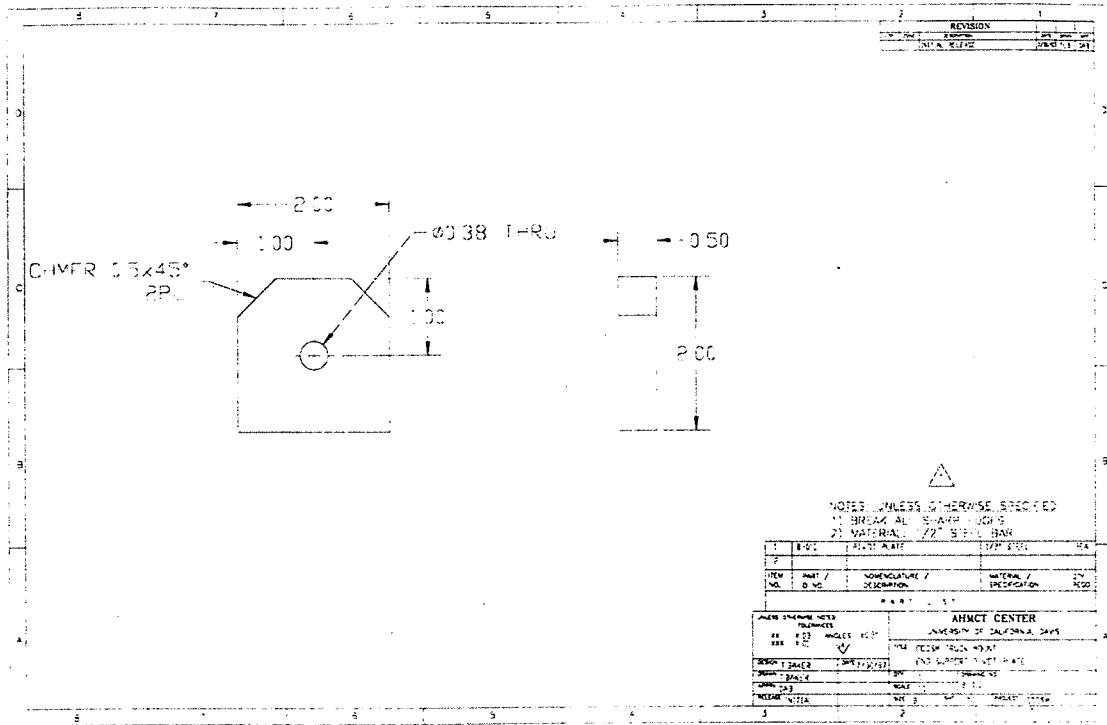


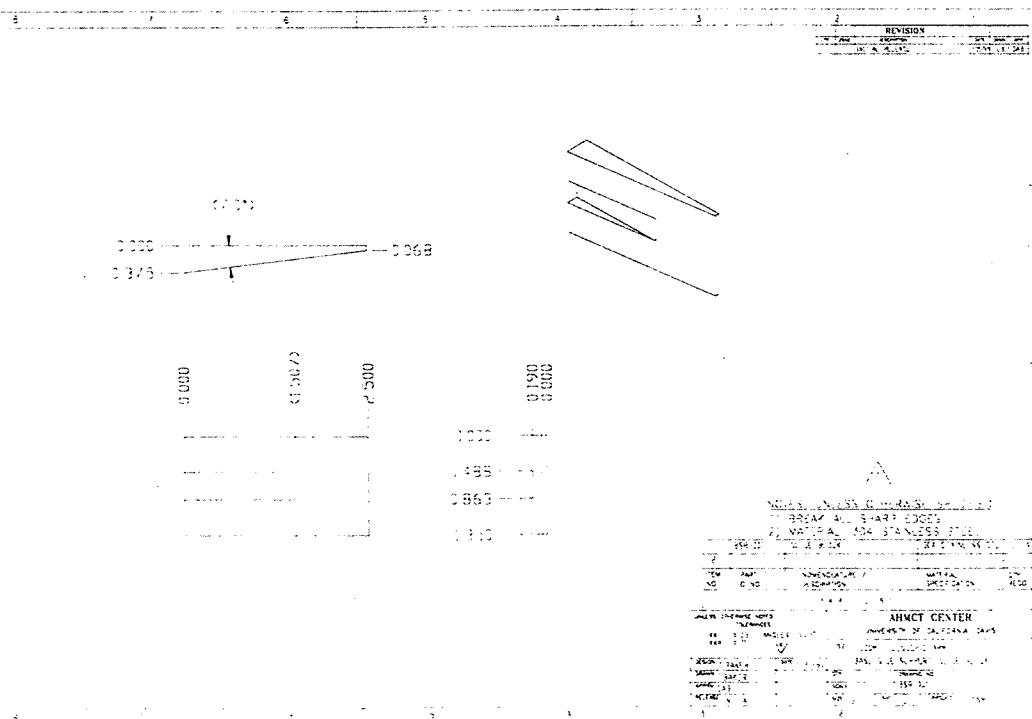
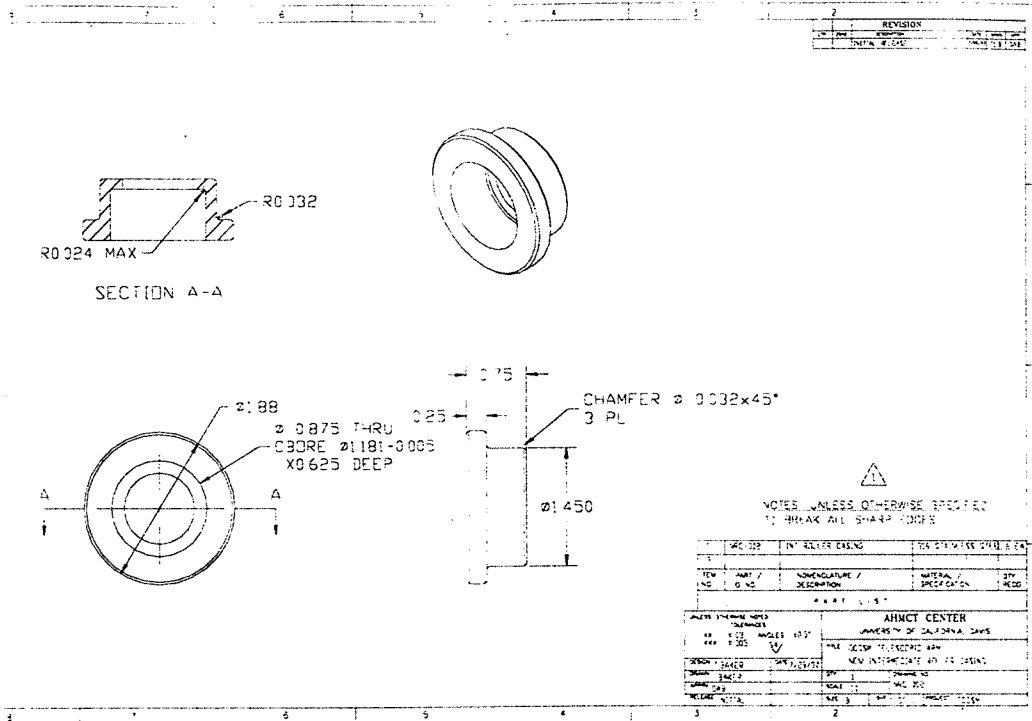


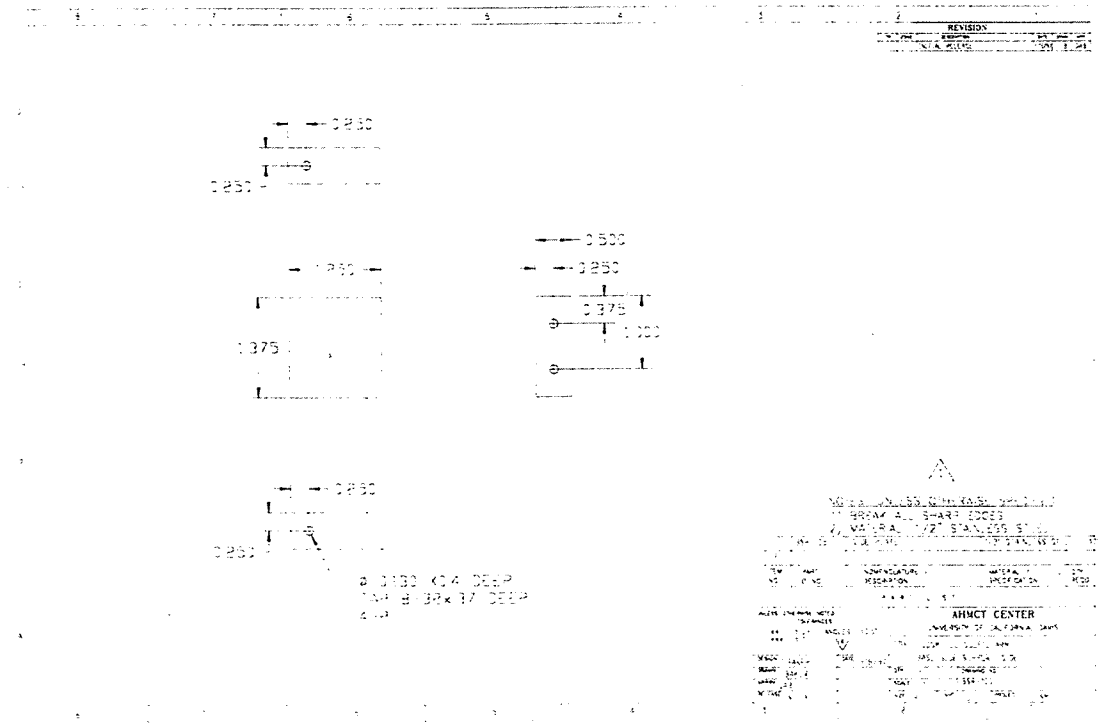
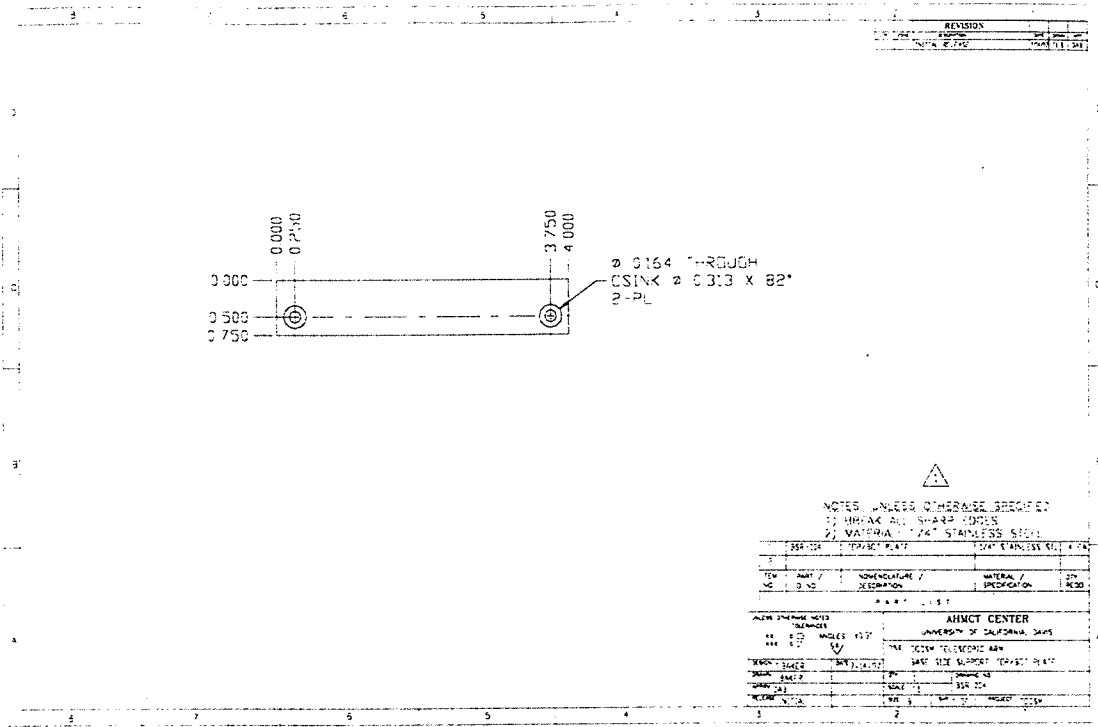
Telescopic Arm Prints Base Section

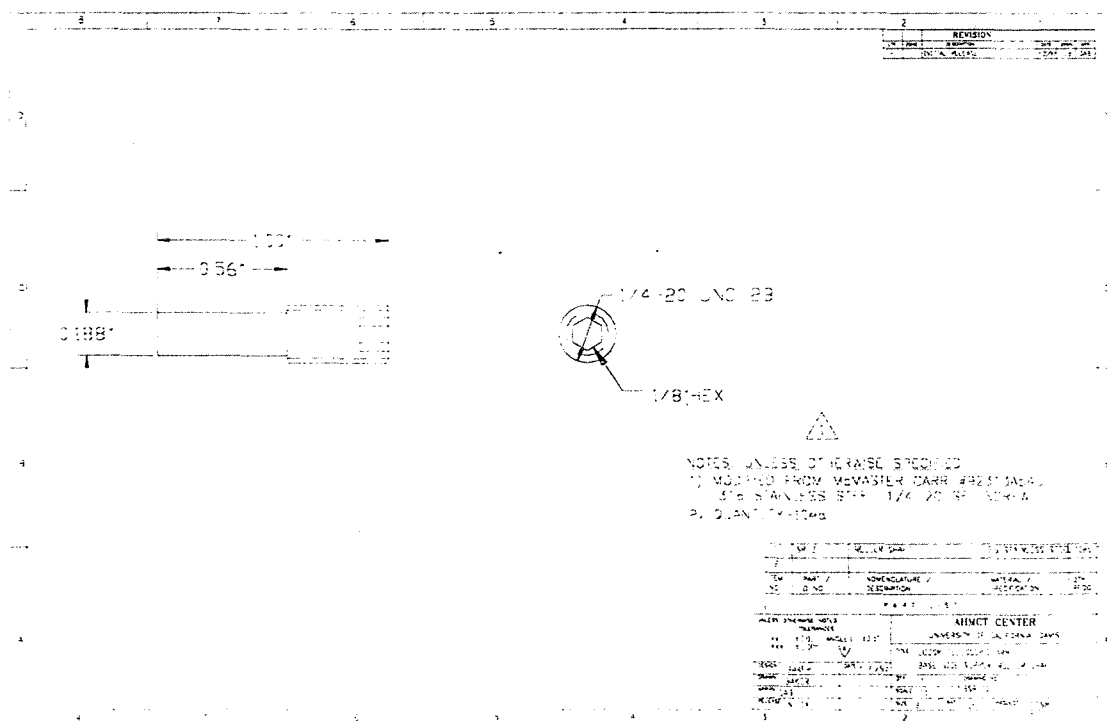
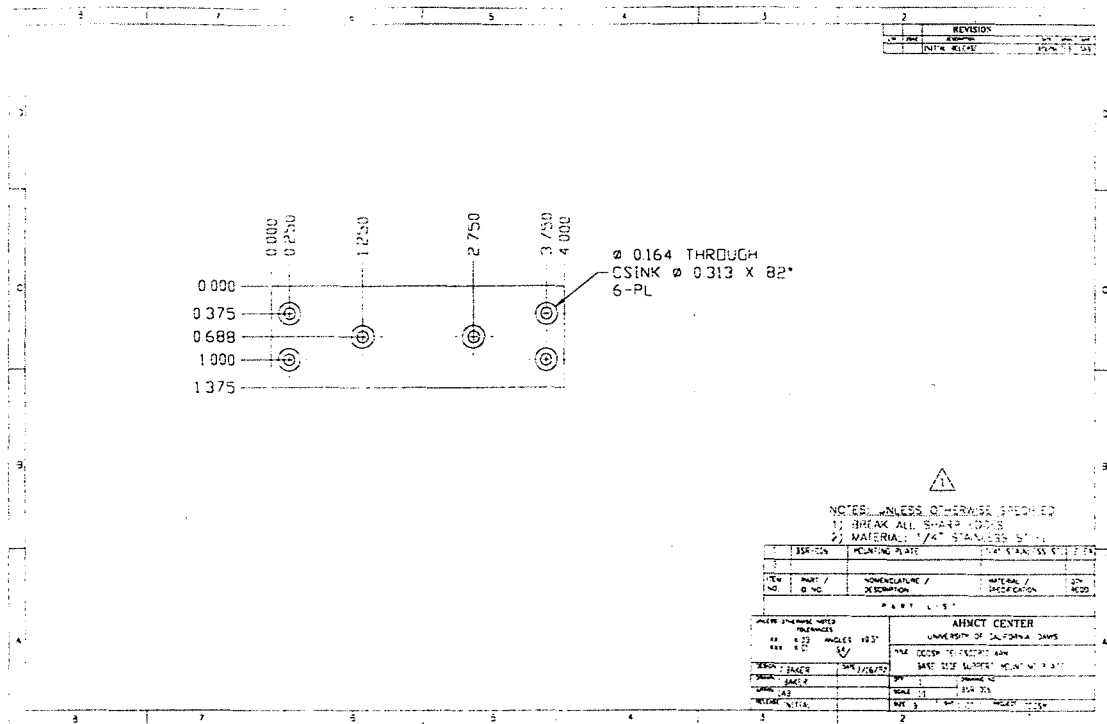


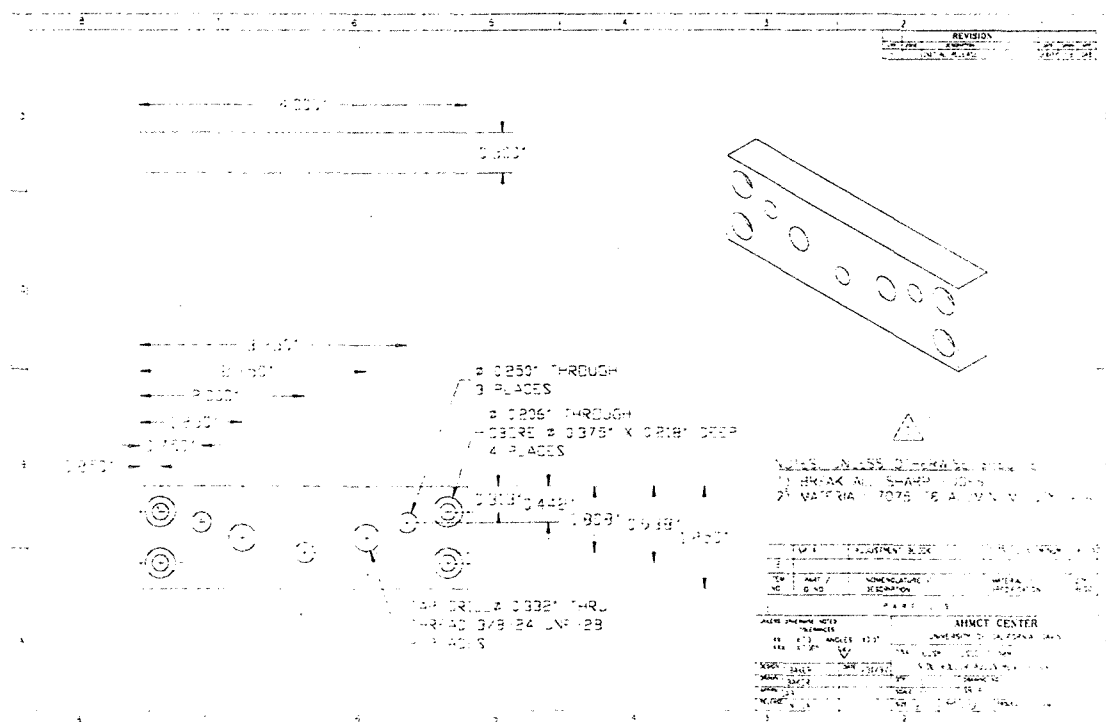
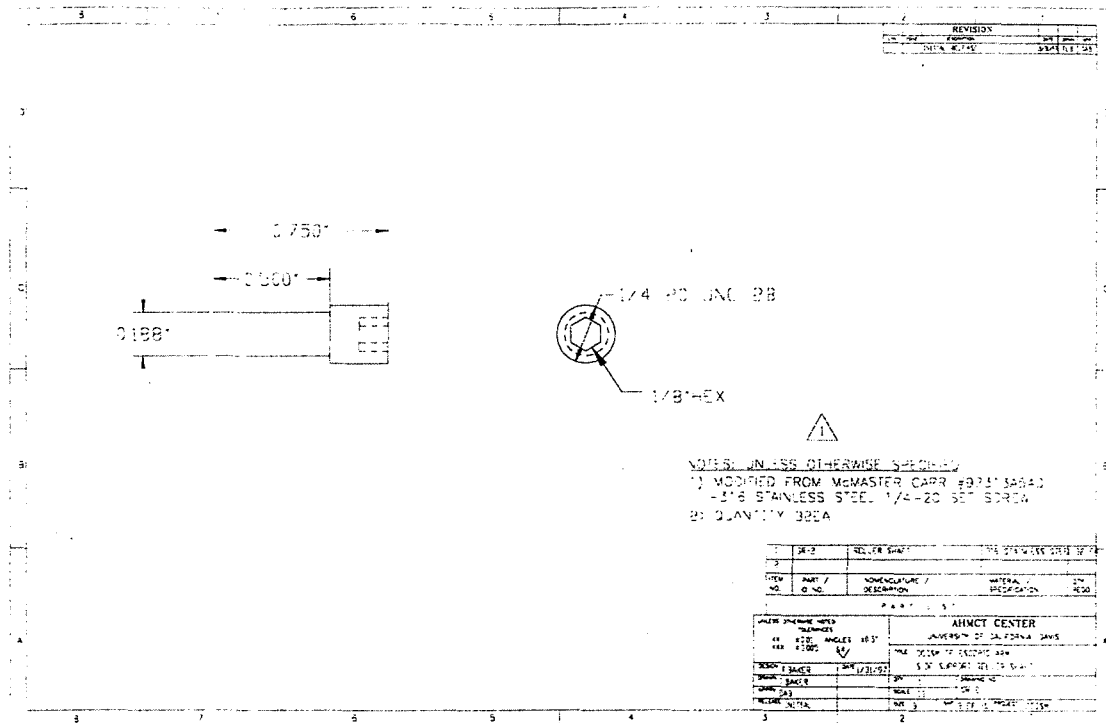


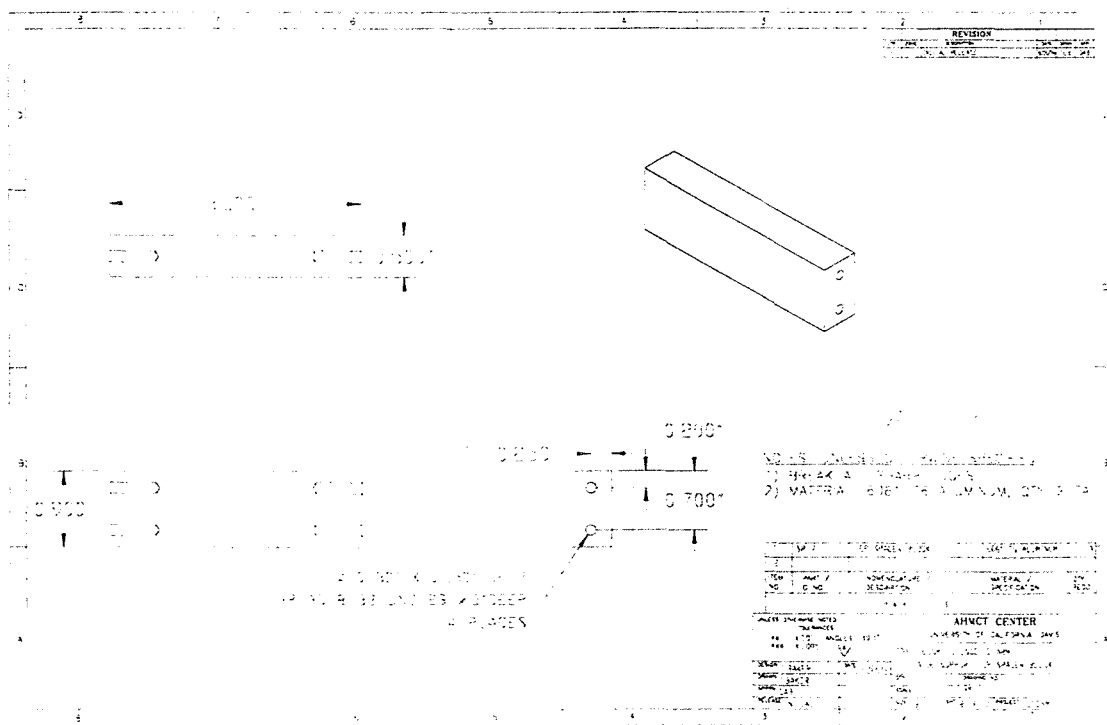
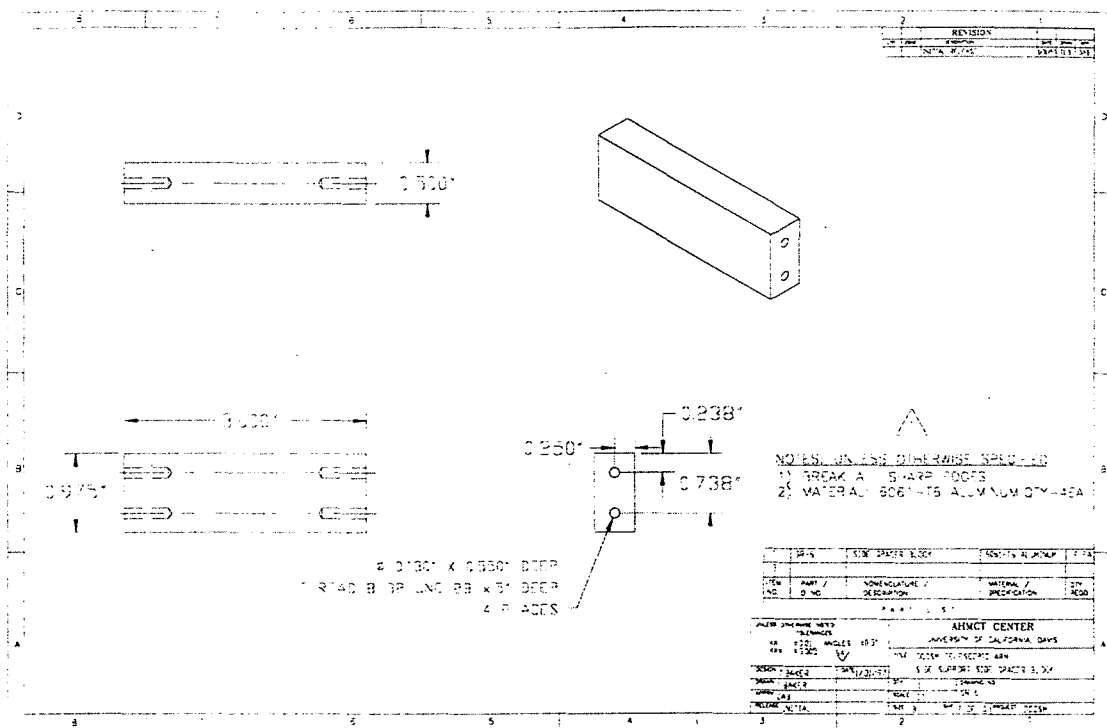


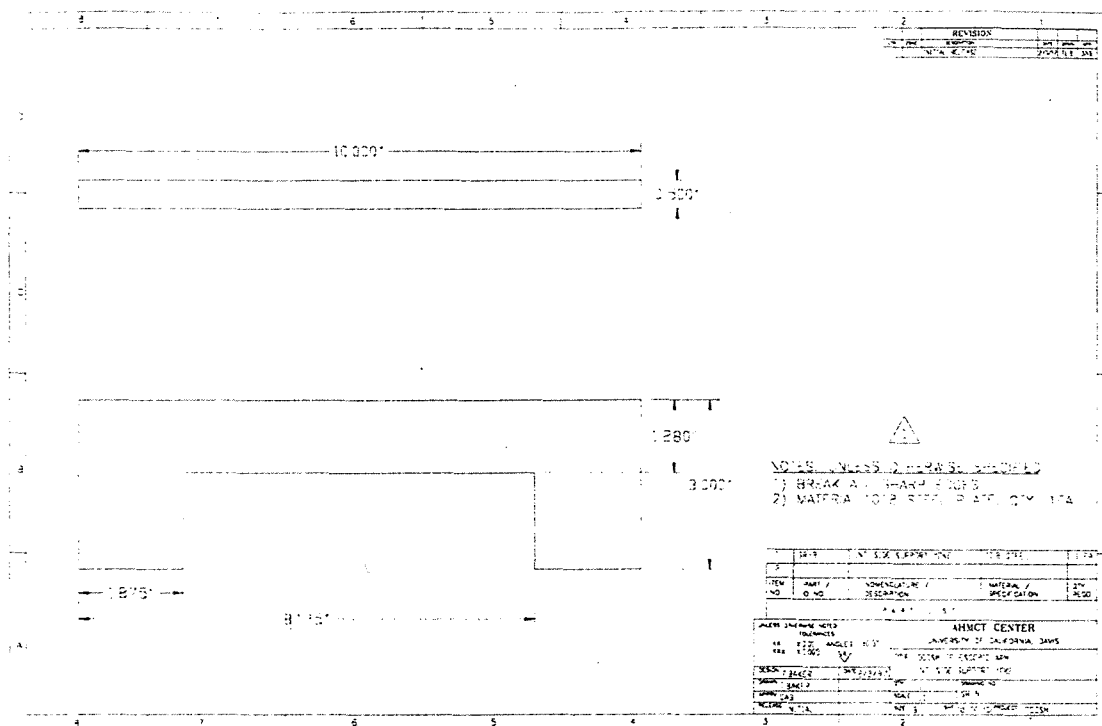




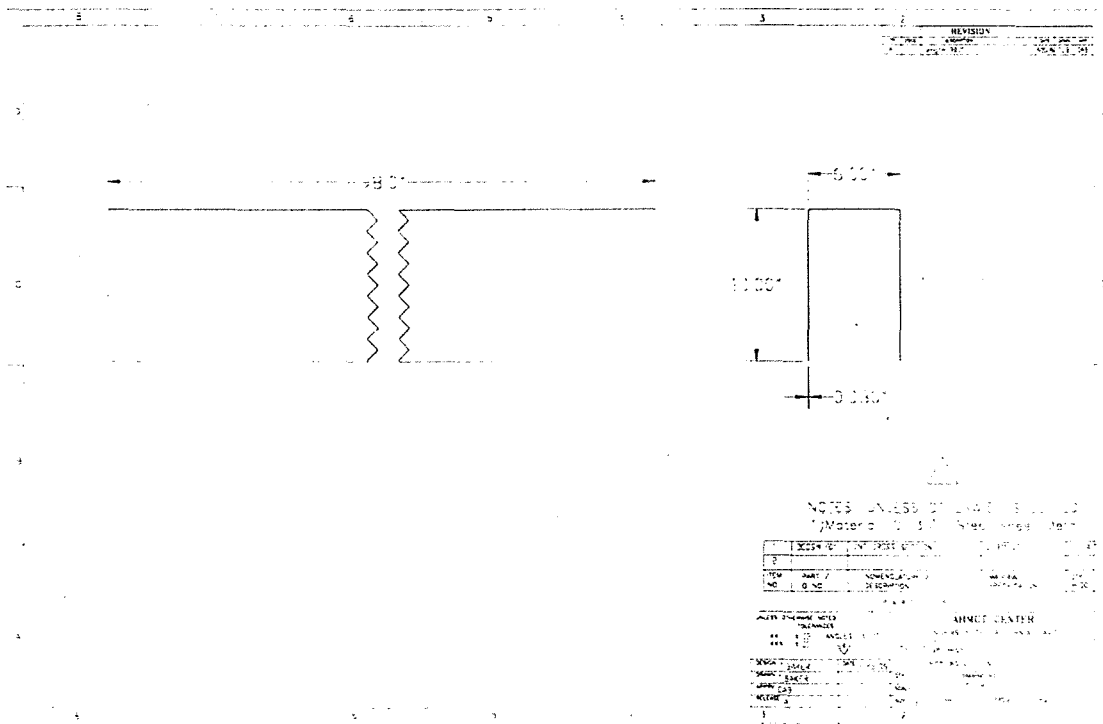
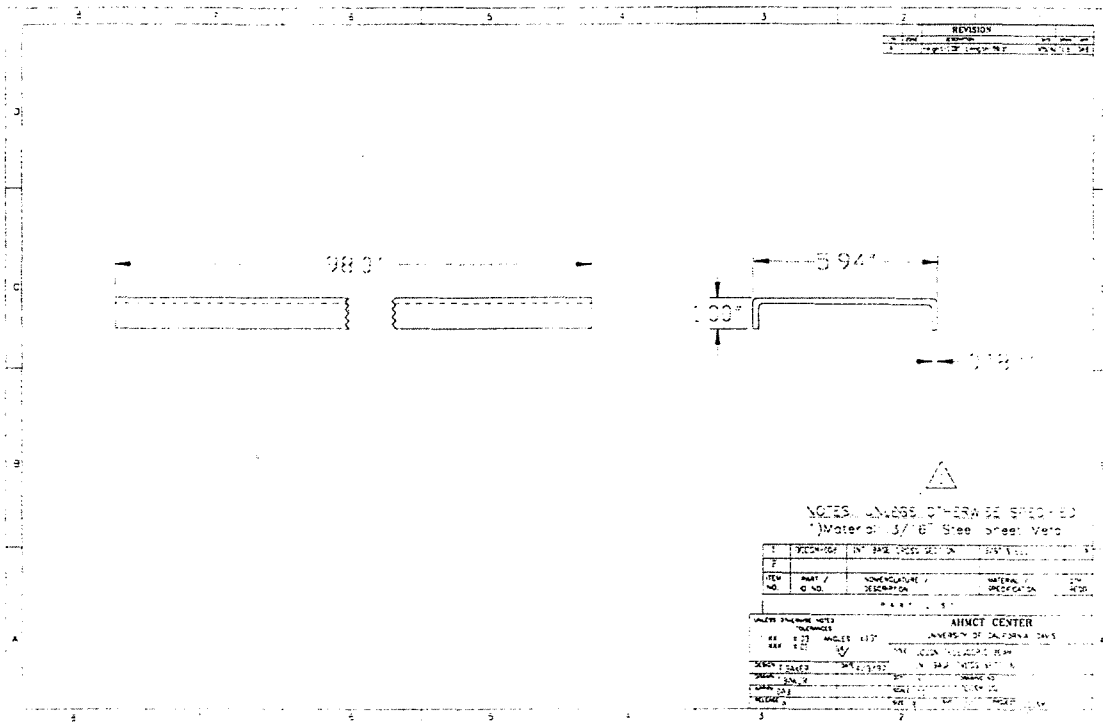


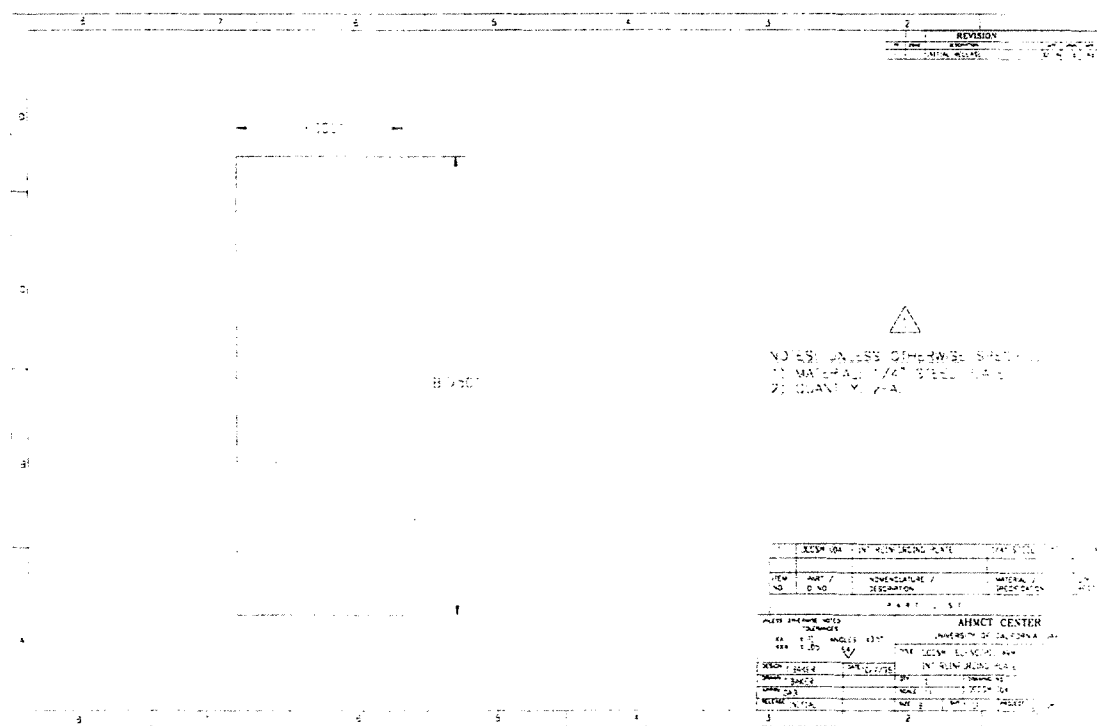
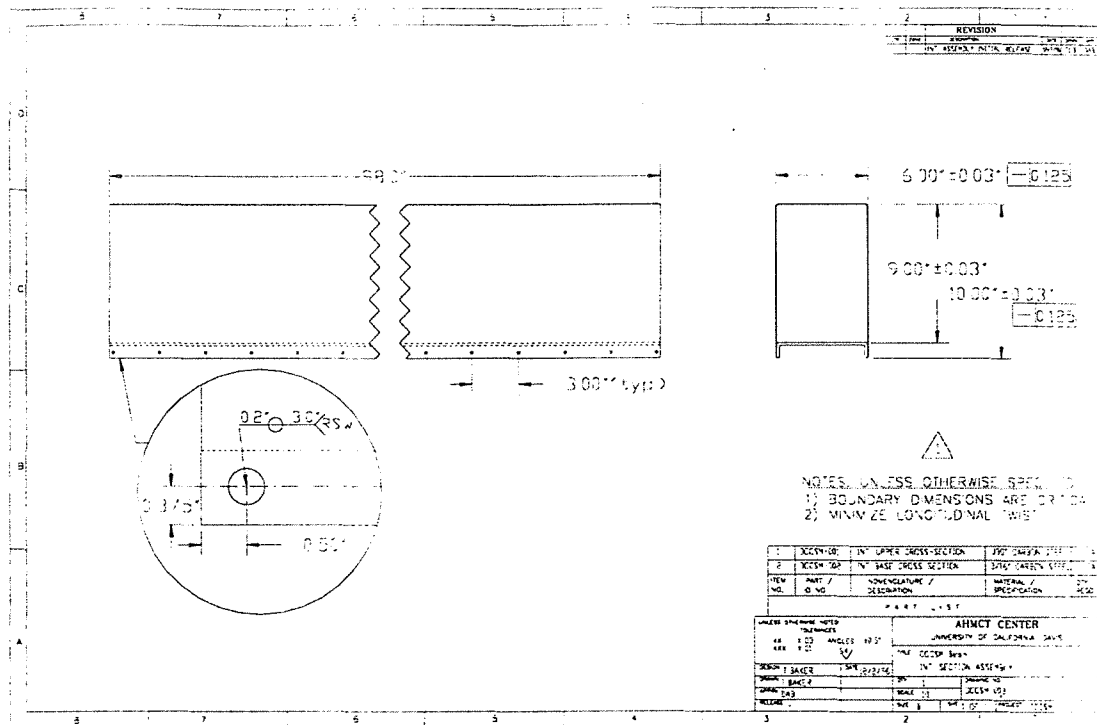


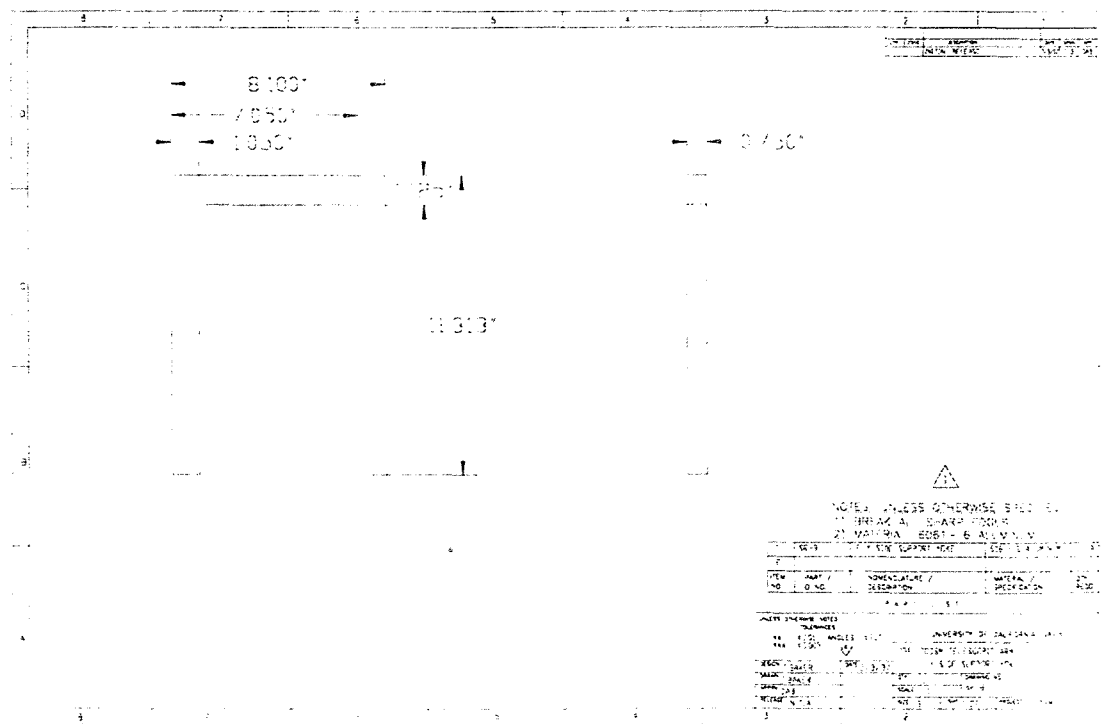
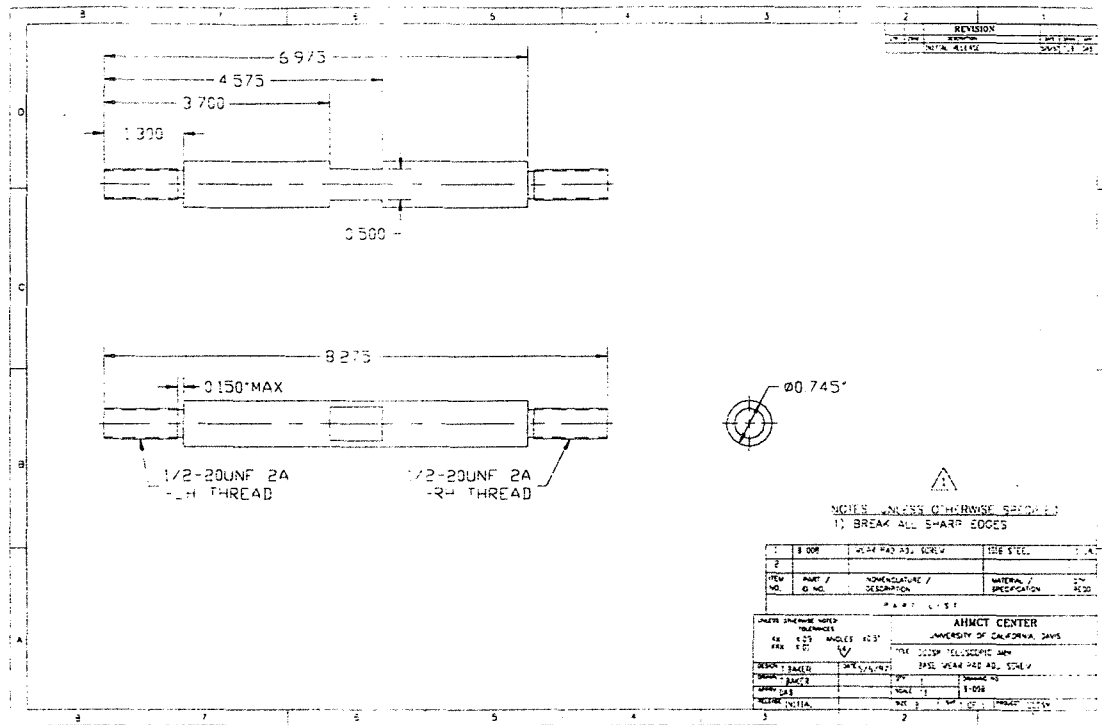


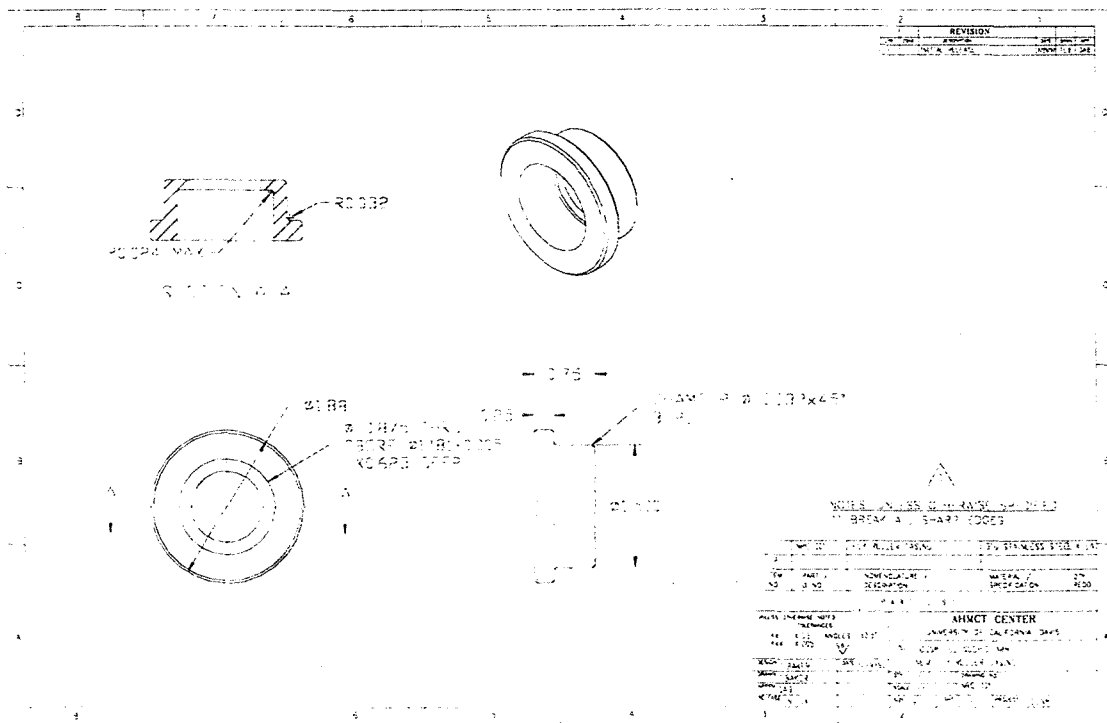
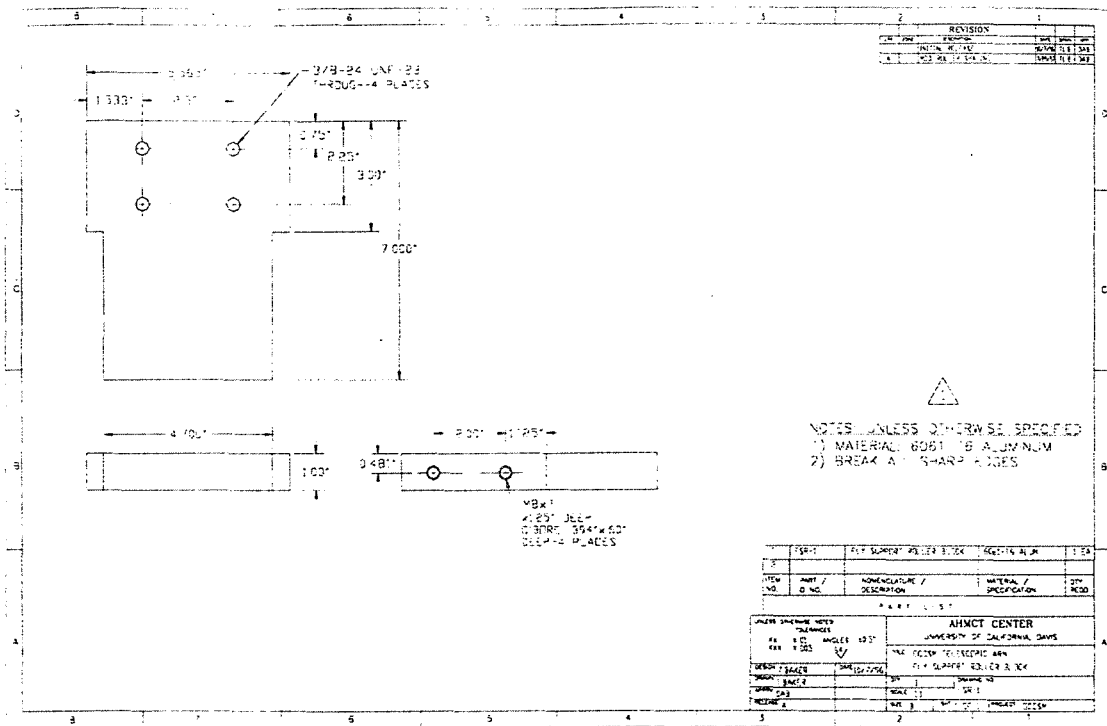


Intermediate Section

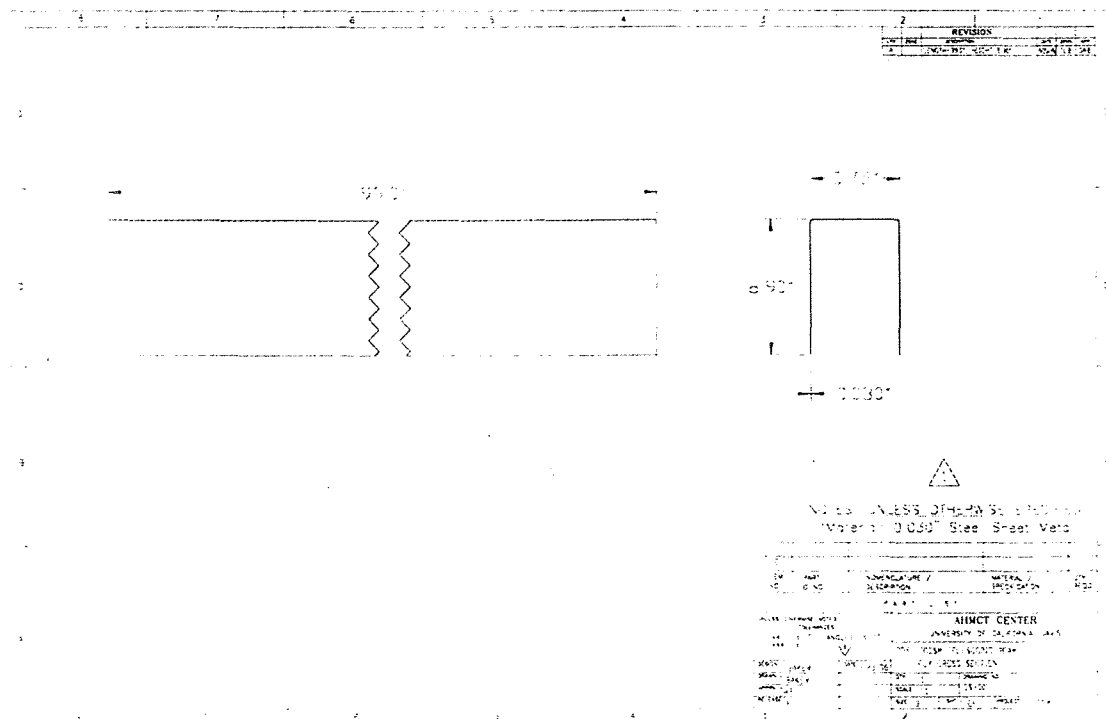
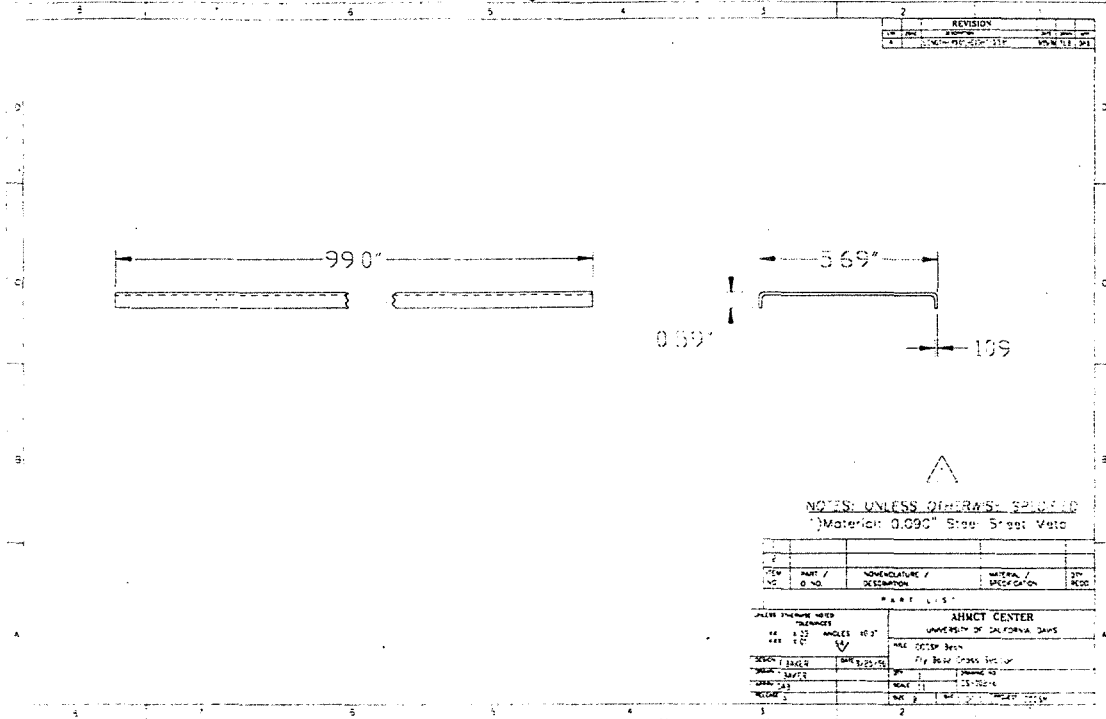


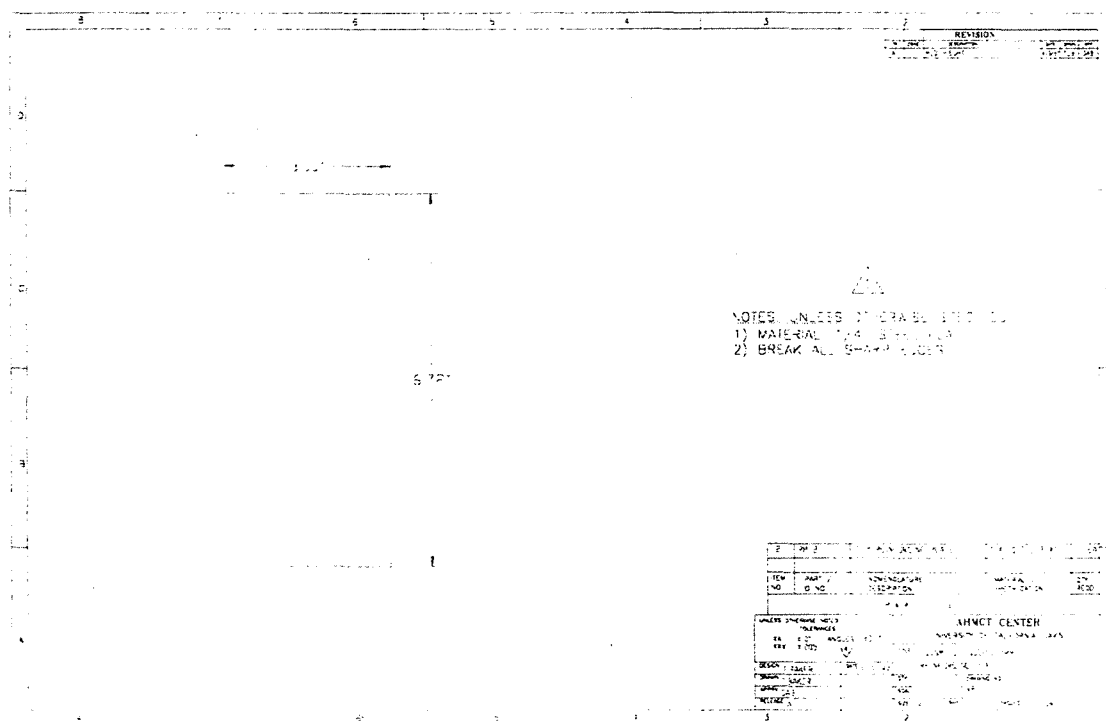
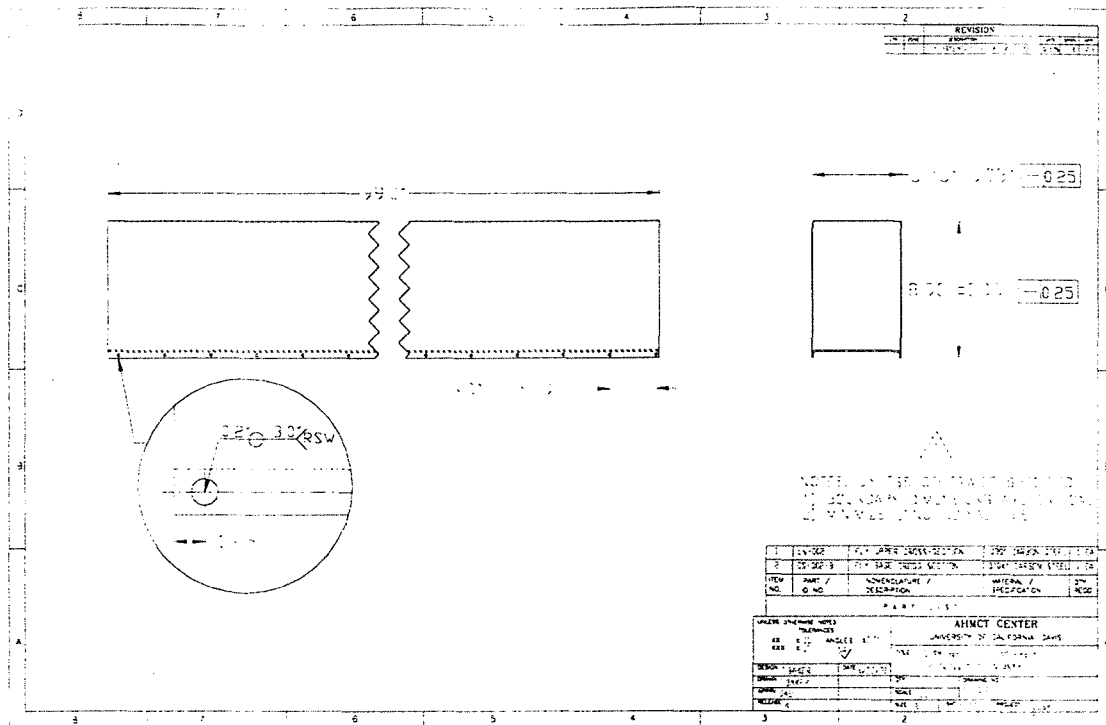


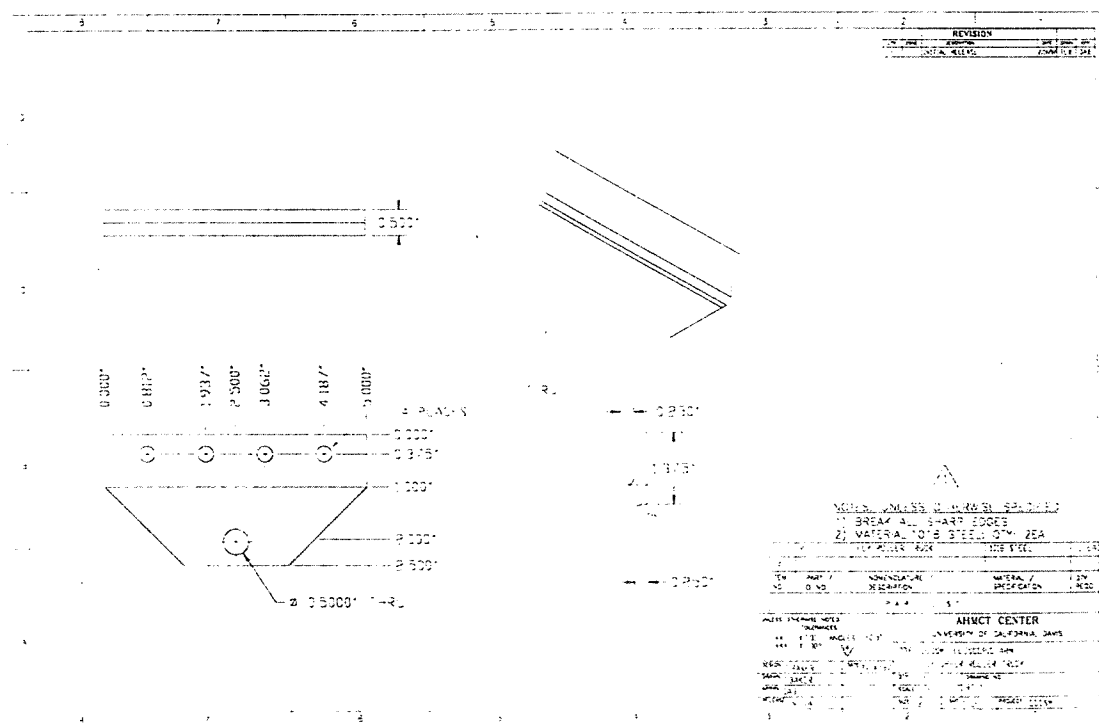
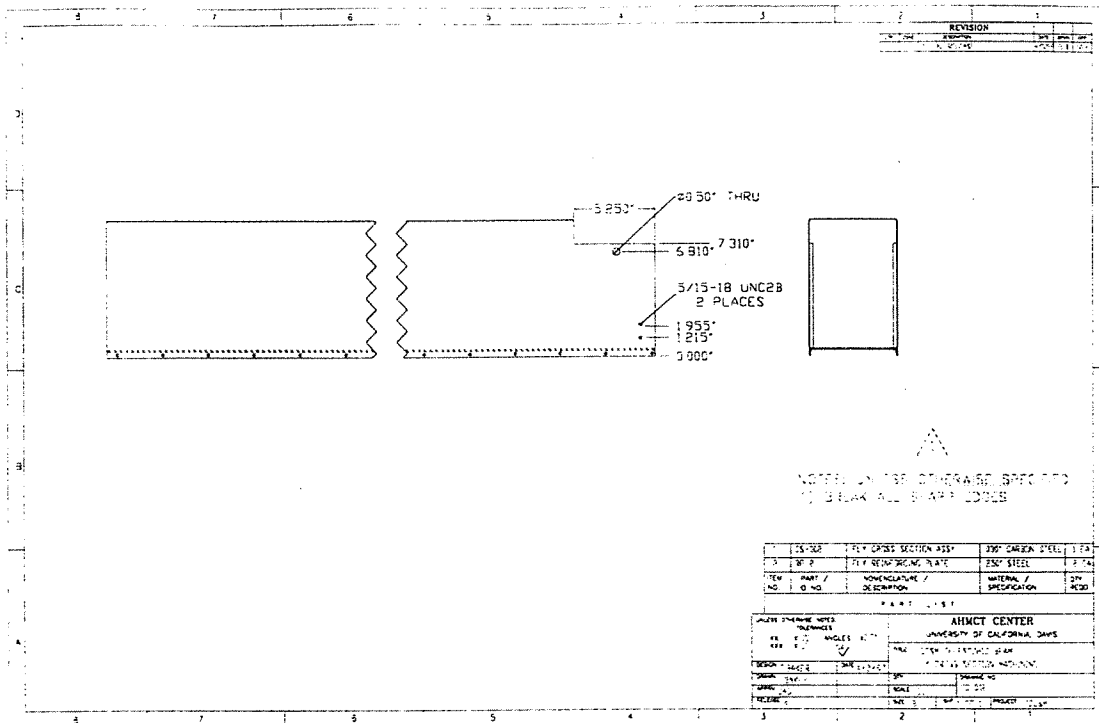




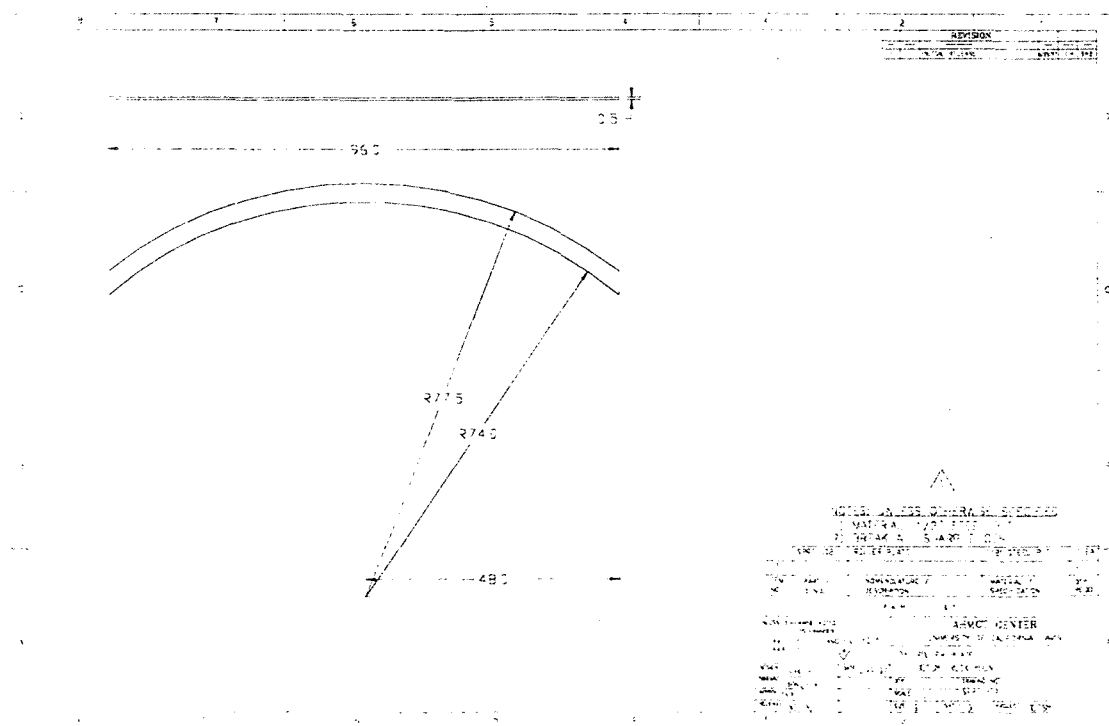
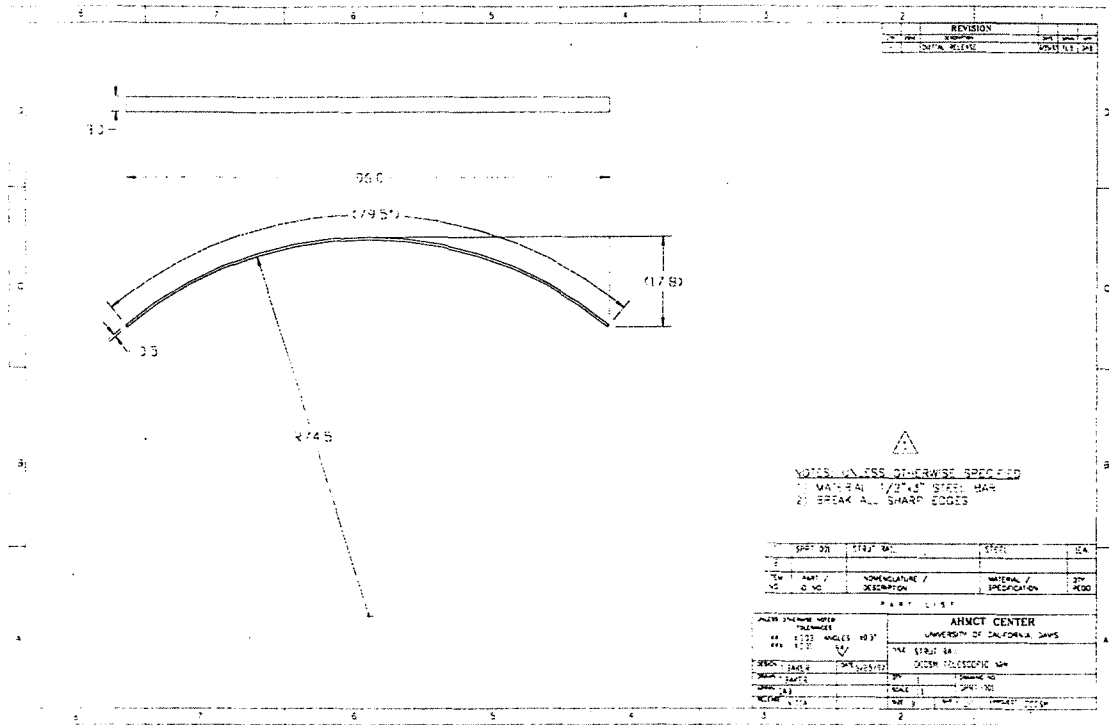
Fly Section

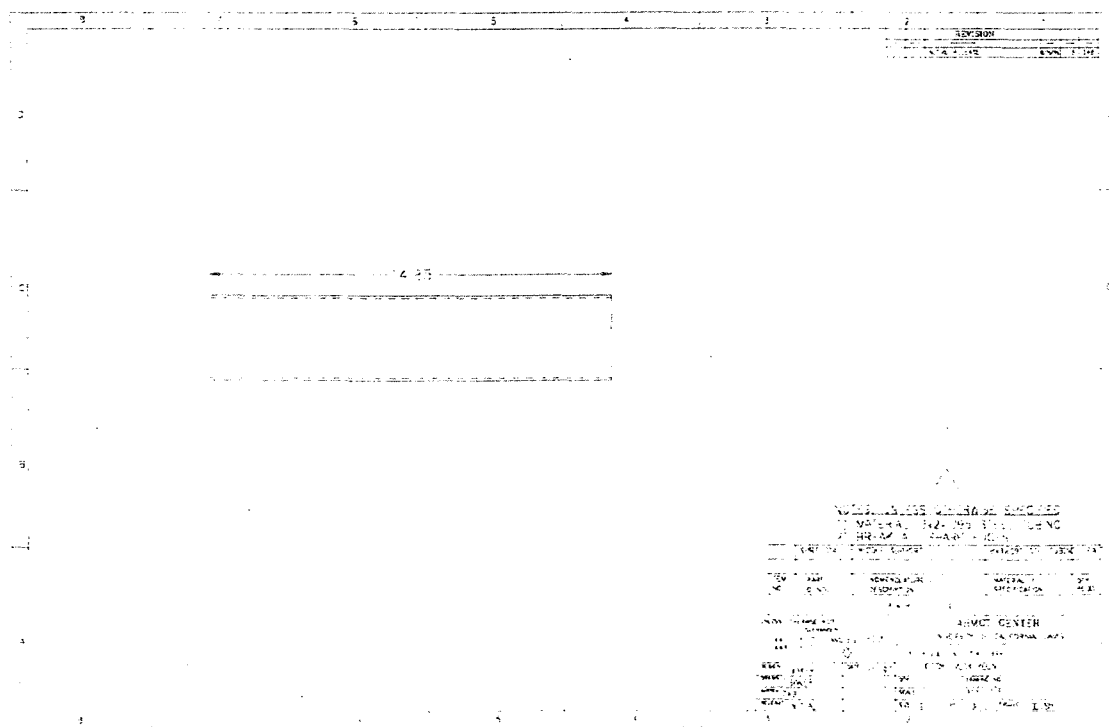
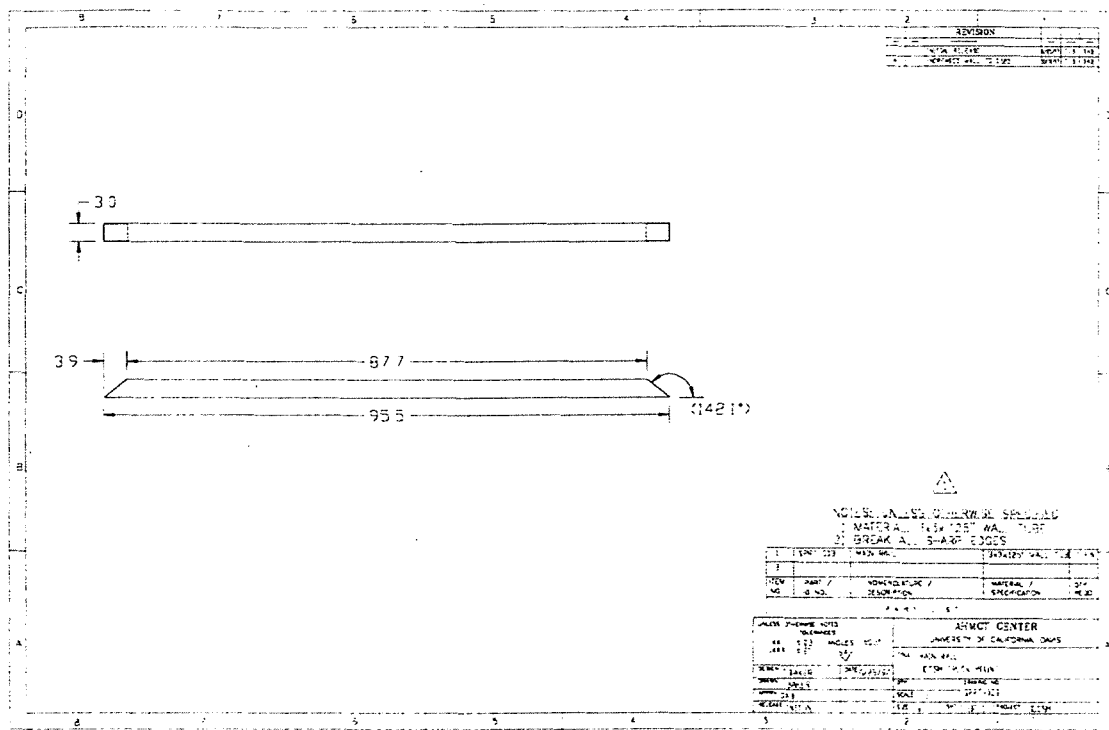


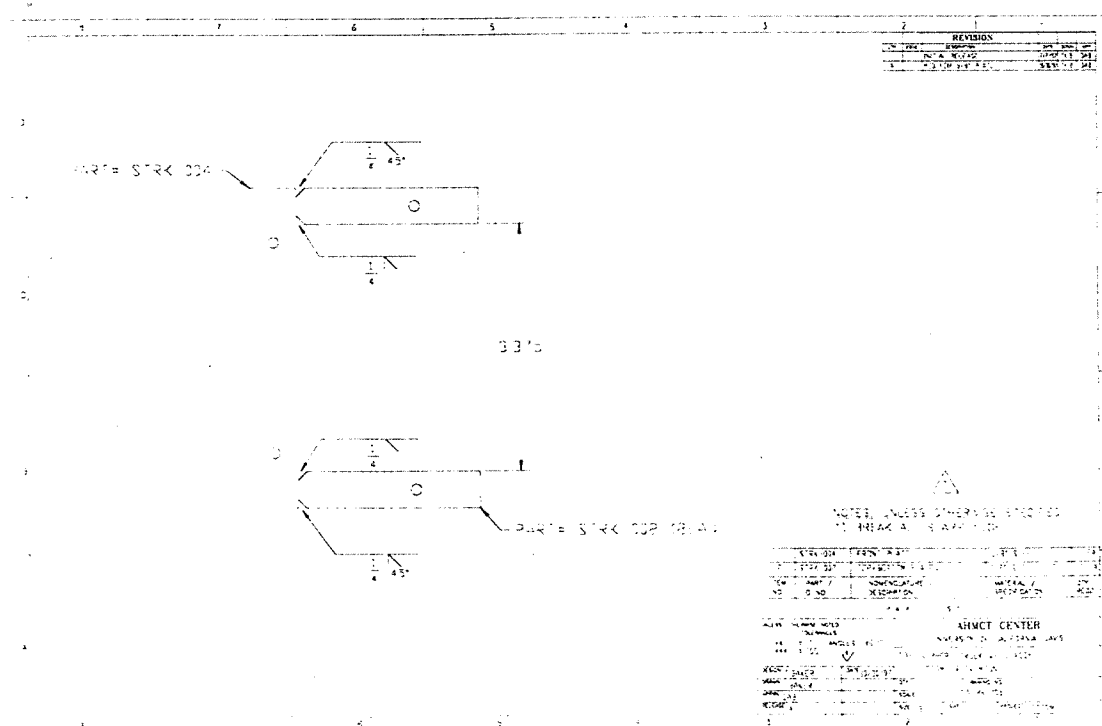
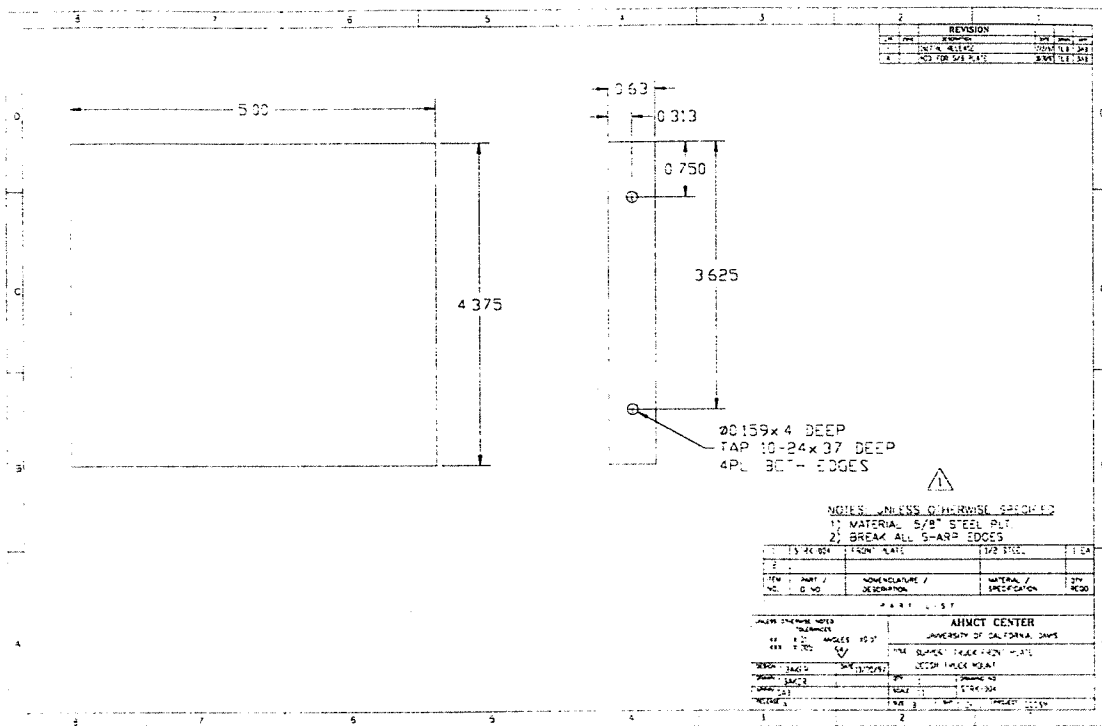


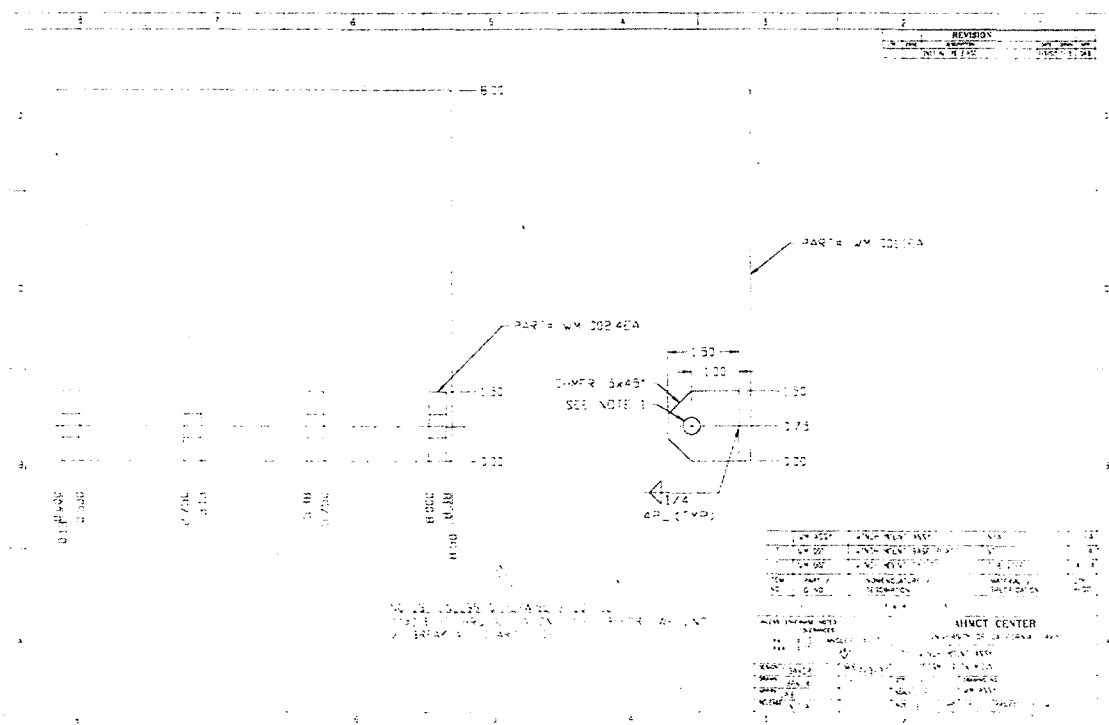
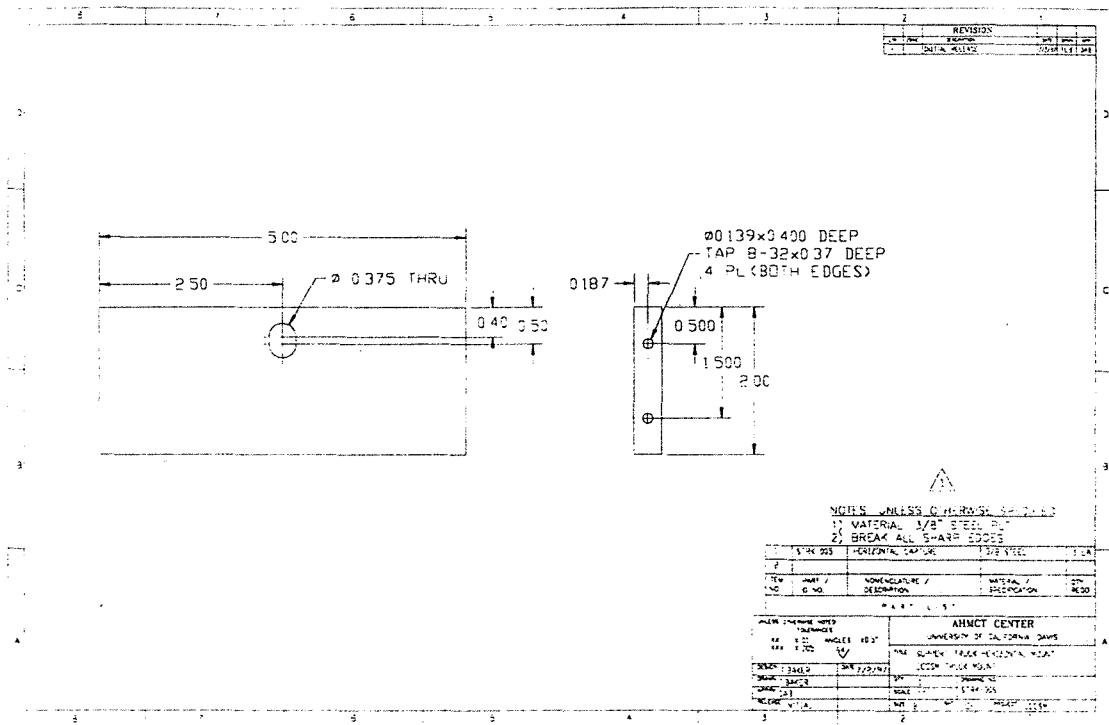


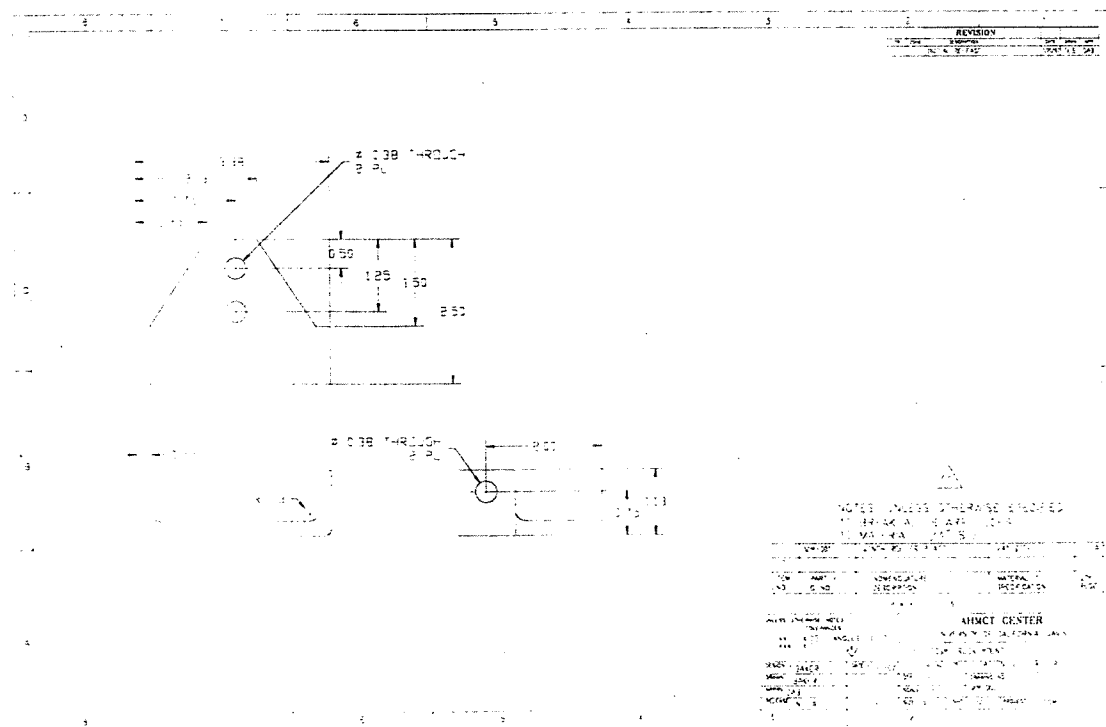
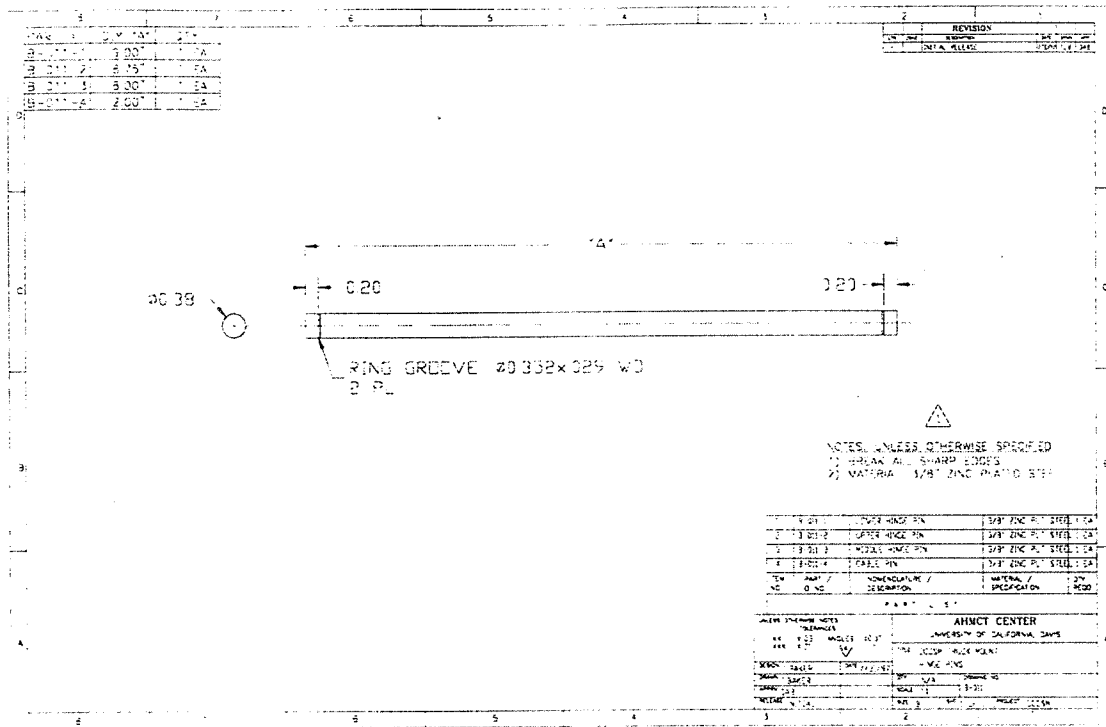
Truck Mount



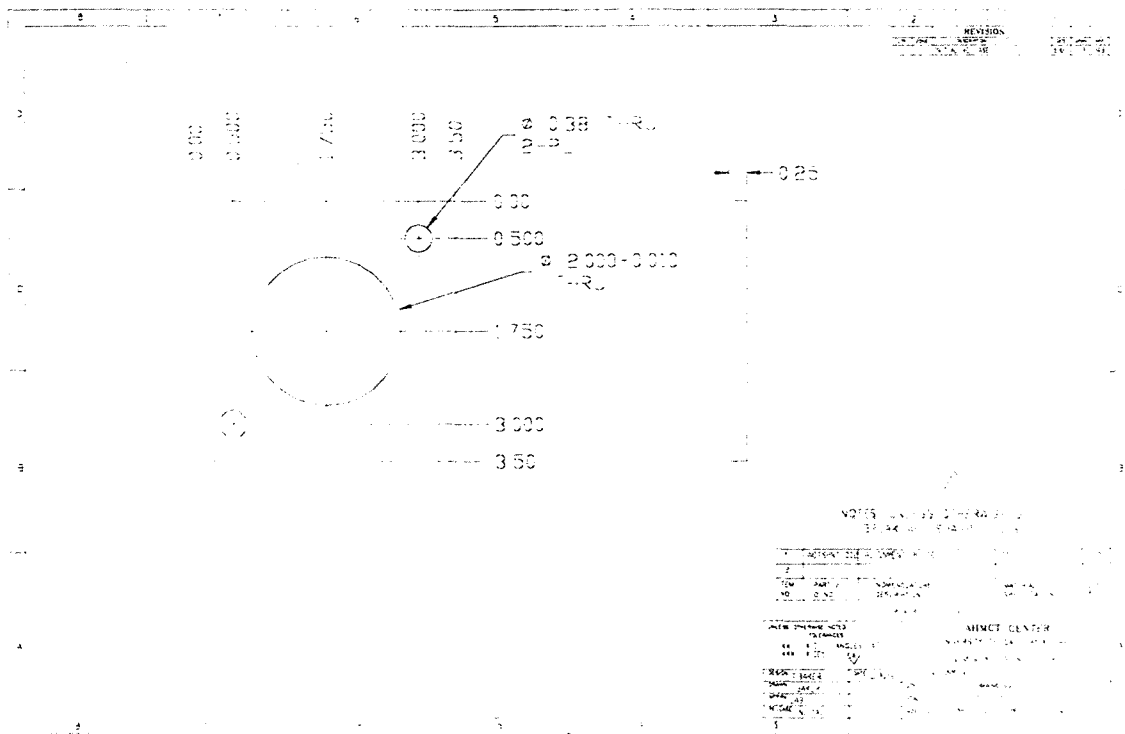
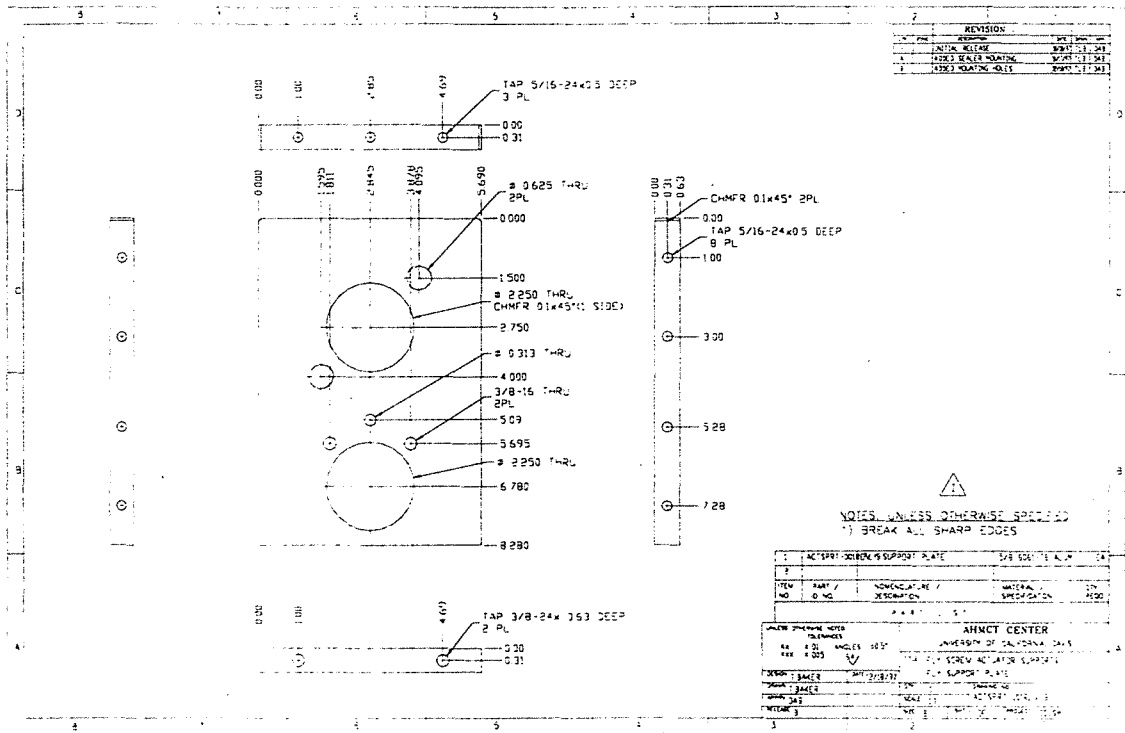


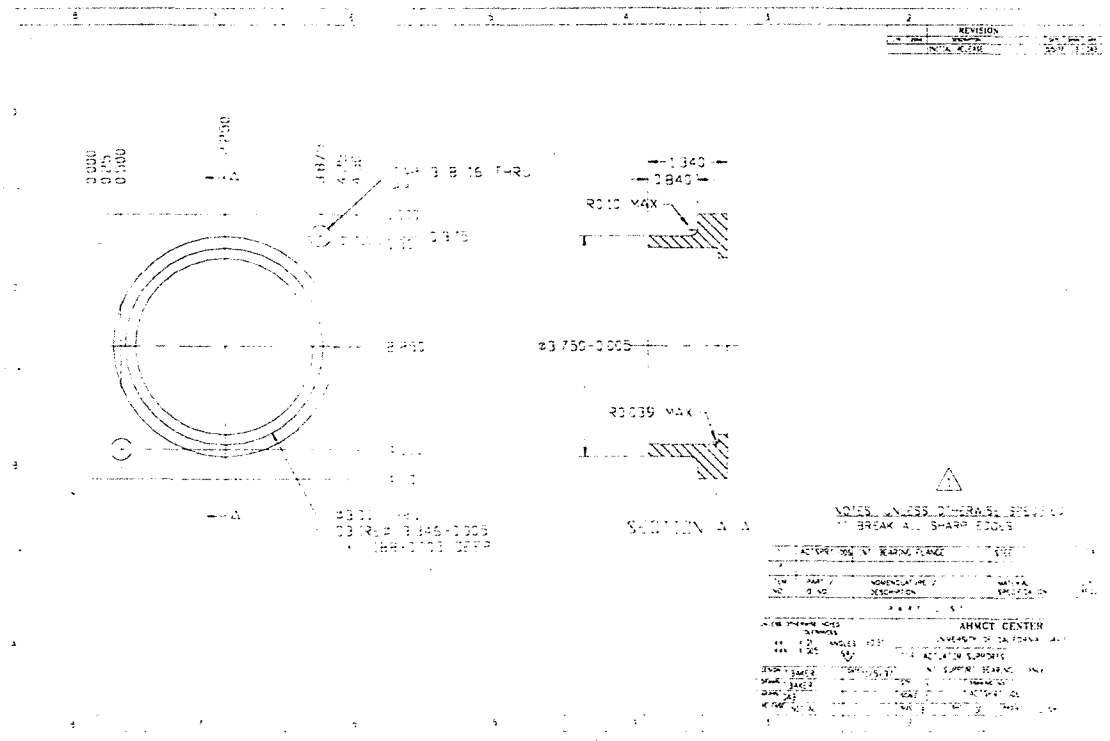
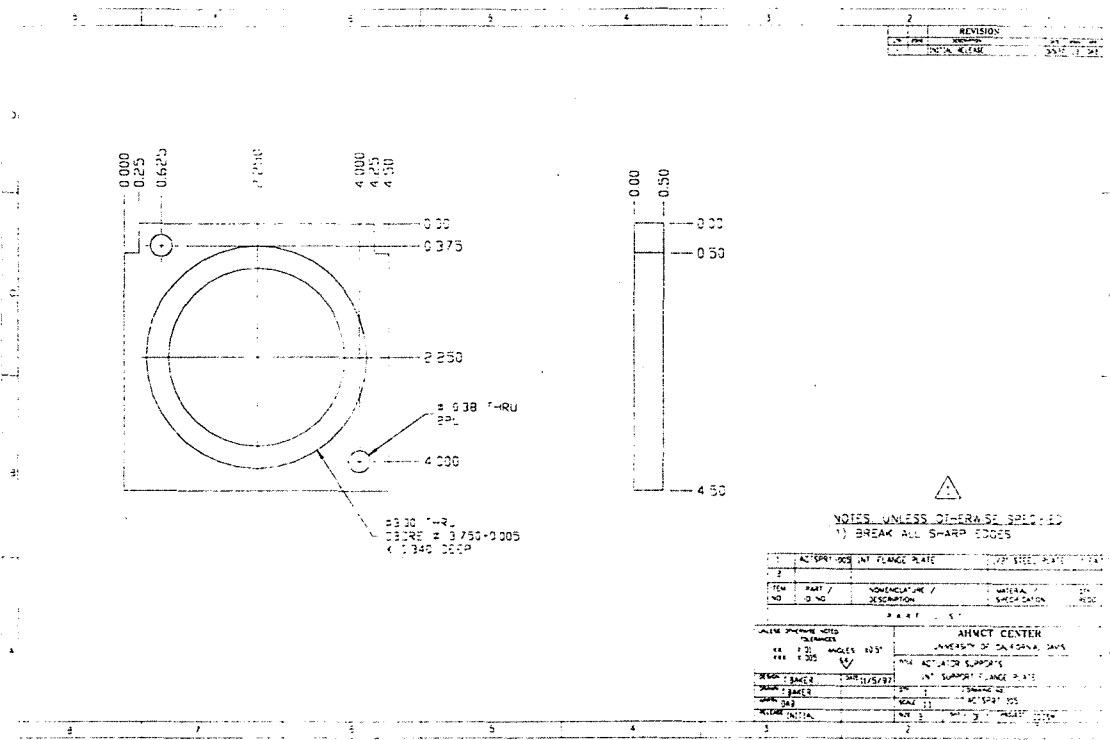


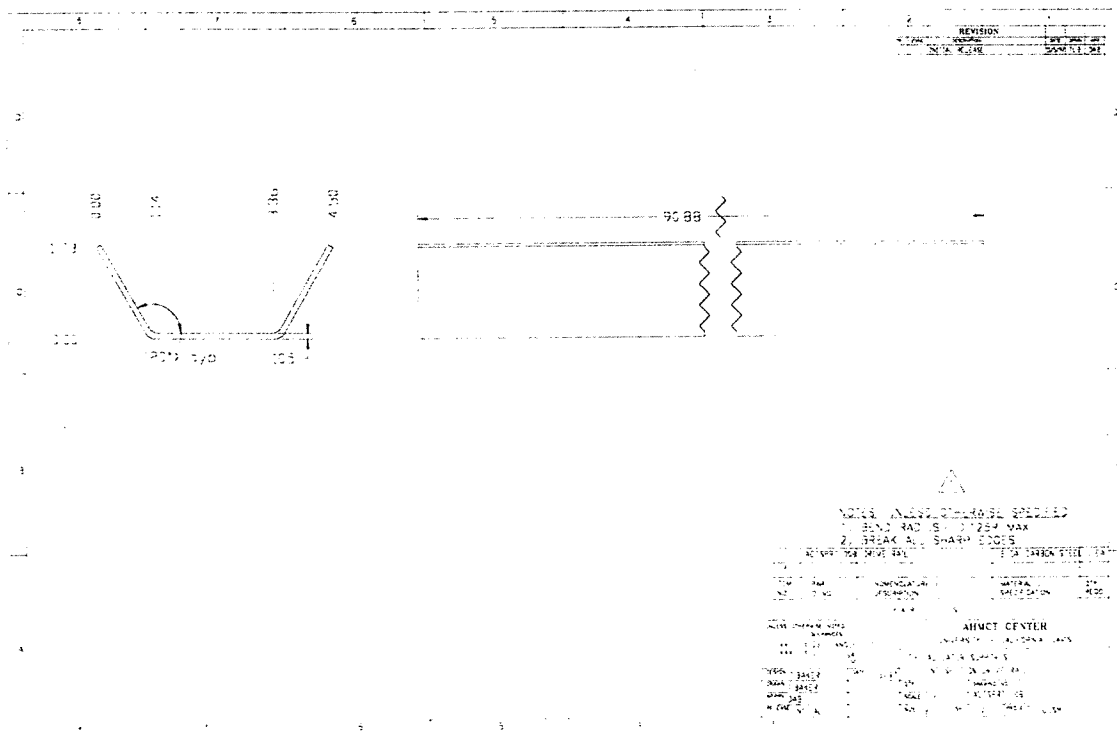
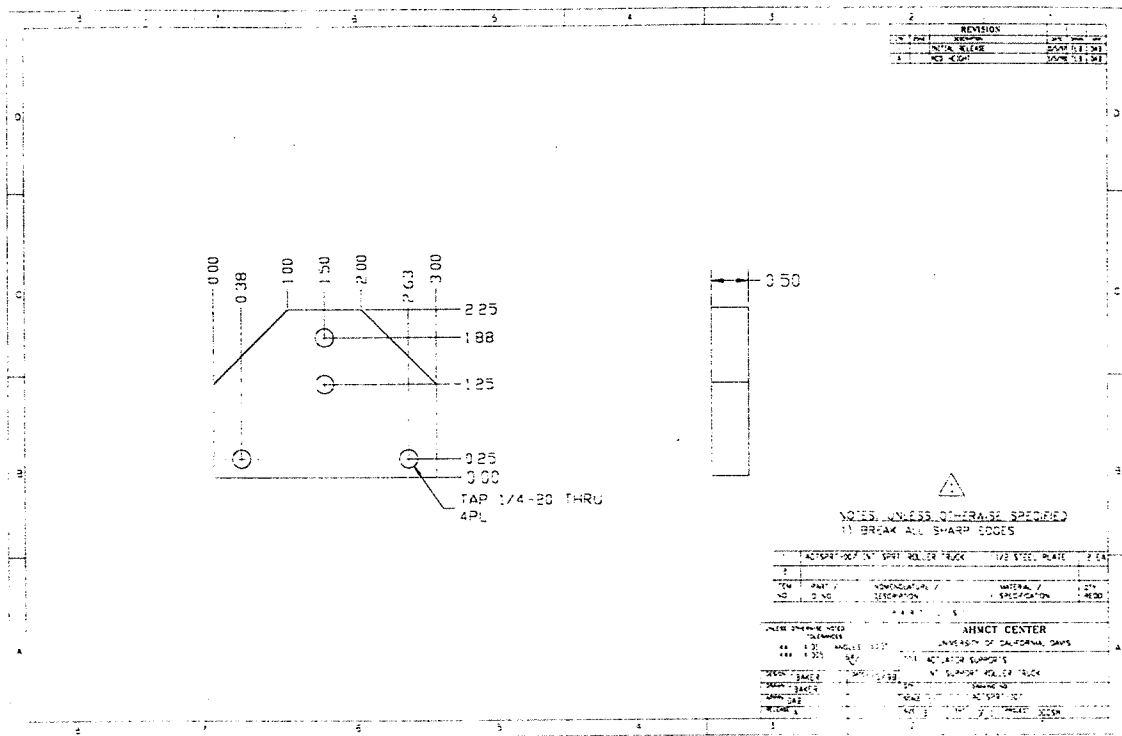


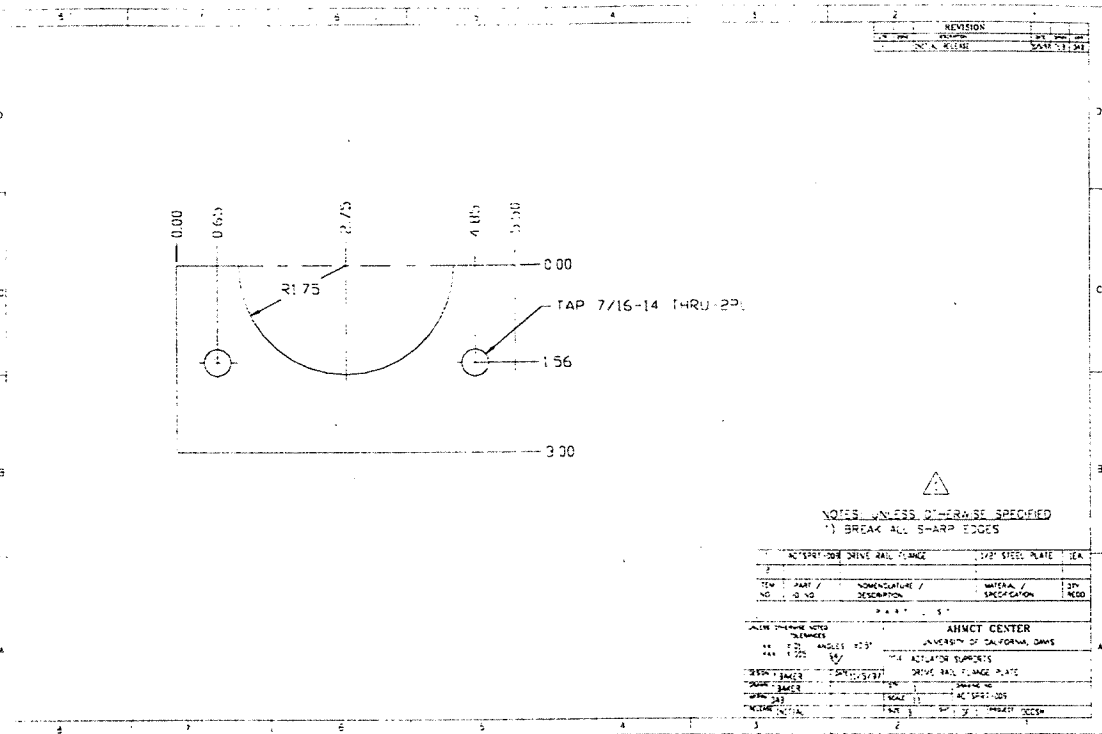


Actuator Supports









Gearbox Mount

